Identification and Modulation of a PPARG-regulated Anti-fibrotic MicroRNA Network in Liver Fibrosis and Hepatocellular Carcinoma

Dissertation

der Mathematisch-Naturwissenschaftlichen Fakultät

der Eberhard Karls Universität Tübingen

zur Erlangung des Grades eines

Doktors der Naturwissenschaften

(Dr. rer. nat.)

vorgelegt von

M. Sc. Catrin Bitter

aus Ludwigshafen am Rhein

Tübingen

2022

Gedruckt mit Genehmigung der Mathematisch-Naturwissenschaftlichen Fakultät der Eberhard Karls Universität Tübingen.

Tag der mündlichen Qualifikation:	27.01.2023
Dekan:	Prof. Dr. Thilo Stehle
1. Berichterstatter:	Prof. Dr. Alfred Nordheim
2. Berichterstatter:	Prof. Dr. Ralf-Peter Jansen

Declaration

All work presented here was performed by Catrin Bitter unless stated otherwise. Contributions of colleagues and collaborators to the three projects are listed in detail in **Chapters 3.2, 4.2,** and **5.2**. The thesis itself was written by Catrin Bitter. The work was performed under the supervision of Prof. Dr. Alfred Nordheim in the period from January 2018 to March 2021 at the Interfaculty Institute for Cell Biology (IFIZ), Eberhard Karls University Tübingen, Germany.

Abstract

The molecular processes underlying chronic liver disease and its progression from fibrosis to cirrhosis and hepatocellular carcinoma (HCC) have been extensively studied in the past, but reliable treatment options remain limited. An important feature of many diseases is the dysregulation of microRNAs (miRNAs). While the functions of miRNAs during hepatic fibrosis and HCC have been described for various individual miRNAs, few studies focus on miRNAs as integral parts of signaling networks.

Therefore, this study aims to identify a signaling network of functionally connected miRNAs and target genes that contributes to fibrosis and HCC. For this, the *SRF-VP16*^{iHep} mouse model of fibrotic HCC was analyzed by global miRNA and transcriptome profiling in combination with bioinformatic tools. The thus identified anti-fibrotic miRNA network (AF-miRNA network) is comprised of 8 miRNAs and 54 extracellular matrix (ECM-) related target genes that influence the fibrotic tumor microenvironment. The AF-miRNA network is not only dysregulated in murine and human HCC but also in murine liver fibrosis independent of HCC. Mechanistically, it was shown that the AF-miRNA network is dysregulated in activated hepatic stellate cells (HSCs) during fibrogenesis, and that the AF-miRNAs are collectively and directly regulated by the transcription factor peroxisome proliferator-activated receptor gamma (PPARG).

This study further shows that the AF-miRNA network is not only conserved between human and mouse, but also to the rat. This expands the available model organisms in which to study the AF-miRNA network with implications for human patients. Expression patterns of the AF-miRNA network were then compared in several rat and mouse models of liver fibrosis, revealing that AF-miRNA dysregulation is highly context-specific and varies considerably between the analyzed fibrosis models.

Additionally, it was investigated whether modulation of the PPARG-regulated AF-miRNA network inhibits liver fibrosis progression. Indeed, the PPARG agonist pioglitazone, while ineffective *in vivo*, enhanced AF-miRNA expression *in vitro* in immortalized HSC cell lines. Since the thus increased AF-miRNA expression inhibited the expression of their fibrotic target genes, it can be concluded that PPARG-mediated AF-miRNA modulation is a possible approach to reduce the fibrotic activity of HSCs during fibrogenesis.

Overall, this study demonstrates how functionally connected miRNAs collectively affect complex biological processes, in this case the microenvironment of fibrosis and HCC. The characterization of the AF-miRNA network in different liver fibrosis models as well as the investigation of how the AF-miRNA network can be modulated *in vitro* and *in vivo* present important steps towards understanding the relevance of the AF-miRNAs as potential therapeutic targets or predictors of disease outcome.

Zusammenfassung

Die molekularen Prozesse, die an der Entwicklung chronischer Lebererkrankungen von Fibrose über Zirrhose zum Hepatozellulären Karzinom (HCC, engl. hepatocellular carcinoma) beteiligt sind, werden seit langer Zeit intensiv erforscht. Trotzdem werden effektive Therapien noch immer benötigt. Eine wichtige Eigenschaft vieler Krankheiten ist die Dysregulation von microRNAs (miRNAs). Obwohl viele Studien die Funktionen individueller miRNAs in Leberfibrose und HCC erforscht haben, beachten nur wenige Studien, dass miRNAs essentielle Bestandteile komplexer Signal-Netzwerke sind.

Daher ist das Ziel dieser Studie, ein Signal-Netzwerk aus funktional zusammenhängenden miRNAs und Zielgenen zu identifizieren, das an der Entwicklung von Leberfibrose und HCC beteiligt ist. Das *SRF-VP16*^{iHep} Mausmodell für fibrotischen HCC wurde verwendet, um globale miRNA- und Transkriptom-Profile zu erstellen und bioinformatisch zu analysieren. Das dadurch identifizierte anti-fibrotische miRNA Netzwerk (AF-miRNA Netzwerk) besteht aus 8 miRNAs und 54 Zielgenen, die mit der extrazellulären Matrix (ECM, engl. extracellular matrix) assoziiert sind. Das AF-miRNA Netzwerk ist an Prozessen im fibrotischen Mikromilieu beteiligt und ist nicht nur in HCC von Maus und Mensch dysreguliert, sondern auch in Mausmodellen der Leberfibrose in Abwesenheit von HCC. Die Dysregulation des Netzwerks findet in aktivierten hepatischen Sternzellen (HSCs, engl. hepatic stellate cells) während der Entstehung von Leberfibrose statt. Dabei werden die AF-miRNAs des Netzwerks direkt und kollektiv durch den Transkriptionsfaktor PPARG (engl. peroxisome proliferator-activated receptor gamma) reguliert.

Diese Studie zeigt weiterhin, dass das AF-miRNA Netzwerk nicht nur zwischen Mensch und Maus konserviert ist, sondern auch zur Ratte. Dadurch vergrößert sich die Anzahl verfügbarer Modellsysteme, in denen das AF-miRNA Netzwerk mit Implikationen für den Menschen erforscht werden kann. Der Vergleich mehrerer Tiermodelle der Leberfibrose in Ratte und Maus zeigte dann, dass die Dysregulation der AF-miRNAs sehr kontextspezifisch ist und stark zwischen den untersuchten Fibrose-Modellen variiert.

In dieser Studie wurde auch untersucht, ob die Modulation des PPARG-regulierten AF-miRNA Netzwerks das Fortschreiten von Leberfibrose reduziert. Obwohl der PPARG-Agonist Pioglitazon im *in vivo* Modell der Leberfibrose keinen Effekt zeigte, konnte er dennoch die Expression der AF-miRNAs *in vitro* in HSC Zellkulturlinien erhöhen. Außerdem bewirkte diese erhöhte AF-miRNA Expression die Inhibition der fibrotischen Zielgene des Netzwerks. Dies zeigt, dass die Modulation der AF-miRNAs mittels Aktivierung von PPARG durchaus ein möglicher Ansatz ist, um die fibrotische Aktivität von HSCs während der Entstehung von Leberfibrose zu reduzieren.

Insgesamt beschreibt diese Studie, wie eine Gruppe funktional verwandter miRNAs gemeinsam komplexe biologische Prozesse beeinflusst, in diesem Fall das Mikromilieu von Leberfibrose und HCC. Die Charakterisierung des AF-miRNA Netzwerks in verschiedenen Modellen der Leberfibrose und die Analyse davon, wie das AF-miRNA Netzwerk *in vitro* und *in vivo* moduliert werden kann, sind entscheidende Schritte, um die Relevanz der AF-miRNAs als potenzielle therapeutische Ziele oder Biomarker besser zu verstehen.

Contents

1 Introduction

1.1 Chronic Liver Disease

Chronic liver disease refers to the long-term pathologic process of continuous destruction of liver function [1]. In response to persistent liver injury, repeated cycles of liver damage and regeneration cause hepatic inflammation and fibrosis [1,2]. Untreated, chronic liver disease progresses to cirrhosis and hepatocellular carcinoma (HCC) [2,3] (**Figure 1.1**). The main risk factors for chronic liver disease, and thus also for fibrosis, cirrhosis, and HCC, are infection with hepatitis B virus (HBV) or hepatitis C virus (HCV), alcoholic liver disease (ALD), non-alcoholic fatty liver disease (NAFLD), and its more progressed form, non-alcoholic steatohepatitis (NASH) [4–6].

Liver fibrosis is typically the first measurable manifestation of chronic liver disease and is characterized by the activation of hepatic stellate cells (HSCs) into extracellular matrix (ECM)-producing myofibroblasts [7]. While these fibrotic processes are essential for the wound-healing response to acute liver injury, they become aberrant if the liver injury persists and becomes chronic [8]. The continuous net accumulation of ECM results in the progressive substitution of liver parenchyma with scar tissue and impairs normal liver function [9]. Liver fibrosis is further accompanied by inflammatory damage, hepatocyte cell death, liver stiffness, and angiogenesis [10]. However, with the removal of the underlying cause of injury or with anti-fibrotic therapies, it is possible for fibrotic liver tissue to resolve to a near-normal liver architecture [9,10] (**Figure 1.1**).

Left untreated, liver fibrosis typically progresses to cirrhosis over the course of 5-50 years [9,10]. Cirrhosis is characterized by severe ECM accumulation and by a distorted liver architecture with abnormal blood flow, eventually leading to portal hypertension [9]. Decompensated cirrhosis is additionally defined by the onset of complications such as ascites, hepatic encephalopathy, and variceal bleeding. Cirrhosis either culminates in loss of liver function or further progresses to HCC [11]. The complete resolution of cirrhosis is rarely feasible, but with removal of the underlying cause of injury or with anti-fibrotic medication, the regression of cirrhosis to less severe fibrotic stages is possible and often improves the patient's clinical outcome [10,12].

Altogether, liver fibrosis is considered the turning point of chronic liver disease. Its regression can result in full resolution of injury, whereas its progression leads to liver cirrhosis and eventually to HCC [13].

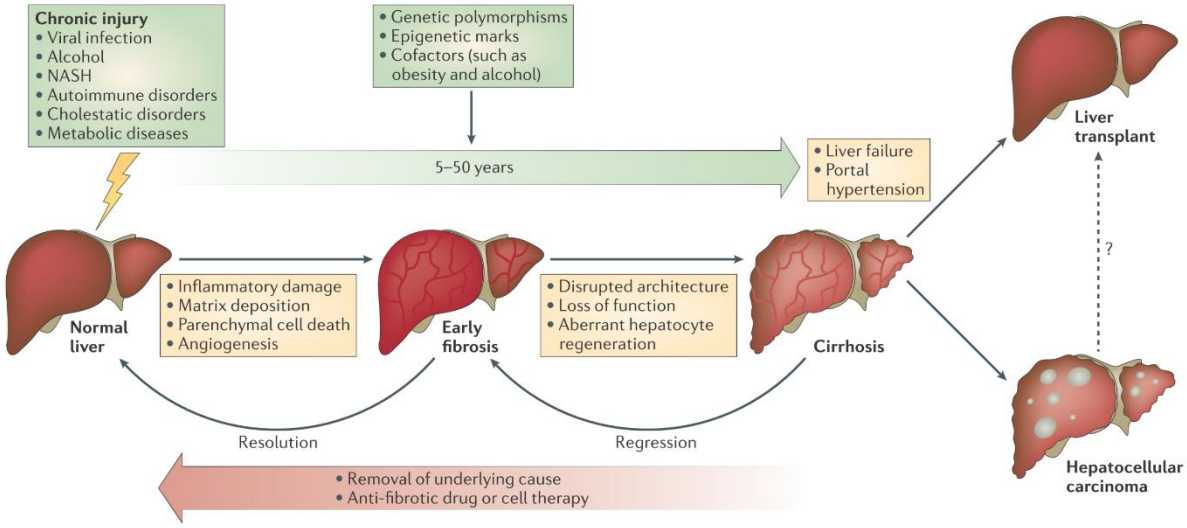

Figure 1.1 | Progression of chronic liver disease from fibrosis to cirrhosis and HCC. (**Green**) Hepatic fibrosis is the aberrant wound-healing response of the liver to diverse causes of chronic injury, of which viral infection, heavy alcohol consumption, and NASH are the most common. Independent of the underlying cause, repeated injury causes inflammatory damage, matrix deposition, parenchymal cell death, and angiogenesis, leading to fibrosis. With persisting cause of injury, fibrosis further progresses to cirrhosis over the course of 5-50 years. Cirrhotic livers are characterized by severe scar tissue accumulation and disrupted liver architecture. Cirrhosis either culminates in loss of liver function and portal hypertension or further progresses to HCC. The risk of liver disease progression is further affected by genetic polymorphisms, epigenetic markers, and cofactors such as obesity and alcohol. (**Red**) With removal of the underlying cause of injury or with anti-fibrotic therapies, the resolution of fibrosis to near-normal liver architecture is possible. Complete resolution of cirrhosis is rarely feasible, but regression to less severe fibrotic stages improves clinical outcomes. In case of liver failure and severe HCC, liver transplantation is the most common treatment besides cancer therapeutics. Figure reprinted from Pellicoro *et al.* (2014) [10]. HCC – hepatocellular carcinoma. NASH – non-alcoholic steatohepatitis.

1.2 HCC as Endpoint of Chronic Liver Disease

1.2.1 Incidence and Risk Factors of HCC

Primary liver cancer was the sixth most commonly diagnosed cancer and the third leading cause of cancer-related deaths worldwide in 2020, with approximately 906,000 new cases and 830,000 deaths [6]. HCC is the most common form of primary liver cancer and accounts for 75-85% of cases [6]. The majority of HCC cases arises in the setting of chronic liver disease independent of its etiology [1,2].

The main risk factors for all stages of chronic liver disease, and thus also for HCC, are HBV/HCV infection, ALD, NAFLD, and NASH [4,5,9]. Additional cofactors such as genetic polymorphisms, obesity, alcohol, smoking, and exposure to aflatoxin are further contributors [6,10]. The incidence and main risk factors vary between geographical regions and are best documented for HCC cases [5,6]. Worldwide, HBV infection accounts for the majority of HCC cases, especially in East Asia, Africa, and South America, where the lower socioeconomic status partially restricts the access to vaccinations [5,14]. Nevertheless, HBV vaccinations have decreased the incidence of HCC in some parts

of Asia, and allow successful treatment of most patients in developed countries [5]. Excessive alcohol consumption is the most common cause of HCC in Central and Eastern Europe and accounts, besides HBV, also for a majority of cases in Africa and South America [5]. In Japan, Western Europe, and North America, HCV infection is the most common etiology of HCC [5].

Interestingly, the major risk factors for HCC appear to be in transition. While the prevalence of HBV and HCV is globally declining, the prevalence of obesity and diabetes is increasing in many regions [6]. Since they are common precursors for NAFLD and NASH, these risk factors are expected to soon become the predominant causes of HCC in high income regions, especially in the Western world [5,6].

1.2.2 Diagnosis of HCC

Since fibrosis typically progresses asymptomatically to cirrhosis and HCC over many years, about 50% of HCC cases are diagnosed at late stages [2]. The first symptoms typically include abdominal pain, weight loss, anorexia, and symptoms of severe liver dysfunction [5]. At such late stages, especially once cirrhosis is established, the available treatment options are very limited [1]. Therefore, surveillance of patients at high risk for HCC development, namely individuals with diagnosed ALD, NAFLD, NASH, or HBV/HCV infections, is strongly advised [5,14]. The currently recommended surveillance strategy consists of semi-annual ultrasound elastography of the liver combined with the measurement of the blood serum marker alpha-fetoprotein [15]. In recent years, other blood serum markers such as circulating tumor DNA [16], extracellular vesicles [17], and circulating tumor cells [18] have become increasingly relevant tools in tumor diagnostics, especially for early disease detection and monitoring of therapeutic response. For asymptomatic patients in surveillance programs as well as for symptomatic late-stage patients, it is standard to confirm an HCC diagnosis by the histopathologic analysis of a liver biopsy [5].

1.2.3 Treatment of HCC

To ensure optimal management of HCC patients, the available treatment options are assigned according to the tumor stage, the degree of liver function impairment, and the patient's performance status [5]. The Barcelona Clinic Liver Cancer (BCLC) system is the most commonly used staging system for HCC and defines treatment options for patients with early-stage, intermediate-stage, and advanced-stage HCC [5,19].

Asymptomatic patients with early-stage HCC, defined by low tumor burden and good liver function, are preferred candidates for local curative treatments such as ablation and resection, or for liver transplantation [5]. While ablation induces tumor necrosis through thermal, chemical, or electrical methods, resection allows surgical removal of single tumor entities [15]. However, recurrence of HCC after resection remains a major challenge because the underlying cirrhosis persists as carcinogenic microenvironment [1,3]. Liver transplantation provides the only definite HCC treatment since it simultaneously removes the tumor and the underlying cirrhosis [15]. While liver transplantation shows excellent outcomes with a 5-year survival of 70%, its application is severely limited by organ shortage and long waiting times [5].

Asymptomatic patients with intermediate-stage HCC, which manifests as multinodular disease with adequate liver function, are preferred candidates for transarterial chemoembolization (TACE) [5]. TACE is a minimally invasive procedure that locally blocks the arterial blood supply of the tumor to induce necrosis and can be combined with local injections of chemotherapeutic drugs [15].

Patients with advanced-stage HCC show either extrahepatic tumor spread, vascular invasion, portal thrombosis, mild cancer-related symptoms, or a combination thereof and are typically treated with systemic therapies [5]. Until 2017, the oral drug sorafenib was the only available standard of care for patients with advanced-stage HCC [20]. As multikinase inhibitor, sorafenib targets tumor angiogenesis and tumor cell proliferation by blocking the serine/threonine-protein kinase Raf as well as vascular endothelial growth factor (VEGF) and platelet-derived growth factor (PDGF) signaling [15]. While further systemic agents have been approved since 2017, the first approach to improve overall survival compared to sorafenib treatment is the combination treatment with bevacizumab (anti-VEGF antibody) and the immune checkpoint inhibitor atezolizumab (anti-PD-L1 antibody) [21].

Overall, HCC treatment is most successful with early diagnosis and early onset of treatment. Therefore, it is most beneficial to target chronic liver disease in its premalignant stages, ideally as early as during liver fibrogenesis, to reduce the risk of HCC development in the first place [2,10].

1.3 Liver Fibrosis as Turning Point of Chronic Liver Disease

1.3.1 Incidence and Risk Factors of Liver Fibrosis

The main risk factors for all stages of chronic liver disease, and thus also for liver fibrosis as its earliest manifestation, are HBV/HCV infection, ALD, NAFLD, and NASH [4,5,9]. Independent of the etiology of chronic liver injury, about 80-90% of HCC cases have underlying fibrosis and approximately one in three patients with cirrhosis will develop HCC in their lifetime [1,3]. Cirrhosis is the leading cause of liver-related deaths worldwide and caused more than 1.32 million deaths globally in 2017, constituting 2.4% of total deaths worldwide [11]. Notably, such estimates of incidence and mortality are likely underestimated for cirrhosis and not widely available for fibrosis due to the often asymptomatic onset of disease [11].

1.3.2 Diagnosis of Liver Fibrosis

Liver fibrosis is the earliest manifestation of chronic liver disease [9]. Therefore, chronic liver disease outcome is strongly improved by reliable diagnosis and treatment of liver fibrosis before it progresses to cirrhosis and HCC [2]. To this day, the golden standard for diagnosis of fibrosis remains the histopathologic analysis of liver biopsies [22]. The Ishak score [23] and the Kleiner score [24] are the most commonly used scoring systems for the staging of chronic hepatitis and NAFLD/NASH, respectively [22]. Both scores assess liver fibrosis, inflammation, and parenchymal necrosis to estimate the patient's prognosis [25]. The degree and pattern of fibrosis is typically visualized by Sirius Red staining of collagen fibers and allows staging as well as identification of the underlying etiology [26,27]. Contrasting their diagnostic importance, liver biopsies are invasive, painful, time-consuming, and costly procedures with a risk of sampling error due to small sample size and heterogeneity in fibrosis distribution [26]. Liver biopsies are therefore not ideal for routine practice and regular screening.

For early detection and regular screening of patients in high risk groups, two main strategies for non-invasive diagnosis of liver fibrosis exist: the measurement of liver stiffness by imaging and the measurement of biochemical markers of liver function in blood serum [26]. The most widely used imaging method in clinical practice is ultrasound elastography, which can differentiate between fibrotic stages, especially late stages and cirrhosis, with high accuracy and sensitivity [28]. While no direct blood serum markers for fibrosis exist, there is a wide range of indirect markers for general liver damage currently in use. The blood serum markers for hepatocyte damage, aspartate aminotransferase (AST) and alanine aminotransferase (ALT), are the most widely used parameters to screen for and monitor patients with any type of liver disease [29]. Further routinely used blood serum markers to diagnose fibrotic liver diseases include bilirubin, albumin, gamma-glutamyltransferase

(GGT), alpha2-macroglobulin, alkaline phosphatase (AP), and platelet count [30–32]. Given the limited ability of individual blood serum markers to differentiate between fibrotic stages and etiology, markers are typically combined into non-invasive scoring systems to increase diagnostic specificity. AST/ALT ratio, APRI score, FIB-4 score, and NAFLD fibrosis score (NFS) are the most widely used scores, especially for initial diagnosis of mild to moderate fibrosis [30,33]. In contrast, the severity and clinical outcome for patients with advanced fibrosis and cirrhosis are typically classified by the Child-Pugh score and the model for end-stage liver disease (MELD) score, which predict the patient's 1-year and 3-months survival rate, respectively [22,34]. The MELD score is further used to assess liver transplant priority [22,34]. Altogether, early detection and diagnosis of liver fibrosis is crucial for the adequate treatment of disease, ideally restoring healthy liver function and improving patient survival [22].

1.3.3 Pathogenesis and Regression of Liver Fibrosis

1.3.3.1 HSC Activation as Key Event in the Pathogenesis of Liver Fibrosis

The healthy liver performs many essential roles in metabolism and clearance and is comprised of four main cell types, namely hepatocytes as the major parenchymal cells, and the three non-parenchymal cell types liver sinusoidal endothelial cells (LSECs), macrophages, and HSCs [35] (**Figure 1.2A**). Hepatocytes comprise about 80% of the total liver volume and perform many of the key functions of the healthy liver including bile production as well as the metabolization of endogenous and exogenous proteins, lipids, carbohydrates, and toxic substances [36]. LSECs constitute about 50% of the non-parenchymal cells of the liver and separate hepatocytes from the sinusoidal blood [35]. The LSEC monolayer is fenestrated and allows passage of small molecules from the blood into the space of Dissé and to hepatocytes [35]. The most common macrophages in the liver are Kupffer cells (KCs), which reside in the blood attached to LSECs [37]. KCs maintain tissue and immune homeostasis, and are the first responders to pathogenic threads and injury [35]. HSCs reside in the space of Dissé between LSECs and hepatocytes and comprise roughly 10% of all liver cells [9]. In the healthy liver, HSCs store vitamin A in the form of retinoid droplets and maintain a non-proliferative, pericyte-like, quiescent phenotype with limited ECM production [8,9] (**Figure 1.2A**).

Fibrogenesis is initiated by acute liver injury which, independent of its etiology, causes damage and ultimately apoptosis or necrosis of hepatocytes (**Figure 1.2B**) [27,38]. Apoptotic hepatocytes release cytokines that activate liver-residing KCs and recruit immune cells to the liver to clear cell debris [38]. Activated KCs are the major source of transforming growth factor beta (TGF-β) and other fibrogenic cytokines [38]. This inflammatory response is a crucial mediator between hepatocyte damage and the key event during fibrogenesis, the activation of HSCs into ECM-producing myofibroblasts [7,37].

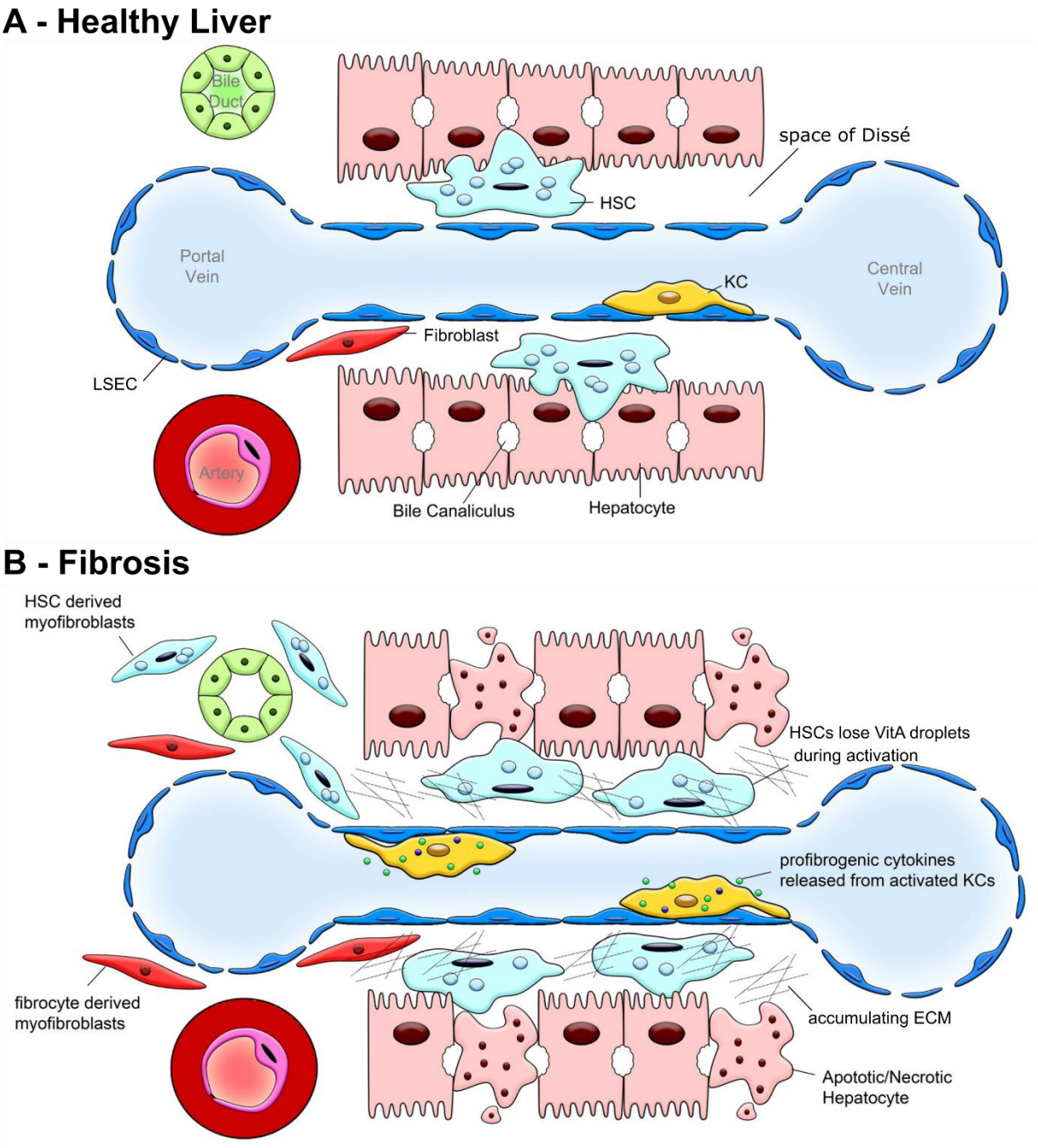

Figure 1.2 | Pathogenesis of liver fibrosis. (**A**) In the hepatic lobule of the healthy liver, the fenestrated LSEC monolayer allows molecules to pass from the sinusoidal blood into the space of Dissé to reach hepatocytes, which perform the metabolic functions of the liver. KCs, the main macrophages of the liver, reside in the sinusoidal blood and regulate tissue and immune homeostasis. HSCs are located in the space of Dissé, where they maintain a non-proliferative, vitamin A-storing, quiescent phenotype. (**B**) In response to chronic liver injury, hepatocytes are damaged and undergo apoptosis or necrosis. This releases cytokines that activate KCs and recruit immune cells to the liver. KCs are the main source of the key fibrogenic cytokine TGF-β, which induces HSC activation together with PDGF. Activated HSCs are characterized by their loss of vitamin A-storing retinoid droplets and their transformation into ECM-producing, contractile myofibroblasts. Liver fibrosis is thus defined by excessive ECM accumulation, increased liver stiffness, and the replacement of hepatocytes with scar tissue, overall disrupting normal liver function. Figure modified from Xu *et al.* (2014) [37]. ECM – extracellular matrix, HSC – hepatic stellate cell, KC – Kupffer cell, LSEC – liver sinusoidal endothelial cell, PDGF – platelet-derived growth factor, TGF-β – transforming growth factor beta, VitA – vitamin A.

HSC activation occurs in two major phases, initiation and perpetuation [27]. Initiation is caused by paracrine stimulation through all neighboring cell types including KCs, recruited immune cells, damaged hepatocytes, and LSECs [3]. Initiation alters the HSC gene expression profile to make them more responsive to further stimuli [7]. Perpetuation of HSC activation occurs when the liver injury becomes chronic, and the activating stimuli persist [27]. Perpetuation is characterized by autocrine as well as paracrine cytokine signaling and causes HSCs to undergo dramatic morphological and functional changes that promote fibrogenesis [7]. The most distinct alterations are the loss of retinoid droplets followed by enhanced proliferation, increased contractility, and the release of more inflammatory, fibrogenic, and mitogenic cytokines that further enhance fibrogenesis through positive feedback loops [9]. Ultimately, activated HSCs migrate to and proliferate at the site of injury, where they transdifferentiate into myofibroblasts and secrete excessive amounts of ECM components [7] (**Figure 1.2B**).

The key fibrogenic cytokines activating HSCs are PDGF and TGF-β [9]. PDGF is a mitogen and chemoattractant that drives proliferation and migration of HSCs to the site of injury through extracellular signal-recruited kinase (ERK)-dependent and ERK-independent pathways [10]. During activation, HSCs increase PDGF production and expression of PDGF receptors to enhance autocrine signaling [7]. As the most potent fibrogenic cytokine, TGF-β promotes ECM production, especially of fibrillar type I and type III collagen, through SMAD2 and SMAD3 signaling cascades [38]. TGF-β also activates mitogen-activated protein kinase (MAPK) signaling to further promote HSC activation [9]. Other important fibrogenic cytokines include VEGF, which is mainly released by LSECs and HSCs to induce HSC proliferation, and connective tissue growth factor (CTGF), which promotes HSC migration, proliferation, survival, and ECM synthesis [9].

Upon activation, HSCs undergo dramatic changes in their gene expression profile that allow clear distinction between quiescent and activated HSCs [7]. The loss of their vitamin A-storing lipid droplets marks HSC differentiation from inactive adipocyte-like cells to activated myofibroblast-like cells and is accompanied by reduced expression of peroxisome proliferator-activated receptor (PPAR) gamma (PPARG) [39]. PPARs are a group of nuclear ligand-activated transcription factors that enable fine-tuning of glucose and fat metabolism, and regulate inflammation and fibrogenesis [4]. PPARG is the most prominent PPAR isotype during liver fibrogenesis and is considered a master regulator of HSC fate [4]. Its reduced expression results in the activation of HSCs and the progression of liver fibrosis, while its overexpression can revert HSCs to their quiescent phenotype [7,40]. Activated HSCs are further characterized by stress fiber formation and increased expression of actin alpha 2 (ACTA2, also known as α-SMA), resulting in increased cell contractility [41]. The enhanced synthesis of key components of fibrillar collagens in the fibrotic ECM, such as collagen type 1 alpha 1 (COL1A1) and collagen type 1 alpha 2 (COL1A2), is another well-established marker for activated HSCs [41]. The

expression of ACTA2 and collagens can be induced through TGF-β/SMAD and TGF-β/early growth response protein 1 (EGR1) signaling [38,42]. Aberrant EGR1 expression or activity is associated with cell growth, cell survival, cell differentiation, and ECM remodeling [43]. Besides transcriptional regulation, HSC activation and ECM synthesis are also mediated through epigenetic regulation, including histone modifications and DNA methylation on the DNA level as well as gene silencing through microRNAs (miRNAs) on the mRNA level [44].

The hepatic ECM is a complex network that not only provides mechanic stability through structural proteins, but also stores growth factors and cytokines [8]. The fibrotic ECM differs in its composition from the ECM in the normal liver, and is mostly composed of collagen I and III, fibronectin, laminin, elastin, and proteoglycans [27]. The fibrotic ECM is further characterized by constant remodeling, which is regulated by the balance between ECM-degrading matrix metalloproteinases (MMPs) and their inhibitors, tissue inhibitors of metalloproteinases (TIMPs) [10,45]. During this ECM remodeling, growth factors like PDGF, TGF-β, CTGF, and VEGF are released [8]. Activated HSCs are the main source of MMPs and also TIMPs, which inhibit MMP-mediated collagen fiber degradation and further enhance ECM accumulation [45]. The accumulating ECM does not only impair normal liver function by replacing hepatocytes with scar tissue, but also actively shapes the fibrotic microenvironment [9].

1.3.3.2 HSCs in the Fibrotic Microenvironment Facilitate HCC Development

The fibrotic microenvironment of the liver is not only comprised of the cellular components hepatocytes, activated HSCs, KCs, LSECs, and immune cells, but also of non-cellular components including the fibrotic ECM the cells reside in and the growth factors, cytokines, and proteins released in the environment [3]. All components of the fibrotic microenvironment constantly interact with each other and actively contribute to tumorigenesis [2]. Therefore, the fibrotic microenvironment is also often referred to as premalignant or carcinogenic microenvironment when facilitating HCC initiation, or as tumor microenvironment when actively interacting with existing HCC tumors [8]. The pathophysiology of HCC is a complex multistep process influenced by liver stiffness, angiogenesis, inflammation, and growth factor signaling, all of which define the fibrotic microenvironment [1,2,46]. Interestingly, activated HSCs contribute significantly to all of these key alterations [8].

Liver stiffness is caused by the enhanced contractility of activated HSCs and the accumulating fibrotic ECM produced by them [2]. Contractile HSCs restrict intrahepatic blood flow and increase sinusoidal pressure, which impedes normal liver function and further enhances ECM stiffness [27,47]. Cells sense ECM stiffness through integrins and other transmembrane receptors promoting proliferation and migration of HSCs (perpetuating fibrogenesis) and hepatocytes (initiating tumorigenesis) [8]. Several

studies confirmed that liver stiffness, as measured by elastography, positively correlates with HCC risk in patients with chronic liver disease [48,49]. Furthermore, the accumulating ECM protects HCC tumors from immune cells and enhances HCC chemotherapy resistance [8].

Liver stiffness and contractile HSCs of the fibrotic microenvironment interfere with normal blood flow and cause vascular disorganization as well as hypoxia [1]. Hypoxia induces angiogenesis to provide the damaged tissue and the growing tumor with nutrients and oxygen [1]. HSCs mediate these angiogenic processes by releasing VEGF and PDGF [9]. VEGF induces the proliferation of endothelial cells to sprout new vessels, while PDGF promotes cell migration and new vessel maturation [2].

The fibrotic microenvironment is further characterized by chronic inflammation, which perpetuates fibrogenesis and stimulates cell death and regeneration cycles in hepatocytes, eventually facilitating HCC development [2]. Inflammation is not only mediated by KCs and other innate and adaptive immune cells densely populating the fibrotic tissue, but also by HSCs [27,50]. Once activated, HSCs acquire important immunologic features. They serve as antigen-presenting cells, they mediate clearance of necrotic and apoptotic hepatocytes, and they are a versatile source of inflammatory mediators such as interleukins (IL) [50]. High levels of IL-6, IL-10, and IL-22 in tumor-surrounding tissue are associated with high risk of HCC development and poor prognosis [2]. HSCs also promote immune-suppressive responses by activating regulatory T cells and inducing T cell apoptosis, thus facilitating tumors to escape immune surveillance [50].

Furthermore, HSCs in the fibrotic tumor microenvironment secrete various growth factors which directly promote tumor proliferation, survival, and migration [1]. Besides its role as mediator of fibrogenesis through HSC activation, TGF-β is also a tumor promoter and immune-suppressor during tumorigenesis [1]. Together with PDGF, TGF-β contributes to tumor migration and invasiveness by facilitating epithelial-mesenchymal transition of hepatocytes [8]. Additionally, activated HSCs secrete hepatocyte growth factor (HGF), which mediates hepatocyte proliferation and survival through MAPK/ERK-signaling as well as HCC invasiveness and chemoresistance through HGF receptor (HGFR) signaling [8].

Altogether, in their complex interplay with the fibrotic microenvironment, HSCs actively contribute to the hallmarks of cancer, namely: sustaining proliferative signaling, evading growth suppressors, resisting cell death, enabling replicative immortality, inducing angiogenesis, evading immune destruction, and activating invasion and metastasis [51].

1.3.3.3 HSCs During Fibrosis Regression

Liver fibrosis is caused by the crosstalk between injured hepatocytes, immune cells, and HSCs upon chronic liver injury [1]. Elimination of the underlying cause of injury is the most effective way to halt or improve liver fibrosis, since it reduces the amount of inflammatory and fibrotic mediators released by damaged hepatocytes [22]. While eliminating the cause of injury has proven effective in experimental models of liver fibrosis induced by ALD, carbon tetrachloride (CCl_4), and bile duct ligation (BDL), human fibrotic diseases are often more complex and eliminating the cause of injury in patients is not always feasible or effective [38,44]. If the cause of injury cannot be eliminated, resolution of liver fibrosis is best achieved by inhibiting the substitution of functional liver tissue with fibrotic ECM [10]. Since activated HSCs are the primary source of fibrotic ECM components, they are attractive targets for anti-fibrotic therapy [37,41]. Three alternative cell fates can eliminate activated HSCs: apoptosis, senescence, and reversion to an inactive phenotype [9,38].

Apoptosis of activated HSCs is induced by external ligands binding to death receptors such as FAS and TNF receptor 1 (TNFR1) on their cell surface [9]. Indeed, stimulating HSC apoptosis pathways was shown to reverse CCl_4-induced liver fibrosis in mice and rats both *in vitro* and *in vivo* [52,53]. However, activated HSCs are often resistant to apoptosis due to their high expression levels of anti-apoptotic proteins such as BCL2 and NF-κB [44]. TIMPs and TGF-β also act as anti-apoptotic signals that promote the survival of HSCs [9].

Senescence of activated HSCs is regulated through p53-dependent and p16-dependent mechanisms and results in HSCs with a senescence-associated secretory phenotype [38]. In this stage, HSCs are characterized by cell cycle arrest, reduced synthesis of ECM components, and by increased secretion of MMPs and other ECM-degrading enzymes [9,38]. Furthermore, senescent HSCs release cytokines that recruit natural killer (NK) cells to induce HSC cell death. Additionally, senescent HSCs are more susceptible to apoptosis signaling due to the upregulation of death receptors such as the TNF-related apoptosis-inducing ligand (TRAIL) [38].

Finally, activated HSCs can revert to an inactive phenotype which is similar to, but distinct from, quiescent HSCs [9]. Inactive HSCs downregulate the expression of fibrotic genes such as *Col1a1*, *Acta2*, and TGF-β receptor 1 (*Tgfbr1*), but fail to express some quiescence-associated genes such as Perilipin-2 (*Plin2*), adiponectin receptor 1 (*Adipor1*), and glial fibrillary acidic protein (*Gfap*) [9]. Furthermore, they regain their functions as pericyte-like, vitamin A-storing cells [38]. However, inactive HSCs remain in a primed state and are easier to reactivate in response to fibrotic stimuli than quiescent HSCs [9].

1.3.4 Treatment of Liver Fibrosis

Liver fibrosis is the manifestation of various chronic liver diseases, and untreated, progresses to cirrhosis and HCC [1]. The most effective treatment of liver fibrosis is the removal of the underlying cause of injury. Depending on the primary cause of disease, specific therapeutic approaches exist [10,22]. For instance, direct-acting antiviral agents decrease fibrosis progression in patients with HCV infection [54]. Furthermore, reduction of alcohol consumption in patients with ALD improves clinical outcomes and prevents progression to cirrhosis, whereas weight reduction by diet or surgery was shown to improve inflammation and fibrosis in patients with NASH [22]. However, targeting the primary cause of liver disease is not always feasible or effective because of drastic live-style changes required by the patient or because the disease is too far progressed. In such cases, liver transplantation is typically the only available treatment [22].

To bridge this gap in treatment options, multiple anti-fibrotic therapies are currently investigated in clinical trials [10,22,41]. In accordance with known fibrosis regression pathways, anti-fibrotic approaches focus on the reduction of accumulating ECM, on modulating inflammatory pathways and, primarily, on the elimination of activated HSCs as drivers of fibrogenesis [10,38,55].

Anti-fibrotic therapies focusing on ECM accumulation include targeting lysyl oxidase-like 2 (LOXL2). LOXL2 is a key component of ECM remodeling and is responsible for collagen cross-linking and ECM stiffness [56]. The monoclonal antibody simtuzumab targets human LOXL2 and is in clinical trials for the treatment of liver fibrosis, where it appears to be well tolerated in NASH patients [22,57]. Additionally, activation or overexpression of the farnesoid X receptor (FXR) is known to inhibit collagen synthesis in HSCs [58]. The FXR agonist obeticholic acid was indeed able to improve fibrosis as well as liver inflammation in clinical trials with NAFLD and NASH patients (ClinicalTrials.gov, NCT00501592 and NCT01265498) [10,59]. Another therapeutic agent, targeting liver inflammation and fibrosis simultaneously, is cenicriviroc, a dual antagonist blocking the C-C chemokine receptors 2 (CCR2) and 5 (CCR5) [60]. Upon ligand binding, CCR2 and CCR5 promote liver fibrosis through activation of inflammatory signaling and the recruitment of immune cells [60]. In patients with NASH or NAFLD, blocking CCR2 and CCR5 with cenicriviroc was well tolerated and resulted in a profound anti-fibrotic benefit (ClinicalTrials.gov, NCT02217475).

Pathways regulating the cell fate of HSCs are also attractive targets for anti-fibrotic therapies [41]. The inhibition of HSC activation is investigated in patients with advanced liver fibrosis using the TGF-β inhibitor pirfenidone, which is already approved for the treatment of idiopathic pulmonary fibrosis (ClinicalTrials.gov, NCT04099407). Additionally, many clinical trials focus on the reversal of activated HSCs to their inactive state using PPARG agonists. PPARG is a nuclear hormone receptor of the PPAR family and typically considered the master regulator of HSC fate [4,61]. High PPARG expression and

activity maintains HSCs in their quiescent state and indeed, various PPARG agonists were able revert activated HSCs to their inactive state [7]. Specifically, PPARG agonists are known to inhibit PDGF-mediated HSC proliferation, TGF-β-mediated HSC activation, and HSC production of collagen and ACTA2 *in vitro* and *in vivo* [41,62–65]. Additionally, PPARG agonists reduce inflammation by inhibiting the expression of IL-1, IL-6, tumor necrosis factor alpha (TNF-α), and other cytokines [66]. The most prominent group of PPARG agonists are the thiazolidinediones (TZDs), of which rosiglitazone and pioglitazone are currently investigated in clinical trials with NASH patients [61,67]. While both TZDs reduce hepatic steatosis, only pioglitazone was repeatedly able to improve fibrosis and inflammation in NASH patients (ClinicalTrials.gov, NCT00492700, NCT00994682, and NCT00063622) [67–70].

Despite the many clinical trials conducted over the years, there are currently no therapies approved by the Food and Drug Administration (FDA) for NASH, NALFD, or other fibrotic liver diseases [59,71]. The results of many of these trials suggest that single drugs are not sufficient to treat the complex pathophysiology of liver fibrosis [71]. Therefore, combination therapies targeting different mechanisms and stages of disease simultaneously are increasingly researched [59]. Nevertheless, the discovery of effective therapeutics remains challenging and continues to benefit from the thorough investigation of known and new molecular pathways involved in liver fibrogenesis.

1.4 MicroRNAs

1.4.1 MicroRNA Function

MicroRNAs (miRNAs) are short (21-23 nucleotides), endogenous, single-stranded RNA molecules that act as important regulators of gene expression [72]. miRNAs are functionally involved in almost all biological processes and aberrant miRNA expression contributes to a wide range of human pathologies, including fibrosis and cancer [73,74].

Mature miRNAs regulate gene expression on the post-transcriptional level [75]. They assemble with Argonaute (AGO) proteins to form the RNA-induced silencing complex (RISC), which is guided by the incorporated miRNA to target messenger RNAs (mRNAs) through complementary base-pairing [72]. In most cases, miRNAs bind to the 3’ untranslated region (3’UTR) of target mRNAs, inducing RISC to mediate degradation, destabilization, or translational inhibition of the target mRNA, ultimately reducing protein expression of the miRNA’s target gene [76,77].

miRNAs recognize their target mRNAs through complementary base-pairing [75]. In plants, and very rarely in mammals, complete complementarity between a miRNA and its target induces endonucleolytic mRNA cleavage by AGO, followed by rapid degradation of the mRNA [78]. In

mammals, miRNAs canonically recognize and inhibit their targets through partial base-pairing of only 6-8 nucleotides at the 5' end of the miRNA (nucleotides 2-8), the so-called seed region [75,79]. On the mRNA, these miRNA binding sites are most prominently located in their 3'UTR, but can also be located in the 5'UTR or coding sequence [77]. Partial base-pairing of a miRNA with its target mRNA typically inhibits gene expression by inducing the CCR4-NOT complex of RISC to deadenylate the mRNA's protective poly(A) tail, resulting in mRNA destabilization and ultimately decay [80]. In an alternative, less common process, partial miRNA:mRNA binding either blocks translation initiation via the CCR4-NOT complex or inhibits translation elongation through ribosome drop-off to repress translation of mRNA into protein [76].

The human genome encodes approximately 2,500 mature miRNAs, and it is overall estimated that more than 60% of protein-coding genes are under control of miRNA regulation [81–83]. A miRNA's influence on target gene inhibition can range from substantial repression of protein output to sensitive fine-tuning effects [84]. The degree of inhibition depends on many factors such as the cell-specific and context-specific expression levels of both the miRNA and its target mRNA, and the affinity of miRNA:mRNA interactions [77,84]. Furthermore, particular miRNAs can target hundreds of different mRNAs, and specific mRNAs can be recognized by multiple miRNAs [81]. In cases where individual miRNAs regulate multiple mRNAs of the same pathway, moderate individual miRNA:mRNA interactions can add up to a stronger response than each single interaction in isolation [85]. These complex networks of multiple miRNAs inhibiting multiple mRNAs to varying degrees depending on cell type and cell stage add an intricate additional layer of regulation to almost all biological processes studied to date [74,85].

1.4.2 MicroRNA Biogenesis

In the human genome, about half of all currently identified miRNA-encoding genes are intergenic, located in independent transcription units of single miRNAs or miRNA clusters regulated by their own promoters. The other half are intragenic, located in introns, and rarely in exons, of protein-coding genes, with which these miRNAs share their promoters [86,87].

Following the canonical pathway of miRNA biogenesis, miRNA-encoding genes are transcribed into primary miRNAs (pri-miRNAs) by RNA polymerase II or III (**Figure 1.3**) [72,77]. A typical pri-miRNA is about 1 kb long and contains a 33-35 bp double-stranded hairpin stem in which the mature miRNA sequences are embedded, a terminal loop, and two single-stranded flanking regions upstream and downstream of the hairpin [72,83]. Endonucleolytic cleavage of the pri-miRNA by the microprocessor complex initiates the miRNA maturation process and occurs either post- or co-transcriptionally in the

nucleus [77]. The microprocessor complex consists of the RNA binding protein DiGeorge syndrome critical region 8 (DGCR8) and the ribonuclease III (RNase III) Drosha [72]. The microprocessor cleaves the single-stranded flanking regions of the pri-miRNA, releasing a hairpin-shaped precursor miRNA (pre-miRNA) of 60-70 nucleotides in length [83].

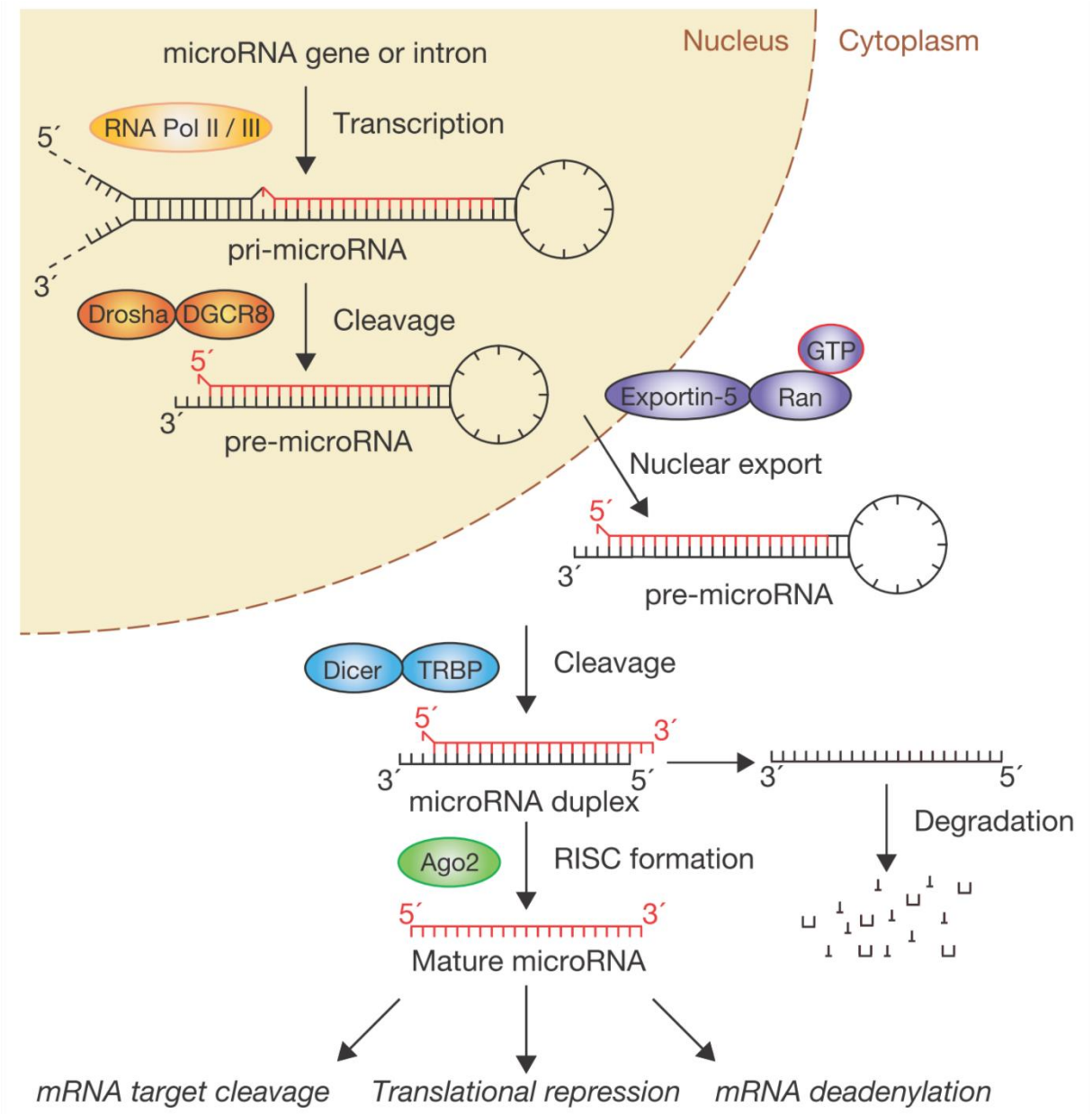

Figure 1.3 | The canonical miRNA biogenesis pathway. In mammals, miRNA genes are typically transcribed by RNA polymerase II or III into pri-miRNA transcripts. The pri-miRNAs fold into hairpins that are processed in the nucleus by the microprocessor complex comprised of the RNase III Drosha and its essential cofactor DGCR8. The resulting pre-miRNA hairpin is exported to the cytoplasm by Exportin-5 and further processed by the RNase III Dicer in complex with TRBP. Dicer cleaves the hairpin loop off the pre-miRNA, creating a miRNA/miRNA* duplex of mature miRNA length. During strand selection, the mature miRNA guide is loaded together with AGO into RISC, while the miRNA* passenger strand is degraded. The mature miRNA guides RISC to its target mRNAs for mRNA degradation through cleavage, for translational repression, or for mRNA destabilization through deadenylation. Figure reprinted from Winter *et al.* (2009) [72]. AGO – Argonaute, DGCR8 – DiGeorge syndrome critical region 8, pre-miRNA – precursor miRNA, pri-miRNA – primary miRNA, RISC – RNA-induced silencing complex, TRBP – TAR RNA-binding protein.

The pre-miRNA is exported from the nucleus by Exportin-5 and further processed in the cytoplasm by another RNase III, Dicer (**Figure 1.3**) [77]. Dicer cleavage removes the terminal loop from the pre-miRNA, producing a small, 21-23 bp miRNA/miRNA* duplex comprised of the mature miRNA guide and the miRNA* passenger strand [72]. Dicer interacts with TAR RNA-binding protein (TRBP), which modulates the processing efficiency of some pre-miRNAs and defines the length of the mature miRNA [83].

The miRNA/miRNA* duplex is then loaded into AGO (AGO1-4 in humans), which forms the effective core of RISC [77]. RISC quickly unwinds the duplex and releases the passenger strand to be degraded, retaining the mature miRNA strand to form the mature RISC [72,83]. Strand selection between mature miRNA and passenger strand depends on their thermodynamic stability, where the strand with the less stable 5' end is usually chosen as mature miRNA [88]. For many miRNAs, strand selection is further influenced by cell type and cellular environment, and ranges from predominant preference for one strand to near equal proportions [77]. Mature miRNAs incorporated into AGO ultimately guide RISC to their target mRNAs, where they inhibit gene expression either by mRNA degradation through cleavage, by mRNA destabilization through deadenylation, or by translational inhibition (**Figure 1.3**) [76].

1.4.3 Regulation of MicroRNA Expression

With their ability to target hundreds of mRNAs simultaneously, miRNAs themselves must be tightly and dynamically regulated. Final miRNA expression levels are controlled during all stages of biogenesis, transcriptionally and post-transcriptionally [83].

The transcription of miRNA-encoding genes is regulated similarly as the transcription of protein-coding genes [89]. Intragenic miRNAs typically share their promoters with their host gene, whereas intergenic miRNAs are regulated by their own promoters [83]. In a comprehensive approach to map the locations of miRNA promoters in the genome, de Rie *et al.* (2017) identified promoters for 1,357 human and 804 mouse miRNAs [90]. Accordingly, the knowledge about transcription factors controlling miRNA expression is constantly expanding. miRNA expression can be positively or negatively regulated by transcription factors, such as transactivation of the miR-34 cluster by p53 or suppression of the miR-200 cluster by zinc finger E-box binding homeobox 1 (ZEB1) and 2 (ZEB2) [83,91]. Expression of miRNA genes further depends on epigenetic factors that influence promoter accessibility such as histone modifications and DNA methylations [83].

Post-transcriptional regulation of miRNA expression can occur during miRNA processing by Drosha and Dicer, during RISC loading, and by controlling mature miRNA stability and accessibility [92–94]. Post-transcriptional modifications such as phosphorylation and ubiquitylation influence Drosha and

DGCR8, Dicer and TRBP as well as AGO of RISC [92]. MAPK signaling leads simultaneously to increased Drosha activity through heavy phosphorylation of its cofactor DGCR8 and to increased stability of the Dicer-TRBP complex through phosphorylation of TRBP [92]. Overall, the activation of the two main miRNA-processing enzymes generates a “pro-growth” miRNA profile with generally increased miRNA production upon MAPK signaling [92]. In addition, the MAPK p38 phosphorylates AGO2 at Ser387, which stabilizes RISC assembly and further promotes miRNA function [93]. In contrast, stress activates mTOR and leads to Drosha ubiquitylation by the E3 ubiquitin-protein ligase MDM2, inducing Drosha degradation by the proteasome and thus reducing overall miRNA processing [93]. Stress also induces EGFR to phosphorylate AGO2 at Tyr393, which inhibits RISC loading and reduces a specific subset of miRNAs [92]. Indeed, lower miRNA expression levels are often observed in cancer [72].

Additionally, many miRNAs are regulated by RNA editing during their biogenesis, where altering the miRNA sequence affects its stability or target specificity [93]. Primarily, miRNA length and sequence are defined by where Drosha and Dicer cleave the precursors [83]. Alternative miRNA cleavage can both modify the miRNA seed region and influence guide strand selection [93]. Furthermore, non-template nucleotide addition (NTA) influences the stability of specific miRNAs by addition of uridyl or adenyl to their 3’ end [93]. A prominent example of NTA-mediated miRNA inhibition is the regulation of the let-7 miRNA family by lin-28 homolog A (LIN28A) [92]. In the cytoplasm, LIN28A recognizes the pre-let-7 miRNA loop and recruits terminal uridyl transferase 4 (TUT4) or 7 (TUT7) to modify pre-let-7, which marks it for degradation and blocks its cleavage by Dicer [92]. Another NTA is the mono-adenylation of miR-122 by the poly(A) RNA polymerase GLD-2 that stabilizes miR-122 in the liver [91]. Besides by NTAs, pri-miRNA and pre-miRNA sequences can also be edited by deamination through adenosine deaminases acting on RNA (ADARs) [83]. ADARs convert adenosine (A) into inosine (I), which is read as guanosine during translation [93]. Such A-to-I editing of miRNAs inhibits Drosha and Dicer cleavage as well as AGO loading, reducing mature miRNA levels [72]. Sequence alterations in the miRNA seed region can even redirect miRNAs to new target mRNAs [93].

Finally, expression levels of mature miRNAs can be regulated by their removal through sequestration or active degradation [93,94]. Long non-coding RNAs (lncRNAs), pseudogenes, and even mRNAs can function as miRNA sponges, binding them and sequestering them away from their target mRNAs [93]. miRNAs can furthermore be transferred from the cytoplasm to the nucleus or to extracellular vesicles, locally separating them from their site of activity [93]. Although miRNAs are considered highly stable molecules, rapid and active miRNA degradation by nucleases nevertheless allows effective reduction of miRNA levels [94]. Several nucleases have been described in the degradation of individual miRNAs, but little is known about their substrate specificity [94].

These mechanisms of regulating mature miRNA expression levels can be performed in different combinations, can be omitted or replaced, and often affect individual miRNAs differently [72]. This complexity of miRNA processing and regulation provides multiple opportunities for the fine-tuning of miRNA function but also for the dysregulation of miRNA processes during disease [72].

1.5 Dysregulated MicroRNAs in Liver Fibrosis and HCC

Dysregulated miRNA expression is frequently observed in disease, and global reduction of mature miRNAs is an emerging feature of cancer [72]. In the liver, miRNA dysregulation is not only observed during HCC, but also during the earlier stages of chronic liver disease caused by HBV/HCV infection, ALD, NAFLD, or NASH [74]. Hepatic miRNAs are known to regulate various biological processes involved in fibrogenesis such as lipid metabolism, apoptosis, cell proliferation, inflammation, and ECM accumulation [74]. Depending on their target genes, miRNAs can be either pro-fibrotic or anti-fibrotic to either support or inhibit chronic liver disease and HCC development [73,95].

Pro-fibrotic miRNAs frequently overexpressed in fibrosis and HCC include miR-21, miR-27, miR-33a, miR-155, miR-221, miR-222 as well as the miR-199 and miR-200 families [95–97]. In HSCs, miR-21 contributes to HSC activation by downregulating SMAD7, a negative regulator of TGF-β signaling, while members of the miR-199 and miR-200 families enhance fibrotic ECM production [98,99]. Furthermore, miR-221 is commonly upregulated in hepatocytes, where it targets tumor suppressors such as p57 and PTEN, ultimately facilitating hepatocyte proliferation and HCC development [73].

In contrast, anti-fibrotic miRNAs such as miR-29, miR-122, miR-133, miR-150, miR-192, and let-7 are frequently downregulated in fibrosis and HCC [9,73,74]. Without the liver-specific miR-122 regulating multiple genes of the hepatic lipid metabolism, miR-122-deficient mice develop steatohepatitis and fibrosis [74]. Furthermore, decreased miR-29 expression is associated with fibrosis in multiple organs including heart, kidney, and skin besides the liver [95]. In inactive HSCs, miR-29 inhibits the production of collagens, integrins, and other ECM components, and directly targets PDGF to maintain low HSC proliferation [100]. Also let-7 maintains a normal ECM by downregulating COL1A1 expression [101]. As tumor suppressors of HCC, let-7 inhibits the oncogene RAS, while miR-29 induces hepatocyte apoptosis through inhibition of the anti-apoptotic proteins BCL2 and MCL1 [73].

Although many studies have elucidated the roles of individual miRNAs in fibrosis and HCC by identifying individual miRNA:target mRNA interactions, they often neglect the complexity of miRNA signaling networks [85]. Due to the intricacy of miRNA expression, the redundancy of miRNA targeting, and their cell-specific and time-specific expression patterns, elucidating the detailed mechanisms of miRNA function during liver disease remains a challenging task and central focus of current research [73,102].

1.6 Aims

Chronic liver disease, progressing from fibrosis to cirrhosis and HCC, poses a major threat to human health [1]. Liver fibrosis is characterized by the activation of HSCs and their excessive production of ECM components [7]. This tissue scarring interferes with normal liver function and generates a fibrotic microenvironment that facilitates HCC development [3]. Despite the frequent occurrence and serious consequences of liver fibrosis and HCC, reliable treatment options remain limited [22].

miRNAs provide a complex regulatory layer to gene expression in almost all biological processes, and their dysregulation contributes to various human diseases, including fibrosis and HCC [73,74]. While their functions during liver disease have been described for various individual miRNAs, few studies focus on miRNAs as integral parts of signaling networks [85]. In such networks, miRNAs typically target multiple, functionally connected genes of related pathways [81]. Such miRNA hubs often explain and influence network behavior, making them potential drug targets or predictors of disease outcome [85].

This study, divided into three projects, aims to identify and characterize a signaling network of functionally connected miRNAs and target genes that contributes to fibrosis and HCC. **Project A** presents our publication "Identification of Pparγ-modulated miRNA hubs that target the fibrotic tumor microenvironment" by Winkler *et al.* (2020) [103]. Here, the *SRF-VP16*^{iHep} mouse model of fibrotic HCC was analyzed by global miRNA and transcriptome profiling, leading to the identification of the anti-fibrotic (AF-) miRNA network. It is comprised of 8 miRNAs and 54 ECM-related target genes involved in the formation of the fibrotic tumor microenvironment. We show that the AF-miRNA network is dysregulated in activated hepatic stellate cells (HSCs) during fibrogenesis and that it is regulated by the transcription factor peroxisome proliferator-activated receptor gamma (PPARG) [103]. **Project B** aims to further expand our understanding of the AF-miRNA network during fibrogenesis as a complex disease with different etiologies. For this, I compare the expression patterns of the AF-miRNA network between different fibrotic stages, experimental models of fibrosis, and model organisms. **Project C** aims to modulate the PPARG-regulated AF-miRNA network to inhibit liver fibrogenesis. For this, I investigate *in vivo* and *in vitro* whether PPARG agonists can collectively increase AF-miRNA expression and whether this reduces fibrotic processes.

Overall, this study aims to thoroughly characterize the PPARG-regulated AF-miRNA network during liver fibrosis and HCC. Using this AF-miRNA network as example, I aim to broaden our scientific knowledge about the intricate interplay between miRNAs, target genes, and transcription factors within complex signaling networks. Furthermore, elucidating the contribution of the AF-miRNAs to the progression of chronic liver disease from fibrosis to HCC may facilitate the identification of new potential therapeutic targets or predictors of disease outcome in the future.

2 Materials and Methods

This material and methods section lists and describes all the procedures performed for **Project B** and **Project C**. The materials and methods used in **Project A** are part of the presented publication by Winkler *et al.* (2020) and are described in detail within the publication and its supporting information available at https://doi.org/10.1073/pnas.1909145117 [103].

2.1 Materials

2.1.1 Animals and Animal Models

Wildtype C57BL/6J Mice

Adult male C57BL/6J mice were purchased from Charles River at the age of 7 weeks.

The *SRF-VP16^{iHep}* Mouse Model

The *SRF-VP16^{iHep}* mouse model was developed by Dr. Stefan Ohrnberger in the group of Prof. Dr. Alfred Nordheim (Department for Molecular Biology, Interfaculty Institute of Cell Biology (IFIZ), University Tübingen, Germany) by cross-breeding the following three transgenic mouse lines (**Table 2.1**) [104].

Table 2.1 | List of mouse lines used to generate *SRF-VP16^{iHep}* mice, their official symbols, and their source.

Mouse Line	Symbol	Information	Source
C57BL/6N	*Genetic wildtype background of all three mouse lines (Charles River)*		
Srf-flex1	Srf$^{tm2.1Nor}$	Floxed *Srf* exon 1	Alfred Nordheim [105]
Alfp-CreER^{T2}	B6.FBV-Tg(Alb-cre/ERT2)Gsc	Hepatocyte-specific CreER^{T2} line	Alfred Nordheim [104]
Stop-floxed SRF-VP16	*Gt(ROSA)26-Sor$^{tm1(SRF-VP16)Antu}$*	Cre-driven SRF-VP16 expressing line	Alfred Nordheim [106]

Stop-floxed SRF-VP16 mice were bred with *Srf-flex1* and *Alfp-CreER^{T2}* mice to generate triple-transgenic *SRF-VP16^{iHep}* (*Srf$^{flex1/wt}$::SRF-VP16$^{+/-}$::Alf-CreER$^{T2+/-}$*) animals with conditional, hepatocyte-specific expression of SRF-VP16 in the absence of functional endogenous serum response factor (SRF) [104]. Tamoxifen-treatment of *SRF-VP16^{iHep}* animals induces Cre-mediated ablation of endogenous SRF and expression of SRF-VP16 in hepatocytes [104,105]. The fusion protein SRF-VP16 is a constitutively active form of SRF, which is comprised of the first 412 residues of human SRF fused to the transcriptional activation domain of the *Herpes simplex* viral protein VP16 [104]. Expression of

SRF-VP16 in hepatocytes enables constitutive activation of SRF target genes independent of upstream stimulation through Rho/actin and Ras/MAPK signaling and results in hepatocyte hyperproliferation [107]. However, spontaneous stochastic Cre activity in the absence of tamoxifen was also observed in some animals and leads to mosaic SRF-VP16 expression in a small number of hepatocytes [104]. Hyperproliferation of affected hepatocytes leads to the formation of premalignant nodules throughout the liver, which gradually progress to fibrotic HCC.

The experimental procedures complied with the guidelines for animal care and were approved by the Regierungspräsidium Tübingen under permit number IM1/14. The HCC tissue samples used in this study are derived from *SRF-VP16*^{iHep} mice with spontaneous Cre activation, while control liver tissue was collected from litter mates that either lack the Cre recombinase or the SRF-VP16 transgene.

Tissue samples (n=4/group) were isolated by Dr. Abhishek Thavamani, while RNA isolation and RNA-seq were performed and the data analyzed by Dr. Ivana Winkler (both from the Department for Molecular Biology, IFIZ, University Tübingen, Germany) as part of Winkler *et al.* (2020) (**Project A**) [103]. The AF-miRNA network was further investigated in the available samples and data, and miRNA and gene expression levels were compared to additional animal models.

The Carbon Tetrachloride Model

The carbon tetrachloride (CCl_4) model serves as experimental *in vivo* model for pericentral liver fibrosis in rodents [108]. The animal experiments were performed as part of Ghallab *et al.* (2019) and complied with the guidelines for animal care approved by the German Animal Care Committee (LANUV, Recklinghausen, Germany) under permit number 84-02.04.2017.A177 [109]. Briefly, adult male C57BL/6N mice (n=6/group) received CCl_4 (1 mg/kg body weight) diluted in olive oil by repeated intraperitoneal injection twice a week for 2 months and 12 months. The control groups were injected with olive oil alone at the same dosage over the same time period. Six days after the last CCl_4 or oil injection, mice were anaesthetized, livers were perfused, and liver specimens from the left liver lobe were collected for RNA isolation. Liver tissue RNA samples isolated by QIAzol (Qiagen) were kindly provided along with the raw RNA-seq data initially published in Ghallab *et al.* (2019) [109]. The AF-miRNA network was investigated in the available samples and data, and miRNA and gene expression levels were compared to further animal models.

The Bile Duct Ligation Model

The bile duct ligation (BDL) model serves as an experimental *in vivo* model for cholestasis and portal liver fibrosis in rodents [45,110]. For this study, samples from two separate BDL experiments were

kindly provided by Prof. Dr. Ralf Weiskirchen (Experimental Gene Therapy and Clinical Chemistry, Institute of Molecular Pathobiochemistry, University Hospital RWTH Aachen, Germany) and Prof. Dr. Sebastian Mueller (Center for Alcohol Research, University of Heidelberg and Salem Medical Center, Heidelberg, Germany).

Mouse BDL model for 2 weeks (Prof. Dr. Ralf Weiskirchen): The experimental protocol complied with the guidelines for animal care approved by the German Animal Care Committee (LANUV, Recklinghausen, Germany) under permit number Az. 84-02.04.2012.A092. BDL was performed on adult male C57BL/6J mice (n=5/group) according to the method of Tag *et al.* (2015) [110]. Control mice were sham-operated. Liver specimens were collected 2 weeks post operation, and liver tissue RNA samples isolated by QIAzol (Qiagen) were kindly provided.

Rat BDL model for 4 weeks (Prof. Dr. Sebastian Mueller): The animal experiments were performed by Teresa Peccerella and complied with the guidelines for animal care approved by the German Animal Care Committee (Regierungspräsidium Karlsruhe, Germany) under permit number 35-9185.81/G-236/11. Adult male Wistar rats were subjected to BDL following standard procedures (n=7), while control rats were sham-operated (n=6) [111]. Liver specimens and blood samples were collected 4 weeks post operation. Snap-frozen liver tissue samples (n=4/group) for RNA analyses and the collected metadata (the blood serum markers ALT, AST, AP, GGT, bilirubin, and albumin as well as qPCR data of relative *Tgfb1* mRNA expression normalized to *Gapdh*, *Hprt*, and *B2m*) of sham (n=6) and BDL (n=7) animals were kindly provided by Prof. Dr. Sebastian Mueller.

The Thioacetamide Model

The thioacetamide (TAA) model provides an experimental *in vivo* model of combined pericentral and periportal liver fibrosis in rodents [112]. The animal experiments were performed by Teresa Peccerella and complied with the guidelines for animal care approved by the German Animal Care Committee (Regierungspräsidium Karlsruhe, Germany) under permit number 35-9185.81/G-236/11. Adult male Wistar rats received TAA (200 mg/kg body weight) diluted in physiological saline solution by repeated intraperitoneal injection twice a week for 4 weeks (n=6) and 10 weeks (n=5) based on standard procedures [113]. Control animals received physiological saline solution alone at the same dosage over the same time courses (n=6 each). Liver specimens and blood samples were collected after 4 weeks or 10 weeks of treatment. Snap-frozen liver samples (n=4/group) for RNA analyses and the collected metadata (the blood serum markers ALT, AST, AP, GGT, bilirubin, and albumin as well as qPCR data of relative *Tgfb1* mRNA expression normalized to *Gapdh*, *Hprt*, and *B2m*) of animals treated with 4 weeks NaCl (n=6), 4 weeks TAA (n=6), 10 weeks NaCl (n=6), and 10 weeks TAA (n=5) were kindly provided by Prof. Dr. Sebastian Mueller.

2.1.2 Cell Lines and Primary Cells

The Hepa1-6 Cell Line

The immortalized hepatoma cell line is derived from the BW7756 tumor carried in C57L/J mice and represents a transformed hepatocyte-derived cell line. The cells secrete several typical liver products including albumin, alpha-fetoprotein, alpha-1-antitrypsin, and amylase [114].

The Col-GFP Cell Line

Col-GFP cells represent immortalized activated HSCs. The cell line is derived from Col-GFP mice expressing green fluorescent protein (GFP) under control of the *Col1a1* promoter/enhancer. These mice were treated with CCl_4 for eight weeks, and the induced HSC activation was reflected in the GFP expression driven by *Col1a1* promoter activity [115]. Activated primary HSCs (pHSCs) were isolated from perfused livers using Nycodenz gradient centrifugation and were cultured as described previously [116]. pHSCs were immortalized by infection with a lentiviral vector construct expressing SV40-large T antigen and hygromycin resistance gene. Individual cell clones were selected by hygromycin-containing media [115]. The Col-GFP cell line was kindly provided by Prof. Dr. Ralf Weiskirchen.

The GRX Cell Line

The continuous GRX cell line is derived from HSCs isolated from fibrotic liver granulomas [117]. As activated HSCs, they display morphologic characteristics of myofibroblasts [7,117]. The GRX cell line was obtained from the Rio de Janeiro Cell Bank (PABCAM, Federal University, Rio de Janeiro, Brazil).

The GRX-Pparg Cell Line

The GRX-Pparg cell line stably overexpresses mouse *Pparg1* and was generated as part of Winkler *et al.* (2020) from GRX cells (**Project A**) [103]. GRX cells were transfected with a modified version of vector pSV-Sport Ppar gamma 1 (Addgene, plasmid #8886) [118], with the neomycine resistance gene inserted into the vector backbone [103]. Cells were maintained in selection medium (700 µg/ml G418) for three weeks to ensure the survival of only stably transfected cells. The resulting polyclonal cell line was defined as GRX-Pparg cell line.

Primary HSCs

Isolation of primary HSCs (pHSCs) was performed at the University Hospital RWTH (Aachen) in collaboration with Prof. Dr. Ralf Weiskirchen. The experimental procedures complied with the guidelines for animal care approved by the German Animal Care Committee (LANUV, Recklinghausen, Germany) under permit number 84.02.04.2015.A028. Murine pHSCs were isolated from C57BL/6J mice essentially according to Weiskirchen *et al.* (2017) [116]. Briefly, the livers of healthy adult mice were perfused with pronase-collagenase solutions through the portal vein. The cells of the enzymatically digested liver were dispersed and subsequently filtered through a nylon mesh. Enrichment of pHSCs was achieved by centrifugation through a Nycodenz density gradient. pHSCs of four animals were pooled and counted on a Neubauer chamber. pHSCs were either immediately collected in TRIzol (inactive pHSCs) or seeded on standard plastic dishes in culture medium (DMEM supplemented with 10% FCS, 100 IU/ml penicillin, 10 µg/ml streptomycin, and 4 mM glutamine) to progress to activated pHSCs. Isolated pHSCs were kindly provided by Prof. Dr. Ralf Weiskirchen.

2.1.3 Vectors

Table 2.2 | List of vectors for luciferase assays with description and source.

Vector	Description	Source
pGL3-$(TSm)_2$-tk120-Fluc	Fluc expression under control of TCF/SRF and tk120 promoters	Dr. Bilge Ergin, Nordheim group (**Supplementary Figure 1**) [119]
pGL3-consPPRE-tk120-Fluc	Fluc expression under control of consensus PPRE and tk120 promoters	Cloned as part of **Project C** (**Supplementary Figure 2**)
pGL3-29cPPRE-tk120-Fluc	Fluc expression under control of miR-29c PPRE and tk120 promoters	Cloned as part of **Project C** (**Supplementary Figure 3**)
pRL-TK	Basal *Renilla* luciferase expression under control of tk120 promoter	Promega (E2241)

2.1.4 Oligonucleotides

Table 2.3 | List of oligonucleotides for molecular cloning. All oligonucleotides were obtained from Sigma-Aldrich.

Primer Name	Sequence (5'-3')
consensus-PPRE-F	CGCACGTAGGGCAAAGGTCACAGAGGGAGAGAGAGGTAGGGCAAAGGTCAGAG AGCCGCGGACAGGTAGGGCAAAGGTCAACTCTGTACTAGCACGTAGGGCAAAGG TCACCCCA
consensus-PPRE-R	TCGATGGGGTGACCTTTGCCCTACGTGCTAGTACAGAGTTGACCTTTGCCCTACCT GTCCGCGGCTCTCTGACCTTTGCCCTACCTCTCTCTCCCTCTGTGACCTTTGCCCTAC GTGCGAGCT
miR29c-PPRE-F	CGCACTGCCCTCTGCCTCTCCAGAGGGAGAGAGAGGAGGGGGAGAGGGGAGAG AGCCGCGGACAGTGCACTCTGGCCTTCACTCTGTACTAGCACTGCCCTCTCCCCCC TCCCCA
miR29c-PPRE-R	TCGATGGGGAGGGGGGAGAGGGCAGTGCTAGTACAGAGTGAAGGCCAGAGTGC ACTGTCCGCGGCTCTCTCCCCTCTCCCCCTCCTCTCTCTCCCTCTGGAGAGGCAGAG GGCAGTGCGAGCT

2.1.5 Primers

Table 2.4 | List of primers for gene expression analyses by qPCR. All primers were obtained from Sigma-Aldrich.

Primer Name	Sequence (5'-3')	Target	Organism
Acta2_F	GAGCGTGAGATTGTCCGTG	Acta2	Mouse
Acta2_R	TAGGTGGTTTCGTGGATGCC		
Col1a1-f	GATGCTAACGTGGTTCGTGA	Col1a1	Mouse
Col1a1-r	TGAGTAGGGAACACACAGGT		
Col1a2_1f	TCAAAGGCGTGAAAGGACAC	Col1a2	Mouse
Col1a2_1r	AGTTCCATTCTCTCCAGGGG		
Col4a2_1f	GAGTGCGGTTCAAAGCGTC	Col4a2	Mouse
Col4a2_1r	CATCCAACTTCTTCACACCCC		
Col4a5_1f	CAGGTATCAAAGGGTCGGTG	Col4a5	Mouse
Col4a5_1r	TCTTGACCTGGCTTGCCTTT		
Col5a2_1f	GGCAAAGATGGAGAAGTTGGT	Col5a2	Mouse
Col5a2_1r	CCCAGGCAGTCCAGTTATCC		
Gapdh-f	TGGATCTGACGTGCCGC	Gapdh	Mouse, rat
Gapdh-r	ATGCCTGCTTCACCACCTTC		
Gusb-f	GATGCTGTTCCCGAAGGAGAG	Gusb	Mouse
Gusb-r	ATTGCTTCCCGTTCATACCACA		
Lamc1_f	GCCTTCCTGACCGACTACAA	Lamc1	Mouse
Lamc1_r	TCCCGAGTGCGCTTATAGAT		
Loxl2_F	GCGTGGAGGTCTACTACGAA	Loxl2	Mouse
Loxl2_R	CCAACGTCTTCAGTGTGCTT		
Loxl4_F	GCCAAAGAAGTGGTGATGAGT	Loxl4	Mouse
Loxl4_R	ACGATCCTCCAAGTACGCC		

Table 2.4 (continued) | List of primers for gene expression analyses by qPCR. All primers were obtained from Sigma-Aldrich.

Primer Name	Sequence (5'-3')	Target	Organism
Pdgfb_f	GATCTCTCGGAACCTCATCG	Pdgfb	Mouse
Pdgfb_r	GGGCTTCTTTCGCACAATCT		
Plin2_ex_f	GGGCTAGACAGGATGGAGGAA	Plin2	Mouse
Plin2_ex_r	CACTGCTCCTTTGGTCTTATCC		
Pparg_f	TAAAGTCCTTCCCGCTGACC	Pparg	Mouse
Pparg_r	CGGCTTCTACGGATCGAAAC		
rno_Acta2_F1	TCCAGCTATGTGTGAAGAGGAA	Acta2	Rat
rno_Acta2_R1	AGTTGGTGATGATGCCGTGT		
rno_Col1a1_F1	CCTGGCAAGAACGGAGATGA	Col1a1	Rat
rno_Col1a1_R1	GCACCATCCAAACCACTGAA		
rno_Col5a2_F1	AGAGTGCCAAGAAGTGCTCAA	Col5a2	Rat
rno_Col5a2_R1	CGACCACGTATGCCCGTTA		
rno_Egr1_F1	CCTGACCACAGAGTCCTTTTC	Egr1	Rat
rno_Egr1_R1	GAGAAGCGGCCAGTATAGGT		
rno_Gusb-F1	TTCATTGGCTGGGTGTGGTA	Gusb	Rat
rno_Gusb-R1	ATCCCATTCACCCACACAACT		
rno_Lamc1_F1	TCAACCGGACCATAGCTGAA	Lamc1	Rat
rno_Lamc1_R1	CAGGTCTGTCACTTCCGAGA		
rno_Loxl2_F1	GAGTGAAGTGCTCAGGAACG	Loxl2	Rat
rno_Loxl2_R1	TCTCGGCGTTAAGTACCAGG		
rno_Pdgfb_F1	GAGACAGTAGTGACCCCTCG	Pdgfb	Rat
rno_Pdgfb_R1	ACTTTCGGTGCTTCCCTTTG		
rno_Plin2_F1	TAGACCAGTACTTGCCGCTC	Plin2	Rat
rno_Plin2_R1	ACATTCTTCCTGGCGAATTCAA		
rno_Pparg_F1	AGCCCTTTGGTGACTTTATGG	Pparg	Rat
rno_Pparg_R1	CAGCAGGTTGTCTTGGATGT		
TBP_F	TTCATGGTGTGTGAAGATAACCC	Tbp	Mouse
TBP_R	AGAGAGACTGTTGGTGTTCTGA		
Tgfb1_ex_f	GCAACAATTCCTGGCGTTAC	Tgfb1	Mouse
Tgfb1_ex_r	GCTGATCCCGTTGATTTCCA		
Tgfbr1_f	CATTTCAGAGGGCACCACCT	Tgfbr1	Mouse, rat
Tgfbr1_r	CAAACTTCTCCAAACCGACCT		
Tpm1_f	TCAAGGTTCTCTCTGACAAGC	Tpm1	Mouse, rat
Tpm1_r	TTGGTTACTGATCTCTCTGCAA		

Table 2.5 | List of primers for miRNA expression analyses by qPCR. All primers were obtained from Sigma-Aldrich.

Primer Name	Sequence (5'-3')	Target	Organism
29c-f	AGCACCATTTGAAATCGGTTAAA	miR-29c-3p (mature)	Mouse, rat
30d-f	TGTAAACATCCCCGACTGGAA	miR-30d-5p (mature)	Mouse, rat
30e-f	TGTAAACATCCTTGACTGGAAGA	miR-30e-5p (mature)	Mouse, rat
335-f	TTTTTCATTATTGCTCCTGACCA	miR-335-3p (mature)	Mouse, rat
338-f	TCCAGCATCAGTGATTTTGTTG	miR-338-3p (mature)	Mouse, rat
let-7a-f	TGAGGTAGTAGGTTGTATAGTTA	let-7a-5p (mature)	Mouse, rat
let-7c-f	TGAGGTAGTAGGTTGTATGGTT	let-7c-5p (mature)	Mouse, rat
let-7g-f	TGAGGTAGTAGTTTGTACAGTT	let-7g-5p (mature)	Mouse, rat
miScript Universal Primer (Qiagen)	Property of Qiagen	Pairs with all small RNA forward primers	
rno-5S-F	TCGTCTGATCTCGGAAGCTA	ribosomal 5S (K01594)	Rat
rno-U87-F	TTTTGCCGTTTACCCAGC	U87 snoRNA (AF272707)	Rat
Rnu6-f	CTTCGGCAGCACATATACTAAA	U6 small nuclear RNA	Mouse
Snord33-f	AGACATCTCCCACTCATGTTC	Snord33	Mouse
Snord35a-f	TGATGTTCTTATTCTCACGATGGTC	Snord35a	Mouse

2.1.6 Reagents

Table 2.6 | List of chemicals, enzymes, and reagents, their manufacturer, and method in which they were used.

Reagent	Manufacturer	Method
1-butanol	Sigma-Aldrich	RNA processing
15-Deoxy-$\Delta^{12,14}$-prostaglandin J2 (PGJ2)	Sigma-Aldrich	Cell treatment
Acetic acid	Sigma-Aldrich	Gel electrophoresis, tissue staining
ACTA2 antibody (ab5694)	Abcam	Tissue staining
AEC Single Solution	Zytomed Systems	Tissue staining
Agar bacteriology grade	AppliChem	Cloning
Agarose LE, DNA grade	Genaxxon	Gel electrophoresis
Carbenicillin, 50mg/ml	AppliChem	Cloning
Carbon tetrachloride (CCl_4)	Merck	Mouse treatment
Carboxymethyl cellulose sodium salt (CMC)	Roth	Mouse treatment
Chloroform	Sigma-Aldrich	RNA isolation
Citrate buffer, pH 6	Dako	Tissue staining
Competent *E. coli* JM109	Promega	Cloning
Corn oil	Roth	Mouse treatment
CutSmart buffer, 10X	NEB	Cloning
DharmaFECT1 Transfection Reagent	Horizon Discovery	Cell transfection
Diethyl ether	Sigma-Aldrich	RNA processing
Dimethyl sulfoxide (DMSO)	AppliChem	Cell cultivation, cell treatment

Table 2.6 (continued) | List of chemicals, enzymes, and reagents, their manufacturer, and method in which they were used.

Reagent	Manufacturer	Method
DNA Loading Dye (6x)	NEB	Gel electrophoresis
Dulbecco's Modified Eagle Medium (DMEM)	Gibco	Cell cultivation
Entellan Neu, mounting medium	Merck Millipore	Tissue staining
Ethanol, 99.9%	Sigma-Aldrich	RNA isolation
Ethanol, denatured	University Tübingen	Tissue staining
Ethidium bromide	AppliChem	Gel electrophoresis
Ethylenediaminetetraacetic acid (EDTA)	AppliChem	Gel electrophoresis
FastStart Universal SYBR Green Master Mix	Roche	qPCR
Fetal calf serum (FCS)	Gibco	Cell cultivation
G418, 100 mg/ml	Invivogen	Cell cultivation
GeneRuler 1kb DNA ladder	Thermo Fisher Scientific	Gel electrophoresis
Glycerol	AppliChem	Cloning
Glycogen, RNase-free, 20 µg/µl	Thermo Fisher Scientific	RNA isolation
Isopropanol	Sigma-Aldrich	RNA isolation, tissue fixation
L-glutamine, 200 mM	Gibco	Cell cultivation
LigFast Buffer, 2x	Promega	Cloning
Midori Green	Nippon Genetics	Gel electrophoresis
MilliQ water (H_2O)	Merck Millipore	General
Opti-MEM I Reduced-Serum Medium	Gibco	Cell transfection
Paraplast paraffin wax	Leica	Tissue fixation
Penicillin-streptomycin, 5,000 U/ml	Gibco	Cell cultivation
Phosphate buffered saline (PBS)	Sigma-Aldrich	Cell cultivation
Picric acid	Sigma-Aldrich	Tissue staining
Pioglitazone-hydrochloride	Sigma-Aldrich	Mouse treatment, cell treatment
Polyview Plus anti-rabbit HRP (ENZ-ACC103)	Enzo	Tissue staining
QuantiTect SYBR Green PCR Master Mix	Qiagen	qPCR
RNA Gel Loading Dye (2x)	Thermo Fisher Scientific	Gel electrophoresis
RNase-free water	Thermo Fisher Scientific	RNA processing
Roti-Histofix, 4%	Roth	Tissue fixation
Roti-Histol	Roth	Tissue staining
SacI-HF	NEB	Cloning
SacII	NEB	Cloning
Sirius Red (Direct Red 80)	Sigma-Aldrich	Tissue staining
SOC medium	Promega	Cloning
T4 DNA Ligase	Promega	Cloning
Trizma base (Tris)	Sigma-Aldrich	Gel electrophoresis
TRIzol Reagent	Invitrogen	RNA isolation
Trypan Blue, 0.4%	Sigma-Aldrich	Cell cultivation

Table 2.6 (continued) | List of chemicals, enzymes, and reagents, their manufacturer, and method in which they were used.

Reagent	Manufacturer	Method
Trypsin-EDTA, 0.05%	Gibco	Cell cultivation
Tryptone	AppliChem	Cloning
XhoI	NEB	Cloning
Yeast extract	AppliChem	Cloning

2.1.7 Commercial Kits

Table 2.7 | List of commercial kits, their manufacturer, and method in which they were used.

Kit	Manufacturer	Method
DNA-free DNA Removal Kit	Invitrogen	RNA processing
Dual Luciferase® Reporter Assay System	Promega	Luciferase assay
EndoFree Plasmid Maxi Kit	Qiagen	Cloning
InnuPREP Plasmid Mini Kit 2.0	Analytik Jena	Cloning
miScript II RT Kit	Qiagen	RNA processing
PureLink Quick Gel Extraction Kit	Invitrogen	Cloning
Qubit dsDNA BR Assay Kit	Invitrogen	RNA processing
Qubit RNA BR Assay Kit	Invitrogen	RNA processing

2.1.8 Laboratory Equipment

Table 2.8 | List of used laboratory devices.

Device	Manufacturer
Aperio AT2 Scanner, digital slide scanner	Leica
AutoStainer XL, automated staining station	Leica
Biometra TRIO, thermocycler	Analytik Jena
E.A.S.Y. Doc Plus, gel documentation system	Herolab
edge® digital pH Meter	Hanna Instruments
EVOS FLoid Cell Imaging Station	Invitrogen
FLUOstar OPTIMA FL, microplate reader	BMG LABTECH
Heraeus Megafuge 16R, centrifuge	Thermo Fisher Scientific
NanoDrop 1000, spectrophotometer	PeqLab
QuantStudio 7 Flex Real-Time PCR System	Applied Biosystems
Qubit 3.0, fluorometer	Invitrogen
RM2155, rotary microtome	Leica
Shandon Citadel 1000, tissue processor	Thermo Fisher Scientific
Shandon Histocentre 2, tissue embedding center	Thermo Fisher Scientific

2.1.9 Software

Table 2.9 | List of used software, its version, and source.

Software	Version	Source
Aperio ImageScope	v12.3.3.5048	Leica
Aperio ScanScope Console	10.2.0.4.6.	Leica
E.A.S.Y. Win	3.2	Herolab
ImageJ Fiji	v1.53b	Schindelin *et al.* (2012) [120]
Inkscape	0.92.4	www.inkscape.org
Lasergene	15.3.0.66	DNASTAR
LinRegPCR	2018.0	Ruijter *et al.* (2009) [121]
MARS Data Analysis Software	v1.20	BMG LABTECH
Microsoft Office	2016	Microsoft
OPTIMA software	v2.20	BMG LABTECH
Prism 8	8.0.2	GraphPad
QuantStudio Real-Time PCR Software	1.3	Applied Biosystems
R package circlize	0.4.12	Gu *et al.* (2014) [122]
R package DESeq2	1.22.2	Love *et al.* (2014) [123]
R package ggplot2	3.3.3	Wickham (2016) [124]
R package pheatmap	1.0.12	Kolde (2019) [125]
R package RColorBrewer	1.1.2	Neuwirth (2014) [126]
R program	4.0.3	www.R-project.org [127]
R Studio	1.1.419	R Studio Team [128]
SnapGene Viewer	v5.2	GSL Biotech

2.2 Methods

2.2.1 Mouse Techniques

Animal Housing

Mice were kept in the animal facilities of the Interfaculty Institute for Cell Biology (IFIZ) at the University Tübingen according to the national guidelines for animal housing GV-SOLAS. Mice were kept under 12 h day/night cycle at 21 °C and 50% relative humidity with unlimited access to dried food pellets and water. Male mice were held in individual cages.

Pioglitazone Treatment of CCl_4-induced Liver Fibrosis in Mice

The animal procedures complied with the guidelines for animal care and were approved by the Regierungspräsidium Tübingen (IZ01/19G). All invasive animal work (injections, blood sample collection, termination of animals) was performed by Dr. Siegfried Alberti and Dr. Michael Orlich (group of Prof. Dr. Alfred Nordheim, Department for Molecular Biology, IFIZ, University Tübingen, Germany).

Adult male C57BL/6J mice were randomly divided into three groups (oil control, CCl_4, and CCl_4+Pio) of 15 animals each. All mice were acclimatized to voluntary oral feeding for eight days (Day -8 to Day 0) before the start of the experiment (**Figure 5.1**). During this phase, all mice received 100 µl honey-CMC (pioglitazone vehicle suspension of honey diluted 1:1 (v/v) with 1% carboxymethyl cellulose sodium salt (CMC) in water) daily by voluntary feeding [129]. For feeding, mice were placed on the cage lid and the suspension was presented from a single-use syringe with a ball-tipped gastric feeding needle until each mouse consumed 100 µl suspension. Feeding was always performed before any other experimental mouse handling. Starting Day 1, mice of the CCl_4 and CCl_4+Pio groups were intraperitoneally injected with CCl_4 (Merck, 0.6 ml/kg body weight) diluted in corn oil twice a week for 4 weeks (Day 1 to Day 28) following standard experimental procedures [130]. Animals of the oil control group received corn oil alone at the same dosage over the same time period. Mice of the CCl_4+Pio group additionally received pioglitazone (30 mg/kg body weight) emulsified in 100 µl honey-CMC daily by voluntary oral feeding, while mice of the oil control and CCl_4 groups were continued to be fed daily with 100 µl of the honey-CMC vehicle.

Before (Day 0) and during the experiment (Days 7, 14, 21), 100 µl blood was collected from n=5 mice/group from the lateral tail vein for analysis of liver function by blood serum markers. At Day 29, mice were sacrificed by carbon dioxide exposure followed by cervical dislocation. The body weight of each mouse was determined, blood was immediately collected by cardiac puncture, and liver tissue specimens were collected for later analyses.

Measurement of Liver Function by the Blood Serum Markers ALT, AST, AP, and Bilirubin

Blood collected from mice was transferred to standard reaction tubes and was allowed to clot at room temperature for 30 min or over night at 4 °C. The samples were centrifuged at 1,500 x g for 15 min at 4 °C to separate the blood serum from the clot. The supernatant serum was transferred to a fresh reaction tube and stored at -80 °C until used for analyses. The enzymatic activity of ALT, AST, and AP as well as the concentration of bilirubin were measured from blood serum samples after 1:10 dilution in PBS. Measurements were performed at the Central Laboratory Facility at the University Hospital RWTH (Aachen) in collaboration with Prof. Dr. Ralf Weiskirchen. Data visualization and statistical analysis were performed with GraphPad Prism 8. Values were compared using one-way ANOVA with Tukey-adjusted post-hoc test and differences were considered statistically significant for p_{adj}-values ≤ 0.05.

Liver Tissue Sample Collection

The whole liver was dissected from sacrificed mice, weighed, and imaged macroscopically. Liver specimens were collected from defined anatomical positions as follows: (i) a specimen of approximately 1 cm size was taken from the right medial liver lobe, fixed in 4% Roti-Histofix, and stored at 4 °C until embedding in paraffin for histolopathologic staining, (ii) a specimen of approximately 100 mg weight was taken from the left lateral liver lobe, homogenized in 1 ml TRIzol, and stored at -80 °C until further RNA isolation, (iii) a specimen of approximately 1 cm size was taken from the left lateral liver lobe, snap-frozen in liquid nitrogen, and stored at -80 °C as backup.

Histopathologic Staining of Paraffin-embedded Liver Tissue Samples

Mouse livers formalin-fixed in 4% Roti-Histofix were dehydrated along an isopropanol gradient (2 h of each 50%, 75%, 90%, and three times 100%). The tissue was cleared in Roti-Histol twice for 2 h, immersed in paraffin twice for 2 h, and embedded in paraffin blocks. For histopathologic stainings, formalin-fixed paraffin-embedded liver sections of 6 µm thickness on glass slides were used.

To assess collagen deposition during liver fibrosis, Sirius Red staining was essentially performed according the protocol of John A. Kiernan published in the IHC world database (www.ihcworld.com/_protocols/special_stains/sirius_red.htm). In short, the samples were deparaffinized in Roti-Histol and rehydrated along an ethanol gradient. The samples were stained for 1 h with picrosirius red (0.1% Direct Red 80 in picric acid) and washed twice for 2 min in acidified water (0.5% acetic acid in water). The samples were dehydrated in ethanol (2 min of each 70% and 100%), cleared in Roti-Histol, and mounted with Entellan Neu mounting medium. Samples were allowed to harden for at least 30 min at room temperature before imaging.

Histologic staining of hematoxylin-eosin (HE) and ACTA2 was performed in collaboration (SFB/TR209) with Dr. med. vet. Tanja Poth (Center for Model System and Comparative Pathology (CMCP), Institute of Pathology, Heidelberg University Hospital, Germany). HE staining was performed according to the standard protocol provided with the Leica AutoStainer XL. For immunostaining with ACTA2, liver sections were deparaffinized in Roti-Histol and rehydrated along an ethanol gradient. Antigen retrieval was performed by boiling the samples for 10 min in citrate buffer, pH 6. Samples were first stained with primary antibody ACTA2 (1:200, Abcam) for 1 h at room temperature and then with HRP-coupled secondary anti-body Polyview Plus anti-rabbit HRP (Enzo) for 1 h at room temperature. Signal detection was performed with AEC Single Solution (Zytomed) for 5 min at room temperature. HE and ACTA2 stained samples were mounted and allowed to harden for at least 30 min at room temperature before imaging.

All samples were imaged by Veronika Eckel for virtual microscopy of up to 40x magnification using the Leica Aperio AT2 Scanner and accompanying software ScanScope Console at the Tissue Bank of the National Center for Tumor Diseases (NCT), Heidelberg, Germany.

Quantification of Sirius Red and ACTA2 Signal Intensity

Quantification of Sirius Red and ACTA2 signal intensity in histopathologic stainings was performed using the image processing software ImageJ Fiji. For this, comparable fields of view (n=9 for Sirius Red, n=3 for ACTA2) were taken per animal (n=15/group) at 20x magnification from virtual microscopy slide files using ImageScope software. Images covered a field of view of 725 µm x 450 µm. Using two ImageJ macros, the images were first blinded for treatment group and then the percent of stained area (%Area) was determined by manual thresholding (**Supplementary Data 1** and **Supplementary Data 2**). The %Area was averaged per animal. The mean %Area per treatment group was then compared by one-way ANOVA and Tukey-adjusted post-hoc test using GraphPad Prism 8. Differences were considered statistically significant for p_{adj}-values ≤ 0.05.

Fibrosis Score (Kleiner Score)

The degree of liver fibrosis was scored by pathologist Dr. med. vet. Tanja Poth (CMCP, Institute of Pathology, Heidelberg University Hospital, Germany) blinded for experimental group. HE stainings were inspected for any histologic alterations such as inflammation, necrosis, altered hepatocyte morphology, or presence of tumors. Fibrotic scoring was performed on Sirius Red stained liver sections according to Kleiner *et al.* (2005), modified by Liang *et al.* (2014), adopted for the present study [24,131]. Scores were averaged per treatment group and compared by one-way ANOVA and Tukey-adjusted post-hoc test using GraphPad Prism 8. Differences were considered statistically significant for p_{adj}-values ≤ 0.05.

2.2.2 Cell Culture Techniques

Cultivation of Cell Lines

All cell lines were maintained under standard growing conditions in a humidified atmosphere at 37 °C with 5% CO_2. Cells were grown in DMEM culture medium (DMEM with 10% FCS, 100 IU/ml penicillin, 10 µg/ml streptomycin, and 4 mM glutamine) until reaching approximately 80% confluency. Culture medium of GRX-Pparg cells was supplemented with 150 µg/ml G418 to ensure persistent plasmid integration.

For passaging, the culture medium was aspirated, the cells were washed with PBS and then detached by addition of trypsin for 2-5 min at 37 °C and 5% CO_2. Trypsin was inactivated by addition of culture medium. To remove trypsin residues from the culture media, cells were pelleted by centrifugation at 800 rpm for 5 min at room temperature. The cell pellet was resuspended in culture medium. Cells were either seeded in appropriate density on a new culture dish for maintenance or harvested for downstream experiments.

Cell Counting

To determine the concentration of living cells, a small aliquot of cell suspension was mixed in a 1:2 ratio (dilution factor) with 0.4% trypan blue. Trypan blue selectively stains dead cells and thus allows determination of living cell count. Cells were counted using a Neubauer counting chamber with 0.1 mm depth and the cell concentration was calculated with the following equation:

$$\text{cell concentration}\left[\frac{\text{cells}}{\text{ml}}\right] = \frac{\text{counted cells}}{\text{counted squares}} \cdot 10^4\ (chamber\ factor) \cdot \text{dilution factor}$$

Freezing and Thawing of Cells

To freeze cells for long term storage, cells in suspension were collected by centrifugation and resuspended in freezing medium (50% culture medium, 40% FCS, 10% DMSO). Cells were transferred to cryovials and frozen in isopropanol freezing containers at -80 °C to ensure slow freezing at 1 °C/min. Cells were stored in liquid nitrogen.

To return cells into culture, cells in cryovials were thawed in a 37 °C water bath and immediately transferred dropwise to a new culture dish containing culture medium. Cells were allowed to attach overnight. The next day, culture medium was changed to remove DMSO, and cells were further cultivated as described above.

Activation and Pioglitazone Treatment of pHSCs

pHSCs were isolated by Prof. Dr. Ralf Weiskirchen according to Weiskirchen *et al.* (2017) [116]. Inactive pHSCs were collected in TRIzol immediately after isolation. Activation of pHSCs occurs when cells are plated and maintained on standard plastic dishes and is characterized by loss of retinoid droplets and increased ECM production [7]. Therefore, freshly isolated pHSCs were seeded on standard plastic dishes in culture medium (DMEM supplemented with 10% FCS, 100 IU/ml penicillin, 10 µg/ml streptomycin, and 4 mM glutamine) for activation (Day -1). The following day (Day 0), the medium of

attached pHSCs was changed to new culture medium supplemented with either 5 µM pioglitazone or DMSO (vehicle, equal volume). Cells were maintained for six days (Day 0 – Day 6) and the medium was changed every second day. Images of cell morphology (bright field) and retinoid droplets (autofluorescence upon UV excitation) were taken daily (Day 1 – Day 6) using FLoid Cell Imaging Station to monitor pHSC activation. On Day 6, pHSCs were collected in TRIzol and stored at -80 °C until further RNA isolation.

Quantification of Retinoid Droplet Autofluorescence Signal

Retinoid droplet autofluorescence signal in pHSC images was quantified to assess pHSC activation [7]. Quantification was performed on n=2 images of Day 1 and n=9 images of Day 6 for each replicate (n=3/group) using ImageJ Fiji. The %Area in the UV channel was determined by manual thresholding. The %Area was first averaged per sample. The mean %Area per treatment group and timepoint was then compared by two-way repeated measures ANOVA with Bonferroni-adjusted post-hoc test using GraphPad Prism 8. Differences were considered statistically significant for p_{adj}-values ≤ 0.05.

Luciferase Assay

Luciferase assay was performed to assess transcriptional activity of PPARG upon stimulation with the PPARG agonists pioglitazone and 15-Deoxy-$\Delta^{12,14}$-prostaglandin J2 (PGJ2). Two different plasmids, containing two variants of the peroxisome proliferator response element (PPRE) of PPARG upstream of the firefly luciferase gene (*Fluc*), were generated. Vector pGL3-consPPRE-tk120-Fluc was cloned to contain four copies of the consensus PPRE sequence of murine PPARG as reported by JASPAR under MA0065.2 [132] (**Supplementary Figure 2**). Vector pGL3-29cPPRE-tk120-Fluc was cloned to contain the four individual PPRE sequences within the miR-29c promoter as identified by us in Winkler *et al.* (2020) (**Project A**) [103] (**Supplementary Figure 3**). Luciferase assay was performed in GRX-Pparg cells. Confluent cells seeded on 24-well plates were transfected with 500 ng of one of the pGL3-PPRE-tk120-Fluc plasmids and 500 ng of the pRL-TK *Renilla* luciferase control plasmid using 1 µl DharmaFECT1 reagent/24-well according to the manufacturer's instructions. 7 h post transfection, cells were washed in PBS and starved in starvation medium (DMEM with 0.1% FCS) over night. The next day, cells were either harvested by protein lysis or further treated by adding pioglitazone (final concentration 20 µM) or PGJ2 (final concentration 2 µM) directly to the starvation medium. Cells were incubated for 24 h and then harvested. Protein lysates were collected and measured using the Dual Luciferase Reporter Assay Kit (Promega) according to the manufacturer's instructions. Firefly and *Renilla* luciferase activities were measured using OPTIMA FluoroSTAR in arbitrary luminescence units.

Firefly luciferase activity was normalized to *Renilla* luciferase activity and was compared between treatments and untreated control by one-way ANOVA with Tukey-adjusted post-hoc test using GraphPad Prism 8. Differences were considered statistically significant for p_{adj}-values ≤ 0.05.

Cell Treatment with the PPARG Agonists Pioglitazone and PGJ2

To study the effects of PPARG agonists on miRNA and gene expression, the cell lines Hepa1-6, Col-GFP, GRX, and GRX-Pparg were treated with pioglitazone or PGJ2. Confluent cells seeded on 6-well plates were washed in PBS and starved in starvation medium (DMEM with 0.1% FCS) for 24 h. The next day, cells were either harvested in TRIzol or further treated by adding pioglitazone (final concentration 20 µM) or PGJ2 (final concentration 2 µM) directly to the starvation medium. Cells were incubated for 4 h or 24 h and harvested in TRIzol for RNA isolation and qPCR measurements.

2.2.3 Molecular Cloning Techniques

Oligonucleotide Annealing

Two single-stranded complementary oligonucleotides were annealed to form a double-stranded DNA fragment that served as insert into a vector backbone. For annealing, 1 µM forward oligonucleotide and 1 µM reverse oligonucleotide (**Table 2.3**) were mixed with 10 µl CutSmart buffer (10x) and water up to 100 µl. The annealing reaction was performed by heating the oligonucleotides to 99 °C for 4 min and letting them cool down to room temperature slowly. The annealed oligonucleotides were stored at -20 °C until used in ligation reaction.

Restriction Digest

Restriction endonucleases were used to cleave double-stranded DNA at specific restriction sites to facilitate the cloning process. The resulting unpaired nucleotide overhangs allow specific ligation of DNA fragments to vector backbones. Standard restriction digestion reactions were prepared on ice according to **Table 2.10**.

Table 2.10 | Standard reaction for restriction endonuclease digestion.

Component	Quantity
10x CutSmart buffer	5 µl
DNA	1 µg
Endonuclease	10 U
Water	up to 50 µl

In case the generation of two different nucleotide overhangs was required, double digestion with two endonucleases was performed in the buffer most suited for both enzymes. Digestion was performed for 1 h at the temperature recommended by the manufacturer followed by heat inactivation of restriction endonucleases for 20 min at 65 °C.

Enzymes XhoI and SacI-HF were used for digestion of plasmid pGL3-$(TSm)_2$-tk120-Fluc to generate the vector backbone for pGL3-consPPRE-tk120-Fluc and pGL3-29cPPRE-tk120-Fluc (**Table 2.2**). Enzyme SacII was used for diagnostic digest of these vectors after oligonucleotide insertion.

Gel Extraction

To separate restriction-digested vector backbone from cut DNA fragments, DNA of the restriction digestion approach was separated by size using gel electrophoresis. The desired vector fragment was excised from the gel and purified with the PureLink Quick Gel Extraction Kit (Invitrogen) according to the manufacturer's instructions. In short, DNA was extracted from the agarose gel by dissolving it in Gel Solubilization Buffer. DNA was collected by binding to a silica membrane spin column. After ethanol washing to remove impurities, the DNA was eluted from the column with water. The DNA yield was quantified with the Qubit fluorometer.

Ligation

The adjacent DNA termini of vector and insert were joined together by DNA ligase. Ligation reaction was prepared on ice using the restriction-digested vector backbone of pGL3-$(TSm)_2$-tk120-Fluc together with the annealed oligonucleotides as insert DNA (**Table 2.11**).

Table 2.11 | Components of ligation reaction.

Component	Quantity
2x LigFast Buffer	5 µl
Vector DNA	100 ng
Insert DNA	30 ng
T4 DNA ligase	1 µl
Water	up to 10 µl

Ligation reaction was performed over night at room temperature. Since the oligonucleotides (**Table 2.3**) were designed to lose their XhoI restriction site upon correct insertion into the vector backbone, ligated plasmids were restriction digested with XhoI before transformation to digest wrongly ligated DNA.

Transformation of *E. coli* JM109

Competent, frozen *E. coli* JM109 were thawed on ice. 10 µl vector DNA from the ligation reaction were added to the cells followed by 10 min incubation on ice. To enable DNA uptake, cells were heat-shocked for 45 s in a water bath at 42 °C followed by 2 min incubation on ice. Cells were allowed to recover by adding 900 µl cold (4 °C) SOC medium and incubation for 60 min at 37 °C with shaking. 100 µl bacterial suspension was plated on LB plates containing selection antibiotics (50 µg/ml carbenicillin) and transformed bacteria were grown over night at 37 °C.

Plasmid DNA Purification

Plasmid DNA was purified from transformed *E. coli* using the InnuPREP Plasmid Mini Kit (Analytik Jena) according to the manufacturer's instructions. Plasmid sequence was confirmed by sequencing before large-scale plasmid DNA isolation was performed using the EndoFree Plasmid Maxi Kit (Qiagen) according to the manufacturer's instructions.

2.2.4 RNA and DNA Techniques

Total RNA Isolation with TRIzol Reagent

TRIzol reagent is a monophasic solution of phenol and guanidine isothiocyanate designed for isolation of high-quality total RNA. RNA isolation was performed according to the manufacturer's instructions. In short, cultured cells were grown to 70-90% confluency in 6-well plates, the medium was aspired, and the cells were lysed in 1 ml TRIzol. Alternatively, 50-100 mg tissue sample was homogenized in 1 ml TRIzol using a homogenizer. After incubation for 5 min at room temperature, 200 µl chloroform was added. The sample was mixed by vigorous shaking and incubated at room temperature for 3 min. Centrifugation at 12,000 x g for 15 min at 4 °C was performed to separate the solution into a lower organic phase, an interphase, and an upper aqueous phase. The aqueous phase containing the RNA was carefully transferred to a new reaction tube. For RNA precipitation, 10 µg RNase-free glycogen as carrier and 500 µl isopropanol were added. The solution was inverted and incubated at room temperature for 10 min before centrifugation at 12,000 x g for 10 min at 4 °C to collect precipitated RNA. The supernatant was removed without disturbing the RNA pellet. The pellet was washed with 75% ethanol and collected by centrifugation at 7,500 x g for 5 min at 4 °C. The supernatant was removed, and the RNA pellet was resuspended in 45 µl RNase-free water preheated to 60 °C and stored at -80 °C.

DNase Treatment of RNA Samples

To remove DNA contaminations from RNA samples, samples were treated with the DNA-free DNA Removal Kit (Invitrogen). The procedure was performed according to the manufacturer's instructions.

RNA Clean-up by 1-Butanol Treatment

In case RNA samples showed contamination with chaotropic salts or organic solvents, they were purified by treatment with 1-butanol and diethyl ether as described by Krebs *et al.* (2009) [133]. In short, the sample volume was adjusted to 150 µl with RNase-free water and 150 µl 1-butanol was added. The sample was vortexed and centrifuged for 1 min at 10,000 x g to separate the upper organic phase from the lower RNA-containing aqueous phase. The upper layer was aspirated, and the 1-butanol extraction was repeated three more times. Residual 1-butanol was removed from the sample by adding 500 µl diethyl ether. The sample was vortexed, centrifuged for 1 min at 10,000 x g and the upper phase aspirated. Diethyl ether extraction was repeated once, and remaining diethyl ether was allowed to evaporate.

Determination of Nucleic Acid Purity

DNA and RNA purity were assessed by measurement of the $A_{260/280}$ and $A_{260/230}$ ratios using the spectrophotometer NanoDrop 1000. $A_{260/280}$ values of 1.8 for DNA and 2.0 for RNA were considered as pure, while acceptable $A_{260/230}$ ratios range from 1.7 to 2.2 for DNA and RNA [134].

Quantification of Nucleic Acids

Fluorescence-based quantification of nucleic acids provides a more specific and sensitive alternative to the historically used spectrophotometric measurement of absorbances at 260 nm [135]. DNA and RNA concentrations were measured using the Qubit 3.0 fluorometer together with the dsDNA BR Assay Kit or the RNA BR Assay Kit, respectively. Quantification was performed according to the manufacturer's instructions.

Determination of DNA and RNA Integrity

Integrity and size of DNA and RNA were verified by agarose gel electrophoresis. For this, 1% agarose gels in TAE buffer (40 mM Tris, 20 mM acetic acid, 1 mM EDTA in H_2O) stained with ethidium bromide were used. DNA mixed with 6x Loading Dye or RNA mixed with 2x Gel Loading Buffer II were separated by gel electrophoresis at 100 V for 1 h. The bands were visualized by UV exposition and documented with the Heraeus E.A.S.Y. Doc Plus system.

2.2.5 Quantification of Relative mRNA and miRNA Expression by qPCR

Reverse Transcription of RNA into cDNA

The miScript II RT Kit (Qiagen) was used for reverse transcription of all RNA species into complementary DNA (cDNA). In the reaction, any non-coding RNAs (ncRNAs) are polyadenylated by poly(A) polymerase and reverse transcribed into cDNA using Oligo-dT primers. To allow simultaneous conversion of ncRNA species (including miRNAs) and mRNAs into cDNA in the same reaction, HiFlex Buffer was used. It contains random nucleotide primers for mRNA conversion in addition to the Oligo-dT primers for ncRNA conversion. The reverse transcription reaction was prepared on ice as described in **Table 2.12**.

Table 2.12| Components of reverse transcription reaction.

Component	Quantity
5x miScript HiFlex Buffer	2 µl
10x miScript Nucleics Mix	1 µl
miScript Reverse Transcriptase Mix	1 µl
RNA	250 ng
RNase-free water	up to 10 µl

Reverse transcription was performed for 60 min at 37 °C followed by heat-inactivation for 5 min at 95 °C. Then, cDNA was diluted 1:40 in RNase-free water and stored at -20 °C until qPCR.

qPCR Measurement

Quantitative polymerase chain reaction (qPCR) allows precise detection and quantification of specific mRNA and miRNA expression levels during amplification. Quantification was achieved using the fluorescent dye SYBR Green, which binds specifically to double-stranded DNA. Thus, fluorescence intensity linearly correlates with the copy number of the cDNA of interest as it accumulates during PCR cycles.

mRNA expression was quantified using FastStart Universal SYBR Green Master Mix (Roche), while mature miRNA expression was quantified using the miScript SYBR Green PCR Kit (Qiagen). To normalize the amount of cDNA between samples, endogenous controls were run alongside the specific mRNAs or miRNAs of interest. In mouse, Glyceraldehyde-3-phosphate dehydrogenase (*Gapdh*), beta-glucuronidase (*Gusb*), and TATA-box binding protein (*Tbp*) served as endogenous controls for mRNA, while U6 small nuclear RNA (*Rnu6*) as well as the small nucleolar RNAs C/D box 33 (*Snord33*) and C/D Box 35A (*Snord35a*) were used to normalize mature miRNAs. In rat, *Gapdh* and *Gusb* were used as endogenous controls for mRNAs, while ribosomal RNA 5S (*5S*) and U87 small nuclear RNA (*U87*) were used to normalize mature miRNAs. Additionally, no template controls were prepared for each primer pair to control for cross-contaminations. Each combination of primer pair and cDNA was measured in triplicates of 10 µl from a 35 µl master mix (**Table 2.13**).

Table 2.13 | Components and quantities of qPCR master mixes for mRNA and miRNA reactions.

Components	**Reagent Amount (mRNA)**	**Reagent Amount (miRNA)**
2x FastStart Universal SYBR Green Master Mix (Roche)	17.5 µl	-
2x SYBR Green PCR Master Mix (Qiagen)	-	17.5 µl
2 µM forward and reverse primer	3.5 µl	-
10x miScript Universal Primer (Qiagen)	-	3.5 µl
2 µM forward primer	-	3.5 µl
cDNA diluted 1:40	14 µl	1.5 µl
RNase-free water	up to 35 µl	up to 35 µl

qPCR amplification reactions were performed on 384-well plates in the QuantStudio 7 Flex Real-Time PCR System (Thermo Fisher Scientific) with the settings QuantStudio 7 Flex System, $\Delta\Delta C_t$, SYBR Green Reagents, and the cycle conditions listed in **Table 2.14** and **Table 2.15** for mRNA and miRNA quantification, respectively.

Table 2.14 | Cycle conditions of the QuantStudio 7 Flex Real-Time PCR System used for mRNA quantification.

Step (Quantification)	**Temperature**	**Time**	
Heat activation of DNA polymerase	95 °C	15 min	
Denaturation	95 °C	15 s	40 cycles
Annealing and elongation (Q)	60 °C	1 min	
Denaturation	95 °C	15 s	Melt curve
Annealing	60 °C	1 min	
Dissociation step (Q during temperature increase)	95 °C	15 s	

Table 2.15 | Cycle conditions of the QuantStudio 7 Flex Real-Time PCR System used for miRNA quantification.

Step (Quantification)	Temperature	Time	
Heat activation of DNA polymerase	95 °C	15 min	
Denaturation	94 °C	15 s	40 cycles
Annealing	55 °C	30 s	
Elongation (Q)	70 °C	30 s	
Denaturation	95 °C	15 s	Melt curve
Annealing	60 °C	1 min	
Dissociation step (Q during temperature increase)	95 °C	15 s	

qPCR Analysis

Data of the completed run were inspected using QuantStudio 7 Flex Real-Time PCR Software. PCR specificity was validated by melt curve analysis. PCR reactions with one defined melt curve peak were judged as specific while reactions with unspecific amplifications were excluded from further analysis.

Post-run data processing was performed with LinRegPCR software (http://LinRegPCR.nl) [121]. LinRegPCR calculates the initial amplicon starting concentration N_0, which is easily compared between different samples. Calculation of N_0 requires estimation of PCR efficiency E, determination of the C_t value, and of the corresponding fluorescence measurement N_C at cycle C_t. The basic equation of PCR kinetics states that the number of amplicons after C_t cycles (N_C) depends on the starting concentration of amplicon (N_0) and the PCR efficiency (E) (**Equation 1**). **Equation 1** is rearranged to calculate the starting concentration N_0 as shown in **Equation 2**.

$$N_C = N_0 \cdot E^{C_t} \qquad \textbf{Equation 1}$$

$$N_0 = \frac{N_C}{E^{C_t}} \qquad \textbf{Equation 2}$$

LinRegPCR first defines the exponential phase of each PCR reaction as the window of linearity (W-o-L) comprising 4-6 data points. The individual PCR efficiency of each sample is derived from the slope of the regression line plotted through the W-o-L data points [136]. To reduce the variability of PCR efficiency values, LinRegPCR calculates the mean efficiency of all reactions using the same amplicon. The PCR efficiency is defined as the fold increase of DNA amount per cycle and ranges from 1 (no amplification) to 2 (complete doubling). LinRegPCR then sets the C_t value for each amplicon group one cycle below the top border of the W-o-L and determines the corresponding fluorescence threshold value N_C for cycle C_t. With these values, N_0 is calculated according to **Equation 2**. N_0 is expressed in arbitrary fluorescence units.

The relative expression of the mRNA or miRNA of interest was calculated by first averaging the N_0 values of technical replicates. To then compare the expression of the mRNA or miRNA of interest across

samples, the N_0 value of the mRNA or miRNA of interest was normalized to the N_0 value of the endogenous control for each sample. In case multiple endogenous controls were used, the N_0 value of interest was normalized to the geometric mean of the endogenous control N_0 values for each sample [121]. The normalized N_0 values of all samples were then shown relative to the mean of the control samples.

Data visualization and statistical analysis were performed with GraphPad Prism 8. Normalized N_0 values were compared using two-sided unpaired t-test, ordinary one-way ANOVA with Tukey-adjusted post-hoc test, or as stated in the figure legends. Differences were considered statistically significant for p-values and p_{adj}-values ≤ 0.05, respectively.

2.2.6 RNA-seq Data Analysis and Visualization

RNA-sequencing (RNA-seq) data of murine *SRF-VP16*^{iHep} tumors and nodules alongside litter mate controls were processed by Dr. Ivana Winkler as part of Winkler *et al.* (2020) (**Project A**) [103]. The processed RNA-seq data, which have been analyzed with the R package DESeq2 (v1.22.2) to calculate normalized reads and differential gene expression values (Supplementary Dataset S02 of Winkler *et al.* (2020)) [103], were re-visited for further analysis in **Project B**.

RNA-seq data of human HCC generated by the cancer genome atlas (TCGA) Research Network (cancergenome.nih.gov) were processed by Dr. Ivana Winkler as part of Winkler *et al.* (2020) [103]. The raw reads available from TCGA were processed to normalized reads using the R package DESeq2 (v1.22.2) and the differential gene expression values were calculated according to the code available at ivanawinkler.github.io/mirna_paper. The processed RNA-seq data in form of normalized reads and differential gene expression values were re-visited for further analysis in **Project B**.

RNA-seq data of 2 months and 12 months CCl_4-induced liver fibrosis and time-matched oil controls were generated by Ghallab *et al.* (2019) and raw reads were kindly provided by Prof. Dr. Jan G. Hengstler (Department of Toxicology, Leibniz Research Centre for Working Environment and Human Factors (IfADo), Dortmund, Germany) [109]. Raw reads were processed using the R package DESeq2 (v1.22.2) according to the code provided as **Supplementary Data 3**. The resulting normalized reads and differential gene expression values were compared to RNA-seq data from *SRF-VP16*^{iHep} tumors and human HCC in **Project B**.

Relative $\log_2$ fold change values of the differential gene expression analysis were visualized using GraphPad Prism 8. Differences were considered statistically significant for p_{adj}-values ≤ 0.05 as

calculated by DESeq2. Heatmaps were generated from the normalized reads datasets using the R package pheatmap (v1.0.12).

2.2.7 Conservation of the AF-miRNA Network from Mouse and Human to Rat

The AF-miRNA network was initially identified by including filtering criteria of miRNA conservation to ensure that the conclusions gained from mouse models can be translated to human patients (**Project A**) [103]. These criteria included the conservation of the miRNAs and target genes themselves but also of the direct miRNA:target interactions. This analysis was revisited and expanded upon in **Project B** to assess to which degree the AF-miRNA network is also conserved to the rat (*Rattus norvegicus*) as additional model organism. For this, the mouse, human, and rat sequences of the 8 AF-miRNAs were retrieved from the TargetScan (v7.2) database and were compared for conservation between the three species [137]. Next, all predicted target genes for each of the 8 AF-miRNAs were extracted from the DIANA microT-CDS (v5.0) database for mouse, human, and rat with the threshold of the miTG target prediction score set to 0 [138,139]. Data analysis was performed using R (v4.0.3) [127]. Target genes were filtered for the 14 target genes experimentally validated in mouse by us in Winkler *et al.* (2020) and their respective homologs in human and rat [103]. The data were further filtered for conservation of direct miRNA:target pairs between species, and for the miTG target prediction score threshold (filtering according to the human miTG score ≥ 0.6 for each miRNA:target pair). The resulting human, mouse, and rat AF-miRNA networks were visualized as circos plots using the R package circlize (v0.4.12) [122].

3 Project A: Identification of a PPARG-regulated AF-miRNA Network that Targets the Fibrotic Tumor Microenvironment

3.1 Summary

Liver fibrosis causes scarring and thickening of liver tissue and increases the risk of HCC development, posing a major threat to human health [1]. In the following publication we identified and characterized a set of 8 miRNAs (let-7a, let-7c, let-7g, miR-29c, miR-30d, miR-30e, miR-338, and miR-335), which target multiple genes of the fibrotic tumor microenvironment [103]. Together, these anti-fibrotic miRNAs (AF-miRNAs) and their target genes form a functionally connected AF-miRNA network.

We showed that the expression of these AF-miRNAs is downregulated not only in the SRF-VP16^{iHep} model of murine HCC, but also in the CCl_4 model of murine liver fibrosis and in murine pHSCs upon activation. We further demonstrated that the predicted fibrotic target genes of these miRNAs, comprising structural, signaling, and remodeling components of the ECM, were upregulated in all model systems. We showed that this network of AF-miRNAs and target genes is also dysregulated in human HCC, invasive breast carcinoma, lung adenocarcinoma, and lung squamous cell carcinoma, which all typically arise in a fibrotic tumor microenvironment [103].

We experimentally validated the direct interactions between miRNAs and their predicted target genes i) on the mRNA level upon modulation of miRNA expression (by miRNA mimics and inhibitors) followed by qPCR as well as ii) on the protein level through luciferase assays for selected target genes. Additionally, we demonstrated that the AF-miRNAs are collectively and directly regulated on the transcriptional level by their transcription factor PPARG.

Mechanistically, we showed that the PPARG-regulated AF-miRNA network operates in HSCs. HSC activation during fibrogenesis results in reduced PPARG expression and thus in reduced transcription of the AF-miRNAs. Without the inhibitory effects of the AF-miRNAs, expression and translation of their fibrotic target genes is elevated. Produced and released by HSCs, these target genes contribute to the fibrotic ECM of the tumor microenvironment.

3.2 Contributions

The following colleagues and collaboration partners contributed to the presented publication "Identification of Pparγ-modulated miRNA hubs that target the fibrotic tumor microenvironment" by Winkler *et al.* (2020). Detailed author affiliations are listed in the presented publication.

Figure	Contribution
1A-B	Abhishek Thavamani isolated liver tissue samples from *SRF-VP16^{iHep}* mice and prepared RNA-seq library. Jan G. Hengstler and Brigitte Begher-Tibbe performed immunostaining of liver samples and acquired images. Ivana Winkler performed signal quantification.
1C and 2A-C	Robert Geffers prepared and sequenced sRNA-seq libraries. Ivana Winkler performed RNA-seq and sRNA-seq analysis as well as miRNA:target gene prediction to identify the AF-miRNA network.
3A-D	Ralf Weiskirchen isolated pHSCs. Ivana Winkler performed pHSC activation. **Catrin Bitter** optimized miRNA quantification by qPCR* (jointly with Ivana Winkler) and performed qPCR measurements.
4A-B	**Catrin Bitter** performed molecular cloning and mutagenesis of the four plasmids for luciferase assays*. **Catrin Bitter** performed miRNA mimic luciferase assays.
4C-D	**Catrin Bitter** generated the Lin28a-overexpressing 3T3 cell line*. **Catrin Bitter** performed miRNA mimic transfections jointly with Ivana Winkler. **Catrin Bitter** performed qPCR measurements.
5A-B	**Catrin Bitter** performed qPCR measurements.
5C	Ivana Winkler performed transcription start site prediction of miRNA-encoding genes and transcription factor binding site prediction.
5D	Ivana Winkler generated the PPARG-overexpressing GRX cell line. **Catrin Bitter** performed qPCR measurements.
5E	Ivana Winkler performed chromatin immunoprecipitation.
6A-B	Ivana Winkler generated graphic summaries.
S1A-B	Jan G. Hengstler and Brigitte Begher-Tibbe performed immunostaining of liver samples and acquired images. Ivana Winkler performed signal quantification.
S1C	Ivana Winkler performed gene set enrichment analysis.
S2A-C	Ivana Winkler performed RNA-seq analysis.
S3	Ivana Winkler imaged pHSCs during activation.
S4A-D	Erawan Borkham-Kamphorst prepared RNA samples of CCl_4-induced murine liver fibrosis. **Catrin Bitter** performed qPCR measurements.
S5A-M	**Catrin Bitter** performed miRNA mimic and miRNA inhibitor transfections, miRNA mimic and miRNA inhibitor luciferase assays, and qPCR measurements.
S6A-C	**Catrin Bitter** performed miRNA mimic luciferase assays jointly with Ivana Winkler.
S7A-E	Ivana Winkler analyzed the TCGA RNA-seq data.
S8-S10	Sebastian Winkler analyzed the TCGA RNA-seq data, methylation data, and CNV data and performed linear regression analysis.
S11A-C	**Catrin Bitter** performed qPCR measurements.
S12	Dieter Weichenhan, Christoph Plass, and Marion Bähr performed DNA methylation analysis of samples prepared by Ivana Winkler.

Figure	Contribution
S13A-B	**Catrin Bitter** performed PGJ2 cell treatments and qPCR measurements.
Other	Ivana Winkler and Alfred Nordheim designed the research. Oliver Kohlbacher supervised Sebastian Winkler. Ivana Winkler, **Catrin Bitter**, Sebastian Winkler, and Dieter Weichenhan analyzed the data. Ivana Winkler, **Catrin Bitter**, Sebastian Winkler, Dieter Weichenhan, Jan G. Hengstler, Ralf Weiskirchen, and Alfred Nordheim wrote the manuscript.

* These experiments were performed by me as part of my Master thesis “Regulation of fibrosis by members of the let-7 miRNA family” (2017) in the group of Prof. Dr. Alfred Nordheim (Department of Molecular Biology, IFIZ, University Tübingen, Germany) [140]. In summary, this included optimization of qPCR for miRNA quantification, generation of the Lin28a-overexpressing 3T3 cell line, and molecular cloning of one of four plasmids used for luciferase assays (pmirGLO-Col1a1). All remaining experimental and other contributions performed by me were part of this PhD thesis.

3.3 Publication

In my PhD work since January 2018, I contributed substantially to most aspects of the presented publication, and especially to the target validation experiments. Importantly, I performed all additional experiments required for the paper revision and helped finalizing the manuscript for successful publication in January 2020 [103].

Winkler, I.*, **Bitter, C.***, Winkler, S., Weichenhan, D., Thavamani, A., Hengstler, J. G., Borkham-Kamphorst, E., Kohlbacher, O., Plass, C., Geffers, R., Weiskirchen, R. & Nordheim, A. Identification of Pparγ-modulated miRNA hubs that target the fibrotic tumor microenvironment. *Proc. Natl. Acad. Sci. U. S. A.* **117**, 454-463 (2020).

*equal contribution

Identification of Pparγ-modulated miRNA hubs that target the fibrotic tumor microenvironment

Ivana Winkler[a,b,c,1], Catrin Bitter[a,b,c,1], Sebastian Winkler[c,d], Dieter Weichenhan[e], Abhishek Thavamani[a,b,c], Jan G. Hengstler[f], Erawan Borkham-Kamphorst[g], Oliver Kohlbacher[c,d,h,i], Christoph Plass[e], Robert Geffers[j], Ralf Weiskirchen[g], and Alfred Nordheim[a,b,c,k,2]

[a]Department for Molecular Biology, Interfaculty Institute of Cell Biology, Eberhard Karls University Tübingen, 72076 Tübingen, Germany; [b]German Cancer Consortium, German Cancer Research Center, 69120 Heidelberg, Germany; [c]International Max Planck Research School, 72076 Tübingen, Germany; [d]Applied Bioinformatics, Department of Computer Science, Eberhard Karls University Tübingen, 72076 Tübingen, Germany; [e]Cancer Epigenomics, German Cancer Research Center, 69120 Heidelberg, Germany; [f]Department of Toxicology, Leibniz Research Centre for Working Environment and Human Factors (IfADo), 44139 Dortmund, Germany; [g]Experimental Gene Therapy and Clinical Chemistry, Institute of Molecular Pathobiochemistry, University Hospital Aachen, 52074 Aachen, Germany; [h]Biomolecular Interactions, Max Planck Institute for Developmental Biology, 72076 Tübingen, Germany; [i]Translational Bioinformatics, University Hospital Tübingen, 72076 Tübingen, Germany; [j]Genome Analytics Unit, Helmholtz Center for Infection Research, 38124 Braunschweig, Germany; and [k]Leibniz Institute on Aging, 07745 Jena, Germany

Edited by Gary Ruvkun, Massachusetts General Hospital, Boston, MA, and approved November 27, 2019 (received for review May 27, 2019)

Liver fibrosis interferes with normal liver function and facilitates hepatocellular carcinoma (HCC) development, representing a major threat to human health. Here, we present a comprehensive perspective of microRNA (miRNA) function on targeting the fibrotic microenvironment. Starting from a murine HCC model, we identify a miRNA network composed of 8 miRNA hubs and 54 target genes. We show that let-7, miR-30, miR-29c, miR-335, and miR-338 (collectively termed antifibrotic microRNAs [AF-miRNAs]) down-regulate key structural, signaling, and remodeling components of the extracellular matrix. During fibrogenic transition, these miRNAs are transcriptionally regulated by the transcription factor Pparγ and thus we identify a role of Pparγ as regulator of a functionally related class of AF-miRNAs. The miRNA network is active in human HCC, breast, and lung carcinomas, as well as in 2 independent mouse liver fibrosis models. Therefore, we identify a miRNA:mRNA network that contributes to formation of fibrosis in tumorous and nontumorous organs of mice and humans.

microRNAs | fibrosis | hepatocellular carcinoma | PPARγ

Hepatocellular carcinoma (HCC) is the most frequent primary human liver malignancy. It represents the fifth most common cancer in men and the seventh in women (1). HCC is currently the third leading cause of cancer-related deaths worldwide (2).

To study molecular and cellular events underlying HCC formation, we have generated *SRF-VP16*^{iHep} mice (3). These mice express in a mosaic, hepatocyte-specific fashion SRF-VP16, a constitutively active variant of serum response factor (SRF). SRF is a ubiquitously expressed transcription factor that regulates a wide range of biological processes (4). As a consequence of SRF-VP16 activity, *SRF-VP16*^{iHep} mice develop hyperproliferative liver nodules that progress to lethal murine HCC (mHCC) (3). SRF-VP16–driven HCCs share several characteristics with human HCC (hHCC), including different features of the tumor microenvironment (3).

The tumor microenvironment is a complex composite of tumor and nontumor cells embedded within an extracellular matrix (ECM), which facilitates malignant tumor progression (5). HCC progression is a multistage process that typically arises in the context of liver fibrosis. Liver fibrosis is the consequence of an exaggerated wound-healing response to reoccurring or chronic liver injury and is characterized by excessive accumulation of ECM. The central event in liver fibrosis is the activation of hepatic stellate cells (HSCs). Activated HSCs (aHSCs) produce components of the ECM and growth factors, thus causing excessive ECM deposition, neoangiogenesis, and inflammation (6). These processes ultimately result in scarring and thickening of affected tissue, which interferes with normal liver function and facilitates HCC tumorigenesis.

Such a fibrotic microenvironment, caused by quantitative and qualitative changes in ECM depositions, is characterized by increased stiffness, which promotes tumorigenesis through elevated integrin signaling. This signaling leads to enhanced growth, survival, and proliferation of tumor cells (7). Furthermore, ECM deposition enhances HCC chemotherapy resistance and offers protection against immune cells (8).

Unfortunately, the sequence of molecular events leading to the formation of a fibrogenic microenvironment, including regulatory networks governing these events, is insufficiently understood.

Significance

Liver fibrosis interferes with normal organ function and supports tumor development in the liver. We uncovered a role of miRNAs in controlling liver fibrosis. In a comprehensive and systematic analysis we specify miRNA activities in targeting the fibrotic cellular microenvironment of the liver, in both mice and humans. We reveal and validate a complex network of 8 functionally connected miRNAs and 54 target genes to regulate structural, signaling, and remodeling components of the fibrotic extracellular matrix. We identify expression of this miRNA network to be controlled by the transcription factor Pparγ. Thus, we expand the antifibrotic function of Pparγ to controlling the synthesis of an antifibrotic miRNA network. This network may serve as a therapeutic target in antifibrotic therapies.

Author contributions: I.W. and A.N. designed research; I.W., C.B., S.W., D.W., A.T., J.G.H., E.B.-K., O.K., C.P., R.G., and R.W. performed research; I.W., C.B., S.W., and D.W. analyzed data; I.W., C.B., S.W., D.W., J.G.H., R.W., and A.N. wrote the paper; and O.K. supervised S.W.

The authors declare no competing interest.

This article is a PNAS Direct Submission.

Data deposition: sRNA-seq and RNA-seq FASTQ data are deposited in the NCBI Sequence Read Archive (SRA), https://www.ncbi.nlm.nih.gov/sra, under accession no. Bioproject: PRJNA522967. Processed sRNA-seq and RNA-seq (differential gene and miRNA expression table and normalized reads) are listed in *SI Appendix*. Output data of the linear regression analysis are also listed in *SI Appendix*. The code for the bioinformatic analysis has been deposited at https://ivanawinkler.github.io/mirna_paper/.

[1]I.W. and C.B. contributed equally to this work.

[2]To whom correspondence may be addressed. Email: alfred.nordheim@uni-tuebingen.de.

This article contains supporting information online at https://www.pnas.org/lookup/suppl/doi:10.1073/pnas.1909145117/-/DCSupplemental.

Accumulating data support a regulatory role of microRNAs (miRNAs) in control of gene expression programs that underline different normal and pathologic processes, including cancer (9). miRNAs are 21- to 23-nucleotide-long RNAs that act as essential regulators of gene expression, directing degradation, destabilization, or translational repression of target mRNAs (10). In mammals, more than 60% of protein-coding genes are believed to be under the control of miRNAs (11). However, in the majority of cases which characterize the regulatory role of miRNAs, the magnitude of the described miRNA:mRNA regulation is mild. This seeming discrepancy of the extensive role that miRNAs have in different biological processes and the mild extent of their influence is explained by the capacity of individual miRNAs to target hundreds of different mRNAs simultaneously. If the miRNA targets are enriched in common pathways, then the sum of modest effects of individual miRNA:mRNA interactions can produce a stronger response than the direct interactions in isolation (12).

Although some miRNAs have already been implicated in the modulation of the fibrotic environment (13), our understanding of the extent of miRNA contribution to the control of fibrosis-related processes, especially in the context of HCC, is still very limited. Studies describing roles that miRNAs have in regulation of fibrosis and HCC typically have identified individual miRNA:target interactions. While these studies provide valuable insight into miRNA-directed regulation, such approaches ignore the complexity of miRNA signaling networks.

Furthermore, with the potential of a single miRNA to regulate hundreds of target mRNAs, miRNAs themselves have to be tightly and dynamically regulated. Specifically, mechanisms controlling miRNA expression, stability, and targeting efficiency may be exerted at all levels of miRNA biogenesis, processing, and functional maturation (14). These miRNA regulatory mechanisms are, currently, poorly defined in the context of fibrosis.

The complexity of regulation of miRNAs and miRNA-directed targeting leads to intricate networks of miRNAs and their target and regulatory genes. The nodes of these networks, which can be either miRNAs or mRNAs, are generally connected to many other nodes in these regulatory networks. Hubs, nodes in the network with an atypically high number of connections, are of special importance, as they represent sites of signaling convergence which can explain the network behavior and serve as potential targets for therapy and prediction of clinical outcome (15).

Therefore, in this study, we investigated and described 1) a miRNA:mRNA network that influences fibrotic microenvironment development in HCC with special emphasis on miRNA hubs which regulate a considerable number of genes in the network, 2) the conservation of the network in different fibrosis settings (e.g., across different fibrosis-facilitated carcinomas and different fibrosis models), and 3) the mechanism of regulation of miRNAs in the network.

As a starting point to investigate the role of miRNAs in regulating HCC-associated fibrosis we utilized the *SRF-VP16*^{iHep} HCC model. Using transcriptome-wide experimental and bioinformatical tools, we identified a miRNA network that regulates different structural, signaling, and remodeling components of the ECM. The identified miRNA:mRNA network was also found to be dysregulated to different degrees in 2 murine fibrosis models, as well as 4 types of human fibrosis-facilitated carcinomas. We show that this complex network is composed of 8 miRNA hubs and 54 target genes which together regulate key components of the fibrotic microenvironment. Taken together, our findings indicate that the let-7 and miR-30 miRNA families, as well as miR-29c, miR-335, and miR-338, are important antifibrotic microRNAs (AF-miRNAs).

Additionally, we observed the dysregulation of the aforementioned miRNAs at the primary (pri-)miRNA level, suggesting transcriptional regulation of pri-miRNA synthesis. Upon investigation of 2 major transcriptional regulatory mechanisms (i.e., transcription factor-mediated regulation and genomic CpG methylation) we identified the transcription factor Pparγ as a direct positive regulator of antifibrotic miRNA synthesis. Furthermore, we observed significant hypermethylation of let-7a, miR-335, and miR-338 gene promoters upon primary HSC (pHSC) activation, suggesting epigenetic mechanisms to contribute to the transcriptional control of these miRNAs.

Results

A Subset of miRNAs Targets ECM-Linked and Fibrosis-Associated Genes in mHCC. To study the role of miRNAs in the regulation of the fibrotic microenvironment during tumor progression we have used the *SRF-VP16*^{iHep} mouse model of HCC formation. To evaluate the progression of fibrosis alongside tumor progression we performed Sirius Red and alpha-smooth muscle actin (Acta2) staining of *SRF-VP16*^{iHep} precancerous nodular and HCC tissue, thereby highlighting fibrotic collagen depositions and HSC activation (16), respectively. This analysis revealed—in correlation with tumor progression—a gradual increase in both area covered by collagen (Fig. 1 *A* and *B*) and density of aHSCs (*SI Appendix*, Fig. S1 *A* and *B*).

To demonstrate that HSC activation occurs in the vicinity of SRF-VP16–expressing hepatocytes, we performed Egr1 immunostaining. As a target gene of SRF, Egr1 is not expressed in control samples, while its expression is high in SRF-VP16 nodular and tumor samples. Colocalization of Acta2 and Egr1 signals confirms that aHSCs are part of the tumor microenvironment, providing further support to the significance of fibrosis in SRF-VP16–driven tumor development (*SI Appendix*, Fig. S1*A*).

To investigate contributions of miRNAs to HCC formation and tumor microenvironment development, we performed small RNA-sequencing analysis (sRNA-seq) of nodular and tumor samples derived from livers of *SRF-VP16*^{iHep} mice and corresponding controls. As the fibrotic microenvironment is more strongly developed in tumor tissue than in nodular tissue (Fig. 1 and *SI Appendix*, Fig. S1), in this study we have focused on miRNA changes in tumors.

To identify miRNA candidates with potential contributions to mHCC formation and microenvironment development, we applied 4 filtering criteria: 1) differential expression in tumors versus controls ($p_{adj} \leq 0.05$), 2) sufficient expression level ($\geq$10 counts across all samples), 3) miRNA conservation (between mice and humans), and 4) similar expression pattern of at least one miRNA family member in hHCCs ($\geq$10% of cases in The Cancer Genome Atlas's [TCGA's] cohort). Criteria 3) and 4) were applied to identify conserved miRNA expressions and functions with the final aim to compare the conclusions gained from our animal model to human patients. Upon applying these criteria, we found that 52 significantly down-regulated and 31 significantly up-regulated mouse miRNAs are dysregulated in at least 10% of human TCGA cases ($\geq$1.5-fold).

Subsequent to identification of tumor-associated miRNAs, we performed screening of potential miRNA targets using the DIANA microT-CDS (17) and TargetScan (18) databases. To increase the accuracy of down-regulated miRNA target predictions, we performed RNA-sequencing (RNA-seq) analyses on largely overlapping samples as used for sRNA-seq (*SI Appendix*, Table S1) and correlated target mRNA candidates generated through bioinformatic analysis with the up-regulated genes found by RNA-seq. Similarly, targets of up-regulated miRNAs were identified.

To profile evolutionary conserved miRNA targeting, an analysis comparable to the above was performed on the TCGA

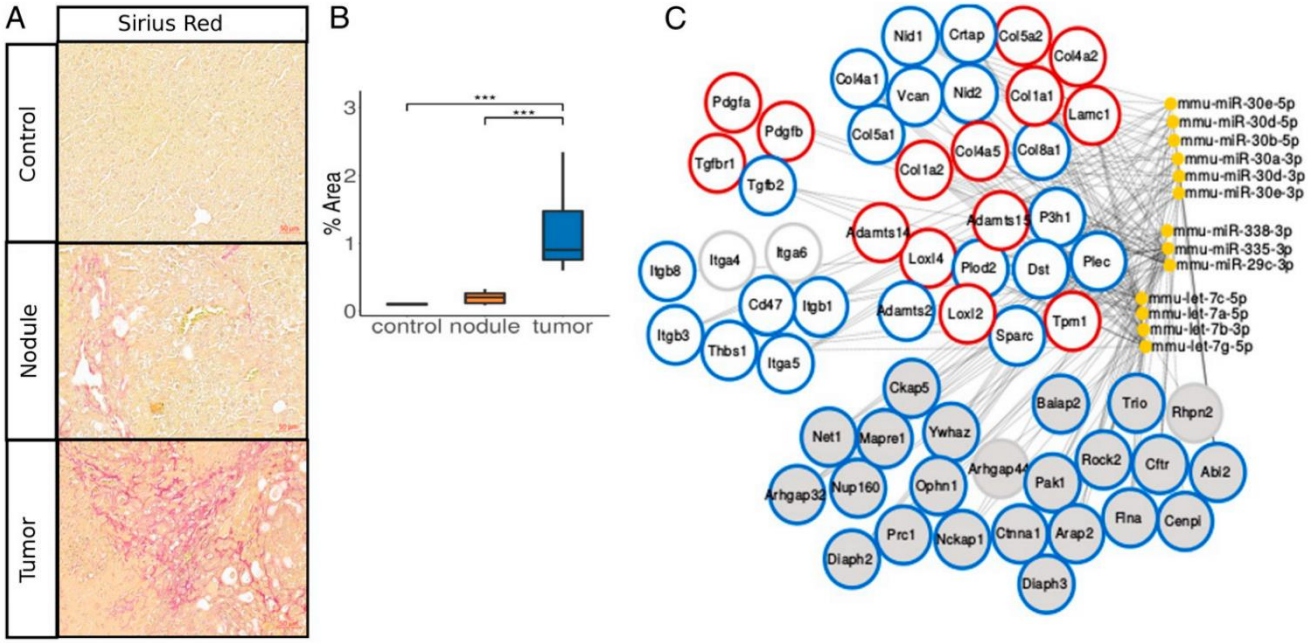

Fig. 1. A subset of miRNAs predicted to target ECM-linked and fibrosis-associated genes in mHCC. (*A*) Sirius Red staining of control, nodular, and tumor liver samples isolated from *SRF-VP16^{iHep}* mice. (Scale bar, 50 μm.) (*B*) Quantification of Sirius Red signal shown in *A*. (*C*) Network of miRNA:mRNA pairs, which encompasses predicted miRNA targeting of genes contributing to the ECM-related pathways highlighted in dark gray in *SI Appendix*, Fig. S1C. Genes are grouped in structural (upper right), signaling (upper left), and remodeling (middle right) components of the ECM, as well as genes related to integrin signaling (middle left) and Rho signaling (bottom). miRNAs mmu-miR-30e-5p, mmu-miR-30d-5p, mmu-miR-338-3p, mmu-miR-335-3p, mmu-miR-29c-3p, mmu-let-7a-5p, mmu-let-7c-5p, and mmu-let-7g-5p, which are predicted to target all ECM-related proteins of the network, were further experimentally characterized in the remainder of this study. Additionally, we chose to further characterize gene expression and predicted miRNA-mediated targeting of a subset of genes, which represent key structural, remodeling, and signaling components of the ECM. We highlighted these genes using red circles. Rims of gene nodes: red, ECM-related genes characterized further in this study and predicted to be targeted by the here-characterized miRNAs; blue, genes not characterized in this study but predicted to be targeted by the here-characterized miRNAs; and gray, genes not characterized in this study and predicted to be targeted by the here-noncharacterized miRNAs. Data are shown as median, first, and third quartiles ("box") and 95% confidence interval of median ("whiskers"). ***p value $\leq$ 0.001.

datasets of hHCCs. Subsequently, miRNA:target mRNA pairs of both murine and human datasets were overlapped and only conserved pairs were further used in gene set enrichment (GSE) analysis, using KEGG (19) and Reactome (20) pathways. GSE analysis of down-regulated miRNAs showed strong overrepresentation of proteins involved in ECM function, integrin signaling, and Rho GTPase-related pathways (*SI Appendix*, Fig. S1*C*), indicating the importance of miRNAs in regulation of the fibrotic microenvironment in HCC development.

Breaking down these pathways into individual genes and their cognate regulatory miRNAs allowed us to identify a miRNA:target mRNA network, composed of a subset of miRNAs down-regulated in tumors. To identify miRNA hubs in the network, all miRNAs which regulate ECM-related genes were filtered for the number of target genes and network coverage. Only miRNAs which target at least 8 ECM-related genes in the network were retained. This miRNA network reveals that the miRNA families miR-30 and let-7, together with miR-335, miR-338, and miR-29c, control a majority of genes related to ECM function as well as integrin and Rho signaling and therefore represent miRNA hubs of the network. For simplicity, we refer to this subset of miRNAs as potential AF-miRNAs.

Collagens represent the most dominant structural proteins of the ECM (21). Most collagen family members in our network are regulated by the let-7 family and miR-29c, with a contribution of miR-335 and miR-338, while laminin gamma 1 (*Lamc1*) is targeted by miR-29c (Fig. 1*C*). ECM remodeling components, i.e., A Disintegrin and Metalloproteinases with a ThromboSpondin motif (*Adamts*) and LOX-like (*Loxl*) family members, are regulated by the let-7 family, miR-29c, and miR-338 (Fig. 1*C*). Components of the TGF-β pathway (*Tgfbr1* and *Tgfbr2*), the most potent positive regulator of fibrosis, are targeted by miR-335 and the let-7 family, while components of the PDGF pathway (*Pdgfa* and *Pdgfb*), responsible for induction of HSC proliferation, are targeted by miR-29c and miR-335. Integrin and Rho-GTPase signaling, which mediate signals from the ECM, are regulated by miR-30 family members. Rho-GTPase signaling is additionally regulated by miR-335 and miR-338 (Fig. 1*C*). Collectively, these results indicate that the identified AF-miRNAs are negative regulators of structural, remodeling, and signaling components of ECM organization.

AF-miRNAs Are Down-Regulated and Fibrosis-Associated Genes Are Up-Regulated in mHCC. sRNA-seq performed on mouse SRF-VP16–driven HCC samples shows that the AF-miRNAs are significantly down-regulated in mHCC (Fig. 2 *B* and *C*).

In this study, we focused on a subset of ECM-related genes which cover structural (*Col1a1*, *Col1a2*, *Col4a2*, *Col4a5*, *Col5a2*, and *Lamc1*), signaling (*Pdgfa*, *Pdgfb*, and *Tgfbr1*), and remodeling (*Loxl2*, *Loxl4*, *Adamts14*, *Adamts15*, and *Tpm1*) components of the ECM (Fig. 2*A*).

All aforementioned genes, except *Col5a2*, show significant up-regulation in the mouse *SRF-VP16^{iHep}* model (*SI Appendix*, Fig. S2 *A–C*). *Col5a2* shows clear, but statistically not significant (p_{adj} value 0.058) up-regulation.

AF-miRNAs Are Down-Regulated and Fibrosis-Associated Genes Are Up-Regulated in the pHSC In Vitro Culture Fibrosis Model and in the In Vivo CCl_4 Murine Fibrosis Model. To probe the generality of our miRNA:mRNA network, we examined the expression of

CELL BIOLOGY

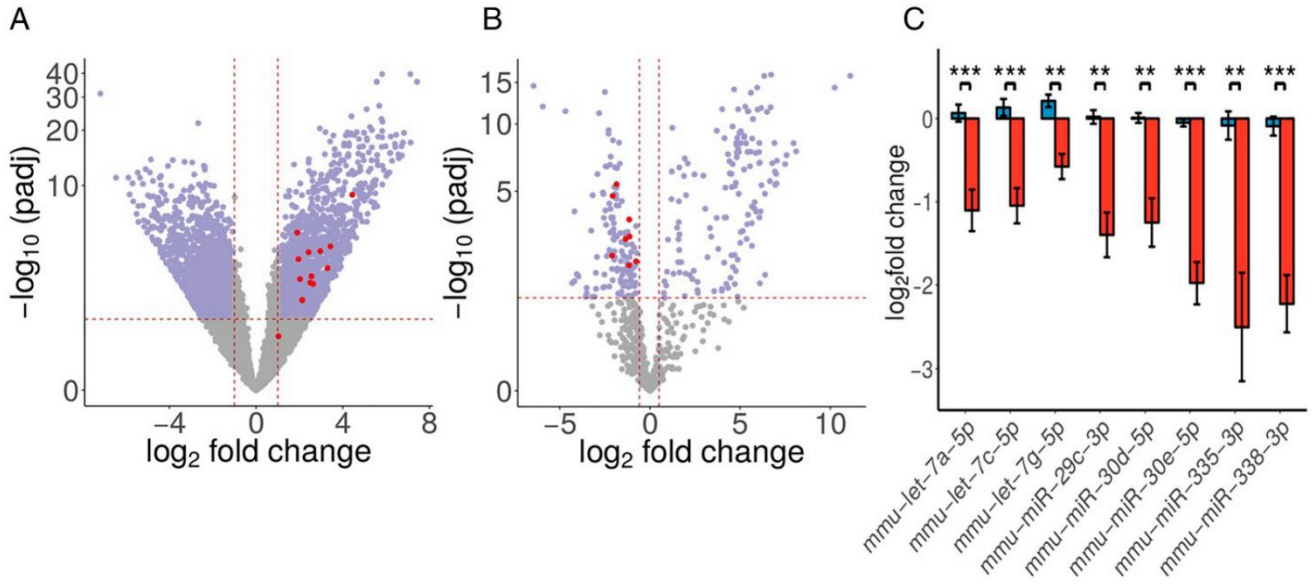

Fig. 2. AF-miRNAs are down-regulated and fibrosis-associated genes are up-regulated in murine HCC. (*A*) Volcano plot of genes identified in RNA-seq. Fibrosis-related genes characterized in this study are shown in red and significantly dysregulated genes (threshold 2-fold) in violet. (*B*) Volcano plot of miRNAs identified in sRNA-seq. AF-miRNAs characterized in this study are depicted in red (also listed in *C*), and significantly dysregulated miRNAs (threshold 1.5-fold) are depicted in violet. (*C*) sRNA-seq–derived, normalized read counts (log_2-transformed) of AF-miRNAs in control (blue bars) and tumor (red bars) samples of *SRF-VP16*^{iHep} mice. Data are shown as mean and SEM. **p_{adj} value $\leq$ 0.01, ***p_{adj} value $\leq$ 0.001.

AF-miRNAs and fibrosis-associated target genes in 2 fibrosis models, pHSC in vitro culture and the carbon tetrachloride (CCl_4) in vivo mouse model.

pHSC activation, evident by loss of retinoid droplets and increased ECM production, occurs when cells are plated on standard plastic dishes (22). To ensure activation of pHSCs, cells were maintained in culture for 7 d (*SI Appendix*, Fig. S3). Using qPCR, we compared freshly isolated (inactive) pHSCs with pHSCs activated by prolonged culturing. The CCl_4 in vivo model was generated by prolonged administration of CCl_4, which leads to hepatic fibrosis development (23).

All AF-miRNAs were found down-regulated in both fibrosis models (Fig. 3*A* and *SI Appendix*, Fig. S4*A*), while all measured structural ECM fibrosis-associated target genes were up-regulated in both models (Fig. 3*B* and *SI Appendix*, Fig. S4*B*). Similarly, all examined remodeling and signaling ECM components were up-regulated, except *Tgfbr1* and *Adamts*, which were up-regulated in the CCl_4 model but down-regulated in the pHSC model (Fig. 3 *C* and *D* and *SI Appendix*, Fig. S4 *C* and *D*).

AF-miRNAs Target Structural, Signaling, and Remodeling Components of the ECM. To experimentally validate the predicted AF-miRNA targeting of fibrosis-related genes, we performed luciferase assays and qPCR analyses (*SI Appendix*, Table S2). To modulate miRNA expression, we employed 3 strategies. First, we used miRNA mimics to overexpress miR-29c, miR-338, let-7a, let-7c, and let-7g. Second, we used miRNA inhibitors to inhibit miR-29c and let-7g. Third, we inhibited let-7a, let-7c, and let-7g expression by overexpressing Lin28a, which down-regulates the entire let-7 family (24).

For luciferase assays, we cloned 3'-untranslated regions (3'-UTRs) of *Col1a1*, *Pdgfa*, *Tgfbr1*, and *Adamts15* genes

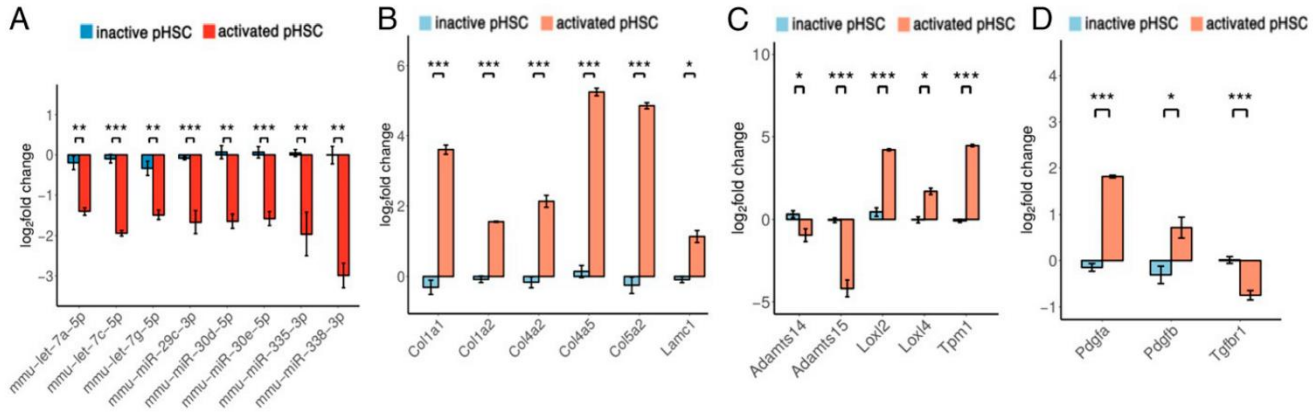

Fig. 3. AF-miRNAs are down-regulated and fibrosis-associated genes are up-regulated in the pHSC fibrosis model. (*A*) Relative expression of mature miRNAs in inactive (freshly isolated) and activated (prolonged in vitro culturing) pHSCs. (*B–D*) Relative expression of fibrosis-associated structural (*B*), remodeling (*C*), and signaling (*D*) genes of the ECM in inactive and activated pHSCs. All samples are normalized to a randomly chosen control sample. Data are shown as mean and SEM. *p value $\leq$ 0.05, **p value $\leq$ 0.01, ***p value $\leq$ 0.001.

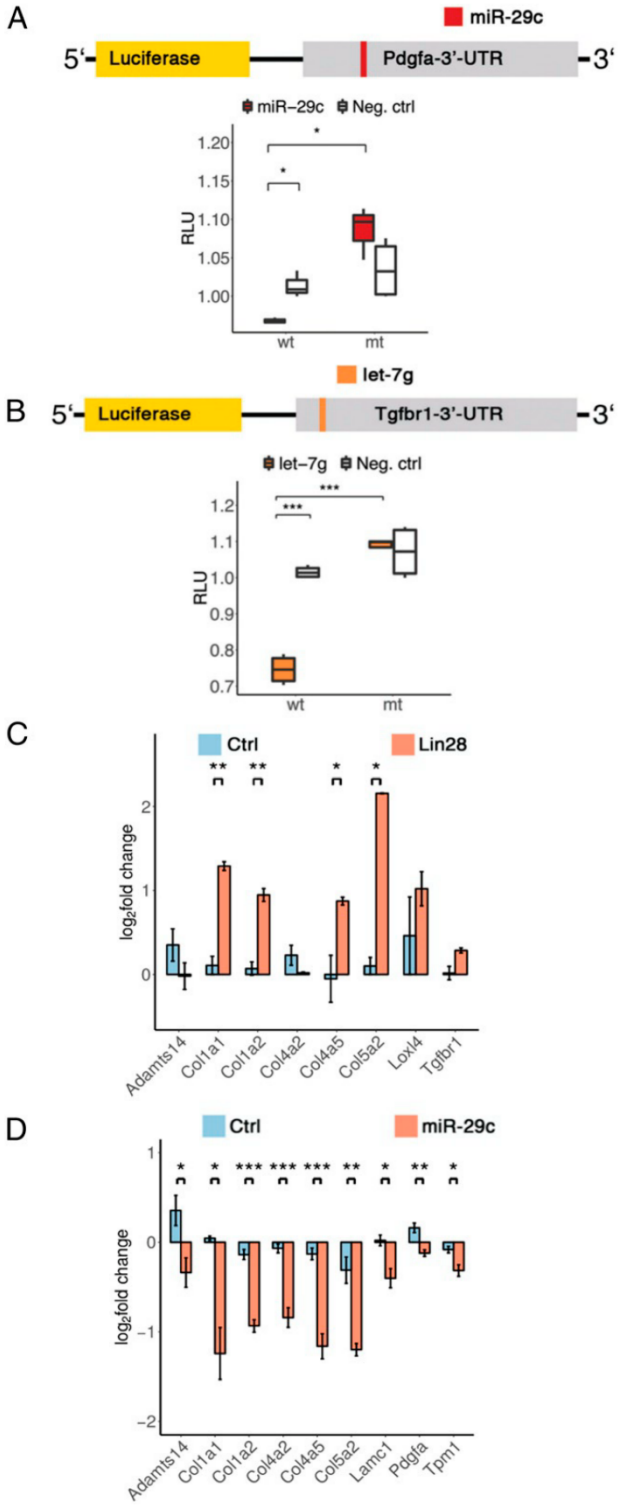

Fig. 4. AF-miRNAs target structural, signaling, and remodeling components of the ECM. (*A* and *B*) Activities of wild-type and mutant (mutated miRNA site) 3′-UTR–luciferase constructs derived from (*A*) *Pdgfa* in NIH/3T3 cells transfected with miR-29c and scrambled miRNA mimic and (*B*) *Tgfbr1* in NIH/3T3 cells transfected with let-7g and scrambled miRNA mimic. Let-7g– and miR-29c–transfected samples are colored in the plots according to the luciferase construct schematic. Samples transfected with scrambled miRNA mimic are shown in white (Neg. ctrl). (*C* and *D*) Relative expression of putative let-7 target genes associated with fibrosis in stable Lin28a-overexpressing NIH/3T3 cells (*C*) and putative miR-29c target genes associated with fibrosis in NIH/3T3 cells transfected with miR-29c mimics (*D*). (*A* and *B*) Data are shown as median, first, and third quartiles ("box") and 95% confidence interval of median ("whiskers"). (*C* and *D*) Data are shown as mean and SEM. *p value $\leq$ 0.05, **p value $\leq$ 0.01, ***p value $\leq$ 0.001.

downstream of the luciferase gene and assayed luciferase expression in NIH/3T3 cells upon miRNA mimic or inhibitor transfection. For validation, we mutated the miRNA binding sites and likewise assayed the mutant 3'-UTR constructs upon miRNA mimic or inhibitor transfection.

The luciferase reporter containing wild-type 3'-UTR of *Col1a1* showed significant down-regulation upon let-7a, let-7c, let-7g, or miR-29c mimic expression compared to scrambled mimic, while the mutant 3'-UTR construct retained comparable levels of expression upon specific miRNA and scrambled mimic transfection (*SI Appendix*, Figs. S5*A* and S6*A*). In agreement, reverse effects were observed for *Col1a1* luciferase assays performed with let-7g and miR-29c inhibitors (*SI Appendix*, Fig. S5*J*).

We observed a similar down-regulation of *Pdgfa* and *Tgfbr1* constructs upon miR-29c and let-7a, let-7c, and let-7g mimics overexpression, respectively (Fig. 4 *A* and *B* and *SI Appendix*, Fig. S6*C*), as well as an up-regulation of the *Tgfbr1* construct upon let-7g inhibitor transfection (*SI Appendix*, Fig. S5*K*). The *Adamts15* luciferase construct showed a significant down-regulation upon miR-338, let-7a, let-7c, let-7g, and miR-29c mimic transfection (*SI Appendix*, Figs. S5*B* and S6*B*).

In qPCR analysis, we assessed the effect of the let-7 family on target gene expression in Lin28a-overexpressing NIH/3T3 cells (Fig. 4*C*). We validated Lin28a overexpression relative to control and confirmed its inhibitory effect on let-7a, let-7c, and let-7g (*SI Appendix*, Fig. S5 *C* and *D*). Lin28a-mediated inhibition of the let-7 family resulted in significant up-regulation of most collagens. While *Tgfbr1* and *Loxl4* showed a similar trend of up-regulation, *Col4a2* and *Adamts14* appeared to be weakly down-regulated (Fig. 4*C*).

Additionally, we investigated the effect of let-7c, let-7g, and miR-29c up-regulation (*SI Appendix*, Fig. S5 *E*–*G*) on target gene expression (Fig. 4*D* and *SI Appendix*, Fig. S5 *H* and *I*) upon miRNA mimic or scrambled mimic transfection. Up-regulation of all 3 miRNAs caused specific down-regulation of their target genes. While miR-29c and let-7c mediate significant inhibition of all their target genes with the exception of *Col4a2* for let-7c (Fig. 4*D* and *SI Appendix*, Fig. S5*I*), the inhibitory effect of let-7g is more subtle (*SI Appendix*, Fig. S5*H*). In agreement with miRNA mimic experiments, inhibition of miR-29c and let-7g by miRNA inhibitor transfection in NIH/3T3 cells caused the up-regulation of most of their target genes (*SI Appendix*, Fig. S5 *L* and *M*).

AF-miRNAs Are Down-Regulated and Fibrosis-Associated Genes Are Up-Regulated in a Subset of Human HCCs. Expression analysis of the AF-miRNAs in the hHCC dataset showed that the same miRNAs are down-regulated in at least 10% of TCGA cases with the exception of hsa-miR-30d-5p, which is down-regulated in only 3.2% of cases (*SI Appendix*, Fig. S7*A*).

The miRNAs hsa-let-7c-5p and hsa-miR-29c-3p show the highest frequency of down-regulation, 71% and 66%, respectively. Hsa-miR-335-3p and hsa-miR-338-3p are down-regulated in a smaller number of cases, 30.1% and 10%. Although hsa-miR-30d-5p is down-regulated in a very small fraction of tumors, hsa-miR-30e-5p, which shares the same targets as miR-30d, is down-regulated in 38% of cases (*SI Appendix*, Fig. S7*A*). In the human TCGA cohort, most of the fibrosis-associated genes show up-regulation ($\geq$2-fold) in the majority of tumors with the exception of *TGFBR1* and *ADAMTS15*, which show up-regulation in 11.8% and 7.5% of cases, respectively (*SI Appendix*, Fig. S7*B*).

CELL BIOLOGY

A total of 29.7% of patients of the TCGA cohort have 25% (17 pairs) of AF-miRNA:fibrosis-associated gene pairs anticorrelated in the same patient (*SI Appendix*, Fig. S7 *C* and *D*). Across the cohort, 20 AF-miRNA:fibrosis-associated gene pairs are anticorrelated in at least 19.4% of patients, ranging from let-7c:COL4A2 which is anticorrelated in 57.8% of patients to miR-338:TGFBR1 which is anticorrelated in 2.2% (*SI Appendix*, Fig. S7*E* and Dataset S5).

The miRNA:mRNA Pairs Show Different Degrees of Association in Human Fibrosis-Facilitated Carcinomas. To examine the recurrence of expression association of the AF-miRNAs and their target mRNAs in a wider range of human carcinomas, we implemented a multivariate linear regression approach (25).

The multivariate model assesses mRNA expression regulation, taking into consideration miRNA expression, changes in DNA copy number (CNV), and promoter methylation status of the respective gene. CNV and methylation data are used to assess the influence of miRNA-unrelated gene regulation. Using the multivariate model, we aimed to assess whether AF-miRNAs considerably contribute to fibrosis-associated gene regulation in vivo in different fibrosis-facilitated carcinomas.

The model was implemented across HCC, invasive breast carcinoma (BRCA), lung adenocarcinoma (LUAD), and lung squamous cell carcinoma (LUSC), i.e., carcinoma types exhibiting fibrotic tumor microenvironments which advance tumor progression (5).

We first examined the recurrence of expression association of the miRNAs and their target mRNAs in individual carcinoma types. In hHCC, most ECM-related genes are consistently targeted by let-7g and miR-29c, while Rho GTPase-related genes are targeted by miR-30e (*SI Appendix*, Fig. S8*B*). Similarly, let-7g and miR-29c consistently inhibit the majority of ECM-related genes in BRCA and LUAD samples. However, in these carcinomas, miR-335 and miR-338 additionally contribute to targeting of ECM genes, while Rho GTPase-related genes are primarily modulated by miR-30d and miR-338 (*SI Appendix*, Figs. S8*A* and S9*A*). Furthermore, miR-335 regulates ECM- and integrin-related genes in LUAD and LUSC (*SI Appendix*, Fig. S9*B*).

Second, we analyzed the association recurrence across all examined carcinomas, defined by the association recurrence (REC) score. A negative REC score of miRNA:mRNA pairs across fibrosis-facilitated carcinomas indicates that miR-29c, let-7g, let-7a, and miR-335 consistently regulate different collagens (*SI Appendix*, Fig. S10). *Adamts14* is regulated by miR-29c, let7a, and let-7g, while *Adamts15* is targeted by let-7g and let-7c. *Loxl2* and *Loxl4* are modulated by miR-29c and let-7c and let-7a, respectively. *Tgfbr1* is primarily regulated by miR-338, let-7a, and let-7c. The linear regression analysis, which assessed the extent of miRNA, DNA methylation, and CNV influence on mRNA expression, showed that identified miRNAs considerably contribute to the expression regulation of the fibrosis-associated genes.

To provide an overview of the characterized miRNA:mRNA interactions we compiled a table, which lists the interactions, the assays in which the interactions were validated, and the REC scores (*SI Appendix*, Table S3). While some validated miRNA:mRNA interactions have a positive REC score and thus the regression model does not provide support for regulation of the mRNA by the miRNA of these interaction pairs in the examined TCGA cohort, the same mRNAs are consistently regulated by other miRNAs of the network as indicated by a negative REC score.

Together, the AF-miRNAs are evidenced to commonly regulate ECM-related genes in human fibrosis-driven carcinomas, albeit to different extents in different carcinoma types.

Transcription Factor Pparγ and DNA Methylation of miRNA-Encoding Gene Promoters Regulate Expression of AF-miRNAs. To identify the mechanism of AF-miRNA regulation during pHSC activation we examined the expression of precursor molecules of AF-miRNAs. As miRNAs can be regulated at different stages of biogenesis, we quantified pri-miRNAs and precursor (pre-)miRNAs of AF-miRNAs using qPCR in inactive and activated pHSCs, as well as in the in vivo CCl_4 fibrosis mouse model.

We established that down-regulation of AF-miRNAs occurs at the pri-miRNA level in both fibrosis models, suggesting transcriptional regulation of pri-miRNA–encoding genes (Fig. 5*B* and *SI Appendix*, Fig. S11*C*). While we find all pri-miRNAs significantly down-regulated in the pHSC model, pri-miRNA down-regulation in the CCl_4 model is clear, albeit less pronounced. In agreement, we also observed pre-miRNA down-regulation in the pHSC model (*SI Appendix*, Fig. S11*A*).

To study how AF-miRNAs are regulated at the transcriptional level, we examined 2 major transcriptional regulation mechanisms: binding of potential transcription factors to the promoters of relevant miRNA-encoding genes and CpG methylation changes in promoters of miRNA-encoding genes upon HSC activation.

First, to identify miRNA promoters, we utilized publicly available Global Run-on sequencing (GRO-seq) data. As pri-miRNAs are rapidly cleaved to pre-miRNAs, mapping miRNA transcription start sites (TSSs) using conventional TSS mapping approaches is highly challenging (26). GRO-seq is a technique used to quantify nascent transcripts. GRO-seq data show sharp peaks around TSSs in both the sense and antisense directions and continuous signal of lower intensity throughout the entire transcript, allowing one to map TSSs of very transient transcripts (27). Nine mouse and 6 human GRO-seq datasets, which were retrieved from the GEO database, were used in miRNA TSS analysis. The source tissue/cells used to generate the retrieved datasets are primary fibroblasts, embryonic stem cells, embryonic fibroblasts, and liver tissue samples. Analysis of all datasets yielded consensus TSSs of miRNA-encoding genes which are present in the large majority of the datasets.

Locations of the identified miRNA promoters display high conservation in human and mouse genomes (Fig. 5*C*), indicating conservation of AF-miRNA regulation between mice and humans. To examine whether a majority of AF-miRNAs are regulated by common transcription factors, we used the FIMO tool of the MEME suite (28) to predict transcription factor binding to the mouse and human promoters of AF-miRNA–encoding genes.

To select final candidates of transcription factors, we applied 3 filtering criteria: 1) DNA binding prediction with $\leq$10% FDR, 2) binding to the majority of mouse and human miRNA promoters, and 3) differential expression ($p_{adj} \leq 0.05$) in inactive versus activated hepatic and pancreatic stellate cells (GEO datasets).

This approach identified Pparγ as a potential transcription regulator of mouse and human let-7a, let-7g, miR-338, miR-29c, miR-30e, and miR-30d genes. Pparγ was additionally identified as a potential regulator of mouse let-7c and human miR-335 (Fig. 5*C*). This prediction further indicates conservation of AF-miRNA regulation in mice and humans.

Next, we examined the expression of *Pparg* in our 2 fibrosis models using qPCR. We found that transcription factor *Pparg* is significantly down-regulated upon pHSC activation in both fibrosis models (Fig. 5*A* and *SI Appendix*, Fig. S11*B*).

We sought to confirm experimentally that Pparγ binds to the identified miRNA-encoding gene promoters using chromatin immunoprecipitation (ChIP). Due to the high number of cells required to perform the procedure, we were unable to perform ChIP on pHSCs. Instead, as we hypothesize that

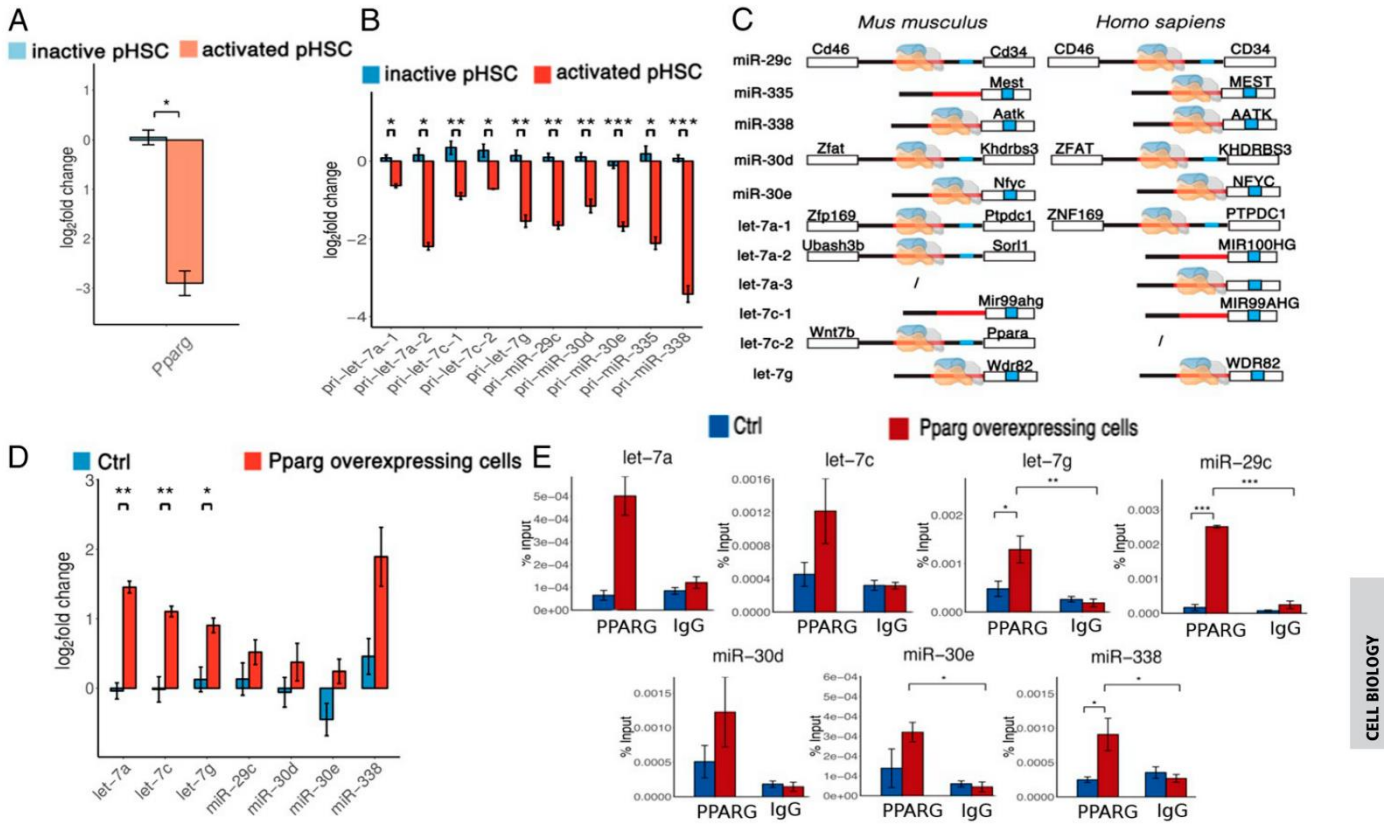

Fig. 5. Transcription factor Pparγ regulates expression of AF-miRNAs. (*A*) Relative expression of *Pparg* in the pHSC in vitro culture model. (*B*) Relative expression of AF-pri-miRNAs in the pHSC in vitro culture model. (*C*) Schematic representation of predicted Pparγ binding to *Mus musculus* (*Left*) and *Homo sapiens* (*Right*) miRNA-encoding gene promoters. miRNA-encoding gene promoters are shown in red, whereas mature miRNAs are indicated in blue. miRNAs located in exons or introns of protein-coding genes share the promoter of the respective protein-coding genes. In the cases of miRNAs located in intergenic regions of the genome, the nearest neighboring genes are shown. Pparγ is depicted on the individual miRNA-encoding gene promoter if it is predicted to bind to the respective promoter. (*D*) Relative expression of AF-miRNAs in a stable Pparγ-overexpressing GRX hepatic stellate cell line. (*E*) ChIP analysis of Pparγ binding to the promoters of AF-miRNAs in a Pparγ-overexpressing GRX (red bars) and control GRX (blue bars) hepatic stellate cell line. (*A–E*) Data are shown as mean and SEM. *p value $\leq$ 0.05, **p value $\leq$ 0.01, ***p value $\leq$ 0.001.

reduced miRNA expression is a consequence of *Pparg* down-regulation, we generated a stable Pparγ-overexpressing GRX hepatic stellate cell line. We used Pparγ-overexpressing and corresponding control cells 1) to quantify mature miRNA expression upon transcription factor up-regulation and 2) to perform ChIP.

All miRNAs predicted to be regulated by Pparγ show a definite trend of up-regulation upon Pparγ overexpression (Fig. 5*D*). miR-335 could not be quantified due to low expression in the GRX cell line.

ChIP analysis showed high-affinity binding of Pparγ to the promoters of AF-miRNA–encoding genes in cells overexpressing Pparγ. Binding of Pparγ was drastically lower in control GRX, demonstrating that expression levels of Pparγ directly modulate its binding to miRNA-encoding gene promoters (Fig. 5*E*).

As genome CpG methylation impinges drastically on gene expression, we examined methylation changes in the promoters of miRNA-encoding genes in pHSCs. We observed significant hypermethylation of let-7a, miR-335, and miR-338 gene promoters upon pHSC activation, suggesting epigenetic mechanisms to contribute to transcriptional control of AF-miRNAs. Although not significant, let-7c-1 and miR-30e promoters were also hypermethylated upon pHSC activation (*SI Appendix*, Fig. S12).

To assess the effects of Pparγ-mediated miRNA expression on fibrotic target genes, stable Pparγ-overexpressing GRX cells were treated with the Pparγ agonist 15-Deoxy-$\Delta^{12,14}$-prostaglandin J_2 (PGJ_2) and simultaneously transfected with either inhibitors of miR-29c or inhibitors of let-7g. In the presence of scrambled inhibitor, the genes *Col1a1*, *Col1a2*, *Col5a2*, and *Adamts14* showed significant down-regulation upon PGJ_2 treatment, whereas the effect was less pronounced for *Loxl2*, *Loxl4*, and *Tgfbr1* (*SI Appendix*, Fig. S13). Inhibition of miR-29c (*SI Appendix*, Fig. S13*A*) and let-7g (*SI Appendix*, Fig. S13*B*) in the presence of PGJ_2 could partially reverse this effect and significantly increase expression of *Col1a1*, *Col1a2*, and *Col5a2* as well as *Tgfbr1*, respectively. These data indicate that multiple fibrosis-associated genes of this network are—at least partially—regulated by Pparγ-mediated expression of the AF-miRNAs miR-29c and let-7g.

In conclusion, we show that AF-miRNAs are significantly down-regulated in our mHCC model, while fibrosis-associated genes are up-regulated. Additionally, we show that AF-miRNAs are significantly down-regulated upon activation of pHSCs. CCl_4 treatment of mice, which induces fibrosis, leads to down-regulation of AF-miRNAs. Furthermore, using a linear regression model, we show that AF-miRNAs significantly contribute to the regulation of fibrosis-associated genes in human fibrosis-associated carcinomas, i.e., HCC, BRCA, LUAD, and LUSC. Also, modulation of AF-miRNA expression (let-7a, let-7c, let-7g, and miR-29c) causes anticorrelated expression of fibrosis-associated target genes. In vitro luciferase assays experimentally

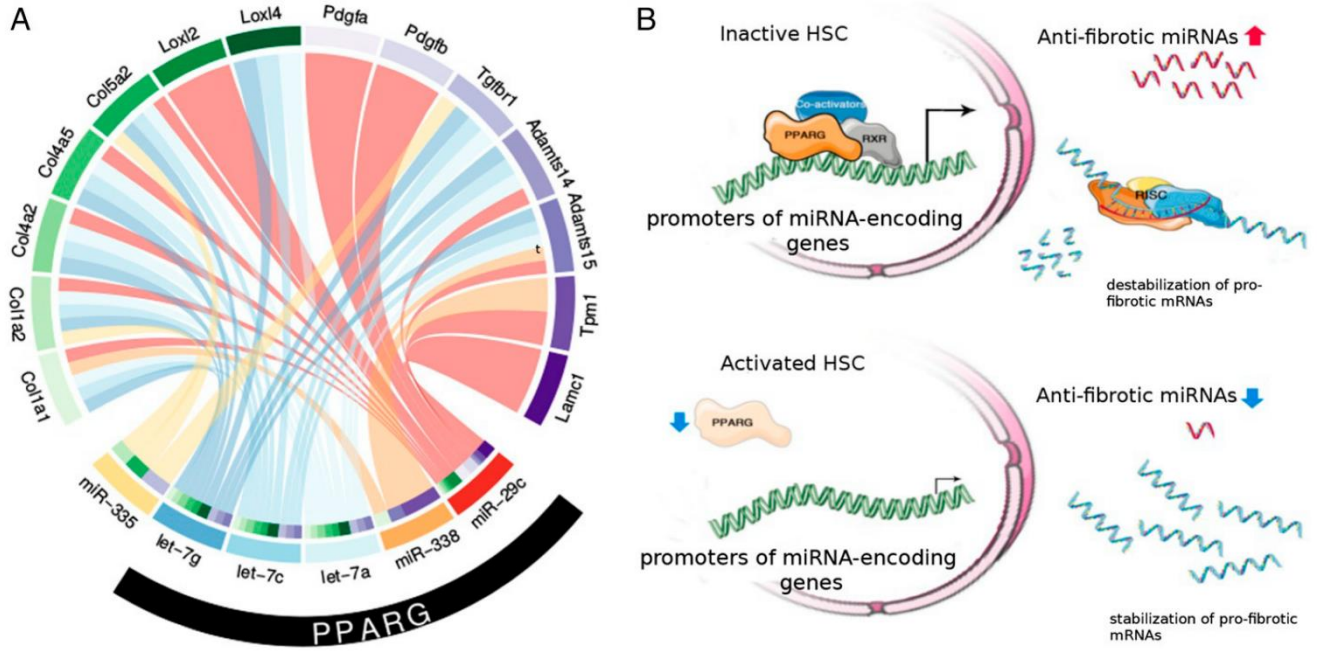

Fig. 6. Schematic displays summarizing the regulation of AF-miRNAs and their target genes. (*A*) Circos plot summarizing the regulation of AF-miRNAs and their target genes. PPARG (black bar) is shown to up-regulate the here-validated miRNAs let-7g-5p, let-7c-5p, let-7a-5p, miR-338-3p, and miR-29c-3p. (*B*) Graphical model summarizing the transcriptional regulation of AF-miRNA–encoding genes by PPARG in HSCs. Reduced expression of PPARG upon activation of HSCs causes down-regulation of AF-miRNA expression. This permits elevated levels of profibrotic mRNAs, leading to the formation of a fibrotic ECM.

confirm predicted targeting of *Col1a1* by miR-29c, let-7a, let-7c, and let-7g; *Pdgfa* by miR-29c; *Tgfbr1* by let-7a, let-7c, and let-7g; and *Adamts15* by miR-29c, miR-338, let-7a, let-7c, and let-7g. Therefore, all results outlined above support the conclusion that AF-miRNAs indeed act as antifibrotic miRNAs.

Based on this conclusion and our findings of AF-miRNA regulation, we propose the following model (Fig. 6): Upon HSC activation, Pparγ expression decreases, consequently causing reduced transcriptional synthesis of antifibrotic pri-miRNAs. Reduced miRNA expression releases their inhibitory effect on fibrosis-associated target mRNAs, thereby increasing the abundance of profibrotic proteins.

Discussion

We identified a network of functionally connected miRNA:mRNA pairs, which regulate cancer-associated fibrosis. This network regulates different structural, signaling, and remodeling ECM components, as well as ECM-linked integrin and Rho-GTPase signaling. We found key miRNA hubs of the network, i.e., miR-29c, miR-335, miR-338, let-7a, let-7c, let-7g, miR-30d, and miR-30e, to be down-regulated in the fibrosis-associated mHCC model, in 2 murine fibrosis models, and in 4 types of human carcinomas.

miR-29c is a known modulator of fibrotic environments in nasopharyngeal carcinoma, shown to reduce mRNA levels of different collagens and LAMC1 (29). We reexamined the role of miR-29c as regulator of fibrosis and experimentally validated *Pdgfa*, *Tpm1*, *Adatms14*, and *Adamts15* as additional fibrosis-linked targets of this miRNA.

McDaniel et al. (30) found the let-7/Lin28 axis to be involved in human HSC activation upon alcoholic liver injury. Given that Lin28 is neither expressed in our mHCC (*SI Appendix*, Table S5, RNA-seq normalized reads) and pHSC culture model nor expressed in the RNA-seq dataset of human HSCs of Zhou et al. (31), we consider Lin28-mediated let-7 regulation in pHSCs and mHCC unlikely. Additionally to Col1a1 (30), we have experimentally validated 4 different collagen family members, Loxl4, and Tgfbr1 as let-7 targets.

To our knowledge, none of the other AF-miRNAs have previously been identified as regulators of fibrosis and none of the AF-miRNAs were previously identified as regulators of fibrotic microenvironments during HCC development.

Our study revealed miRNA-mediated targeting of relevant structural components of the ECM, namely laminin and collagens. Collagens represent the most abundant ECM component and collagen I deposition has been associated with increased incidence of tumor formation and metastasis (21). A study by Ramaswamy et al. (32) found a gene expression signature that distinguishes primary and metastatic adenocarcinomas and predicts the metastatic probability of tumors. A considerable proportion of the gene-expression signature described by Ramaswamy et al. (32) is composed of components of the tumor microenvironment, such as *COL1A1* and *COL1A2*.

We show that, additionally to *Col1a1* and *Col1a2*, AF-miRNAs also regulate other collagen subunits, such as *Col5a2*. Although collagen V is a minor constituent of the ECM compared to collagen I, collagen V is essential for fibrillogenesis, as its deletion leads to inability of collagen fibril assembly (33).

We also demonstrate that AF-miRNAs target components of the PDGF and TGF-β signaling pathways. TGF-β is considered the most potent fibrogenic cytokine. TGF-β binds to type I receptor (Tgfbr1) and causes phosphorylation of downstream SMADs (34), thus inducing SMAD-mediated increased collagen I and III transcription (35). PDGF is a critical mitogen in the liver, which induces HSC proliferation (36).

Furthermore, we have shown that AF-miRNAs regulate remodeling components of the ECM. Tropomyosin 1 (Tpm1), an actin-binding protein, helps in orienting depositions of collagen and laminin in the ECM (37). Adamts proteases process procollagens and regulate collagen fibril deposition (38). We show that *Adamts14* and *Adamts15* are up-regulated in *SRF-VP16*^{iHep}-driven tumors and the CCl_4 mouse model,

but down-regulated in the pHSC model, possibly indicating the necessity of higher Adamts abundance in tissues, where more extensive ECM remodeling may be required. Loxl proteins are primarily responsible for the regulation of collagen cross-linking. Loxl expression strongly correlates with tumor progression, metastasis, and consequently decreased patient survival (39).

Increased ECM stiffness, a consequence of elevated ECM deposition and remodeling, causes activation of MAPKs and Rho-GTPases via integrin signaling. Although we experimentally focus on miRNA-mediated ECM targeting, it is worth mentioning that the identified AF-miRNAs were also predicted to target integrin and Rho-GTPase signaling. These pathways are strong stimulators of tumor migration, invasion, and proliferation (40). Integrin $\alpha5\beta1$ promotes cell invasion by sensitizing cancer cells to the changes in the ECM (41), while Rho-GTPases are indispensable in the regulation of cell migration and control of multiple aspects of M phase and G_1 progression of the cell cycle (40).

Mechanistically, we show that AF-miRNAs are regulated by the transcription factor Pparγ. We show that *Pparg* expression, along with AF-miRNAs, is reduced in vivo and in vitro upon HSC activation and that overexpression of *Pparg* leads to increased AF-miRNA expression. Furthermore, we demonstrate direct Pparγ binding to the AF-miRNA–encoding promoters.

Pparγ heterodimerizes with the retinoid acid receptor (Rxr) and, upon DNA binding, recruits RNA polymerase and coactivators with histone acetyl transferase activity, causing remodeling of chromatin and enhancing transcription (42). Pparγ:Rxr interacts with the peroxisome-proliferator response element (PPRE) in the promoter of its target genes. PPREs are typically found in various genes involved in lipid metabolism and energy homeostasis (43).

Additional to its role in the regulation of lipid metabolism, Pparγ's involvement in HSC activation has also been described. Pparγ sustains HSC quiescence and promotes deactivation of HSCs (44). A study by Marra et al. (45) showed that PPARγ inhibits HSC proliferation, migration, and chemokine expression, thus inhibiting fibrogenesis. Furthermore, HSC-specific interference of PPARγ signaling aggravates liver damage and fibrosis induced by CCl_4 treatment (46). Studies conducted so far concluded that PPARγ exerts its antifibrotic effects primarily by antagonizing TGF-β signaling (38). Here, we propose an additional mechanism of Pparγ-mediated regulation of fibrosis via stimulation of antifibrotic miRNA expression.

Transcription factors frequently regulate one or more classes of functionally related protein-coding genes. Pparγ has been previously identified as a regulator of lipid-metabolism–related genes (43) and of fibrosis. Here, we find Pparγ regulates a functionally connected class of miRNAs with antifibrotic properties. However, our discovery of antifibrotic miRNAs targeting key fibrosis-associated genes and Pparγ-directed regulation of antifibrotic miRNAs describes an intricate coherent feed-forward loop, whereby miRNAs and transcription factors regulate common targets, thus significantly adding to the understanding of Pparγ's role in fibrosis regulation.

Activation of HSCs and down-regulation of miRNA expression occur in quite a short time (up to 7 d) in our experimental setup. Initial miRNA down-regulation correlates well with down-regulation of the positive regulator of AF-miRNA expression *Pparg*. However, we also identified hypermethylation of let-7a, let-7c-1, miR-335, miR-338, and miR-30e gene promoters upon pHSC activation. In our window of measurement, the identified methylation changes in all miRNA gene promoters are quite subtle. However, it is possible that initial changes in miRNA expression are mediated through transcription factor regulation, while more long-term changes are established through changes in the methylation of miRNA promoters.

In the last decade, several individual miRNA:target interactions have been characterized in fibrosis and HCC. However, such approaches ignore the complexity of miRNA signaling networks. Therefore, we use transcriptome-wide experimental and bioinformatical tools to identify miRNA hubs that influence HCC and its fibrotic microenvironment. We show a complex network of 8 miRNA hubs that target 54 ECM-related genes together regulate structural, signaling, and remodeling components of the fibrotic microenvironment.

Our findings indicate that the let-7 and miR-30 miRNA families, as well as miR-29c, miR-335, and miR-338, are important antifibrotic microRNAs. We show that these miRNAs are down-regulated in the fibrosis-associated mHCC model, in 2 murine fibrosis models, and in 4 types of human carcinomas.

Using a multivariate model, which assesses whether examined genes are indeed more likely to be targeted by miRNAs or by CpG methylation and CNV, we showed that AF-miRNAs considerably contribute to fibrosis-associated gene regulation in vivo in different human fibrosis-facilitated carcinomas and that changes in fibrosis-associated gene expression are more consistent with changes in miRNA expression than with changes in CNV or methylation.

The fact that a substantial part of the proteins in the described network is regulated through the activity of such a limited number of miRNAs emphasizes the relevance of miRNAs as powerful mediators of complex biological processes, in this case fibrosis.

A noteworthy aspect of our study is the identification of Pparγ as a major transcription factor which regulates 7 of 8 miRNA hubs, therefore identifying Pparγ as a regulator of a functionally connected class of miRNAs with antifibrotic properties.

Additionally, as all aforementioned miRNAs, with the exception of miR-335, are regulated—to a major extent—by Pparγ, this transcription factor represents an attractive stimulatory target for antifibrotic therapy.

Materials and Methods

To profile the whole miRNome, sRNA-seq was performed on liver tumor and nodular tissue of *SRF-VP16^{iHep}* mice alongside the corresponding controls. The library was generated using TruSeq Small RNA Library Prep Kits v2 (Illumina) according to the manufacturer's protocol. Subsequent to identification of tumor-associated miRNAs, we performed screening of potential miRNA targets using the DIANA microT-CDS (17) and TargetScan (18) databases. To increase the accuracy of down-regulated miRNA target predictions, we performed RNA-seq analyses on largely overlapping samples as used for sRNA-seq.

To quantify mature miRNA, pre-miRNA, and pri-miRNA expression in RNA samples of fibrosis models, total RNA was reverse transcribed using the miScript II RT Kit (Qiagen) and the miScript SYBR Green PCR Kit (Qiagen) was used to quantify the RNA expressions.

To experimentally validate the functionality of predicted miRNA targeting, a luciferase gene reporter assay was used.

To validate PPARγ binding to miRNA promoters, the ChIP protocol based on the procedure described by Daniel et al. (47) was used with some modifications.

Detailed description of all animal models, materials, and methods is contained in *SI Appendix*.

Data Availability. sRNA-seq and RNA-seq FASTQ data are deposited in the NCBI Sequence Read Archive (SRA) under accession no. Bioproject: PRJNA522967.

The code for the bioinformatic analysis is available at https://ivanawinkler.github.io/mirna_paper/.

Requests for resources and reagents should be directed to and will be fulfilled by the corresponding author (A.N.).

ACKNOWLEDGMENTS. We thank Elisa Izaurralde, who sadly passed away, for her continuous support. Brigitte Begher-Tibbe, Marion Bähr, and Heidemarie Riehle provided excellent technical support in immunostainings, methylation studies, and cell culture work, respectively. This work received financial support from the International Max Planck Research School (University Tübingen) (to I.W., C.B., S.W., O.K., and A.N.). Further support to

A.N., I.W., and C.B. came from the Deutsche Konsortium für Translationale Krebsforschung (DKTK) Joint Funding Consortium "Noncoding mutations in cancer genomes." Additional support to A.N. came from the Deutsche Forschungsgemeinschaft (DFG [German Research Foundation] - Project-ID 314905040 - TRR 209) and the German Cancer Aid (Project 109886). Further funding was provided by the Deutsches Bundesministerium für Bildung und Forschung (BMBF; LiSyM Project 031L0045, to J.G.H.). R.W. is supported by the DFG (SFB/TRR 57) and the Interdisciplinary Center for Clinical Research within the Faculty of Medicine at the Rheinisch-Westfälische Technische Hochschule (RWTH) Aachen (Project O3-1).

1. H. B. El-Serag, Hepatocellular carcinoma. *N. Engl. J. Med.* **365**, 1118–1127 (2011).
2. A. Forner, M. Reig, J. Bruix, Hepatocellular carcinoma. *Lancet* **391**, 1301–1314 (2018).
3. S. Ohrnberger *et al.*, Dysregulated serum response factor triggers formation of hepatocellular carcinoma. *Hepatology* **61**, 979–989 (2015).
4. E. N. Olson, A. Nordheim, Linking actin dynamics and gene transcription to drive cellular motile functions. *Nat. Rev. Mol. Cell Biol.* **11**, 353–365 (2010).
5. V. Hernandez-Gea, S. Toffanin, S. L. Friedman, J. M. Llovet, Role of the microenvironment in the pathogenesis and treatment of hepatocellular carcinoma. *Gastroenterology* **144**, 512–527 (2013).
6. V. Hernandez-Gea, S. L. Friedman, Pathogenesis of liver fibrosis. *Annu. Rev. Pathol.* **6**, 425–456 (2011).
7. R. Kalluri, M. Zeisberg, Fibroblasts in cancer. *Nat. Rev. Cancer* **6**, 392–401 (2006).
8. F. Heindryckx, P. Gerwins, Targeting the tumor stroma in hepatocellular carcinoma. *World J. Hepatol.* **7**, 165–176 (2015).
9. A. Lujambio, S. W. Lowe, The microcosmos of cancer. *Nature* **482**, 347–355 (2012).
10. D. P. Bartel, MicroRNAs: Target recognition and regulatory functions. *Cell* **136**, 215–233 (2009).
11. M. Ha, V. N. Kim, Regulation of microRNA biogenesis. *Nat. Rev. Mol. Cell Biol.* **15**, 509–524 (2014).
12. C. P. Bracken, H. S. Scott, G. J. Goodall, A network-biology perspective of microRNA function and dysfunction in cancer. *Nat. Rev. Genet.* **17**, 719–732 (2016).
13. Y. A. Lee, M. C. Wallace, S. L. Friedman, Pathobiology of liver fibrosis: A translational success story. *Gut* **64**, 830–841 (2015).
14. J. Winter, S. Jung, S. Keller, R. I. Gregory, S. Diederichs, Many roads to maturity: MicroRNA biogenesis pathways and their regulation. *Nat. Cell Biol.* **11**, 228–234 (2009).
15. E. Anastasiadou, L. S. Jacob, F. J. Slack, Non-coding RNA networks in cancer. *Nat. Rev. Cancer* **18**, 5–18 (2018).
16. S. L. Friedman, Hepatic stellate cells: Protean, multifunctional, and enigmatic cells of the liver. *Physiol. Rev.* **88**, 125–172 (2008).
17. M. Reczko, M. Maragkakis, P. Alexiou, I. Grosse, A. G. Hatzigeorgiou, Functional microRNA targets in protein coding sequences. *Bioinformatics* **28**, 771–776 (2012).
18. R. C. Friedman, K. K. Farh, C. B. Burge, D. P. Bartel, Most mammalian mRNAs are conserved targets of microRNAs. *Genome Res.* **19**, 92–105 (2009).
19. M. Kanehisa, S. Goto, KEGG: Kyoto encyclopedia of genes and genomes. *Nucleic Acids Res.* **28**, 27–30 (2000).
20. A. Fabregat *et al.*, Reactome graph database: Efficient access to complex pathway data. *PLoS Comput. Biol.* **14**, e1005968 (2018).
21. D. M. Gilkes, G. L. Semenza, D. Wirtz, Hypoxia and the extracellular matrix: Drivers of tumour metastasis. *Nat. Rev. Cancer* **14**, 430–439 (2014).
22. S. Weiskirchen, C. G. Tag, S. Sauer-Lehnen, F. Tacke, R. Weiskirchen, Isolation and culture of primary murine hepatic stellate cells. *Methods Mol. Biol.* **1627**, 165–191 (2017).
23. D. Scholten, J. Trebicka, C. Liedtke, R. Weiskirchen, The carbon tetrachloride model in mice. *Lab. Anim.* **49**(Suppl. 1), 4–11 (2015).
24. M. A. Newman, J. M. Thomson, S. M. Hammond, Lin-28 interaction with the Let-7 precursor loop mediates regulated microRNA processing. *RNA* **14**, 1539–1549 (2008).
25. A. Jacobsen *et al.*, Analysis of microRNA-target interactions across diverse cancer types. *Nat. Struct. Mol. Biol.* **20**, 1325–1332 (2013).
26. Q. Liu *et al.*, Identification of active miRNA promoters from nuclear run-on RNA sequencing. *Nucleic Acids Res.* **45**, e121 (2017).
27. L. J. Core, J. J. Waterfall, J. T. Lis, Nascent RNA sequencing reveals widespread pausing and divergent initiation at human promoters. *Science* **322**, 1845–1848 (2008).
28. C. E. Grant, T. L. Bailey, W. S. Noble, FIMO: Scanning for occurrences of a given motif. *Bioinformatics* **27**, 1017–1018 (2011).
29. S. Sengupta *et al.*, MicroRNA 29c is down-regulated in nasopharyngeal carcinomas, up-regulating mRNAs encoding extracellular matrix proteins. *Proc. Natl. Acad. Sci. U.S.A.* **105**, 5874–5878 (2008).
30. K. McDaniel *et al.*, The let-7/Lin28 axis regulates activation of hepatic stellate cells in alcoholic liver injury. *J. Biol. Chem.* **292**, 11336–11347 (2017).
31. C. Zhou *et al.*, Long noncoding RNAs expressed in human hepatic stellate cells form networks with extracellular matrix proteins. *Genome Med.* **8**, 31 (2016).
32. S. Ramaswamy, K. N. Ross, E. S. Lander, T. R. Golub, A molecular signature of metastasis in primary solid tumors. *Nat. Genet.* **33**, 49–54 (2003).
33. J. K. Mouw, G. Ou, V. M. Weaver, Extracellular matrix assembly: A multiscale deconstruction. *Nat. Rev. Mol. Cell Biol.* **15**, 771–785 (2014).
34. R. Derynck, Y. E. Zhang, Smad-dependent and Smad-independent pathways in TGF-beta family signalling. *Nature* **425**, 577–584 (2003).
35. D. A. Mann, F. Marra, Fibrogenic signalling in hepatic stellate cells. *J. Hepatol.* **52**, 949–950 (2010).
36. A. Pellicoro, P. Ramachandran, J. P. Iredale, J. A. Fallowfield, Liver fibrosis and repair: Immune regulation of wound healing in a solid organ. *Nat. Rev. Immunol.* **14**, 181–194 (2014).
37. A. J. Hayes, M. Benjamin, J. R. Ralphs, Role of actin stress fibres in the development of the intervertebral disc: Cytoskeletal control of extracellular matrix assembly. *Dev. Dyn.* **215**, 179–189 (1999).
38. C. Bonnans, J. Chou, Z. Werb, Remodelling the extracellular matrix in development and disease. *Nat. Rev. Mol. Cell Biol.* **15**, 786–801 (2014).
39. H. E. Barker, T. R. Cox, J. T. Erler, The rationale for targeting the LOX family in cancer. *Nat. Rev. Cancer* **12**, 540–552 (2012).
40. A. B. Jaffe, A. Hall, Rho GTPases: Biochemistry and biology. *Annu. Rev. Cell Dev. Biol.* **21**, 247–269 (2005).
41. H. Hamidi, J. Ivaska, Every step of the way: Integrins in cancer progression and metastasis. *Nat. Rev. Cancer* **18**, 533–548 (2018).
42. J. M. Peters, Y. M. Shah, F. J. Gonzalez, The role of peroxisome proliferator-activated receptors in carcinogenesis and chemoprevention. *Nat. Rev. Cancer* **12**, 181–195 (2012).
43. L. Michalik, B. Desvergne, W. Wahli, Peroxisome-proliferator-activated receptors and cancers: Complex stories. *Nat. Rev. Cancer* **4**, 61–70 (2004).
44. L. Michalik, W. Wahli, Involvement of PPAR nuclear receptors in tissue injury and wound repair. *J. Clin. Invest.* **116**, 598–606 (2006).
45. F. Marra *et al.*, Ligands of peroxisome proliferator-activated receptor gamma modulate profibrogenic and proinflammatory actions in hepatic stellate cells. *Gastroenterology* **119**, 466–478 (2000).
46. T. Tsuchida, S. L. Friedman, Mechanisms of hepatic stellate cell activation. *Nat. Rev. Gastroenterol. Hepatol.* **14**, 397–411 (2017).
47. B. Daniel, B. L. Balint, Z. S. Nagy, L. Nagy, Mapping the genomic binding sites of the activated retinoid X receptor in murine bone marrow-derived macrophages using chromatin immunoprecipitation sequencing. *Methods Mol. Biol.* **1204**, 15–24 (2014).

3.4 Discussion

Here, I expand on the discussion of our publication "Identification of Pparγ-modulated miRNA hubs that target the fibrotic tumor microenvironment" by Winkler *et al.* (2020) (**Project A**) [103]. To summarize, we initially identified the 8 AF-miRNAs let-7a, let-7c, let-7g, miR-29c, miR-30d, miR-30e, miR-338, and miR-335 to be downregulated in the SRF-VP16^{iHep} model of murine HCC. We further showed that these AF-miRNAs are also downregulated in liver fibrosis independent of HCC. Mechanistically, we demonstrated that these miRNAs collectively regulate fibrotic target genes comprising structural, signaling, and remodeling components of the ECM, thus forming an interconnected AF-miRNA network. We experimentally confirmed direct miRNA:target interaction for 14 of these fibrotic target genes, namely *Col1a1*, *Col1a2*, *Col4a2, Col4a5*, *Col5a2*, laminin gamma 1 (*Lamc1*), *Loxl2*, lysyl oxidase-like 4 (*Loxl4*), *Pdgfa*, *Pdgfb*, *Tgfbr1*, Tropomyosin 1 (*Tpm1*) as well as ADAM metallopeptidase with thrombospondin type 1 motif 14 (*Adamts14*) and 15 (*Adamts15*). We further showed that the miRNAs and genes themselves as well as most of the miRNA:target interactions are conserved between mouse and human. We identified HSCs as the cell type in which the AF-miRNA network is active and showed mechanistically, that the AF-miRNAs are collectively regulated by the transcription factor PPARG [103].

Of the AF-miRNAs identified by us in liver fibrosis, miR-29c was previously reported to exert anti-fibrotic functions [96,97]. miR-29c is known to modulate LAMC1 and different collagens in the fibrotic microenvironment of nasopharyngeal carcinoma [141] as well as LAMC1 during prostate cancer cell migration [142]. We confirmed targeting of *Lamc1* and collagens by miR-29c also in liver fibrosis and in the fibrotic HCC microenvironment, and we further identified *Pdgfa*, *Adamts14*, *Adamts15*, and *Tpm1* as additional fibrotic targets of miR-29c [103]. Huang *et al.* (2020) showed that *Tpm1* is also targeted by miR-29c in murine renal fibrosis [143], thus confirming our findings and expanding the role of miR-29c as anti-fibrotic miRNA outside the liver. Furthermore, Yin *et al.* (2020) showed that miR-29b of the highly conserved miR-29 family [144] as well as miR-30d both directly target LOXL4 in human breast cancer cells [145]. Even though we could not confirm direct *Loxl4* targeting by miR-29c and did not perform target validation experiments for the miR-30 family, we have however shown direct *Loxl4* targeting by the let-7 miRNA family [103]. We further found *Loxl4* upregulated in all tested models of HCC and liver fibrosis and thus defined *Loxl4* as part of the AF-miRNA network [103]. In addition to *Loxl4*, we experimentally validated the collagens *Col1a1*, *Col1a2*, *Col4a2*, *Col4a5*, and *Col5a2* as well as *Tgfbr1* as targets of the let-7 family, of which, to our knowledge, only *Col1a1* was previously reported as let-7 target by McDaniel *et al.* (2017) [101]. To our knowledge, we were also the first to describe the miR-30 family as well as miR-338 and miR-335 as

regulators of fibrosis and are the first to identify an interconnected network of miRNAs and ECM-related target genes to regulate the fibrotic microenvironment of HCC [103].

We identified the AF-miRNAs to collectively target genes encoding structural, signaling, and remodeling ECM components [103]. Excessive accumulation of structural ECM components, especially collagens and laminins, is characteristic for fibrosis and the fibrotic tumor microenvironment [56]. Here, we validated five members of the collagen family as well as the laminin *Lamc1* as targets of the AF-miRNAs [103]. We further validated the AF-miRNAs to target components of the PDGF and TGF-β signaling pathways, namely *Pdgfa*, *Pdgfb*, and *Tgfbr1* [103]. While PDGF, composed of PDGFA and PDGFB in one of three dimeric forms (-AA, -AB, and -BB), is a critical mitogen stimulating HSC proliferation and migration, TGF-β is generally considered the most potent fibrogenic cytokine driving HSC activation upon binding to its receptor TGFBR1 [9,146]. Besides structural and signaling components of the ECM, we also showed that the AF-miRNAs regulate the ECM-remodeling genes *Tpm1, Adamts14*, *Adamts15, Loxl2*, and *Loxl4* [103]. TPM1 is an actin-binding protein which facilitates correct orientation of collagen depositions within the forming ECM [147]. Of the ADAMTS protease family, ADAMTS14 processes pro-collagens and regulates collagen fibril deposition, while ADAMTS15 cleaves proteoglycans in the ECM, allowing the release of signaling molecules and growth factors [56,148]. The Lysyl oxidase (LOX) family, including LOXL2 and LOXL4, mediates collagen cross-linking that results in increased ECM stiffness [56]. Indeed, it was shown that LOXL2 inhibition reduced liver fibrosis progression in a TAA mouse model [149] and targeting the LOX family is currently researched for anti-cancer drug development [57]. In addition to the experimentally validated target genes, we also predicted the AF-miRNAs to target further ECM-related genes as well as multiple components of the integrin and Rho-GTPase signaling pathways [103]. Integrins on the cell surface connect the ECM to the actin cytoskeleton via Rho-GTPase signaling, which regulates cell migration via actin dynamics [150]. Increased ECM stiffness, which is a hallmark of liver fibrosis, activates such integrin pathways and promotes migration, invasion, and proliferation of both fibroblasts and tumor cells [56].

Mechanistically, we demonstrated that the AF-miRNAs are directly and collectively regulated by the transcription factor PPARG [103]. PPARG is a ligand-activated transcription factor which heterodimerizes with a retinoid X receptor (RXR) to bind to peroxisome proliferator response elements (PPREs) in promoter regions of genomic DNA [61]. DNA binding induces transcription of diverse PPARG target genes involved in glucose and lipid metabolism and in cell differentiation [151]. Additionally, PPARG is known to influence HSC activation and fibrosis progression in the liver [9]. HSC activation is associated with reduced PPARG expression and activity, while PPARG overexpression or activation through agonists can revert HSCs to a quiescent phenotype [40,62]. Accordingly, we observed reduced *Pparg* expression, along with reduced AF-miRNA expression, *in vitro* during HSC activation as well as

in vivo in CCl_4-induced liver fibrosis in mice [103]. So far, PPARG has been described to maintain HSC quiescence mainly through antagonizing pro-fibrotic TGF-β signaling [152]. Here, we suggest a new supplementary mechanism, where PPARG maintains high AF-miRNA expression in quiescent HSCs to inhibit overexpression of ECM-related genes in healthy tissue [103].

Since the discovery of miRNAs as post-transcriptional regulators of gene expression, the function of individual miRNAs in linear signaling cascades has been studied excessively, and several miRNA:target gene pairs have been characterized in fibrosis and HCC [95–97]. However, the complexity of signaling networks and miRNA networks is often neglected. Transcription factors and miRNAs typically regulate multiple – often functionally connected – downstream genes simultaneously and represent points of signal convergence in a network [85]. These points of signal convergence, also known as hubs, are likely able to explain network behavior and are therefore especially suited as targets for drug development or as predictors of clinical outcome [85]. In the here identified AF-miRNA network, comprised of 8 miRNAs targeting 54 fibrosis-associated genes, each of the AF-miRNAs targets at least 8 ECM-related genes, making them key hubs of the network [103]. Regulating 7 of the 8 identified AF-miRNAs, the transcription factor PPARG is considered an additional hub of the AF miRNA network [103].

Overall, the identified PPARG-regulated AF-miRNA network demonstrates how a limited number of functionally connected miRNAs can collectively regulate complex biological processes, in this case fibrosis and the formation of a fibrotic tumor microenvironment [103].

4 Project B: The AF-miRNA Network in Different Liver Fibrosis Models, Fibrotic Stages, and Model Organisms

4.1 Summary

We previously identified the AF-miRNA network in *SRF-VP16*^{iHep} mice, where 8 AF-miRNAs were found downregulated and their fibrosis-associated target genes upregulated in the fibrotic microenvironment of HCC tumors (**Project A**) [103]. We further confirmed that the AF-miRNA network is also dysregulated in a 6 weeks CCl_4-induced liver fibrosis model, emphasizing its importance in fibrosis progression independent of HCC.

Liver fibrosis is a complex disease arising from different etiologies [9]. To assess how variations in liver fibrogenesis affect the AF-miRNA network, I studied its expression patterns in several rodent models of liver fibrosis along three different parameters. One, I assessed to which degree the AF-miRNA network is conserved to the rat as most common model organism besides the mouse [153]. For this, conservation of individual miRNA:target gene pairs between mouse and rat was examined bioinformatically, and gene expression patterns of the AF-miRNA network were compared in a mouse model and a rat model of BDL-mediated liver fibrosis. Furthermore, I investigated the expression of the AF-miRNA network at different stages of liver fibrosis progression. In the mouse, a 2 months and a 12 months CCl_4-induced liver fibrosis model were compared to the previously analyzed 6 weeks CCl_4-induced liver fibrosis model and *SRF-VP16*^{iHep} mouse model of fibrotic HCC [103]. In the rat, expression of the AF-miRNA network was compared between a 4 weeks and a 10 weeks TAA-induced liver fibrosis model. Lastly, in the model systems of CCl_4-induced, TAA-induced, and BDL-mediated liver fibrosis, different procedures are applied to induce liver fibrosis [112]. These fibrosis models were compared to assess how the cause and context of fibrosis influences the AF-miRNA network.

Studying the AF-miRNA network in these liver fibrosis models in mouse and rat, I demonstrate that AF-miRNA dysregulation is highly context-specific and differs most strongly between the fibrotic ECM of the liver fibrosis models on the one hand and the fibrotic tumor microenvironment of the *SRF-VP16*^{iHep} model of HCC on the other hand.

4.2 Contributions

The following colleagues and collaboration partners contributed to the results of **Project B**.

Figure	Contribution
4.1-4.2	Abhishek Thavamani[1] prepared RNA-seq libraries from liver tissue samples of *SRF-VP16^{iHep}* mice and Ivana Winkler[1] processed *SRF-VP16^{iHep}* and TCGA RNA-seq data as part of **Project A** [103]. Jan G. Hengstler[2] provided RNA-seq data and RNA samples of 2 months and 12 months CCl_4-treated mice generated in Ghallab *et al.* (2019) [109]. **Catrin Bitter**[1] analyzed and visualized RNA-seq data and performed miRNA qPCR measurements.
4.3	**Catrin Bitter** performed conserved miRNA targeting analyses and generated circos plots.
4.4-4.6	Teresa Peccerella[3] performed 4 weeks and 10 weeks TAA as well as 4 weeks BDL experiments in rat. Sebastian Mueller[3] provided rat data of blood serum markers and rat liver tissue samples. **Catrin Bitter** analyzed and visualized data of blood serum markers and isolated RNA from rat liver tissue. Ralf Weiskirchen[4] provided RNA samples isolated from liver tissue of a 2 weeks mouse BDL experiment. **Catrin Bitter** performed gene and miRNA qPCR measurements of the four rodent models.
S4	**Catrin Bitter** analyzed and visualized RNA-seq data described for Figure 4.1.
S5-S8	**Catrin Bitter** generated heatmaps from RNA-seq data described for Figure 4.1.
S9	**Catrin Bitter** performed qPCR of 2 weeks mouse BDL samples described for Figure 4.4.
Other	**Catrin Bitter** designed the research together with Alfred Nordheim[1] as supervisor. **Catrin Bitter** analyzed the presented data and wrote the results and discussion presented below.

[1] Dr. Abhishek Thavamani, Dr. Ivana Winkler, Catrin Bitter, and Prof. Dr. Alfred Nordheim: Department for Molecular Biology, IFIZ, Eberhard Karls University Tübingen, Germany.

[2] Prof. Dr. Jan G. Hengstler: Department of Toxicology, Leibniz Research Centre for Working Environment and Human Factors (IfADo), Dortmund, Germany.

[3] Dr. Teresa Peccerella and Prof. Dr. Sebastian Mueller: Center for Alcohol Research, University of Heidelberg and Salem Medical Center, Heidelberg, Germany.

[4] Prof. Dr. Ralf Weiskirchen: Experimental Gene Therapy and Clinical Chemistry, Institute of Molecular Pathobiochemistry, University Hospital RWTH Aachen, Germany.

4.3 Results

4.3.1 The AF-miRNA Network During Progression of CCl_4-induced Liver Fibrosis in Mice

We previously identified the AF-miRNA network, comprised of 8 miRNAs and 54 fibrotic target genes, in the *SRF-VP16*^{iHep} mouse model of murine HCC, where it regulates the fibrotic tumor microenvironment (**Project A**) [103]. We showed that the described network also operates to varying degrees in human HCC as well as in three other human cancers typically arising in fibrotic microenvironments. Since the AF-miRNAs function in HSCs by targeting fibrotic genes, we further investigated the AF-miRNA network in liver fibrosis independent of HCC and confirmed downregulation of AF-miRNAs and upregulation of their targets in liver fibrosis induced by 6 weeks of CCl_4 treatment in mice [103].

To investigate how the AF-miRNA network behaves over the time course of liver fibrosis progression, I analyzed RNA samples and RNA-seq data of C57BL/6 mice after 2 months and 12 months of CCl_4-induced liver fibrosis and their time-matched oil controls generated by Ghallab *et al.* (2019) [109]. First, the degree of liver fibrosis progression in these samples was assessed on Sirius Red stainings of liver specimens to visualize collagen depositions (Figure 1 of Ghallab *et al.* (2019)) [7,109]. After 2 months of CCl_4 treatment, fibrosis was relatively mild but progressed into severe fibrosis after 12 months, characterized by wide streets of Sirius Red positive areas as well as the development of fibrosis-associated tumor nodules (Figure 1 of Ghallab *et al.* (2019)) [109]. The degree of liver fibrosis after 12 months of CCl_4 treatment was comparable to the fibrotic microenvironment of tumorous livers of *SRF-VP16*^{iHep} mice (Figure 1A, B of Winkler *et al.* (2020)) [103].

After confirming progressing liver fibrosis in these samples, the provided RNA-seq data of 2 months and 12 months CCl_4-treated mice were analyzed for gene expression of the fibrotic target genes of the AF-miRNA network. Initially, the AF-miRNA network was defined by identification of anti-correlated miRNA:target gene pairs dysregulated in *SRF-VP16*^{iHep} tumors and conserved to human HCC (TCGA cohort) [103]. This bioinformatic analysis had revealed upregulation of 59 fibrosis-associated genes including structural, signaling, and remodeling components of the ECM as well as genes related to integrin signaling and Rho-GTPase signaling, which are collectively targeted by the AF-miRNAs (Figure 1C of Winkler *et al.* (2020)) [103]. To compare expression levels of these fibrotic target genes in the *SRF-VP16*^{iHep} tumors and in human HCC (TCGA cohort) to the 2 months and 12 months CCl_4-induced fibrosis models, I re-visualized the available RNA-seq data of **Project A** [103] to demonstrate significant upregulation of all fibrotic target genes in *SRF-VP16*^{iHep} tumors of murine HCC (**Figure 4.1a**, **Supplementary Figure 4a** and **Supplementary Figure 5**) as well as significant upregulation of most fibrotic target genes in the TCGA cohort of human HCC (**Figure 4.1b**, **Supplementary Figure 4b**, and **Supplementary Figure 6**).

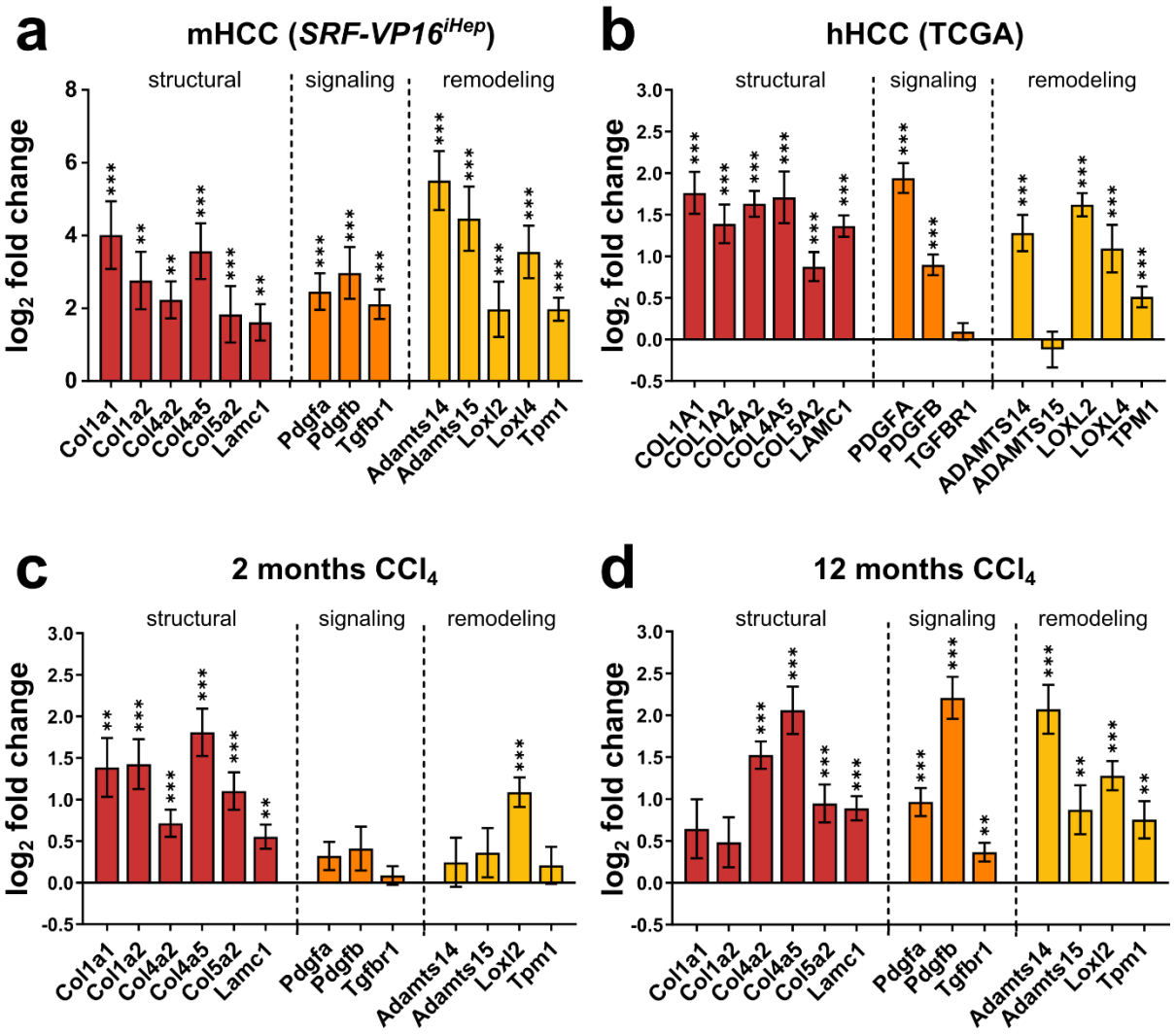

Figure 4.1 | Expression of the 14 validated fibrotic target genes of the AF-miRNA network in HCC and liver fibrosis. Relative gene expression of structural, signaling, and remodeling ECM components of the AF-miRNA network in (**a**) mHCC (*SRF-VP16*^{iHep} tumors) (n=4/group), (**b**) hHCC (TCGA cohort) (n=50 controls, n=374 tumors), and in (**c**) 2 months and (**d**) 12 months CCl_4-induced liver fibrosis (n=6/group each). Data are shown as log_2 fold change in disease (mHCC/hHCC/2 months CCl_4/12 months CCl_4) compared to control (litter mate/healthy liver/2 months oil/12 months oil) in each RNA-seq dataset as analyzed by DESeq2. Data are shown as mean and SEM. * $p_{adj} \leq 0.05$, ** $p_{adj} \leq 0.01$, *** $p_{adj} \leq 0.001$. CCl_4 – carbon tetrachloride, hHCC – human HCC, mHCC – murine HCC, HCC – hepatocellular carcinoma.

Of the 59 fibrotic target genes of the AF-miRNA network, 50 were detected in RNA-seq of 2 months and 12 months CCl_4-induced liver fibrosis (**Supplementary Figure 4c**, **d**, **Supplementary Figure 7**, **Supplementary Figure 8**). After 2 months of CCl_4 treatment, 18 of the 50 target genes were significantly upregulated (**Supplementary Figure 4c**), including 7 of the 14 target genes experimentally validated by us in Winkler *et al.* (2020), namely *Col1a1*, *Col1a2*, *Col4a2*, *Col4a5*, *Col5a2*, *Lamc1*, and *Loxl2* (**Figure 4.1c**) [103]. With progressed fibrosis after 12 months of CCl_4 treatment, significant upregulation was observed for 42 of the 50 fibrotic target genes (**Supplementary Figure 4d**), including the 11 validated target genes *Col4a2*, *Col4a5*, *Col5a2*, *Lamc1*, *Pdgfa*, *Pdgfb*, *Tgfbr1*, *Adamts14*,

Adamts15, *Loxl2*, and *Tpm1* (**Figure 4.1d**). Interestingly, *Col1a1* and *Col1a2* were not significantly upregulated in the RNA-seq data, while Sirius Red staining indicated massive collagen depositions after 12 months of CCl_4 treatment (Figure 1 of Ghallab *et al.* (2019)) [109]. Since Sirius Red simultaneously stains collagens type I and III [154], it is possible that most of the collagen deposition detected by Sirius Red staining is derived from other collagen members not part of the AF-miRNA network. Most fibrotic target genes of the AF-miRNA network showed higher log_2 fold change values after 12 months than after 2 months of CCl_4 treatment (**Figure 4.1**, **Supplementary Figure 4**). Overall, this demonstrates that liver fibrosis progressed from 2 months to 12 months of CCl_4 treatment, at which point the degree of fibrotic target gene upregulation was comparable to the TCGA cohort of human HCC, but lower than in *SRF-VP16*^{iHep} tumors (**Figure 4.1**, **Supplementary Figure 4**).

The observed upregulation of the fibrotic target genes suggests that the AF-miRNA network is active in the CCl_4 model of liver fibrosis [103]. However, qPCR expression analysis of the 8 AF-miRNAs in 2 months and 12 months CCl_4-induced liver fibrosis showed only mild overall downregulation of the AF-miRNAs (**Figure 4.2a, b**). Only two AF-miRNAs were significantly downregulated, miR-29c at 2 months and let-7g at 12 months. In contrast, the 8 AF-miRNAs were all significantly downregulated in the microenvironment of *SRF-VP16*^{iHep} tumors, measured both by sRNA-seq (Figure 2B, C of Winkler *et al.* (2020)) [103] as well as by qPCR (**Figure 4.2c**) in the same samples. This confirms that miRNA expression can be reliably quantified by qPCR, and subsequently also that the mild AF-miRNA downregulation in CCl_4-treated fibrosis is a reliable observation (**Figure 4.2a, b**).

We identified the transcription factor PPARG as direct and positive regulator of AF-miRNA expression [103]. Therefore, differences in AF-miRNA expression between the model systems may result from altered PPARG expression levels or altered PPARG activity. As PPARG target gene outside the AF-miRNA network, *Plin2* expression was assessed as readout for PPARG activity [155,156]. In *SRF-VP16*^{iHep} tumors, collective miRNA downregulation correlated with significantly reduced *Plin2* expression and therefore more with reduced PPARG activity than expression levels (**Figure 4.2c**). However, the AF-miRNA network was also shown to be active in a 6 weeks CCl_4-induced liver fibrosis model, where we measured consistent *Pparg* and AF-miRNA downregulation alongside fibrotic target gene upregulation (Figures S11B and S4 of Winkler *et al.* (2020)) [103]. In accordance with these data, *Pparg* expression levels and PPARG activity were both reduced in the 2 months CCl_4-induced liver fibrosis model. Nevertheless, AF-miRNA expression was only partially downregulated at this stage (**Figure 4.2a**). After 12 months of CCl_4 treatment, *Pparg* expression was significantly upregulated, but the unchanged PPARG activity (*Plin2* expression) may explain the relatively unchanged AF-miRNA expression at this timepoint (**Figure 4.2b**).

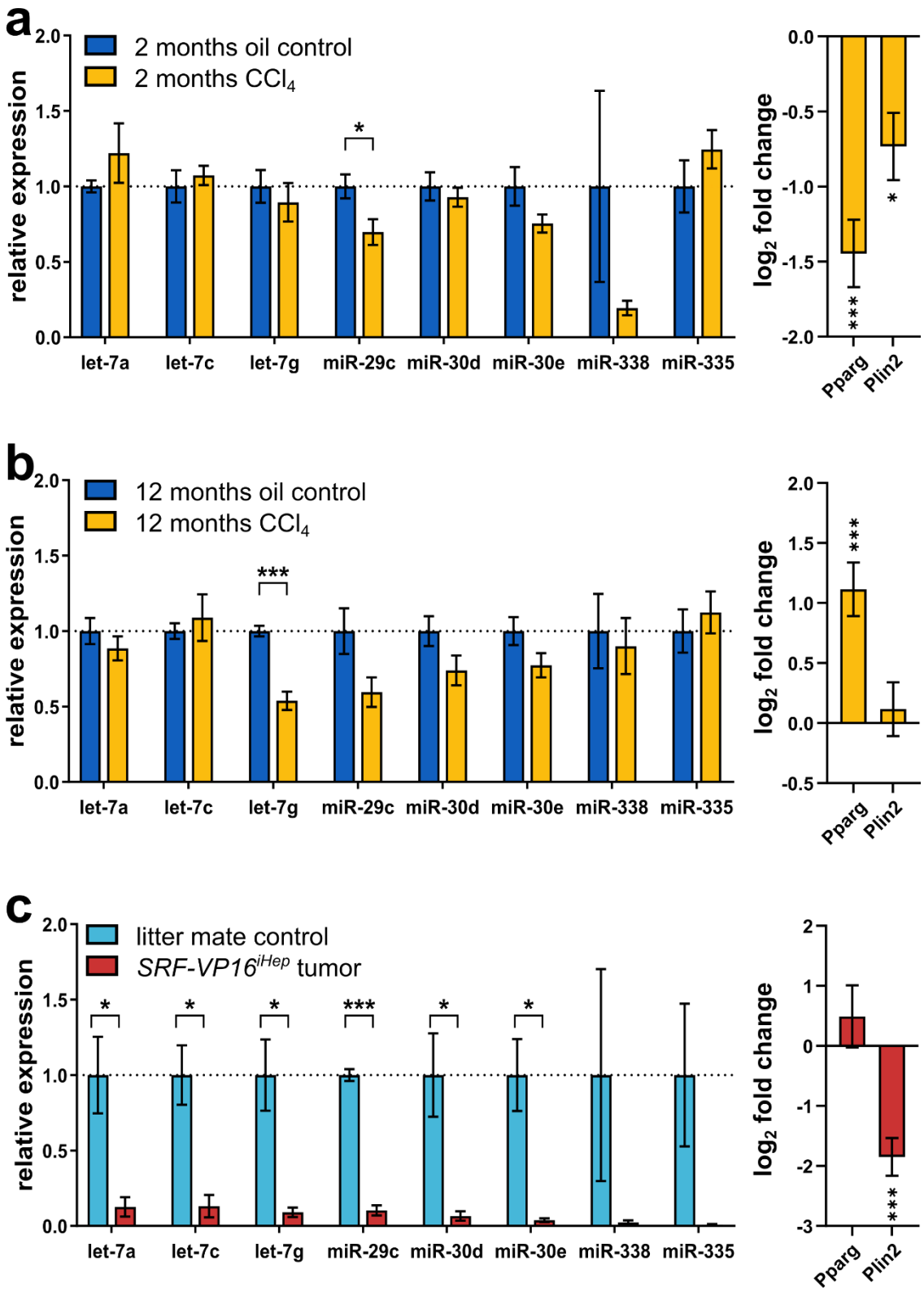

Figure 4.2 | Expression of the miRNAs of the AF-miRNA network and *Pparg* in progressing liver fibrosis and murine HCC. Relative expression of the AF-miRNAs measured by qPCR (**left**) as well as gene expression of transcription factor *Pparg* and its target gene *Plin2* measured by RNA-seq (**right**) in (**a**) 2 months and (**b**) 12 months CCl_4-induced liver fibrosis (n=4/group each) as well as in (**c**) mHCC (*SRF-VP16*^{iHep} tumors) (n=3/group). qPCR data were normalized to *Snord33* and *Snord35a* and are shown relative to the control mean. Statistical comparison of qPCR data by two-sided unpaired t-test. RNA-seq data are shown as log_2 fold change in disease (2 months CCl_4/12 months CCl_4/mHCC) compared to control (2 months oil/12 months oil/litter mate) in each dataset as analyzed by DESeq2. Data are shown as mean and SEM. * $p_{(adj)} \leq 0.05$, ** $p_{(adj)} \leq 0.01$, *** $p_{(adj)} \leq 0.001$. CCl_4 – carbon tetrachloride, mHCC – murine hepatocellular carcinoma.

Together, these data suggest that AF-miRNA expression depends more on PPARG activity than on *Pparg* expression levels. Furthermore, the AF-miRNAs were significantly downregulated in early fibrosis after 6 weeks of CCl_4 treatment and in the fibrotic tumor microenvironment of murine HCC [103], while AF-miRNA expression was only weakly downregulated in intermediate and late-stage CCl_4-induced liver fibrosis, indicating time-sensitive alterations in AF-miRNA expression during fibrosis progression.

4.3.2 Conservation of the AF-miRNA Network from Mouse and Human to Rat

We initially identified the AF-miRNA network in RNA-seq and sRNA-seq data of *SRF-VP16*^{iHep} mice, where the AF-miRNAs were found downregulated and their target genes upregulated in HCC tumors compared to healthy liver controls. To ensure that the conclusions gained from mouse models are translatable to human patients, only those miRNAs, targets, and specific miRNA:target interactions were retained that are conserved from mouse to human (**Project A**) [103].

The rat (*Rattus norvegicus*) is the most commonly used laboratory species besides the mouse [153]. To expand the available model systems in which to investigate the AF-miRNA network, the previous analysis was revisited and expanded upon to assess to which degree the AF-miRNA network is also conserved to rat.

First, the sequences of the 8 AF-miRNAs were retrieved from the TargetScan database and compared for conservation between mouse, human, and rat (**Table 4.1**) [137]. As described by us in Winkler *et al.* (2020), the AF-miRNAs are completely conserved between mouse and human [103]. The miRNAs let-7a-5p, let-7c-5p, let-7g-5p, miR-29c-3p, miR-30d-5p, and miR-30e-5p are also completely conserved to rat. Rat miR-338-3p possesses one more base at the 3'-end than mouse miR-338-3p, but this does not interfere with its targeting properties [79]. miR-335-3p is however not conserved to rat and was thus excluded from further analyses of the AF-miRNA network in rat.

Table 4.1 | Sequence comparison of the 8 AF-miRNAs in human, mouse, and rat. Bases differing from the human miRNA are labeled in bold.

AF-miRNA	Human Sequence (5' – 3')	Mouse Sequence (5' – 3')	Rat Sequence (5' – 3')
let-7a-5p	ugagguaguagguuguauaguu	ugagguaguagguuguauaguu	ugagguaguagguuguauaguu
let-7c-5p	ugagguaguagguuguaugguu	ugagguaguagguuguaugguu	ugagguaguagguuguaugguu
let-7g-5p	ugagguaguaguuuguacaguu	ugagguaguaguuuguacaguu	ugagguaguaguuuguacaguu
miR-29c-3p	uagcaccauuugaaaucgguua	uagcaccauuugaaaucgguua	uagcaccauuugaaaucgguua
miR-30d-5p	uguaaacaucccgacuggaag	uguaaacaucccgacuggaag	uguaaacaucccgacuggaag
miR-30e-5p	uguaaacauccuugacuggaag	uguaaacauccuugacuggaag	uguaaacauccuugacuggaag
miR-335-3p	uuuuucauuauugcuccugacc	uuuuucauuauugcuccugacc	u**caagagca**au**aa**c**gaaaa**a**ugu**
miR-338-3p	uccagcaucagugauuuuguug	uccagcaucagugauuuuguug	uccagcaucagugauuuuguug**a**

Next, all predicted target genes for each of the 8 AF-miRNAs were extracted from the DIANA microT-CDS (v5.0) database for mouse, human, and rat along with the miTG target prediction score for each miRNA:target pair with the miTG threshold set to 0 [138,139]. For each species, the target genes were then filtered to only include the 14 targets of the network (*Col1a1*, *Col1a2*, *Col4a2*, *Col4a5*, *Col5a2*, *Lamc1*, *Pdgfa*, *Pdgfb*, *Tgfbr1*, *Adamst14*, *Adamts15*, *Loxl2*, *Loxl4*, *Tpm1*) experimentally validated by us in Winkler *et al.* (2020) or their respective homologs in human and rat [103]. This resulted in the identification of 85 miRNA:target pairs in mouse and 80 miRNA:target pairs in human. In rat, the AF-miRNA network, comprised of 7 AF-miRNAs and 14 targets, encompasses 43 miRNA:target pairs and is thus smaller than the networks in mouse and human.

The AF-miRNA networks in mouse, human, and rat were then each filtered to only retain miRNA:target pairs with miTG target prediction scores ≥ 0.6 to omit miRNA:target pairs with low targeting probability. This reduced the mouse network from 85 to 51 miRNA:target pairs, the human network from 80 to 52 miRNA:target pairs, and the rat network from 43 to 28 miRNA:target pairs.

The three datasets were then compared with each other to only retain direct miRNA:target pairs conserved between all three species. With miTG = 0 filtering, 40 miRNA:target pairs are conserved between all three species (**Supplementary Data 4**), while with miTG ≥ 0.6 filtering, 28 miRNA:target pairs are conserved. These 28 conserved miRNA:target pairs are all part of the rat network (at miTG ≥ 0.6) and are all contained within the mouse and human AF-miRNA networks (**Figure 4.3**).

The AF-miRNA networks in mouse and human only differ in the additional miR-29c:*LAMC1* miRNA:target pair in human (**Figure 4.3**). The predicted AF-miRNA network in the rat is overall smaller than the network confirmed in mouse and human [103]. It comprises 7 of 8 AF-miRNAs and 11 of 14 validated fibrotic target genes as 28 predicted direct miRNA:target pairs. Nevertheless, AF-miRNA targeting is conserved to the rat to a large extend so that fibrotic rat model systems can be used to further investigate the AF-miRNA network.

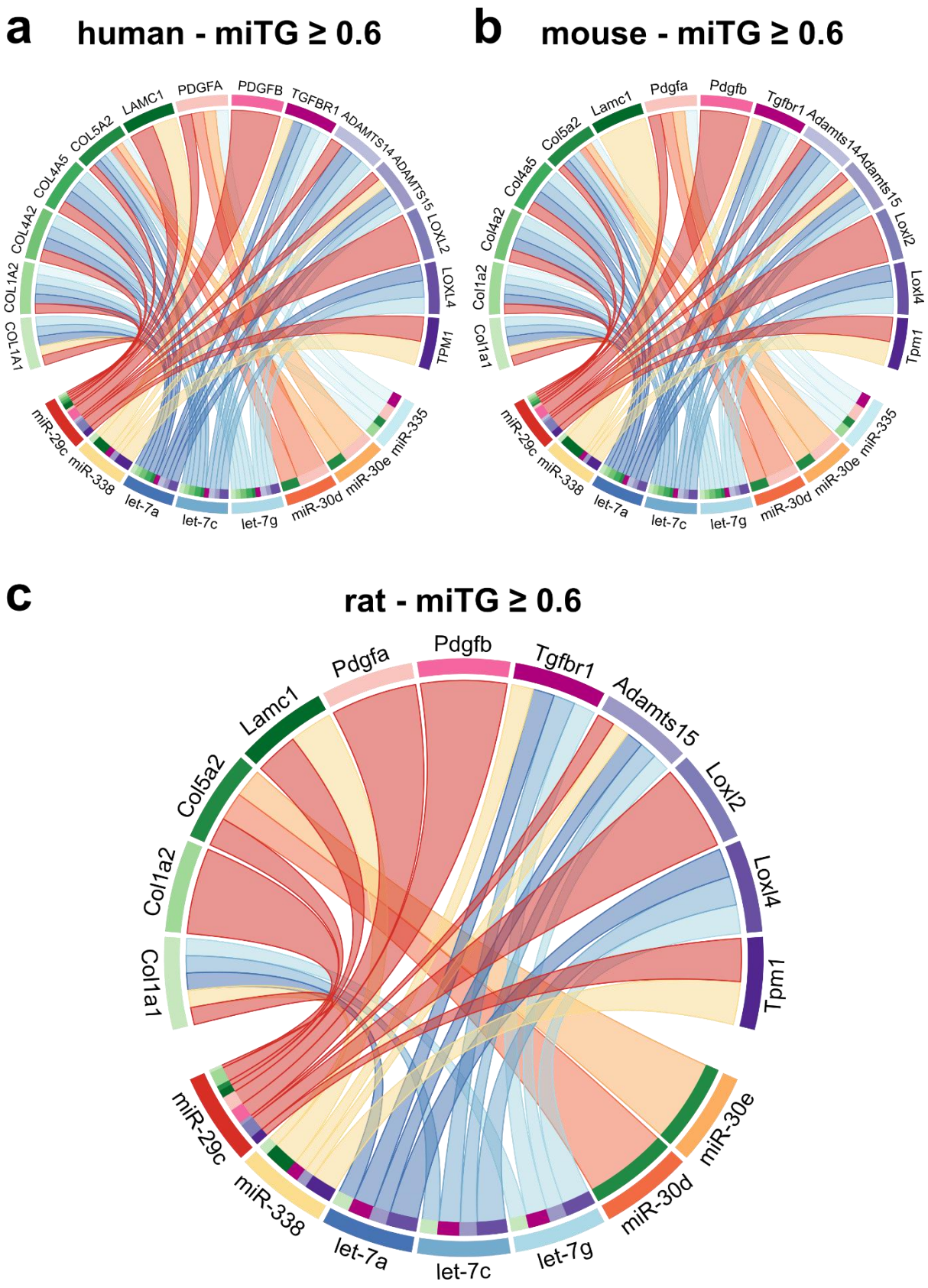

Figure 4.3 | The AF-miRNA network is largely conserved between human, mouse, and rat. Circos plots depicting the miRNA:target interactions of the AF-miRNA network in (**a**) human, (**b**) mouse, and (**c**) rat with miTG target prediction score ≥ 0.6. AF-miRNA targeting is conserved between mouse (51 miRNA:target pairs) and human (52 miRNA:target pairs) except for the additional miR-29c:*LAMC1* interaction present in the human network. The rat AF-miRNA network consists of 28 miRNA:target pairs, which are all present in the mouse and human networks. The rat network (**c**) thus also depicts the network conserved between all three species.

4.3.3 The AF-miRNA Network in Rodent TAA-induced and BDL-mediated Liver Fibrosis

The degree of AF-miRNA downregulation varied between different stages of CCl_4-induced liver fibrosis and the fibrotic microenvironment of murine HCC (**Chapter 4.3.1**). To assess whether the observed differences only vary between different degrees of liver fibrosis or whether the cause of liver fibrosis also influences the AF-miRNA network, two further commonly used liver fibrosis models were investigated. The TAA-induced liver fibrosis model develops early peri-central and peri-portal fibrosis progressing to bridging fibrosis in later stages similar to CCl_4, while the common BDL model develops obstructive cholestasis that progresses to portal fibrosis and portal inflammation [112].

The degree of liver fibrosis was assessed by blood serum markers of liver function for two rat TAA-induced fibrosis models after 4 weeks and 10 weeks of TAA treatment as well as for a 4 weeks rat BDL model (**Figure 4.4**). ALT and AST were significantly increased in all three model systems (**Figure 4.4a, b**). ALT and AST are general markers for hepatocellular damage as it typically occurs during various liver injuries [31]. Therefore, elevated ALT and AST activities indicate here that liver fibrosis was successfully induced by both TAA-treatment and BDL.

Increased enzymatic activity of AP and GGT as well as elevated bilirubin concentration are markers especially for cholestasis, but also for other types of liver damage, including fibrosis and cirrhosis [32]. In all three models, AP and GGT were significantly increased, while bilirubin levels were increased in the 10 weeks TAA and the BDL model, further indicating fibrotic liver damage in these models (**Figure 4.4c-e**). Of note, GGT and bilirubin were about 2-fold and 8-fold more elevated in BDL than in the TAA models, respectively. This emphasizes the different etiologies of TAA-induced liver fibrosis and BDL, where the experimental bile duct obstruction causes cholestasis-mediated fibrosis [110]. Albumin is exclusively produced in hepatocytes so that severe liver damage can be assessed by reduced albumin concentrations in blood serum [157]. Albumin concentration was significantly decreased after 10 weeks of TAA-treatment, but not after 4 weeks of TAA treatment, indicating that the induced liver fibrosis may start to progress to cirrhosis at this later timepoint (**Figure 4.4f**).

Collectively, the assessed blood serum markers of liver function showed that all three experimental models successfully induced liver fibrosis in the rat, but also that TAA-induced and BDL-mediated liver fibrosis may differ on a molecular level due to their different experimental origin and thus different fibrotic etiology.

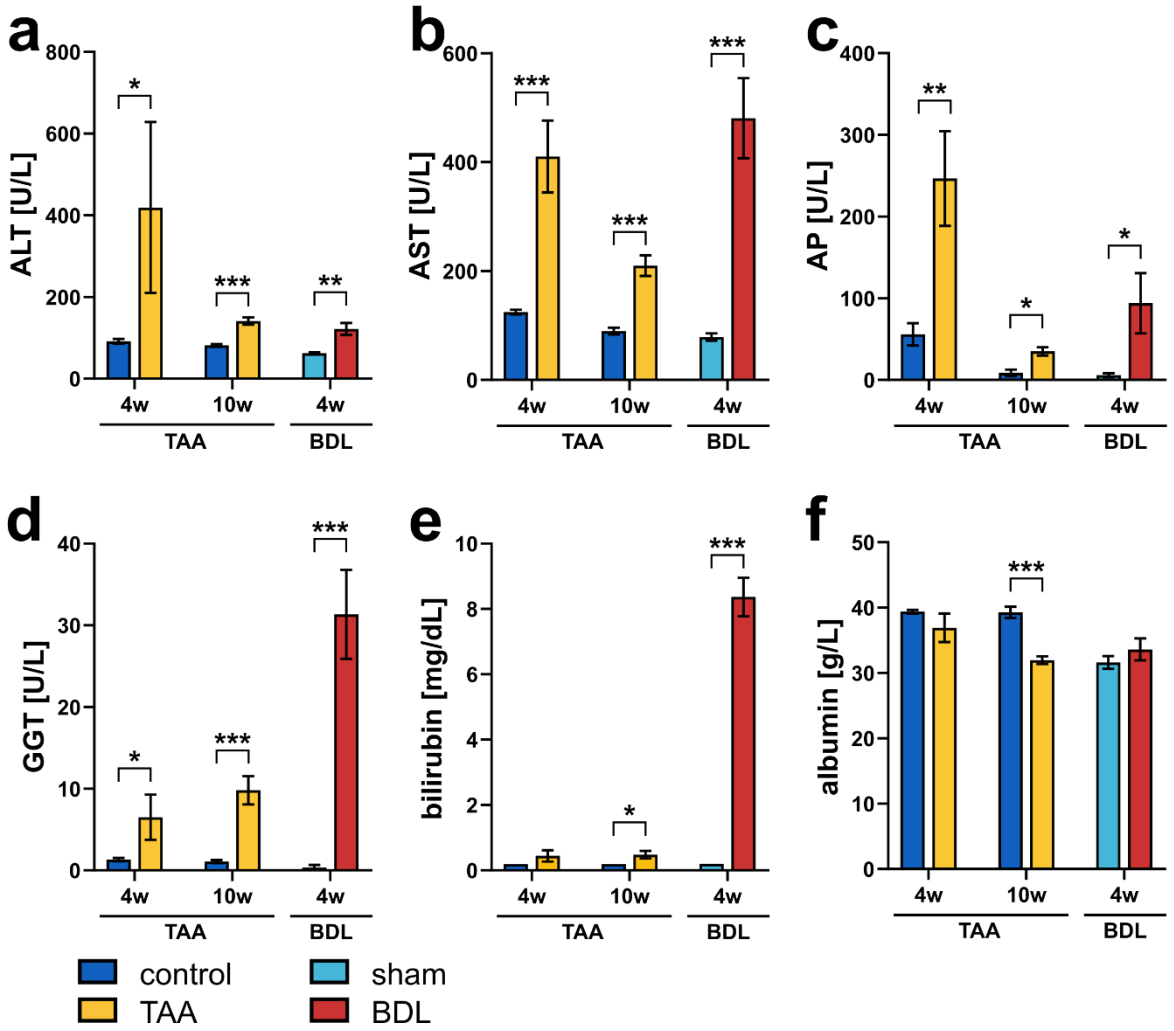

Figure 4.4 | Blood serum markers of liver function in TAA-induced and BDL-mediated liver fibrosis in the rat. Enzymatic activity of (**a**) ALT, (**b**) AST, (**c**) AP, and (**d**) GGT as well as concentration of (**e**) bilirubin and (**f**) albumin were measured in blood serum collected after 4 weeks or 10 weeks TAA or NaCl control treatment and 4 weeks after BDL or sham operation (n=6, 6, 5, 6, 7, 6 for 4w TAA, 4w NaCl, 10w TAA, 10w NaCl, BDL, sham). Data are shown as mean and SEM. Statistical comparison by two-sided unpaired t-test. * p≤0.05, ** p≤0.01, *** p≤0.001. ALT – alanine aminotransferase, AP – alkaline phosphatase, AST – aspartate aminotransferase, BDL – bile duct ligation, GGT – gamma-glutamyltransferase, TAA – thioacetamide, w – weeks.

Next, the AF-miRNA network was assessed in these fibrotic model systems. On the one hand, the 4 weeks and 10 weeks rat TAA models were compared to determine whether the duration of TAA exposure influences the degree of HSC activation as well as the expression levels of genes and miRNAs of the network (**Figure 4.5a-d**). On the other hand, the rat BDL model was compared to a mouse BDL model to determine whether the AF-miRNA network behaves similarly in both species (**Figure 4.5e-h**).

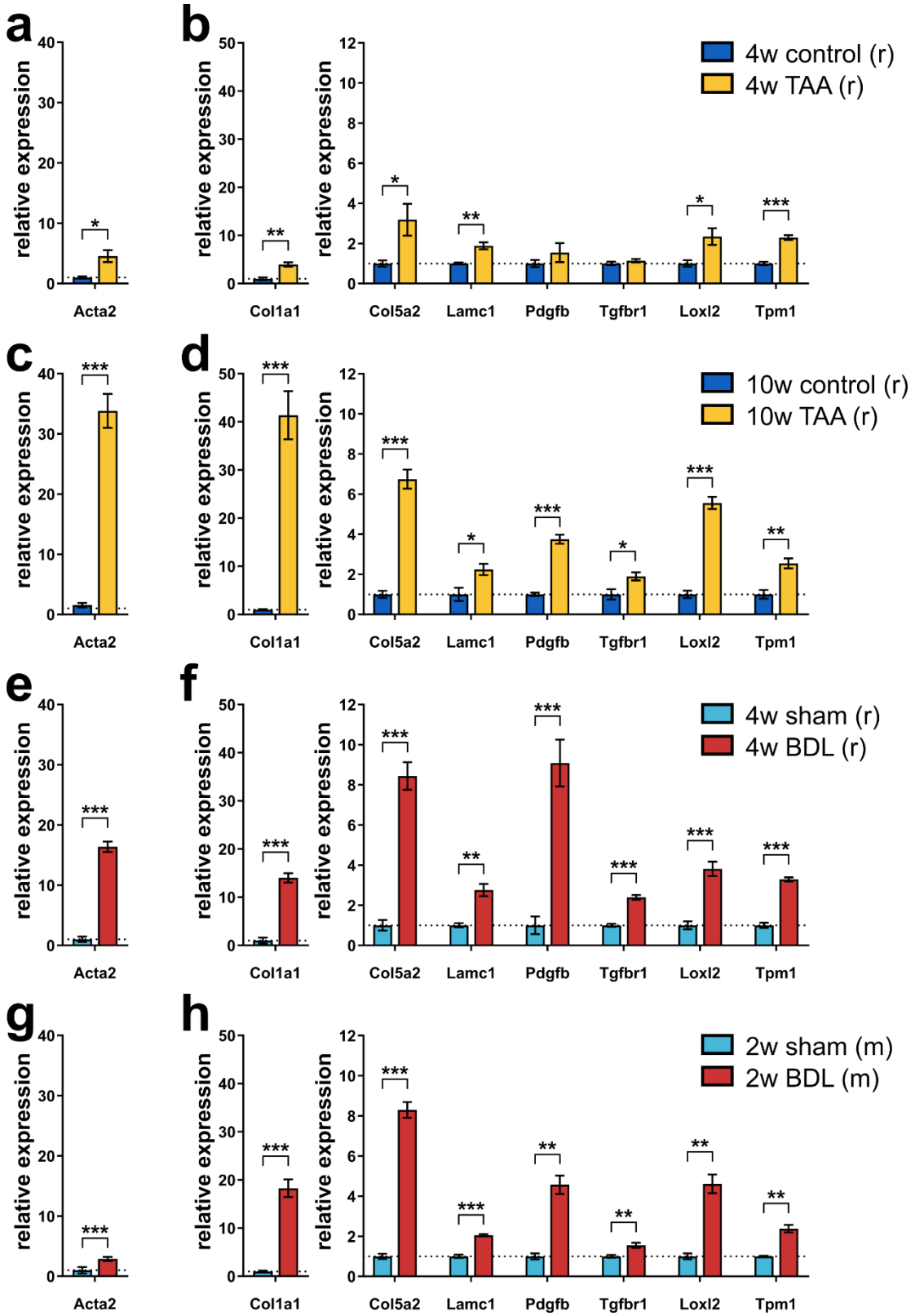

Figure 4.5 | Expression of *Acta2* and fibrotic target genes of the AF-miRNA network in TAA-induced and BDL-mediated liver fibrosis. Relative gene expression of *Acta2* and selected fibrotic target genes of the AF-miRNA network in (**a**, **b**) 4 weeks and (**c**, **d**) 10 weeks TAA-induced liver fibrosis in rat as well as (**e**, **f**) 4 weeks after BDL in rat and (**g**, **h**) 2 weeks after BDL in mouse (n=4/group for all models). qPCR data were normalized to *Gapdh* and *Gusb* for the rat models and to *Gapdh* and *Tbp* for mouse BDL and are shown relative to the control mean (4w NaCl/10w NaCl/4w sham/2w sham). Data are shown as mean and SEM. Statistical comparison by two-sided unpaired t-test. * p≤0.05, ** p≤0.01, *** p≤0.001. BDL – bile duct ligation, m – mouse, r – rat, TAA – thioacetamide, w – weeks.

In the mechanistic model of the AF-miRNA network, the activation of HSCs is marked by *Pparg* and AF-miRNA downregulation and subsequently by increased expression and secretion of fibrotic target genes [103]. Induction of ACTA2 is the most reliable marker of HSC activation and *Acta2* gene expression was thus measured in all model systems (**Figure 4.5**) [7]. *Acta2* expression was significantly increased 4.55(±1.01)-fold after 4 weeks and 33.82(±2.84)-fold after 10 weeks of TAA treatment compared to time-matched controls, confirming stronger HSC activation in more progressed fibrosis after prolonged TAA treatment (**Figure 4.5a, c**). Furthermore, *Acta2* expression was significantly increased 16.37(±1.09)-fold 4 weeks after BDL in rat and 2.88(±0.60)-fold 2 weeks after BDL in mouse compared to time-matched sham operated animals, which again indicates stronger HSC activation in later stages of fibrosis (**Figure 4.5e, g**).

As part of the AF-miRNA network, a subset of fibrotic target genes conserved between mouse and rat (**Figure 4.3c**) was quantified in all four model systems. *Col1a1*, *Col5a2*, *Lamc1*, *Pdgfb*, *Tgfbr1*, *Loxl2*, and *Tpm1* were all found significantly upregulated in 4 weeks and 10 weeks TAA-induced rat fibrosis as well as 4 weeks after rat BDL and 2 weeks after mouse BDL relative to corresponding controls, with the only exception being *Pdgfb* and *Tgbfr1* in the 4 weeks TAA model (**Figure 4.5b, d, f, h**). Additionally measured fibrotic target genes of the mouse AF-miRNA network (**Figure 4.3b**) 2 weeks after mouse BDL were also all found significantly upregulated (**Supplementary Figure 9**). Generally, the fibrotic target genes were more elevated after 10 weeks than after 4 weeks of TAA treatment compared to time-matched controls, further suggesting fibrosis progression with prolonged TAA treatment. Moreover, the relative expression patterns of the measured fibrotic target genes were comparable between the 10 weeks TAA model and the two BDL models, indicating similar degrees of liver fibrosis in these three models. Given the different time courses over which fibrosis was induced, fibrosis appears to develop fastest in the mouse BDL model and slowest in the rat TAA model.

Since upregulation of the fibrotic target genes implied that the AF-miRNA network is active in all four models, the expression of the AF-miRNAs was analyzed next (**Figure 4.6a, c, e, g**). Surprisingly, relative expression of most AF-miRNAs was either unchanged or even significantly upregulated in all four model systems. Only miR-30d was significantly downregulated after 4 weeks of TAA treatment, where none of the other AF-miRNAs were significantly changed (**Figure 4.6a**). Of note, the miRNAs let-7a, let-7c, and let-7g were significantly upregulated to comparable degrees after 10 weeks of TAA treatment, 4 weeks after BDL in rat, and 2 weeks after BDL in mouse. Furthermore, miR-30d was found significantly upregulated in both BDL models and miR-29c significantly upregulated in the mouse BDL model (**Figure 4.6c, e, g**).

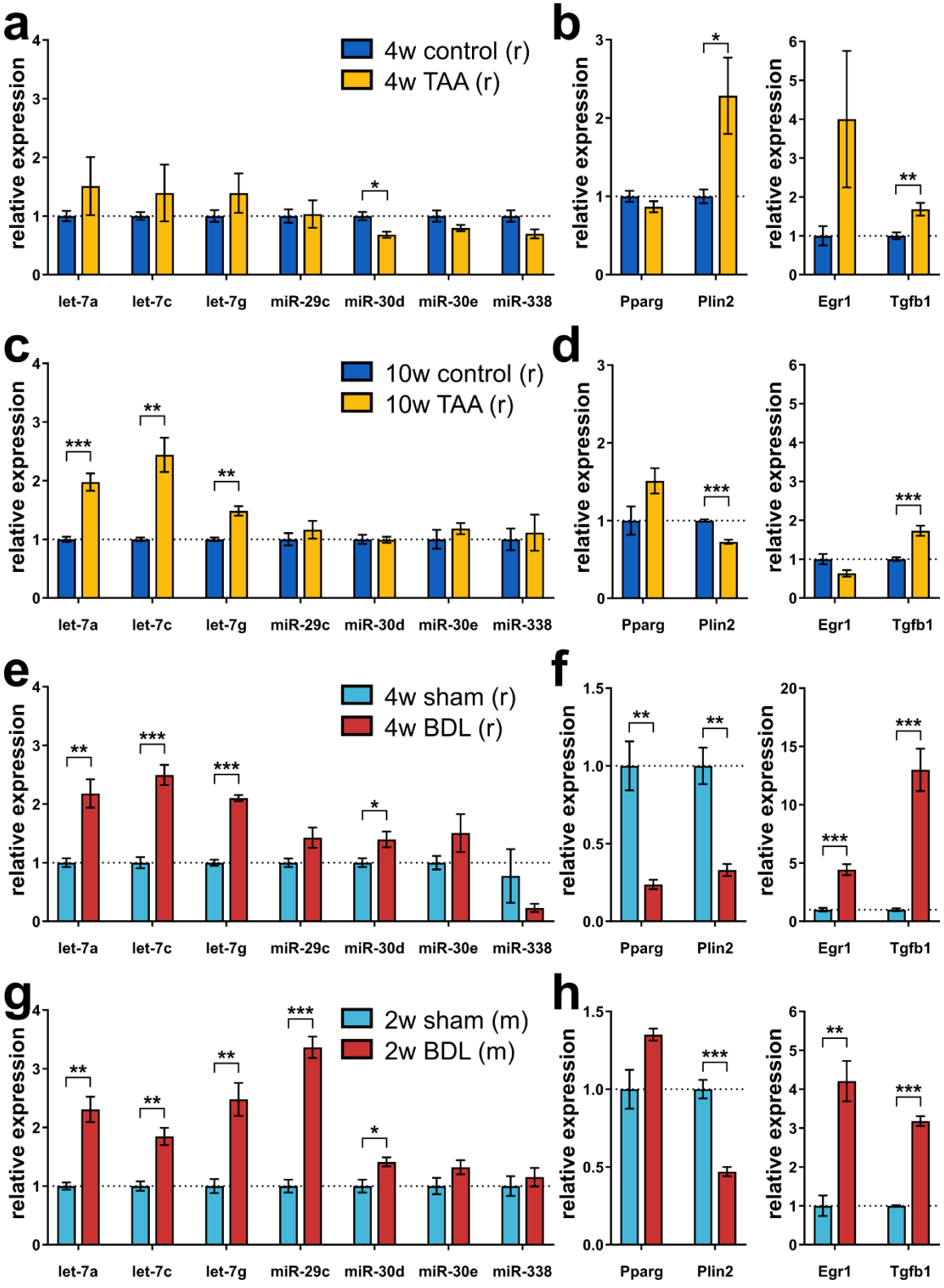

Figure 4.6 | Expression of AF-miRNAs and their transcription factors *Pparg* and *Egr1* in TAA-induced and BDL-mediated liver fibrosis. Relative expression of the AF-miRNAs (**left**), *Pparg* and its target gene *Plin2* (**middle**) as well as *Egr1* and its target gene *Tgfb1* (**right**) in (**a**, **b**) 4 weeks and (**c**, **d**) 10 weeks TAA-induced liver fibrosis in rat as well as (**e**, **f**) 4 weeks after rat BDL and (**g**, **h**) 2 weeks after mouse BDL (n=4/group for all models). qPCR data were normalized to *5S* and *U87* for rat miRNAs, to *Gusb* and *Tbp* for rat genes, to *Rnu6* and *Snord33* for mouse miRNAs, and to *Gapdh* and *Tbp* for mouse genes. qPCR data are shown relative to the control mean (4w NaCl/10w NaCl/4w sham/2w sham). Data are shown as mean and SEM. Statistical comparison by two-sided unpaired t-test. * p≤0.05, ** p≤0.01, *** p≤0.001. BDL – bile duct ligation, m – mouse, r – rat, TAA – thioacetamide, w – weeks.

It was then assessed whether upregulation of the AF-miRNAs during fibrosis, which does not correspond to the AF-miRNA network model postulated by us in Winkler *et al.* (2020), correlates with increased expression or activity of their known transcription factors. Besides PPARG, which we identified as direct positive regulator of the seven AF-miRNAs let-7a, let-7c, let-7g, miR-29c, miR-30d, miR-30e, and miR-338 in Winkler *et al.* (2020), Ivana Winkler has further identified the transcription factor EGR1 as direct regulator of the AF-miRNAs let-7a, let-7c, let-7g, miR-30d, and miR-30e in her PhD thesis (2019) [103,158].

Therefore, both the relative expression of the two transcription factors PPARG and EGR1 as well as their activity was assessed. As readout for PPARG and EGR1 activity, the relative expression of *Plin2* and *Tgfb1* as their target genes outside the AF-miRNA network, respectively, were measured (**Figure 4.6b, d, f, h**) [155,156,159]. During progression of liver fibrosis from 4 weeks to 10 weeks of TAA treatment, *Pparg* expression remained unchanged, but its activity measured by *Plin2* expression was significantly increased after 4 weeks and significantly decreased after 10 weeks of TAA treatment. While *Egr1* expression was also relatively unchanged at both time points, EGR1 activity measured by *Tgfb1* expression was significantly elevated after 4 weeks as well as 10 weeks of TAA treatment (**Figure 4.6b, d**). A similar trend of reduced PPARG activity (accompanied by reduced *Pparg* expression 4 weeks after BDL) and increased EGR1 expression and activity was also observed both 4 weeks after BDL in rat and 2 weeks after BDL in mouse (**Figure 4.6f, h**).

Overall, these data suggest three things. First, BDL-mediated fibrosis, including the AF-miRNAs, their fibrosis-associated target genes, and their transcription factors, develops similarly in rat and mouse species. Second, the AF-miRNAs appear transcriptionally regulated by EGR1 rather than PPARG in the here analyzed fibrosis models of TAA treatment and BDL. Third, the AF-miRNAs are mostly upregulated rather than downregulated in fibrogenesis, which implies that they have additional functions, potentially unrelated to fibrotic processes, in the here analyzed liver fibrosis model systems of TAA-induced and BDL-mediated liver fibrosis.

4.4 Discussion

4.4.1 The AF-miRNA Network During Progression of CCl_4-induced Liver Fibrosis in Mice

It is well established that the activation of HSCs, as the fibroblasts of the liver, is the key event driving liver fibrosis [160]. Furthermore, there is accumulating evidence that activated HSCs and liver fibrosis actively contribute to the development of HCC through shaping the premalignant and tumor microenvironment [8,56]. Of all HCCs, more than 80% develop in fibrotic or cirrhotic livers [14]. To discern in more detail how the AF-miRNA network behaves at different stages of liver fibrosis

progression to HCC, expression of the AF-miRNAs and their target genes was assessed in the mouse models of 2 months and 12 months CCl_4-induced liver fibrosis generated by Ghallab *et al.* (2019) [109]. These data were then compared to our data of the 6 weeks CCl_4-induced liver fibrosis model and the *SRF-VP16*^{iHep} mouse model of fibrotic HCC as well as to the TCGA cohort of human HCC processed by us in Winkler *et al.* (2020) (**Project A**) [103].

RNA-seq data analysis of 2 months and 12 months CCl_4-induced liver fibrosis samples revealed that both the degree of fibrotic target gene upregulation and the number of significantly upregulated fibrotic target genes increased with prolonged CCl_4-treatment. The degree of fibrotic target gene upregulation after 12 months of CCl_4 treatment was comparable to human HCC. Fibrotic target gene upregulation was overall strongest in the *SRF-VP16*^{iHep} model of murine HCC. In accordance with this fibrotic target gene expression analysis, the published Sirius Red stainings of Ghallab *et al.* (2019) also indicate the progression of liver fibrosis from 2 months to 12 months of CCl_4 treatment [109]. However, comparison of Sirius Red stainings of 12 months CCl_4-treated mice [109] and of the fibrotic HCC microenvironment of *SRF-VP16*^{iHep} mice [103] indicate similar degrees of fibrosis, while the RNA-seq data suggest more progressed fibrosis in the HCC microenvironment. Here, signal quantification or fibrotic scoring of the Sirius Red stainings is required to clarify whether the degree of fibrosis differs between 12 months CCl_4-induced fibrosis and the fibrotic HCC microenvironment of *SRF-VP16*^{iHep} mice.

We previously showed that the AF-miRNA network is dysregulated in a 6 weeks CCl_4-induced fibrosis model, including upregulation of the 14 experimentally validated fibrotic target genes [103]. The degree of fibrotic target gene upregulation after 2 months of CCl_4 treatment was very comparable, especially for collagens, *Lamc1*, and *Loxl2*, to this 6 weeks CCl_4-induced fibrosis model. On the one hand, this indicates that the two additional weeks of CCl_4 administration do not accelerate liver fibrosis progression substantially. On the other hand, the minor differences in the degree of fibrotic target gene upregulation can also be explained by the fact that the experiments were performed in different laboratories with some variations in experimental procedures [103,109]. Overall, fibrotic target gene expression levels and Sirius Red stainings demonstrate that the mouse models of 2 months and 12 months CCl_4 treatment and the *SRF-VP16*^{iHep} mouse model represent suitable model systems to study fibrosis progression from mild fibrosis over severe fibrosis to fibrotic HCC.

According to the mechanistic model of the AF-miRNA network, the increasing fibrotic target gene expression during fibrogenesis is negatively correlated with the expression of the AF-miRNAs [103]. Therefore, stronger AF-miRNA downregulation in later stages of fibrosis was expected. However, while most AF-miRNAs were strongly downregulated at the earliest available timepoint of mild fibrosis after 6 weeks of CCl_4 treatment [103], AF-miRNAs were less downregulated after 2 months and 12 months of CCl_4 treatment. Interestingly, AF-miRNA expression was again found to be strongly downregulated

in the severely fibrotic HCC tumors of *SRF-VP16*^{iHep} mice, measured both by sRNA-seq [103] and confirmed here by qPCR.

These findings indicate a time-sensitive regulation of AF-miRNA expression during fibrosis progression. The AF-miRNAs were strongly downregulated in earlier stages of fibrogenesis, as measured in pHSCs and in the 6 weeks CCl_4 model [103]. Often, miRNAs function as molecular switches, maintaining low baseline expression of their target genes under healthy conditions until a sufficiently strong disturbance arises [75]. A switch-like reduction in AF-miRNA expression to allow the accumulation of their fibrotic target genes may be especially important for a fast response to acute liver injury or other early fibrotic signals. While a fast and timely limited response to such signals is beneficial for effective wound-healing, persistent signaling typically becomes harmful and induces fibrogenesis [10]. However, AF-miRNA downregulation may become less relevant In later stages of fibrogenesis, once a certain threshold is overcome and alternative regulatory mechanisms additionally act on the excessive expression of fibrotic and ECM-related genes [160]. In the late-stage fibrotic microenvironment of *SRF-VP16*^{iHep} tumors, the AF-miRNAs were again strongly downregulated. These miRNAs may thus possess additional tumor-suppressive functions less relevant in non-tumorous fibrosis. For example, the miRNAs miR-29c and let-7c/g were shown to inhibit apoptosis pathways during HCC by targeting MCL1 and BCL-xL of the BCL2 family, respectively [161,162]. Reduced expression of these miRNAs would thus enhance HCC growth. Additionally, the AF-miRNAs likely respond differently to the different contextual cues that a fibrotic tumor microenvironment and a non-tumorous fibrotic ECM provide.

With PPARG as direct and positive regulator of AF-miRNA expression [103], the differences in AF-miRNA expression between the fibrotic model systems either result from differences in *Pparg* gene expression levels or from differences in PPARG activity as assessed by *Plin2* expression [155,156]. PPARG downregulation is reportedly associated with HSC activation during fibrosis [62]. Reduced *Pparg* expression was indeed observed in the 6 weeks CCl_4 model [103] and in the 2 months CCl_4 model along with AF-miRNA downregulation, but not in the later stages of fibrosis in the 12 months CCl_4 model. Of note, *Pparg* expression was not downregulated in the *SRF-VP16*^{iHep} model, even though the strongest AF-miRNA downregulation was observed here. As PPARG typically requires activation through agonist binding to induce transcription, the expression of PPARG targets is not only decreased by a reduction in PPARG availability, but also by a reduction in its activity [61]. Indeed, PPARG activity was reduced in the 2 months CCl_4 model and in the *SRF-VP16*^{iHep} model along with AF-miRNA downregulation. To clarify whether the observed AF-miRNA and *Pparg* downregulation in the 6 weeks CCl_4 model of Winkler *et al.* (2020) [103] was accompanied by reduced PPARG activity, it would be beneficial to measure *Plin2* gene expression in this model. However, this analysis was beyond the scope of this PhD study. Overall, the available data on the three model systems of 2 months and 12 months

CCl_4-induced fibrosis and on the *SRF-VP16*^{iHep} model of HCC suggest that the AF-miRNA downregulation during fibrogenesis depends more on PPARG activity than on *Pparg* gene expression.

While alterations in PPARG expression and activity may account for the different degrees of AF-miRNA downregulation during fibrogenesis, it is also possible that other transcription factors besides PPARG regulate the AF-miRNAs. In her PhD thesis, Dr. Ivana Winkler identified EGR1 as another transcription factor of the AF-miRNAs [158]. It is therefore possible that EGR1-mediated AF-miRNA transcription maintains higher AF-miRNA expression levels even in the absence or inactivity of PPARG during later stages of fibrosis. Furthermore, we demonstrated in Winkler *et al.* (2020) that the AF-miRNAs are also partially regulated through epigenetic changes in promoter methylation [103] that can additionally influence time-sensitive changes in AF-miRNA expression during fibrogenesis.

4.4.2 Conservation of the AF-miRNA Network from Mouse and Human to Rat

In Winkler *et al.* (2020), we defined the AF-miRNA network as a group of 8 AF-miRNAs and 14 experimentally validated ECM-related target genes that are, together with their specific miRNA:target interactions, conserved between mouse and human (**Project A**) [103]. To expand the available model systems in which to investigate the AF-miRNA network, bioinformatic analyses were performed to assess the degree to which this AF-miRNA network is further conserved to the rat (*Rattus norvegicus*) as the most commonly used laboratory species besides the mouse [153]. The resulting AF-miRNA network conserved between all three species is comprised of 7 of the 8 AF-miRNAs excluding miR-335-3p, of 11 of the 14 experimentally validated ECM-related target genes excluding *Col4a2*, *Col4a5*, and *Adamts14,* and of 28 miRNA:target pairs conserved between all three species.

While miR-335 exists in the rat, its sequence [137], and thus its targetome and biological function [138,139], differs from mouse and human miR-335. Rat miR-335 nevertheless targets some genes of the AF-miRNA network, including interactions present in mouse and human (*Col5a2* and *Tgfbr1*) and rat-specific interactions (*Col1a1, Lamc1*, and *Tpm1*) [138,139]. However, these rat miR-335:target interactions all possess low target prediction scores (miTG ≤ 0.5) and are, most importantly, mediated by other miRNA:target sequence interactions than in mouse and human. Therefore, rat miR-335 and its target interactions are not suited to translate miR-335 functions from rat to human and were thus excluded from the AF-miRNA network conserved between the three species. Of the AF-miRNA target genes, rat *Col4a2*, *Col4a5*, and *Adamts14* do not appear in the DIANA microT-CDS database (v5.0) of rat genes used for miRNA target prediction [138,139]. For these three genes, the prediction of miRNA targeting was therefore not possible in the rat. The DIANA microT-CDS database sources its gene information from Ensembl, where the mRNAs of rat

Col4a2, *Col4a5*, and *Adamts14* are annotated as predicted transcripts with limited experimental evidence of their biological expression [163]. The three genes were thus excluded from the AF-miRNA network conserved between the three species. Within the individual AF-miRNAs and genes conserved to the rat, not all miRNA:target interactions were conserved. This becomes most evident for *Col1a2*, which is targeted by 5 AF-miRNAs in mouse and human but only by miR-29c in the rat. *Col5a2* and *Pdgfa* are also targeted by fewer miRNAs in the rat than in mouse and human. Given that the AF-miRNAs are conserved in their sequence, the lack of several miRNA:target interactions in the rat is best explained by non-conserved AF-miRNA binding sequences in the 3'UTRs of the mRNAs of the rat genes [75].

The used DIANA microT-CDS database [138,139] is only one of many miRNA target prediction algorithms [164]. Other databases may thus identify additional miRNA:target interactions or predict certain interactions as more or less likely than the DIANA microT-CDS algorithm. The current standard operating procedures suggest to integrate data from multiple target prediction databases [165], either manually or by using integrative platforms like miRWalk [166], which scan and compare multiple databases. However, the DIANA microT-CDS algorithm was used here to ensure that filtering for the rat AF-miRNA network resembled the initial analysis performed to identify the AF-miRNA network conserved between mouse and human [103]. Overall, target prediction analysis showed that the AF-miRNA network is sufficiently conserved between mouse, human, and rat so that rat models of liver fibrosis can be used to further investigate AF-miRNA and target gene expression.

4.4.3 The AF-miRNA Network in Rodent TAA-induced and BDL-mediated Liver Fibrosis

The varying degree of AF-miRNA downregulation during progressing stages of CCl_4-induced liver fibrosis as well as in the fibrotic microenvironment of *SRF-VP16*^{iHep} tumors suggests that AF-miRNA dysregulation is context-specific and varies depending on the cause of liver fibrosis. This hypothesis was investigated in two further commonly used liver fibrosis models, TAA-induced fibrosis and BDL-mediated fibrosis. Two BDL-mediated liver fibrosis models, one in the rat and one in the mouse, were analyzed to assess whether the AF-miRNA network behaves similarly in both species under comparable experimental conditions. Moreover, two rat TAA-induced liver fibrosis models after 4 weeks and 10 weeks of TAA treatment were analyzed to assess the AF-miRNA network during hepatotoxin-induced fibrosis progression in the rat, and to compare the effects of TAA on the rat to the effects of CCl_4 as another hepatotoxin on the mouse.

In the three rat models of 4 weeks TAA, 10 weeks TAA, and BDL-mediated fibrosis, blood serum markers of liver function were analyzed to determine the degree of liver fibrosis compared to their

respective controls. In all three models, the assessed blood serum markers indicated the presence of fibrosis, hepatocellular damage as well as biliary obstruction [31,32]. As also described by Tarcin *et al.* (2011), the fibrotic markers AST, GGT, and bilirubin were found upregulated 4 weeks after BDL in the rat [167]. In accordance with the experimental cause of fibrosis, the two fibrotic markers for biliary obstruction, GGT and bilirubin, were more elevated in the BDL model, where the bile duct is artificially obstructed [111], than in the TAA-induced fibrosis model. Furthermore, the blood serum markers AST and ALT were more increased after 4 weeks than after 10 weeks of TAA treatment. Since massive hepatocyte damage and death occurs especially in acute and acute-to-chronic fibrosis but is typically subdued in later stages of fibrosis [29], this indicates more progressed liver fibrosis with prolonged TAA administration. Collectively, the blood serum markers show that fibrosis was successfully induced in all three liver fibrosis models of the rat. Because blood serum markers were not available for the mouse BDL model, *Acta2* gene expression was measured in all four model systems as additional marker of liver fibrosis and HSC activation [7]. Increased *Acta2* expression in the three rat models of 4 weeks TAA, 10 weeks TAA, and BDL-mediated fibrosis corresponded to the blood serum marker measurements, while increased *Acta2* expression in the mouse BDL model was a first indicator for the presence of fibrosis in this model.

The elevated gene expression of the fibrotic target genes of the AF-miRNA network further confirmed the presence of fibrosis in all four models. The fibrotic target genes *Col5a2*, *Pdgfb*, *Tgfbr1*, *Loxl2,* and *Tpm1* of the network as well as *Acta2* were stronger upregulated in the 10 weeks than in the 4 weeks TAA-induced fibrosis model of the rat. Together with AST and ALT measurements, this further supports the basic concept of more progressed fibrosis and stronger HSC activation with prolonged TAA treatment. The standard operating procedure of TAA-induced fibrosis in the rat by Wallace *et al.* (2015) as well as several studies on TAA-induced liver fibrosis also describe a time-dependent increase in diverse fibrotic markers [112,113,168,169], further confirming the here observed increasing fibrosis with prolonged TAA administration.

Comparison of the 4 weeks rat BDL model and the 2 weeks mouse BDL model revealed that, overall, the degree of gene upregulation was similar in both species except for a stronger upregulation of *Acta2* and *Pdgfb* in the 4 weeks rat BDL model. The observed *Col1a1* and *Col5a2* upregulation 4 weeks after BDL in the rat corresponds to the collagen protein accumulation reported by Tarcin *et al.* (2011) in their rat model 4 weeks after BDL [167]. In our 2 weeks BDL mouse model, *Col1a1* gene expression was about 20-fold increased compared to sham-operated mice. This value lies between the 6-fold increase reported by Sigal *et al.* (2010) [170] and the 40-fold increase reported by Georgiev *et al.* (2008) [171] for C57BL/6 mice 2 weeks after BDL. A high variation in the degree of *Col1a1* upregulation within the same model of liver fibrosis was also reported for CCl_4-induced liver fibrosis in mice [130]. Even though the degree of *Col1a1* upregulation varies between studied fibrosis models and species,

Col1a1 upregulation remains a key alteration in the fibrotic ECM and is thus nevertheless one of the most reliable markers for liver fibrosis [27]. While the observed upregulation of *Col1a1* and other fibrotic target genes confirms the presence of liver fibrosis in both BDL models, it cannot be clearly distinguished whether the degree of fibrosis differs between the two models. However, the comparable degree of fibrotic target gene upregulation, especially of *Col1a1*, *Col5a2*, *Lamc1*, and *Loxl2*, after a shorter period of bile duct obstruction rather suggests that mice are more susceptible to BDL-mediated fibrosis than rats. Time-matched BDL experiments in rat and mouse are required to pursue this hypothesis in future studies.

Altogether, liver fibrosis was successfully induced in the three rat models of 4 weeks TAA, 10 weeks TAA, and 4 weeks BDL as well as in the mouse model of 2 weeks BDL. In all four models, liver fibrosis was accompanied by the upregulation of the fibrotic target genes of the AF-miRNA network. In accordance with literature, the mild liver fibrosis present after 4 weeks of TAA treatment progressed to significant liver fibrosis after 10 weeks of TAA treatment [112,113,168,169], while BDL caused liver fibrosis in the mouse after 2 weeks and in the rat after 4 weeks [110,167,170,171]. The animal models analyzed here thus confirm that liver fibrosis develops faster after BDL operation than with TAA treatment.

According to the mechanistic model of the AF-miRNA network, increased fibrotic target gene expression is negatively correlated with the expression of the AF-miRNAs as well as the expression or activity of their transcription factor PPARG (**Project A**) [103]. However, even though all four animal models were shown to cause liver fibrosis in general as well as the upregulation of the fibrotic target genes of the AF-miRNA network specifically, the AF-miRNAs themselves were not found downregulated. Instead, the expression of most AF-miRNAs was unchanged after 4 weeks of TAA treatment in the rat, while the expression of multiple AF-miRNAs, and most consistently the let-7 family, was even found upregulated after 10 weeks of TAA treatment in the rat as well as 4 weeks after rat BDL and 2 weeks after mouse BDL. Given that the AF-miRNA upregulation was consistent in both BDL models indicates that it is more likely caused by BDL as method of fibrosis induction and not by a species-specific effect.

Even though the diverse members of the let-7 family are continuously reported by us [103] and others [101,172,173] as anti-fibrotic miRNAs downregulated in progressing liver fibrosis in mouse and human, the let-7 AF-miRNAs were upregulated in TAA-induced and BDL-mediated fibrosis. Interestingly, upregulation of let-7 family members was also observed in a 10 weeks TAA mouse model by Hong *et al.* (2017) and in a 1 week BDL mouse model by Zhang *et al.* (2019) [174,175]. However, neither of the two studies identified any let-7 target genes so that the biological role of let-7 upregulation during TAA-induced and BDL-mediated fibrosis remains unclear [174,175]. Nevertheless,

the observed upregulation of the let-7 AF-miRNAs suggests that they possess additional functions, potentially unrelated to fibrotic processes, in the TAA-induced and BDL-mediated liver fibrosis models. Of note, especially BDL-mediated liver fibrosis is typically accompanied by inflammation [112]. Polikepahad *et al.* (2010) described a pro-inflammatory role of let-7 miRNAs through inhibition of IL-13 and other anti-inflammatory interleukins in an asthma lung disease mouse model [176]. Similar processes may also occur in inflamed fibrotic livers and may explain why let-7 expression was upregulated in the TAA-induced and BDL-mediated fibrosis models.

The AF-miRNAs are transcriptionally regulated by the transcription factor PPARG [103]. In accordance with literature [7,39,62,103], *Pparg* expression was found downregulated in fibrotic livers 4 weeks after BDL in the rat, and its activity, as assessed by *Plin2* expression, was reduced in the 10 weeks rat TAA, 4 weeks rat BDL, and 2 weeks mouse BDL models. Considering that the reduced expression and activity of PPARG was not accompanied by reduced AF-miRNA expression in these models, it is likely that the unexpected AF-miRNA upregulation in TAA-induced and BDL-mediated fibrosis is caused by alternative transcription factor activities. In her PhD thesis, Dr. Ivana Winkler identified EGR1 as another anti-fibrotic transcription factor directly regulating the AF-miRNAs *in vitro*, where it is downregulated in activated pHSCs together with the AF-miRNAs [158]. However, the role of EGR1 *in vivo* in the CCl_4-induced liver fibrosis mouse model and in the *SRF-VP16*^{iHep} mouse model of fibrotic HCC was less clear and suggests that EGR1-mediated AF-miRNA expression is context-specific [158]. While EGR1 is repeatedly associated with liver fibrosis, its role in fibrogenesis is quite controversial, with different studies identifying anti-fibrotic [43,158,177,178] as well as pro-fibrotic [42,43,179] functions of EGR1. In contrast to the anti-fibrotic function through regulating AF-miRNA expression in pHSCs [158], EGR1 is also known as direct regulator of the pro-fibrotic cytokine TGF-β, which plays a major role in HSC activation and induction of ECM synthesis during fibrogenesis [42,160]. In accordance with their pro-fibrotic functions, both *Egr1* and *Tgfb1* expression was increased in the TAA-induced as well as in the BDL-mediated liver fibrosis models in rat and mouse. It is thus possible that EGR1 activation induces AF-miRNA upregulation in these fibrosis models, competing with and abrogating PPARG-dependent AF-miRNA functions.

4.4.4 Context-specific AF-miRNA Dysregulation in Different Liver Fibrosis Models

In **Project B**, I analyzed the AF-miRNA network in different stages of CCl_4-induced liver fibrosis in the mouse, in the *SRF-VP16*^{iHep} mouse model of fibrotic HCC, in BDL-mediated fibrosis in the mouse and in the rat as well as in different stages of TAA-induced liver fibrosis in the rat. While the expression of the fibrotic target genes of the AF-miRNA network as well as additional fibrotic markers confirmed the

presence of liver fibrosis in all analyzed models, expression of the AF-miRNAs and their transcription factors varied considerably between the different models.

This observation strongly suggests a context-specific regulation of the AF-miRNAs due to the different etiologies of the analyzed models, which differ, among other factors, in the initiating nature of liver injury and the speed of fibrosis progression [112]. The strongest and most consistent AF-miRNA downregulation was observed in HCC-bearing livers of *SRF-VP16*^{iHep} mice. The analysis of further fibrotic HCC models is required to investigate whether the AF-miRNAs are generally stronger dysregulated in the fibrotic tumor microenvironment than in fibrotic non-tumorous tissues.

AF-miRNA expression patterns also differed between the liver fibrosis models. In the rat, Khimji *et al.* (2008) observed higher EGR1 protein levels in HSCs of BDL-injured livers than in HSCs of CCl_4-injured livers [180], which provides a possible explanation for the observed differences in AF-miRNA expression between these models. Alternatively, other transcription factors besides PPARG and EGR1 can be involved in AF-miRNA regulation depending on the fibrotic context. For instance, the transcription factor PU box binding protein (PU.1) was shown to positively regulate miR-29c in HSCs during TAA-induced liver fibrosis in mice [181]. In contrast to PPARG-regulated miR-29c expression which decreases with fibrosis progression [103], PU.1-mediated miR-29c expression resulted in more activated HSCs and more severe fibrosis through an alternative miR-29c targeting network [181].

Other mechanisms that mediate context-specific differences in miRNA expression include epigenetic accessibility of miRNA promoters and various post-transcriptional processes such as alternative miRNA processing, post-translational modifications of AGO proteins, and miRNA transport to the cytoplasm [93]. It is also important to consider that miRNA function is essentially defined by the mRNAs they target. Since miRNA targeting is highly context-specific [182], the molecular differences between the studied liver fibrosis models can result in different AF-miRNA expression patterns targeting additional or alternative genes beyond the AF-miRNA network described by us (**Project A**) [103]. Overall, the observed differences in AF-miRNA expression between the different fibrosis models emphasize the complexity of miRNA biology and regulation, which depends on various contextual cues such as cell type, cause of fibrotic injury, and severity of fibrosis.

5 Project C: Using PPARG Agonists to Target Murine Liver Fibrosis through Modulation of the PPARG-regulated AF-miRNA Network

5.1 Summary

In Winkler *et al.* (2020), we identified the PPARG-regulated AF-miRNA network, which influences the fibrotic microenvironment not only in HCC, but also in CCl_4-induced liver fibrosis and *in vitro* in pHSCs (**Project A**) [103]. Mechanistically, we postulate that the reduced AF-miRNA expression during HSC activation is directly mediated by the reduced expression and activity of their transcription factor PPARG. Without the inhibitory effects of the AF-miRNAs, their fibrotic target genes accumulate and contribute to liver fibrogenesis [103].

Here, I investigated whether modulation of the PPARG-regulated AF-miRNA network reduces liver fibrogenesis. In the mouse, PPARG directly and positively regulates 7 out of 8 AF-miRNAs of the network [103]. To collectively increase AF-miRNA expression, I aimed to increase the transcriptional activity of PPARG using the PPARG agonists pioglitazone and PGJ2 [61]. Experimentally, I performed pioglitazone treatments of an *in vivo* CCl_4-induced liver fibrosis mouse model and of an *in vitro* pHSC model. I further assessed the effects of pioglitazone and PGJ2 on PPARG activity as well as AF-miRNA and target gene expression *in vitro* using different immortalized hepatic cell lines.

Pioglitazone neither increased AF-miRNA expression in the *in vivo* CCl_4 model nor in the *in vitro* pHSC model. Yet, both pioglitazone and PGJ2 enhanced AF-miRNA expression directly through PPARG *in vitro* in immortalized HSC cell lines. I further showed that the thus increased AF-miRNA expression inhibits the expression of their fibrotic target genes *in vitro*, confirming that PPARG-mediated AF-miRNA modulation is a possible approach to reduce the fibrotic activity of HSCs during fibrogenesis.

5.2 Contributions

The following colleagues and collaboration partners contributed to the results of **Project C**.

Figure	Contribution
5.1	**Catrin Bitter**[1] designed the animal experiment. Siegfried Alberti[1] performed all invasive animal work with support from Michael Orlich[1] (injections, blood withdrawal, termination of animals). **Catrin Bitter** performed daily animal feedings and collected liver tissue and blood samples for further analyses.
5.2	**Catrin Bitter** prepared blood serum. Ralf Weiskirchen[2] measured markers of liver function in blood serum.
5.3a-c	**Catrin Bitter** prepared formalin-fixed paraffin-embedded liver sections and performed Sirius Red staining. Tanja Poth[3] performed HE and ACTA2 stainings. Veronika Eckel[4] imaged samples. Tanja Poth performed fibrotic scoring. **Catrin Bitter** quantified Sirius Red and ACTA2 signals.
5.3d and 5.4	**Catrin Bitter** isolated RNA from liver tissue samples and performed qPCR measurements.
5.5-5.6	Ralf Weiskirchen isolated pHSCs. **Catrin Bitter** performed pHSC activation and treatment, imaged cells, performed signal quantification, isolated RNA, and performed qPCR measurements.
5.7	**Catrin Bitter** generated luciferase reporter plasmids and performed luciferase assay.
5.8-5.10	Ralf Weiskirchen provided Col-GFP cell line. Ivana Winkler[1] generated GRX-Pparg cell line as part of **Project A** [103]. **Catrin Bitter** treated cells, isolated RNA, and performed qPCR measurements.
S1-S3	Bilge Ergin[1] generated vector pGL3-2x-TSm-tk120-Fluc. **Catrin Bitter** generated luciferase reporter vectors pGL3-consPPRE-tk120-Fluc and pGL3-29cPPRE-tk120-Fluc.
Other	**Catrin Bitter** designed the research together with Alfred Nordheim[1] as supervisor. **Catrin Bitter** analyzed the presented data and wrote the results and discussion presented below.

[1] Catrin Bitter, Dr. Siegfried Alberti, Dr. Michael Orlich, Dr. Ivana Winkler, Dr. Bilge Ergin, and Prof. Dr. Alfred Nordheim: Department for Molecular Biology, IFIZ, Eberhard Karls University Tübingen, Germany.

[2] Prof. Dr. Ralf Weiskirchen: Experimental Gene Therapy and Clinical Chemistry, Institute of Molecular Pathobiochemistry, University Hospital RWTH Aachen, Germany.

[3] Dr. med. vet. Tanja Poth and team (Heike Conrad, Sarah Lammer, Diana Lutz, Karin Rebholz, Jutta Scheuerer, Christine Schmitt, Elisabeth Specht-Delius): CMCP, Institute of Pathology, Heidelberg University Hospital, Germany.

[4] Veronika Eckel: Tissue Bank of the NCT, Heidelberg, Germany.

5.3 Results

5.3.1 Pioglitazone Treatment to Target CCl_4-induced Liver Fibrosis in Mice through the AF-miRNA Network

Besides its role in regulating the fibrotic tumor microenvironment of HCC, we also showed that the PPARG-regulated AF-miRNA network regulates fibrotic processes independent of HCC (**Project A**) [103]. We showed significant downregulation of *Pparg* and the AF-miRNAs as well as significant upregulation of their fibrotic target genes in a CCl_4-induced liver fibrosis mouse model (Figures S4 and S11B of Winkler *et al.* (2020)) [103].

With PPARG as transcription factor directly regulating AF-miRNA expression, PPARG agonists are promising compounds to enhance PPARG activity and thus AF-miRNA expression collectively. Even though we and others showed anti-fibrotic effects of the endogenous PPARG agonist PGJ2 in cell culture experiments (Figure S13 of Winkler *et al.* (2020)) [103,183,184], PGJ2 is not easily administered *in vivo* [185]. However, pioglitazone is another well-known PPARG agonist, which serves as clinically approved drug for the treatment of diabetes and is additionally researched as therapeutic drug to treat liver fibrosis (ClinicalTrials.gov, e.g. NCT04584242) [61,186].

To investigate *in vivo* whether pioglitazone increases PPARG-mediated AF-miRNA expression and thus reduces fibrosis progression, CCl_4-induced liver fibrosis in mice was treated with pioglitazone as shown in **Figure 5.1**. Mice received repeated injections of CCl_4 over a period of 4 weeks to induce liver fibrosis (CCl_4 group), while the control group received oil injections (oil control group). A third group of mice received pioglitazone orally in addition to CCl_4 injections (CCl_4+Pio group). According to the working hypothesis, pioglitazone is expected to preventively reduce the CCl_4-mediated fibrotic effects in this group.

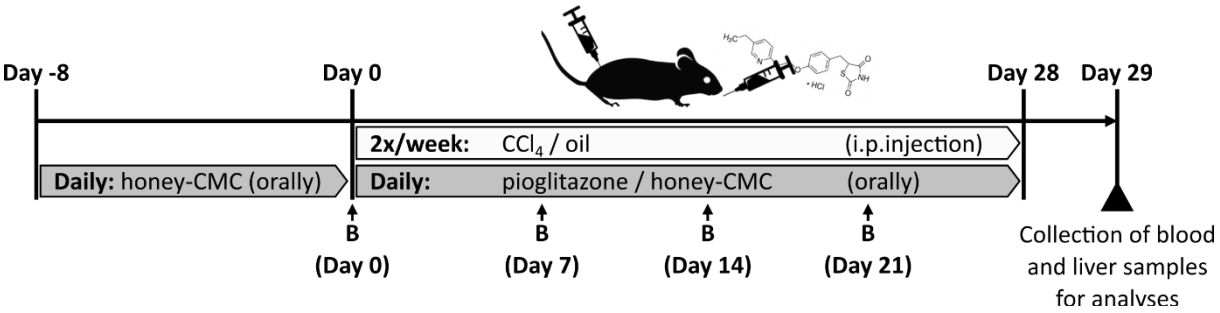

Figure 5.1 | Experimental design for pioglitazone treatment of CCl_4-induced liver fibrosis in mice. Adult, male C57BL/6J mice (n=15/group) were acclimatized to daily oral voluntary feeding with honey-CMC (vehicle) for eight days (Day -8 to Day 0) before the start of the experiment. Starting Day 1, mice either received CCl_4 (CCl_4 and CCl_4+Pio group) or corn oil (oil control group) twice a week for 4 weeks by i.p. injection (**white**). In parallel, animals were either fed pioglitazone (CCl_4+Pio group) or honey-CMC (oil control and CCl_4 group) daily by oral voluntary feeding (**grey**). Blood samples were collected from n=5 mice before and during the experiment (B) and from all n=45 mice terminally at Day 29 together with liver samples. B – blood sample collection. CMC – carboxymethyl cellulose salt. i.p. – intraperitoneal.

To monitor disease progression over the course of the experiment, blood samples were taken from a subset of mice before and during the experiment. After 4 weeks (Day 29), blood and liver samples were collected from all mice for further analyses.

The degree of liver fibrosis was initially assessed by four blood serum markers of liver function, the enzymatic activity of ALT, AST, and AP as well as bilirubin concentration (**Figure 5.2**). AST and ALT activity was measured to assess the degree of hepatocellular necrosis typical for almost all liver diseases, including toxin-induced damage [31]. As markers especially for cholestasis, but also for other types of liver damage including fibrosis and cirrhosis, AP activity and bilirubin concentration were measured [32].

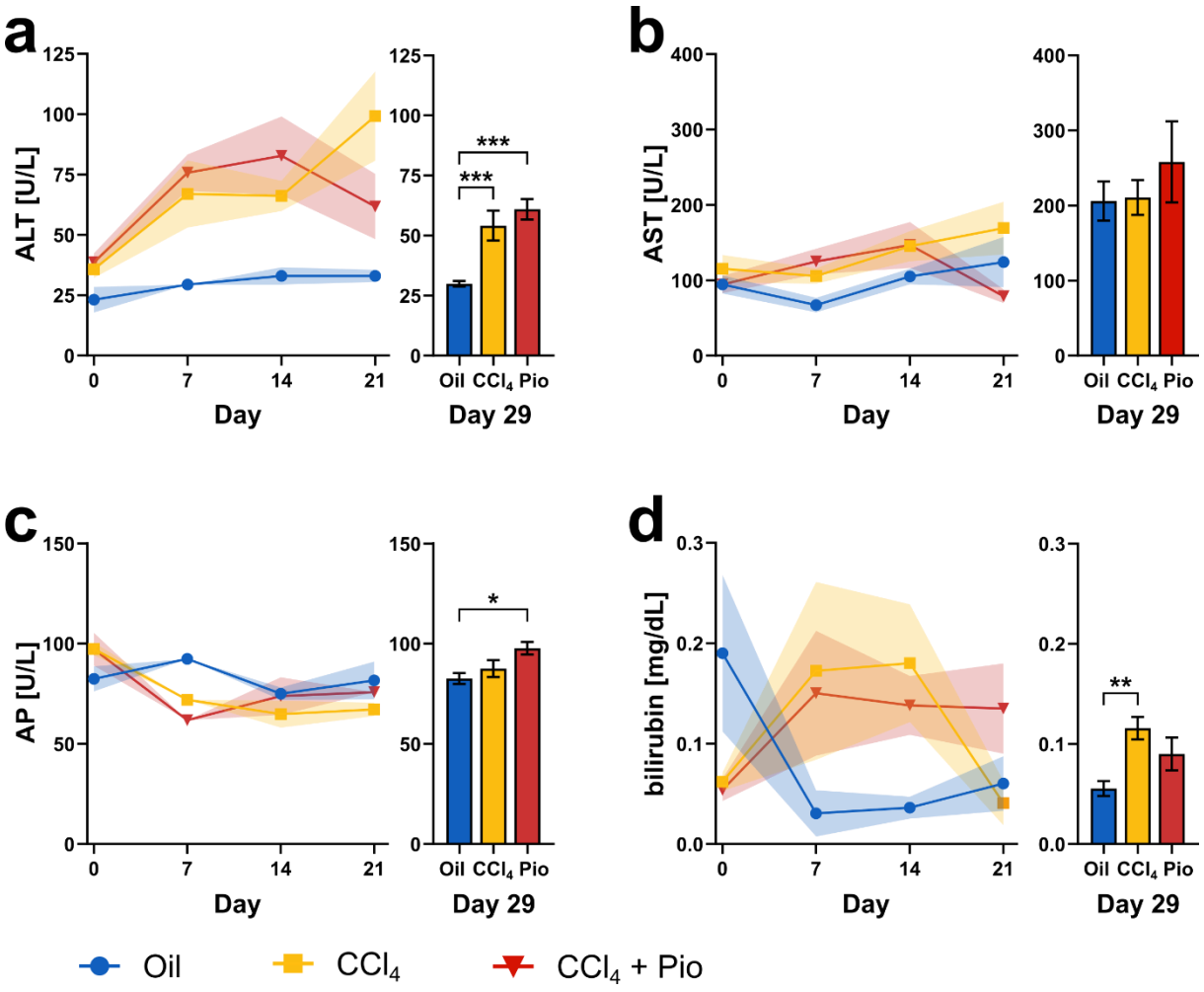

Figure 5.2 | Blood serum markers of liver function during the 4 weeks of pioglitazone-treated CCl_4-induced liver damage in mice. Enzymatic activity of (**a**) ALT, (**b**) AST, and (**c**) AP as well as (**d**) concentration of bilirubin were measured in blood serum collected before (Day 0) and during (Days 7, 14, 21) the experiment (n=5/group) as well as terminally (Day 29) in oil control, CCl_4, and CCl_4+Pio treated animals (n=15, 15, 14). Data are shown as mean and SEM. Statistical comparison of Day 29 data by ordinary one-way ANOVA with Tukey-adjusted post-hoc test. * $p_{adj} \leq 0.05$, ** $p_{adj} \leq 0.01$, *** $p_{adj} \leq 0.001$. ALT – alanine aminotransferase, AP – alkaline phosphatase, AST – aspartate aminotransferase, CCl_4 – carbon tetrachloride, Pio – pioglitazone.

Enzymatic activity of ALT was increased with CCl_4 and CCl_4+Pio treatment as early as Day 7 and remained elevated over the course of the experiment. After 4 weeks, ALT activity significantly increased to similar degrees with both CCl_4 and CCl_4+Pio treatment compared to oil control (**Figure 5.2a**). In contrast, even though AST activity increased slowly from about 100 U/L to 200 U/L over the time course of the experiment, it did so for all three treatment groups, and this did not result in any significant differences between the groups at Day 29 (**Figure 5.2b**). AP activity was relatively stable over the course of the experiment but was significantly increased in CCl_4+Pio-treated animals after 4 weeks compared to oil control (**Figure 5.2c**). Bilirubin concentration was, similar to ALT activity, increased with CCl_4 and CCl_4+Pio treatment as early as Day 7 and remained, apart from CCl_4 treatment at Day 21, elevated over the course of the experiment. After 4 weeks, bilirubin concentration was significantly increased in the CCl_4 group compared to oil control (**Figure 5.2d**). Together, the measured blood serum markers, especially ALT and bilirubin, suggest that 4 weeks of CCl_4-treatment did induce liver damage to a certain degree. However, when comparing the CCl_4 and CCl_4+Pio groups, pioglitazone treatment did not significantly reduce the CCl_4-induced liver damage measured by these markers.

The degree of liver fibrosis was further assessed in liver specimens by Sirius Red staining of collagen depositions and by ACTA2 staining of activated HSCs (**Figure 5.3**) [7]. Sirius Red staining revealed the presence of bridging fibrosis after 4 weeks of CCl_4 treatment in both the CCl_4 and CCl_4+Pio group. This was accompanied by the activation of HSCs as indicated by the increased ACTA2 signal in both CCl_4-treated groups compared to oil control (**Figure 5.3a**). Quantification of the Sirius Red and ACTA2 signals in the microscopic images confirmed that both, collagen deposition and HSC activation, respectively, are significantly increased in both CCl_4-treated groups compared to oil control (**Figure 5.3c**). Sirius Red signal quantification further showed that collagen deposition was significantly reduced in the presence of pioglitazone (**Figure 5.3c**). Pathologic scoring of liver fibrosis based on Sirius Red stainings showed that CCl_4 treatment induced fibrosis in both the CCl_4 and CCl_4+Pio group. However, no significant effect of pioglitazone reducing the degree of fibrosis in the CCl_4+Pio group compared to the CCl_4 group was observed (**Figure 5.3b**). Furthermore, the significantly increased *Acta2* gene expression upon CCl_4 treatment in both the CCl_4 and CCl_4+Pio group reflects the ACTA2 protein levels that were also increased independent of the absence or presence of pioglitazone (**Figure 5.3c, d**).

In summary, the analysis of the blood serum markers of liver function and of the liver specimens shows that CCl_4 administration successfully induced liver fibrosis over a time course of 4 weeks but that the effect of pioglitazone on the degree of liver fibrosis is at most very limited.

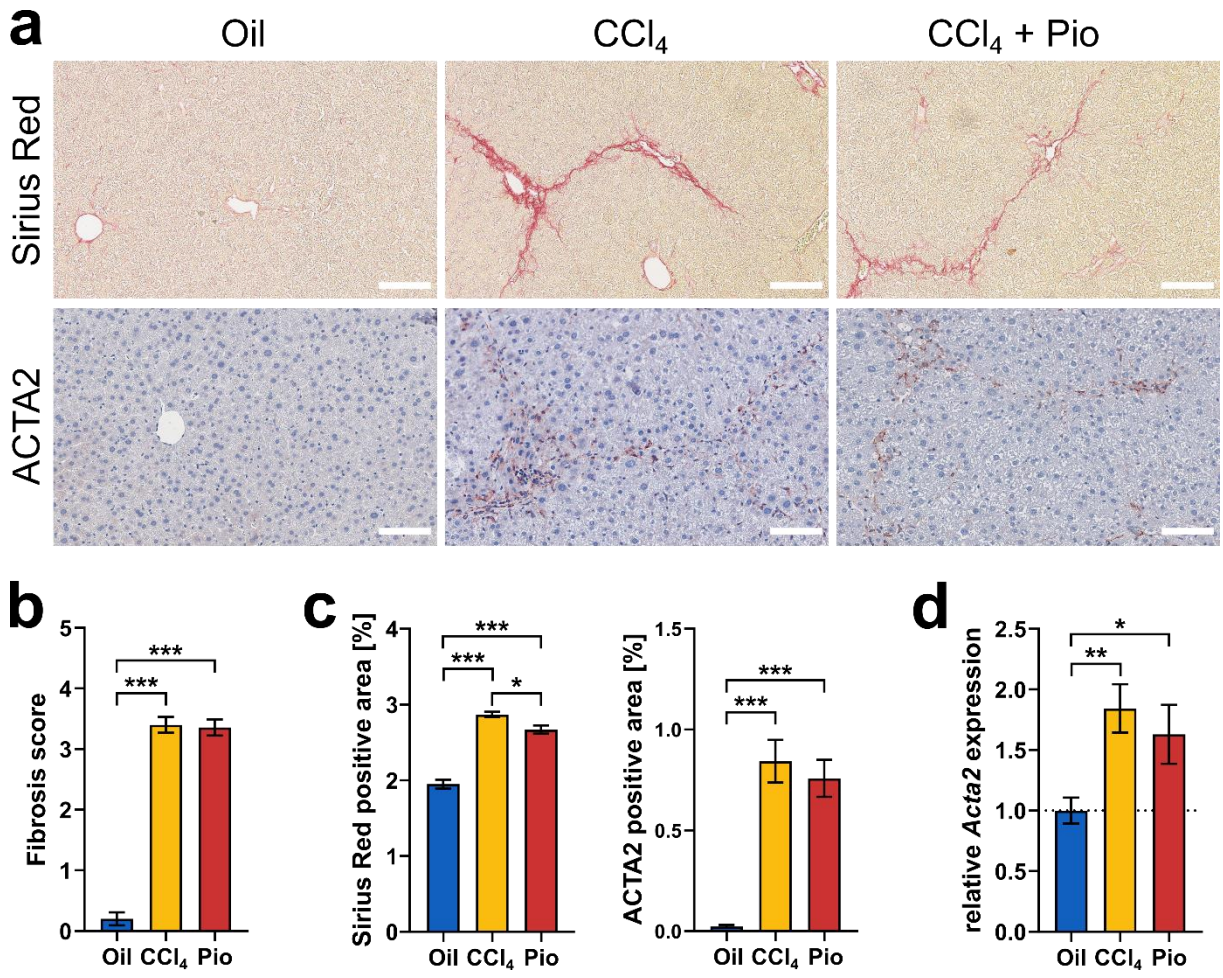

Figure 5.3 | Liver fibrosis assessment of pioglitazone-treated CCl_4-induced liver damage in mice. (**a**) Representative images of liver specimens stained for collagen depositions by Sirius Red and for HSC activation by ACTA2. Scale bar: 100 µm. (**b**) Fibrosis score determined by pathologist Dr. med. vet. Tanja Poth based on Sirius Red stainings. (**c**) Quantification of Sirius Red and ACTA2 positive areas shown in **a**. (**d**) Relative *Acta2* gene expression measured by qPCR normalized to *Gusb* and *Tbp* and shown relative to the oil control mean. (**a**-**d**) n=15, 15, 14 for oil control, CCl_4, and CCl_4+Pio mice. (**b**-**d**) Data are shown as mean and SEM. Statistical comparison by ordinary one-way ANOVA with Tukey-adjusted post-hoc test. * $p_{adj} \leq 0.05$, ** $p_{adj} \leq 0.01$, *** $p_{adj} \leq 0.001$. CCl_4 – carbon tetrachloride, Pio – pioglitazone.

Nevertheless, a subset of the AF-miRNA network was analyzed in liver tissue samples of oil control, CCl_4, and CCl_4+Pio mice to assess on the molecular level whether pioglitazone has any anti-fibrotic effects on *Pparg*, the AF-miRNAs or their target genes (**Figure 5.4**). Further indicating HSC activation upon fibrotic changes in the liver, *Pparg* expression was significantly downregulated with CCl_4 treatment in both the CCl_4 and CCl_4+Pio group compared to oil control (**Figure 5.4a**). However, expression of the measured AF-miRNAs was unaltered with any treatment (**Figure 5.4b**). Still, the fibrosis-associated target genes *Col1a1* and *Loxl2* were significantly upregulated in the CCl_4 and CCl_4+Pio group, while *Pdgfb* expression was not increased with CCl_4 treatment (**Figure 5.4c**). Again, neither the reduction in *Pparg* expression nor the increase in *Col1a1* and *Loxl2* expression upon CCl_4 treatment was diminished by the presence of pioglitazone.

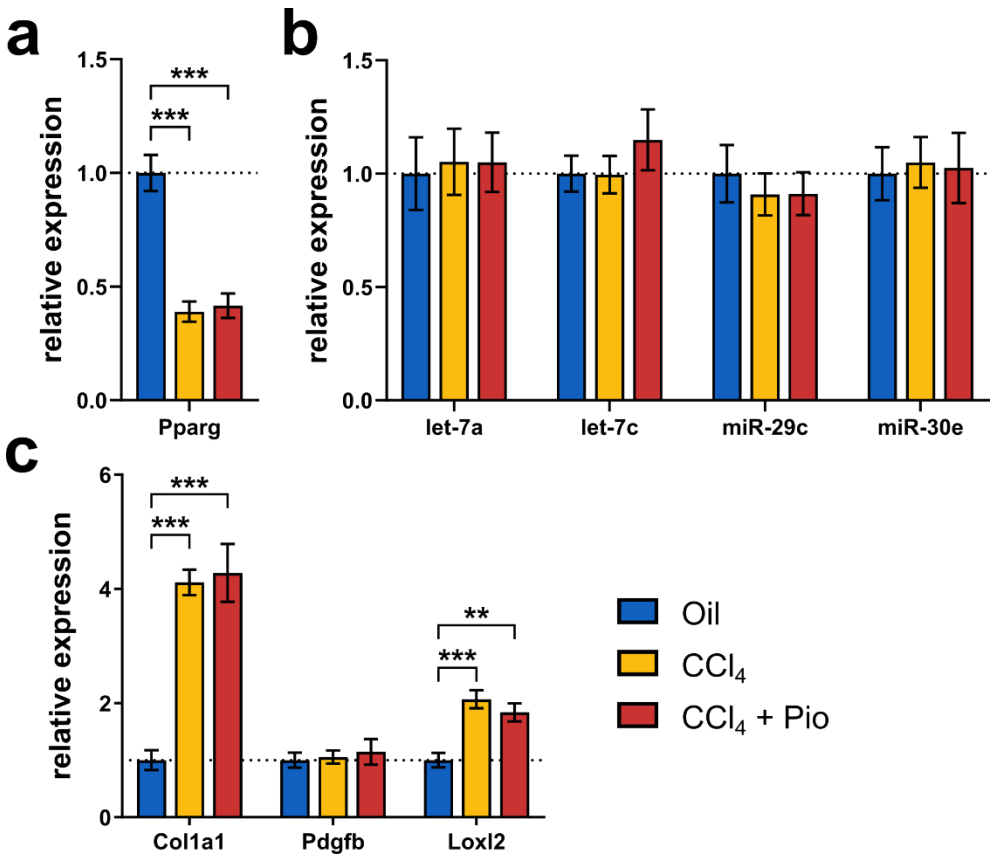

Figure 5.4 | Expression of the PPARG-regulated AF-miRNA network in pioglitazone-treated CCl_4-induced liver fibrosis in mice. Relative expression of (**a**) *Pparg*, (**b**) selected AF-miRNAs, and (**c**) a subset of their target genes in oil control, CCl_4, and CCl_4+Pio mice (n=15, 15, 14). qPCR data were normalized to *Gusb* and *Tbp* for genes and to *Rnu6* and *Snord33* for miRNAs and are shown relative to the oil control mean. Data are shown as mean and SEM. Statistical comparison by ordinary one-way ANOVA with Tukey-adjusted post-hoc test. * $p_{adj} \leq 0.05$, ** $p_{adj} \leq 0.01$, *** $p_{adj} \leq 0.001$. CCl_4 – carbon tetrachloride, Pio – pioglitazone.

In conclusion and contrary to the working hypothesis, pioglitazone did not reduce the progression of CCl_4-induced liver fibrosis *in vivo* in mice over the time course of 4 weeks. While most parameters of liver fibrosis responded to CCl_4 treatment and confirmed the development of fibrosis over 4 weeks, this effect was only reduced for one parameter – Sirius Red quantification of collagen depositions – with pioglitazone treatment.

5.3.2 Pioglitazone Treatment to Target pHSC Activation through the AF-miRNA Network

Even though pioglitazone treatment did not reduce CCl_4-induced liver fibrosis preventively *in vivo* (**Chapter 5.3.1**), it remains to be shown whether pioglitazone is able to modulate the PPARG-regulated AF-miRNA network on a cellular level during HSC activation as it occurs in fibrogenesis. pHSCs are a valuable tool to study activation processes of HSCs *in vitro*. Isolated from mice in their inactive state, pHSCs undergo spontaneous activation with prolonged growth on standard plastic culture dishes [7].

This activation is accompanied by their transformation into myofibroblast-like cells and their loss of retinoid droplets as it also typically occurs during HSC activation *in vivo* [7,116]. We previously showed that the AF-miRNA network operates in such pHSCs, where activation caused significant downregulation of *Pparg* and the AF-miRNAs as well as significant upregulation of fibrotic target genes (Figures 3, 5A, and S3 of Winkler *et al.* (2020)) (**Project A**) [103].

To investigate whether pioglitazone reduces activation of HSCs through the PPARG-regulated AF-miRNA network, murine pHSCs were isolated in their inactive state and were either immediately harvested or cultured for six days to induce HSC activation as performed by us in Winkler *et al.* (2020) [103]. During cultivation, pHSCs were maintained in the absence or presence of pioglitazone to assess its effect on HSC activation (**Figure 5.5**) and the AF-miRNA network (**Figure 5.6**).

The observed morphologic changes and loss of retinoid droplets after six days in culture confirmed activation of pHSCs during prolonged growth on standard plastic culture dishes (**Figure 5.5**). However, pioglitazone treatment did not reduce the degree of HSC activation assessed by these parameters.

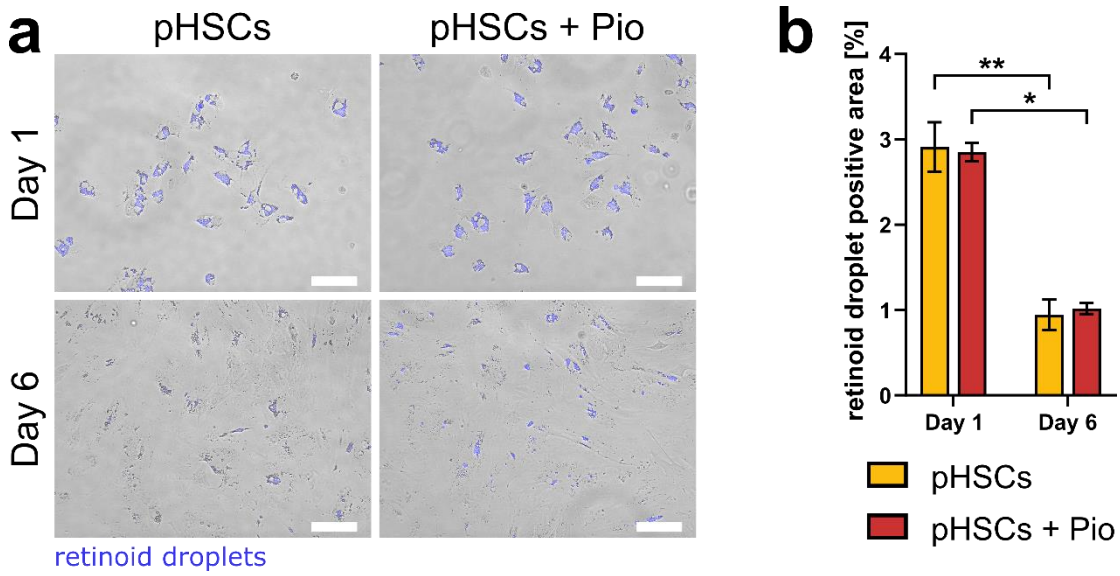

Figure 5.5 | Pioglitazone treatment of pHSCs during *in vitro* activation. Inactive pHSCs were cultured for six days in the absence or presence of 5 µM pioglitazone (n=3/group). (**a**) Spontaneous *in vitro* activation of pHSCs by prolonged growth on standard plastic culture dishes is characterized by morphologic changes (phase contrast) and loss of retinoid droplets (autofluorescence upon UV excitation). Scale bar: 100 µm. (**b**) Quantification of retinoid droplet positive area shown in **a**. Data are shown as mean and SEM. Statistical comparison by two-way repeated measures ANOVA with Bonferroni-adjusted post-hoc test. * $p_{adj} \leq 0.05$, ** $p_{adj} \leq 0.01$, *** $p_{adj} \leq 0.001$. pHSCs – primary hepatic stellate cells, Pio – pioglitazone.

To determine whether pioglitazone nonetheless affected the degree of HSC activation on the molecular level, *Acta2* gene expression was quantified in pHSCs activated by prolonged cultivation relative to inactive pHSCs (**Figure 5.6a**). In accordance with the microscopic data (**Figure 5.5**), *Acta2* gene expression was drastically increased in activated pHSCs independent of pioglitazone.

Next, the effect of pHSC activation and pioglitazone treatment on PPARG was determined (**Figure 5.6b**). *Pparg* expression was downregulated significantly in activated compared to inactive pHSCs in accordance with our previous findings (Figure 5A of Winkler *et al.* (2020)), but pioglitazone did not reduce this effect [103]. As agonist, pioglitazone rather influences PPARG activity than gene expression [61]. Therefore, expression of the PPARG target gene *Plin2* was assessed as readout for PPARG activity [155,156]. *Plin2* was significantly downregulated in activated pHSCs, but this reduction in PPARG activity was also not diminished by pioglitazone treatment (**Figure 5.6b**).

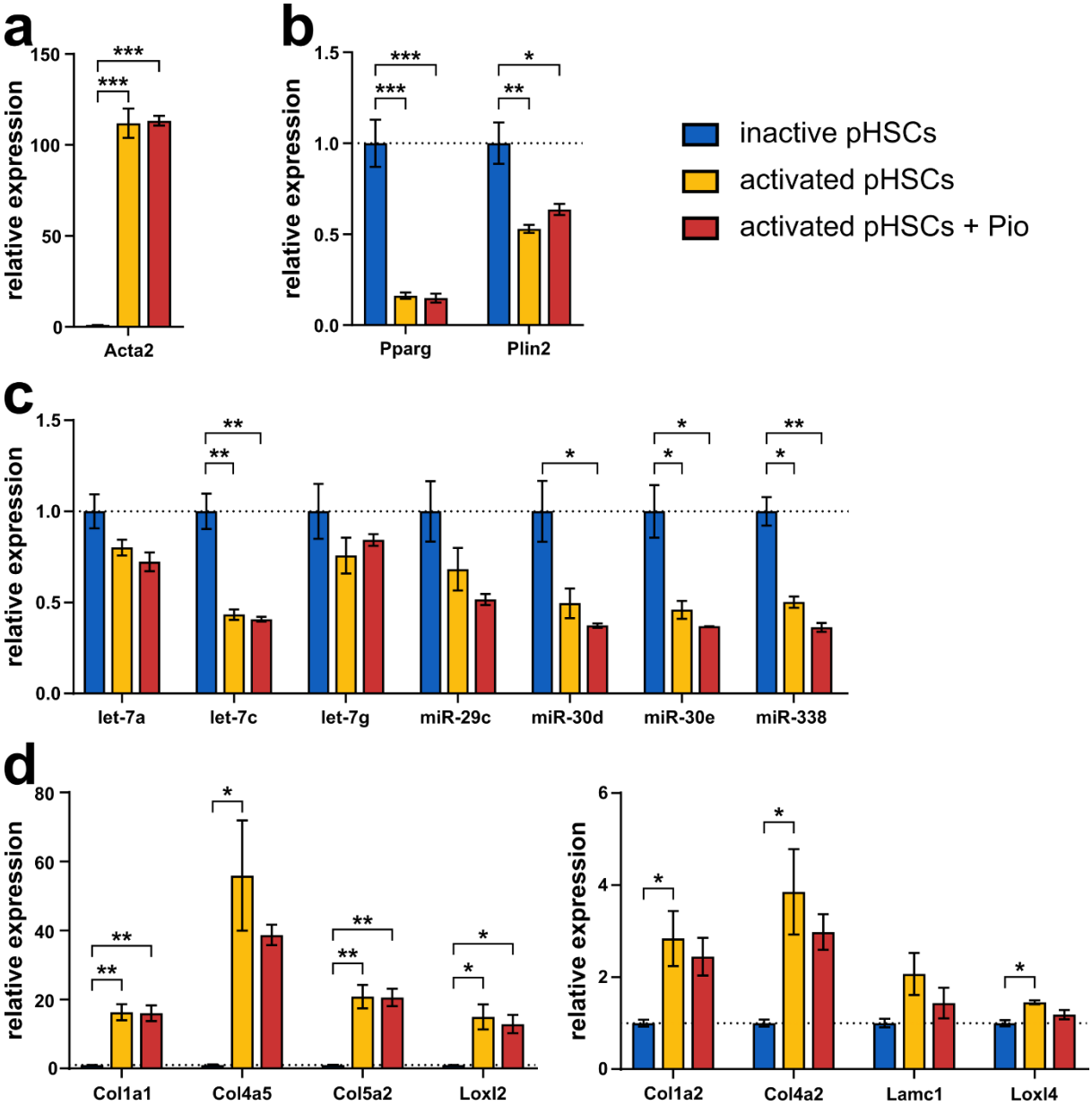

Figure 5.6 | Expression of *Acta2* and the PPARG-regulated AF-miRNA network in pioglitazone-treated activated pHSCs. Relative expression of (**a**) *Acta2*, (**b**) *Pparg* and its target gene *Plin2*, (**c**) the PPARG-regulated AF-miRNAs, and (**d**) a subset of their target genes in inactive, activated, and pioglitazone-treated activated pHSCs (n=3/group). qPCR data were normalized to *Gapdh*, *Gusb*, and *Tbp* for genes and to *Snord33* and *Snord35a* for miRNAs and are shown relative to the inactive pHSCs mean. Data are shown as mean and SEM. Statistical comparison by ordinary one-way ANOVA with Tukey-adjusted post-hoc test. * $p_{adj} \leq 0.05$, ** $p_{adj} \leq 0.01$, *** $p_{adj} \leq 0.001$., pHSCs – primary hepatic stellate cells, Pio – pioglitazone.

Analyzing the PPARG-regulated AF-miRNA network, 4 of the 7 AF-miRNAs (let-7c, miR-30d, miR-30e, and miR-338) were significantly downregulated while 7 of the 8 measured target genes (*Col1a1*, *Col4a5*, *Col5a2*, *Loxl2*, *Col1a2*, *Col4a2*, and *Loxl4*) were significantly upregulated in activated pHSCs relative to inactive pHSCs (**Figure 5.6c, d**). While the observed dysregulation of the AF-miRNA network with HSC activation confirms our previous data (Figure 3 of Winkler *et al.* (2020)), pioglitazone did not prevent these dysregulations of the AF-miRNA network during pHSC activation (**Figure 5.6c**, **d**).

On the one hand, these data successfully reproduced the pHSC experiment from **Project A** with the activation of pHSCs accompanied by downregulation of *Pparg* and the AF-miRNAs as well as upregulation of their target genes [103]. On the other hand, the degree of pHSC activation over the time course of six days was not prevented by treatment with 5 µM pioglitazone.

5.3.3 Modulation of the AF-miRNA Network in Immortalized HSC Cell Lines through the PPARG Agonists Pioglitazone and PGJ2

Even though pioglitazone treatment did neither modulate PPARG-mediated AF-miRNA expression *in vivo* in the 4 weeks CCl_4-induced liver fibrosis model (**Chapter 5.3.1**) nor during pHSC activation (**Chapter 5.3.2**), it remains to be shown whether PPARG agonists are molecularly and mechanistically able to modulate the AF-miRNAs and their target genes *in vitro*. Given the limited success of 5 µM pioglitazone in modulating AF-miRNA expression in previous experiments, the following cell-culture based assays were performed with 20 µM pioglitazone to account for the relatively low binding affinity of pioglitazone to PPARG [61,187]. The endogenous, higher-affinity PPARG agonist PGJ2 [61,185] was additionally investigated for its ability to modulate the AF-miRNA network.

Mechanistically, agonist binding induces PPARG heterodimerization with an RXR to bind to PPREs in promoter regions of genomic DNA, which induces the transcription of PPARG target genes and miRNAs [61,103]. Here, luciferase assays were performed to test whether pioglitazone and PGJ2 induce PPARG-mediated transcription of the firefly luciferase reporter gene (*Fluc*) under control of two different PPREs.

First, a consensus PPRE sequence was designed to represent the most frequent base at each PPRE position as reported by JASPAR's (v2020) position frequency matrix for the murine PPARG binding motif (MA0065.2) [132]. Vector pGL3-consPPRE-tk120-Fluc was cloned to contain four identical copies of this consensus PPRE (**Figure 5.7a**, **Supplementary Figure 2**). Second, we previously identified PPARG as transcription factor of the AF-miRNAs based on the presence of PPRE motifs in their promoter regions and confirmed PPARG binding to these PPREs by chromatin immunoprecipitation (Figure 5e of Winkler *et al.* (2020)) (**Project A**) [103]. The four individual PPRE motifs found in the promoter regions

of murine miR-29c were cloned into vector pGL3-29cPPRE-tk120-Fluc to test, representatively on miR-29c, whether PPARG agonists can induce transcription through the specific PPREs present in AF-miRNA promoters (**Figure 5.7a**, **Supplementary Figure 3**). In both vector constructs, the four PPREs were positioned upstream of the basal thymidine kinase promoter (tk120), which drives basal Fluc reporter expression.

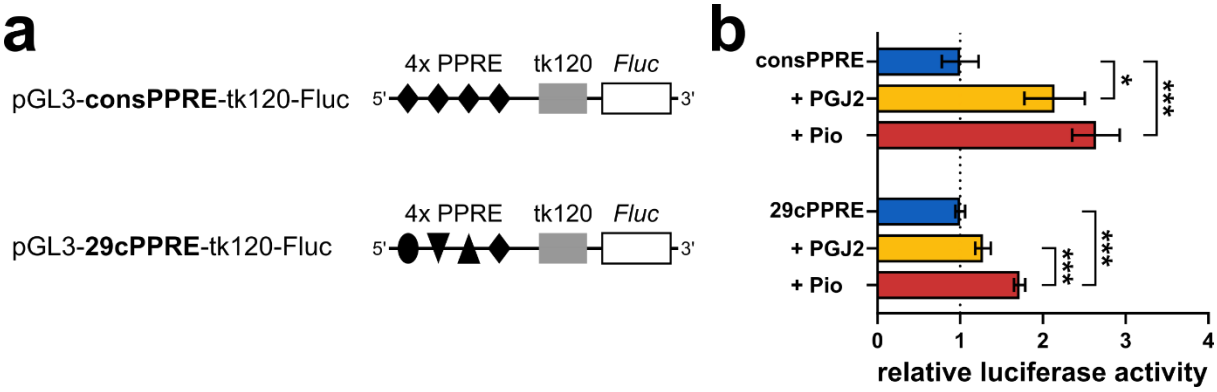

Figure 5.7 | PPARG drives luciferase activity via consensus PPREs and miR-29c PPREs upon PGJ2 and pioglitazone treatment. (**a**) Schematic display of luciferase reporter constructs which either contain 4 identical repeats of the consensus PPRE (**top**) or the 4 individual PPRE sequences within the miR-29c promoter regions (**bottom**) upstream of the basal promoter tk120, which drives *Fluc* cDNA expression. (**b**) Relative luciferase activity in reporter-transfected GRX-Pparg cells after 24 h of treatment with 2 µM PGJ2 or 20 µM pioglitazone compared to untreated cells (n=4/group). Relative luciferase activity represents firefly luciferase (Fluc) activity normalized to basal *Renilla* luciferase activity from co-transfected vector pRL-TK and is shown relative to the untreated control mean. Data are shown as mean and SEM. Statistical comparison by ordinary one-way ANOVA with Tukey-adjusted post-hoc test. * $p_{adj} \leq 0.05$, ** $p_{adj} \leq 0.01$, *** $p_{adj} \leq 0.001$. 29cPPRE – PPREs in the miR-29c promoter, consPPRE – consensus PPRE according to JASPAR [132], *Fluc* – firefly luciferase reporter gene, PPRE – peroxisome proliferator response element. PGJ2 – 15-Deoxy-$\Delta^{12,14}$-prostaglandin J2, Pio – pioglitazone.

Luciferase assay was performed in GRX-Pparg cells, which stably overexpress murine PPARG. Reporter-transfected cells without additional treatment served as control and showed basal luciferase activity based on tk120 promoter activity (**Figure 5.7b**). PPARG stimulation with both PGJ2 and pioglitazone for 24 h significantly increased relative luciferase activity under control of the consensus PPREs. Relative luciferase activity under control of the miR-29c PPREs was also significantly increased by pioglitazone, but not by PGJ2 (**Figure 5.7b**). Both PGJ2 and pioglitazone increased luciferase activity more via the consensus PPREs than via the miR-29c PPREs. Of note, luciferase activity under control of the miR-29c PPREs was significantly more increased by pioglitazone than by PGJ2 (**Figure 5.7b**).

Luciferase assay showed that both PPARG agonists can indeed enhance PPARG activity to induce transcription of downstream target genes under control of consensus and miRNA-specific PPREs. Therefore, different immortalized hepatic cell lines were treated with pioglitazone and PGJ2 to assess their effect on AF-miRNA gene expression under control of their natural PPREs. For this, the three HSC cell lines Col-GFP, GRX, and GRX-Pparg were compared. Col-GFP cells are derived from pHSCs isolated

from CCl_4-induced fibrotic livers, while GRX cells stem from HSCs isolated from fibrotic liver granulomas [115,117]. GRX-Pparg cells were generated from GRX cells to stably overexpress mouse PPARG [103]. These HSC cell lines were further compared to the hepatocyte cell line Hepa1-6 [114] to assess in an *in vitro* approach whether different hepatic cell types respond differently to PPARG agonist treatments.

Considering that PGJ2 and pioglitazone function through direct interaction with PPARG [61], first, baseline expression levels of *Pparg* as well as *Plin2*, as readout for PPARG activity [155,156], were compared by qPCR in these four cell lines (**Figure 5.8**). *Pparg* expression levels were similar in the two HSC cell lines Col-GFP and GRX and were in both cases significantly lower than in Hepa1-6 cells (**Figure 5.8a**). The fact that *Pparg* expression was significantly and drastically higher in GRX-Pparg cells than in GRX cells confirmed successful *Pparg* overexpression in these stably transfected cells. *Pparg* expression levels in GRX-Pparg cells were also significantly higher than in Hepa1-6 and Col-GFP cells (**Figure 5.8a**).

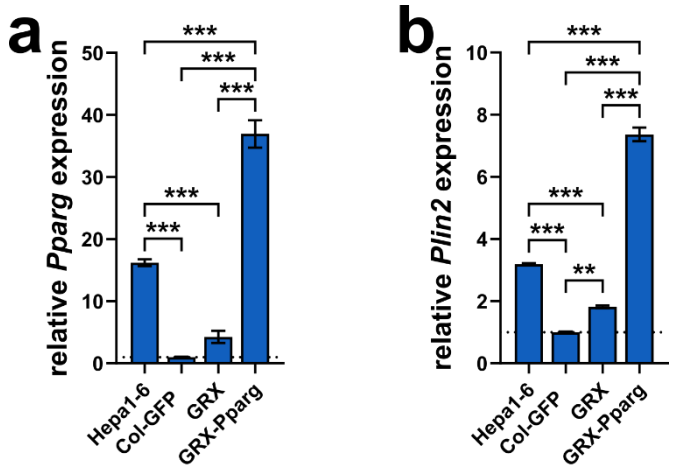

Figure 5.8 | Comparative PPARG expression and activity in different hepatic cell lines. Relative expression of (**a**) *Pparg* and (**b**) its target gene *Plin2* in the hepatocyte cell line Hepa1-6 as well as in the HSC cell lines Col-GFP, GRX, and GRX-Pparg (n=4/group). qPCR data were normalized to *Gapdh*, *Gusb*, and *Tbp* and are shown relative to the arbitrarily chosen Col-GFP mean. Data are shown as mean and SEM. Statistical comparison by ordinary one-way ANOVA with Tukey-adjusted post-hoc test. * $p_{adj} \leq 0.05$, ** $p_{adj} \leq 0.01$, *** $p_{adj} \leq 0.001$.

Plin2 showed a similar expression pattern as *Pparg* and was significantly different between all four cell lines (**Figure 5.8b**). *Plin2* expression was highest in GRX-Pparg cells, second highest in Hepa1-6 cells and lowest in Col-GFP cells. Additionally, *Plin2* expression was significantly higher in GRX than in Col-GFP cells. Overall, it was observed that a high baseline *Pparg* expression positively correlated with a high baseline *Plin2* expression (**Figure 5.8**).

Next, all four cell lines were treated with PGJ2 and pioglitazone to assess to which degree AF-miRNA expression is upregulated by these PPARG agonists and whether the baseline amount of PPARG available for agonist binding influences their responsiveness to the PPARG agonists. Cells were treated for 4 h and 24 h to investigate potential time-sensitive responses to PGJ2 and pioglitazone (**Figure 5.9**). Interestingly, AF-miRNA expression in Hepa1-6 cells did not respond to PGJ2 or pioglitazone, neither after 4 h nor 24 h of treatment (**Figure 5.9a**).

In Col-GFP cells, PGJ2 treatment did not increase expression of any of the measured AF-miRNAs (**Figure 5.9b**). Instead, let-7a was even significantly downregulated after 24 h of PGJ2 treatment compared to untreated control and compared to 4 h of PGJ2 treatment. However, Col-GFP cells showed significantly upregulated let-7a expression after 4 h of pioglitazone treatment which declined significantly from 4 h to 24 h to return to the initial expression levels observed in untreated cells (**Figure 5.9b**). Even though not significant, let-7g, miR-29c, and miR-30d showed a similar trend of upregulation after 4 h of pioglitazone treatment, which declined again after 24 h for let-7g and miR-29c. When comparing the effect of the two PPARG agonists on Col-GFP cells at each timepoint, pioglitazone induced significantly higher let-7a expression than PGJ2 after 4 h and 24 h, and significantly higher let-7g expression after 4 h (**Figure 5.9b**).

In GRX cells, the PPARG agonists affected miR-29c and miR-30d expression, rather than let-7a and let-7g expression as they did in Col-GFP cells (**Figure 5.9**). PGJ2 treatment only induced significant upregulation of miR-29c after 24 h of treatment, while pioglitazone significantly upregulated miR-29c and miR-30d, and already after 4 h of treatment (**Figure 5.9c**). After 4 h of treatment, pioglitazone thus induced significantly higher miR-29c expression than PGJ2. The pioglitazone-induced upregulation of miR-29c and miR-30d after 4 h was significantly reduced after 24 h of treatment (**Figure 5.9c**). While miR-30d expression returned to the initial expression levels observed in untreated cells after 24 h of pioglitazone treatment, miR-29c expression levels after 24 h of pioglitazone treatment remained significantly higher than in untreated GRX cells.

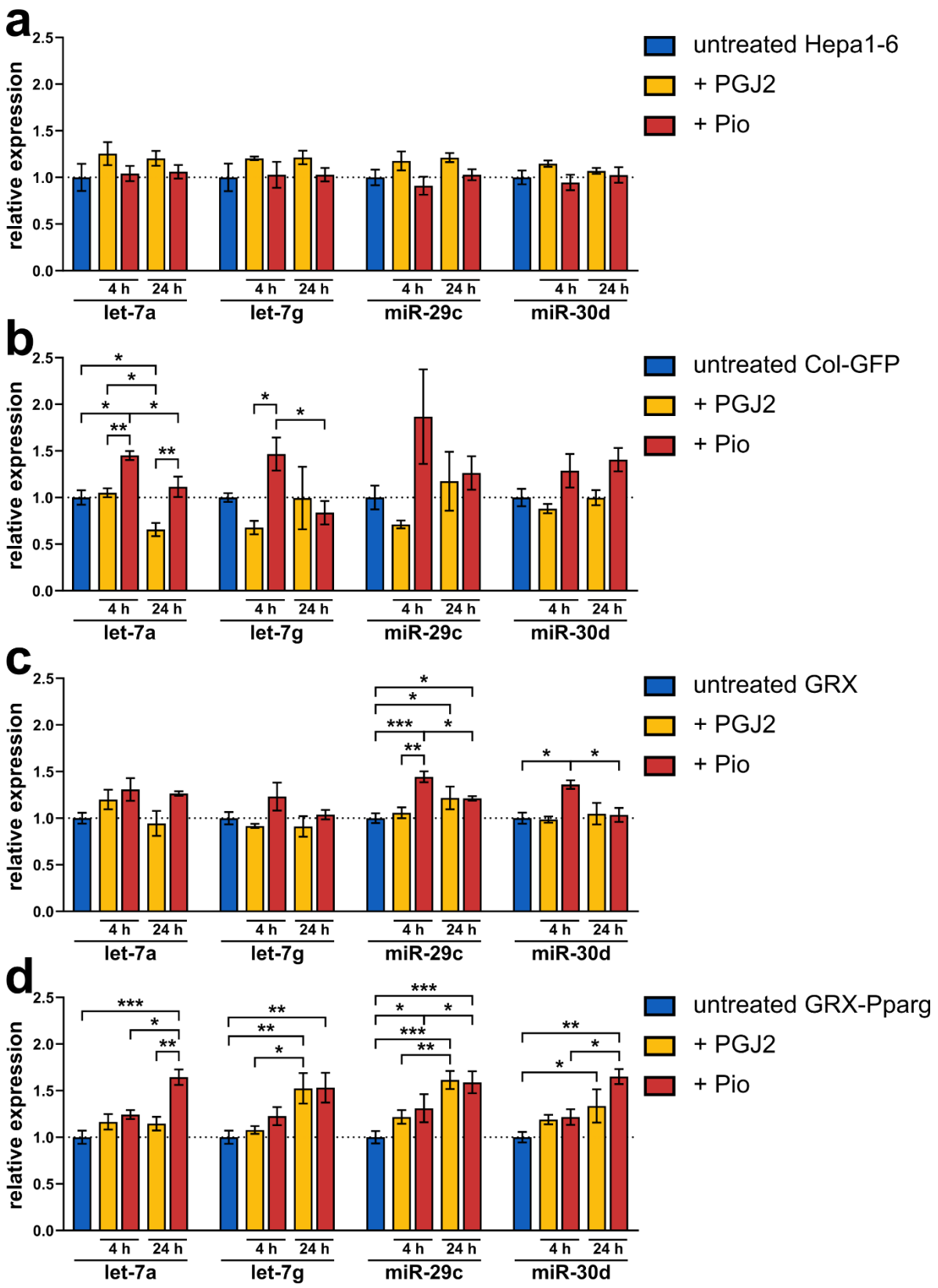

Figure 5.9 | Effects of PGJ2 and pioglitazone on AF-miRNA expression in different hepatic cell lines. Relative expression of a subset of the AF-miRNAs in (**a**) the hepatocyte cell line Hepa1-6 as well as in the HSC cell lines (**b**) Col-GFP, (**c**) GRX, and (**d**) GRX-Pparg. Cells were treated with 2 µM PGJ2 or 20 µM pioglitazone for 4 h or 24 h and were compared to untreated cells (n=3/group). qPCR data were normalized to *Rnu6*, *Snord33*, and *Snord35a* and are shown relative to the untreated cells mean. Data are shown as mean and SEM. Statistical comparison by two-way ANOVA with Tukey-adjusted post-hoc test over time and Sidak-adjusted post-hoc test to compare treatments. * $p_{adj} \leq 0.05$, ** $p_{adj} \leq 0.01$, *** $p_{adj} \leq 0.001$. PGJ2 – 15-Deoxy-$\Delta^{12,14}$-prostaglandin J2, Pio – pioglitazone.

In GRX-Pparg cells, both PPARG agonists showed the strongest effect on all measured AF-miRNAs compared to the other cell lines (**Figure 5.9**). While 4 h of PGJ2 treatment did again not increase AF-miRNA expression significantly, 24 h of PGJ2 treatment induced significant upregulation of let-7g, miR-29c, and miR-30d compared to untreated GRX-Pparg cells (**Figure 5.9d**). The upregulation of let-7g and miR-29c was significantly higher after 24 h than after 4 h of PGJ2 treatment. Interestingly, pioglitazone also induced stronger AF-miRNA upregulation after 24 h than after 4 h in GRX-Pparg cells, contrasting previous observations in Col-GFP and GRX cells (**Figure 5.9b, c**). While let-7a, let-7g, miR-29c, and miR-30d were all significantly upregulated in GRX-Pparg cells after 24 h of pioglitazone treatment, only miR-29c was also significantly upregulated after the shorter period of 4 h of treatment (**Figure 5.9d**). For let-7a, miR-29c, and miR-30d, upregulation was significantly higher after 24 h than after 4 h of pioglitazone treatment. Comparing the effect of the two PPARG agonists on GRX-Pparg cells at each timepoint, pioglitazone induced significantly higher let-7a expression than PGJ2 after 24 h of treatment. Other than that, the effect of both agonists on the measured AF-miRNAs was comparable after 4 h as well as 24 h in this cell line (**Figure 5.9d**).

Overall, AF-miRNA expression was not modulated by the PPARG agonists PGJ2 and pioglitazone in the hepatocyte cell line Hepa1-6. However, AF-miRNA expression was modulated to varying degrees in the three HSC cell lines Col-GFP, GRX, and GRX-Pparg upon PGJ2 and pioglitazone treatment. Even though PGJ2 increased the expression of miR-29c in GRX cells after 24 h and the expression of let-7g, miR-29c, and miR-30d in GRX-Pparg cells after 24 h, it also decreased expression of let-7a in Col-GFP cells after 24 h. In all three HSC cell lines, pioglitazone induced significant upregulation of at least one AF-miRNA. While AF-miRNA upregulation was strongest after 4 h of pioglitazone treatment in Col-GFP and GRX cells and declined back to initial levels after 24 h, AF-miRNA upregulation was most consistent after 24 h of pioglitazone treatment of GRX-Pparg cells (**Figure 5.9**).

Given that both PPARG agonists induced the strongest AF-miRNA upregulation in GRX-Pparg cells after 24 h, the AF-miRNA network was further investigated under these treatment conditions (**Figure 5.10**). While *Pparg* expression was not altered by either PGJ2 or pioglitazone treatment after 24 h, *Plin2* expression as readout for PPARG activity was significantly increased by both PGJ2 and pioglitazone (**Figure 5.10a**). Interestingly, pioglitazone treatment induced significantly higher *Plin2* upregulation than PGJ2, mirroring the luciferase assay data of the miR-29c PPRE (**Figure 5.7**) and the let-7a expression in GRX-Pparg cells after 24 h of treatment (**Figure 5.9**).

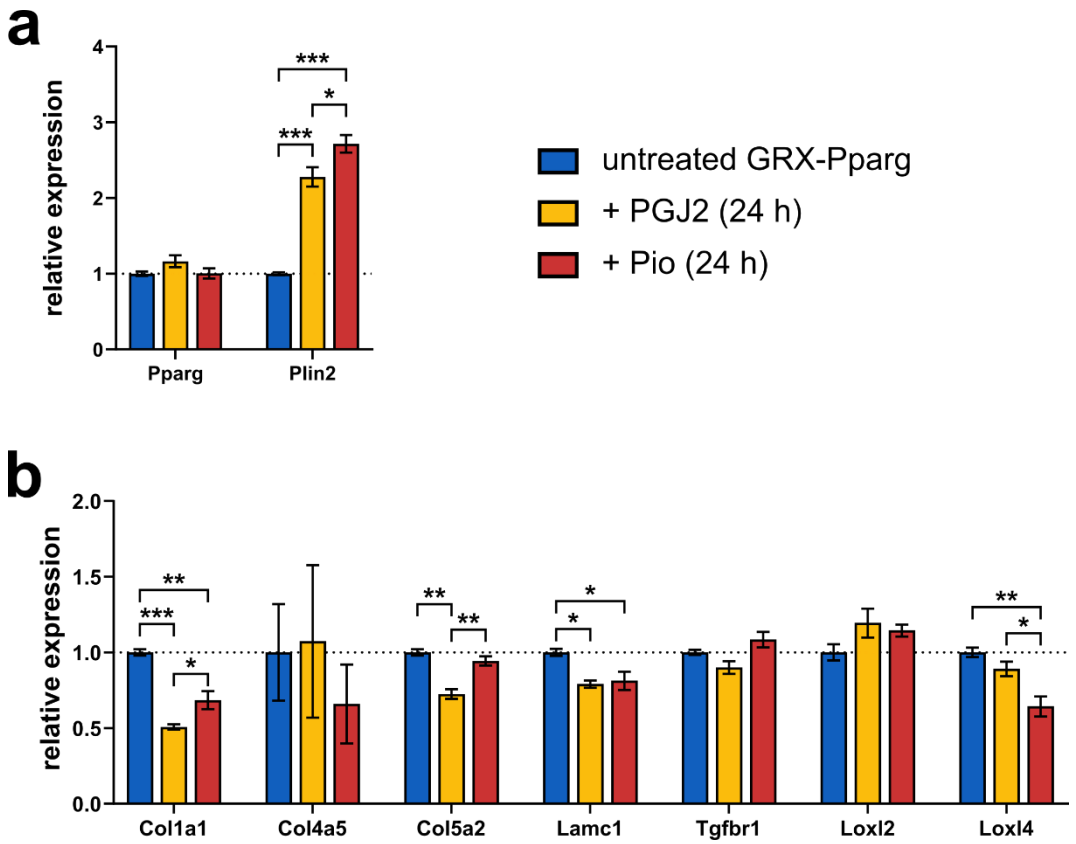

Figure 5.10 | PGJ2 and pioglitazone increase PPARG activity and thus reduce expression of fibrotic target genes through the AF-miRNA network in GRX-Pparg cells. Relative expression of (**a**) *Pparg* and its target gene *Plin2* as well as (**b**) a subset of fibrotic target genes of the AF-miRNA network in GRX-Pparg cells after 24 h of treatment with 2 µM PGJ2 or 20 µM pioglitazone compared to untreated cells (n=3/group). qPCR data were normalized to *Gusb* and *Tbp* and are shown relative to the untreated cells mean. Data are shown as mean and SEM. Statistical comparison by ordinary one-way ANOVA with Tukey-adjusted post-hoc test. * $p_{adj} \leq 0.05$, ** $p_{adj} \leq 0.01$, *** $p_{adj} \leq 0.001$. PGJ2 – 15-Deoxy-$\Delta^{12,14}$-prostaglandin J2, Pio – pioglitazone.

Next, a subset of the fibrotic target genes of the AF-miRNA network was analyzed by qPCR to assess whether the PPARG-mediated upregulation of the AF-miRNAs was able to reduce expression of the fibrotic target genes in GRX-Pparg cells (**Figure 5.10b**). Indeed, expression of *Col1a1*, *Col5a2*, and *Lamc1* was significantly reduced after 24 h of PGJ2 treatment, while expression of *Col1a1*, *Lamc1*, and *Loxl4* was significantly reduced after 24 h of pioglitazone treatment. PGJ2 reduced expression of *Col1a1* and *Col5a2* significantly more than pioglitazone but pioglitazone reduced *Loxl4* expression significantly more than PGJ2 (**Figure 5.10b**). *Col4a5*, *Tgfbr1*, and *Loxl2* expression was not affected by either PGJ2 or pioglitazone treatment.

Even though downregulation of the fibrotic target genes was limited in some of the tested genes, it was shown that *in vitro*, both PGJ2 and pioglitazone can indeed mechanistically modulate the PPARG-regulated AF-miRNA network identified by us in Winkler *et al.* (2020) [103].

5.4 Discussion

5.4.1 Pioglitazone Treatment to Target CCl_4-induced Liver Fibrosis in Mice through the AF-miRNA Network

We previously showed that the AF-miRNA network is dysregulated during fibrogenesis, especially in the fibrotic tumor microenvironment of murine HCC and in a 6 weeks CCl_4-induced liver fibrosis mouse model (**Project A**) [103]. According to our mechanistic model, AF-miRNA downregulation in HSCs during fibrogenesis is caused by reduced PPARG expression and activity and facilitates the increased expression of ECM-related target genes [103]. Thus, we hypothesize that maintenance of high AF-miRNA expression levels reduces fibrosis progression and can be collectively achieved through enhanced activity of their transcription factor PPARG.

Given that PPARG is known to influence HSC activation and fibrosis progression in the liver through multiple mechanisms, PPARG agonists have been studied previously for their ability to reduce liver fibrosis using a wide range of agonists, cell culture models, and animal models [9,63,188–190]. Pioglitazone is a well-studied PPARG agonist known to reduce hepatic fibrotic processes such as HSC activation and collagen accumulation in *in vitro* and *in vivo* rodent models [63–65,189]. Furthermore, pioglitazone serves as clinically approved drug for the treatment of diabetes and is additionally researched as therapeutic drug to treat human liver fibrosis [61,186].

Pioglitazone was therefore used in this study to investigate its effects on the PPARG-regulated AF-miRNA network in a 4 weeks CCl_4-induced liver fibrosis mouse model. Induction of CCl_4-mediated fibrosis over 4 weeks was chosen as experimental model considering multiple factors. First, CCl_4 administration is one of the most commonly used methods to induce liver fibrosis in animal models [130]. Second, 4 weeks of CCl_4 treatment is considered sufficient to induce progressed fibrosis [112]. Third, we found the AF-miRNA network to be most dysregulated in the 6 weeks CCl_4-induced liver fibrosis mouse model (**Project A**) [103] compared to the 2 months and 12 months CCl_4-induced liver fibrosis mouse models (**Project B**), suggesting stronger dysregulation of the AF-miRNA network at earlier stages of CCl_4-induced liver fibrosis.

Before analyzing the effects of CCl_4 and pioglitazone on the PPARG-regulated AF-miRNA network, the degree of liver fibrosis was assessed by several parameters. Measurement of the four blood serum markers of liver function ALT, AST, AP, and bilirubin indicated an early onset of fibrotic liver damage 1 week after CCl_4 treatment, which persisted until 4 weeks after CCl_4 treatment independent of pioglitazone administration. Considering the increased ALT activity but unaltered AST activity observed 4 weeks after CCl_4 treatment compared to the oil control, the degree of induced liver fibrosis was considered acute and mild [31]. In contrast, pathologic scoring of liver fibrosis sections revealed the

presence of bridging fibrosis in all, and cirrhosis in some CCl_4-treated murine livers, which are both typically considered signs of severe fibrosis [131]. The increased collagen accumulation assessed by Sirius Red staining and the presence of activated HSCs assessed by ACTA2 protein staining and *Acta2* gene expression in CCl_4-treated mice further indicate the presence of moderate to severe liver fibrosis [7]. Altogether, it was concluded that 4 weeks of CCl_4 treatment induces sufficient, most likely moderate to severe, liver fibrosis and demonstrates the successful establishment of this fibrosis mouse model in our laboratory.

However, pioglitazone administration to CCl_4-treated mice did not reduce the degree of liver fibrosis according to these parameters. Gene expression analysis further demonstrated that, also on the molecular level, pioglitazone neither increased *Pparg* and AF-miRNA expression nor decreased fibrotic target gene expression in CCl_4-treated livers. It is further important to note that, independent of pioglitazone administration, none of the measured AF-miRNAs were found downregulated after 4 weeks of CCl_4 treatment. This contrasts our previous findings, where we observed significant downregulation of 6 out of 7 PPARG-regulated AF-miRNAs after 6 weeks of CCl_4-induced liver fibrosis [103]. This indicates that *in vivo*, the AF-miRNA dysregulation in HSCs is time-sensitive and depends on a stronger HSC activation than present after 4 weeks of CCl_4 treatment. Alternatively, other cell types of the liver may mask HSC-specific effects in the whole liver tissue samples used for this analysis. A further *in vivo* experiment, where pHSCs are isolated from perfused livers of oil control, CCl_4, and CCl_4+Pio mice will allow to study the HSC-specific effects of these treatments on the AF-miRNA network [191,192].

As a well-studied PPARG agonist, pioglitazone has been investigated as anti-fibrotic drug in diverse rodent models [9,63,65,188–190]. Even though pioglitazone appears to reduce fibrosis more reliably in rats than in mice [63,65,188,190], mice were chosen as model organism in this study to ensure comparability to our previous findings on the AF-miRNA network [103]. Other experimental parameters of pioglitazone administration were designed to correspond to literature, where pioglitazone administration by daily oral gavage rather than addition to diet [63,190] and an early onset of pioglitazone administration during fibrogenesis [189] are considered most effective against liver fibrosis. However, the different pioglitazone studies mainly demonstrate that the therapeutic effect of pioglitazone varies considerably depending on the cause of fibrotic injury, on the duration of fibrogenesis, and on the drug administration route. It is therefore possible that with an alternative study design, pioglitazone nevertheless reduces fibrosis progression *in vivo* through modulation of the AF-miRNA network.

Other PPARG agonists besides pioglitazone are also known to reduce fibrosis progression and investigating their influence on the AF-miRNA network is of further interest. For instance, Galli *et al.*

(2002) show that both pioglitazone and rosiglitazone reduce liver fibrosis induced by CCl_4, BDL, and dimethylnitrosamine (DMN) in rats [188]. Furthermore, Alatas *et al.* (2020) report anti-fibrotic effects of thiazolidinedione in a rat BDL fibrosis model, where it reduces HSC activation, collagen accumulation, and the transcription of the fibrogenic cytokines PDGFB and TGF-β [193]. Interestingly, three recent studies reported successful anti-fibrotic and anti-inflammatory *in vivo* effects of the pan-PPAR agonist lanifibranor, which targets PPARA, PPARG, and PPARD simultaneously [194–196]. Wettstein *et al.* (2017) comprehensively tested the effects of different specific PPAR agonists and lanifibranor on a prophylactic and a therapeutic CCl_4 mouse model and showed that lanifibranor prevents and reverses CCl_4-induced fibrosis more effectively than specific PPAR agonists [194]. Similarly, Lefere *et al.* (2020) demonstrate that lanifibranor reduces inflammation, liver damage, and fibrosis in two NAFLD mouse models. Again, they show that lanifibranor combines and exceeds the effects of specific PPAR agonists, including pioglitazone [195]. Furthermore, Boyer-Diaz *et al.* (2021) report successful reduction of TAA-induced advanced cirrhosis in rats as well as reduced *in vitro* activation of cirrhotic human pHSCs upon lanifibranor treatment [196]. The therapeutic potential of lanifibranor is currently further evaluated in a clinical trial in adults with NASH (ClinicalTrials.gov, NCT03008070) [41]. To further understand the molecular involvement of the AF-miRNA network in fibrogenesis, it will be valuable to investigate whether lanifibranor mediates its anti-fibrotic effects, at least partially, through PPARG-mediated AF-miRNA upregulation.

5.4.2 Pioglitazone Treatment to Target pHSC Activation through the AF-miRNA Network

Contrary to the working hypothesis, pioglitazone did not reduce the progression of CCl_4-induced liver fibrosis *in vivo* in mice over the time course of 4 weeks. However, the whole liver tissue used for this analysis is not only comprised of HSCs, where the AF-miRNA network is active [103], but also of hepatocytes, macrophages, and other cell types [7]. It is therefore not clear whether the *in vivo* administered pioglitazone was ineffective in modulating AF-miRNA expression because it was not efficiently delivered to HSCs or because HSCs did not respond to it.

Therefore, I studied in pHSCs how the PPARG-regulated AF-miRNA network responds to pioglitazone. Such pHSCs can either be isolated from fibrotic and control animals after their *in vivo* activation in fibrosis models or they can be isolated in their inactive state from healthy animals followed by *in vitro* cell culture activation [191,192]. Even though *in vivo* activation of HSCs represents a more physiological process, *in vitro* pHSC activation allows to study HSC biology in a well-defined cell culture context and is less time-consuming due to the use of healthy untreated animals [191].

Here, inactive mouse pHSCs isolated from healthy adult mice were incubated with or without pioglitazone during their spontaneous *in vitro* activation [7,116] and were compared to inactive pHSCs harvested immediately after isolation. Pioglitazone was applied throughout the pHSC activation process to resemble the preventive approach also used in the 4 weeks CCl_4 *in vivo* study (**Chapter 5.3.1**). The degree of pHSC activation by prolonged cultivation is typically assessed by their loss of retinoid droplets and their increased *Acta2* and *Col1a1* gene expression [7]. Indeed, I observed successful pHSC activation after six days in culture as previously described by us in Winkler *et al.* (2020) (**Project A**) [103], where the same experimental design was used. Furthermore, pHSC activation was accompanied by decreased PPARG expression and activity, by decreased AF-miRNA expression, and by increased expression of fibrotic target genes of the AF-miRNA network. Therefore, these data reliably reproduce the AF-miRNA network dysregulations we initially characterized in pHSCs during activation [103]. However, treatment with 5 µM pioglitazone neither reduced the degree of pHSC activation nor the degree of *Pparg* and AF-miRNA downregulation nor the degree of fibrotic target gene upregulation.

While pHSC activation through prolonged cell cultivation is a well-established model for mouse, rat, and human pHSCs, the efficacy of pioglitazone and other PPARG agonists varies between studies. Resembling my own observations, Morais *et al.* (2007) report that neither higher concentrations of pioglitazone (10 µM) nor PGJ2 as alternative PPARG agonist reduce the activation of mouse pHSCs [190]. In contrast with these findings, both pioglitazone and PGJ2 were reported to inhibit the activation of rat pHSCs [64,187,197]. Also in human pHSCs, the PPARG agonists pioglitazone, rosiglitazone, troglitazone, and PGJ2 all successfully reduced parameters of pHSC activation including proliferation, migration, and *Col1a1* expression [62,188]. Of note, in these studies, pHSC activation in rat and human was effectively reduced with pioglitazone concentrations of 5 µM and lower [64,188]. These studies complement the notion that also *in vivo*, PPARG agonists have stronger anti-fibrotic effects on rats than on mice [63,65,188,190]. It is therefore of interest to study whether not only pHSC activation but also the fibrotic dysregulations of the AF-miRNA network respond differently to pioglitazone and other PPARG agonists in mouse, rat, and human pHSCs.

5.4.3 Modulation of the AF-miRNA Network in Immortalized HSC Cell Lines through the PPARG Agonists Pioglitazone and PGJ2

Since pioglitazone did not modulate the AF-miRNA network, neither *in vivo* nor in pHSCs, I next investigated whether AF-miRNAs are at all molecularly able to respond to PPARG agonists in HSCs. Due to the limited availability of pHSCs, different immortalized murine HSC cell lines were used for these *in vitro* experiments. Furthermore, the pioglitazone concentration was increased to 20 µM to account

for the limited response of mouse HSCs to lower pioglitazone concentrations [190], and for the relatively low binding affinity of pioglitazone to PPARG compared to other agonists [61]. Kawaguchi *et al.* (2004) showed in rat pHSCs, that 20 µM pioglitazone effectively reduced HSC activation without being damaging to cells [187]. Additionally, the prostaglandin and endogenous PPARG agonist PGJ2 [61] was investigated for its ability to modulate the AF-miRNA network through PPARG activation *in vitro*. PGJ2 binds with higher affinity to PPARG than pioglitazone and is known to exert anti-fibrotic functions, especially in acute fibrosis models [185,198,199].

Mechanistically, the binding of agonists like pioglitazone and PGJ2 activates PPARG and allows it to recognize PPREs in promoter regions, inducing the transcription of PPARG target genes and miRNAs [61,103]. Using chromatin immunoprecipitation, we showed in Winkler *et al.* (2020) that the overexpression of PPARG in the HSC cell line GRX-Pparg enhances PPARG binding to the PPREs in promoters of AF-miRNA-encoding genes compared to the GRX control cell line (**Project A**) [103]. We also observed that PPARG overexpression concurs with increased AF-miRNA expression in GRX-Pparg compared to GRX cells [103]. Performing luciferase assay in GRX-Pparg cells, I demonstrated here that it is indeed the binding of PPARG to PPREs that directly induces the transcription of genes under control of both consensus PPREs [132] and AF-miRNA-specific PPREs [103]. Moreover, I showed that this PPRE-mediated transcription can be further enhanced by the PPARG agonists pioglitazone and PGJ2. Pioglitazone and PGJ2 also induce transcription of reporter genes under control of other PPREs, as demonstrated by luciferase assays performed in human pHSCs by Marra *et al.* (2000) and Galli *et al.* (2002) [62,188]. Of note, these luciferase assays further demonstrate that both the type of PPARG agonist as well as the exact PPRE sequence influence the level of induced transcription.

After demonstrating that PPARG agonists are mechanistically able to induce PPARG-mediated AF-miRNA transcription in murine HSCs, the effect of pioglitazone and PGJ2 on AF-miRNA expression under control of their endogenous PPREs was investigated in different immortalized HSC cell lines. Both PPARG agonists successfully increased AF-miRNA expression in the three tested HSC cell lines Col-GFP, GRX, and GRX-Pparg. AF-miRNA upregulation was strongest after 4 h of agonist treatment in Col-GFP and GRX cells and declined back to initial levels after 24 h. In contrast, GRX-Pparg cells only responded after 24 h, but then with consistent upregulation of all four tested AF-miRNAs. In all three HSC cell lines, pioglitazone induced stronger overall AF-miRNA upregulation than PGJ2. Most likely, the 10-fold higher pioglitazone (20 µM) than PGJ2 (2 µM) concentration the cells were treated with compensated for the higher PPARG affinity of PGJ2 [61].

The responsiveness of the cell lines to the PPARG agonists seems to depend on the baseline level of PPARG expression, which is directly correlated with its activity as measured by *Plin2* expression [155,156]. Col-GFP and GRX cells, which express *Pparg* and *Plin2* in comparable levels, both

responded less effectively to pioglitazone and PGJ2 than GRX-Pparg cells, which stably overexpress transcriptionally active PPARG. Even though we previously demonstrated that PPARG overexpression alone is sufficient to increase AF-miRNA expression in GRX-Pparg cells compared to GRX cells [103], here I showed that PPARG agonists increase AF-miRNA transcription even further. Accordingly, Galli *et al.* (2002) reported in human pHSCs that PPRE-regulated reporter gene transcription induced by PPARG overexpression is further enhanced by the agonists pioglitazone, PGJ2, and rosiglitazone [188]. Thus, I demonstrate here that HSCs are able to modulate AF-miRNA expression in response to both PPARG overexpression and to PPARG agonist treatment. The strongest effect is observed when combining both approaches, in which case the increased amount of available PPARG likely facilitates and prolongs the agonist-induced AF-miRNA upregulation.

For *in vivo* administration of PPARG agonists, it is important to consider potential off-target effects in other liver cell types besides HSCs, especially hepatocytes [7]. Interestingly, neither pioglitazone nor PGJ2 modulated AF-miRNA expression in the hepatocyte cell line Hepa1-6. Generally, a miRNA can regulate different target genes depending on the cell type in which it is expressed [75,200]. Thus, the irresponsiveness of the AF-miRNAs in hepatocytes reduces the chance of adverse side effects caused by modulating unknown hepatocyte-specific miRNA pathways. Of note, baseline expression and activity of PPARG was higher in the hepatocyte cell line Hepa1-6 than in the HSC cell lines Col-GFP and GRX, where PPARG agonists did upregulate AF-miRNA expression. While this suggests that hepatocytes are generally irresponsive to PPARG agonists, it must also be considered that, as transcription factor, PPARG regulates other pathways besides the AF-miRNA network. Indeed, Shannon *et al.* (2017) reported that pioglitazone inhibits glucose synthesis and increases insulin resistance in hepatocytes, which is beneficial for the treatment of diabetes mellitus type 2 [201]. Moreover, Tomita *et al.* (2004) demonstrated that pioglitazone prevents the progression of alcoholic hepatic steatosis to fibrosis by reducing lipid accumulation in hepatocytes [202]. Even though PPARG regulates different pathways in hepatocytes and HSCs, the effect of pioglitazone on hepatocytes appears to supplement the anti-fibrotic effect of AF-miRNA upregulation in HSCs.

The anti-fibrotic function of AF-miRNA upregulation is defined by their ability to reduce expression of their fibrotic target genes in HSCs [75,103]. Since both PPARG agonists induced the strongest AF-miRNA upregulation in GRX-Pparg cells after 24 h, the strongest target gene downregulation was expected under these treatment conditions. Indeed, both PPARG agonists significantly reduced expression of a subset of the anti-fibrotic target genes of the AF-miRNA network under these conditions. In Winkler *et al.* (2020), we previously showed that target gene downregulation induced by PGJ2 treatment can be inhibited by miRNA inhibitors, demonstrating that it is indeed the PGJ2-mediated AF-miRNA upregulation that causes target gene downregulation in GRX-Pparg cells [103]. Here, I showed for the first time that the AF-miRNAs as well as *Plin2* as positive control for

PPARG activation are indeed upregulated with PGJ2 treatment of GRX-Pparg cells. Furthermore, I reproduced the PGJ2-mediated downregulation of *Col1a1* and *Col5a2* [103] and demonstrated that PGJ2 treatment additionally downregulates *Lamc1*. Most importantly, I demonstrated that pioglitazone induces the same anti-fibrotic effects as PGJ2, upregulating AF-miRNA expression and downregulating their fibrotic target genes. Pioglitazone even induced stronger PPARG activation than PGJ2, as demonstrated by luciferase assay, by *Plin2* upregulation in GRX-Pparg cells, and by AF-miRNA upregulation in all three tested HSC cell lines.

With the here described cell culture models, I demonstrated that PPARG-mediated modulation of the AF-miRNA network is possible in HSCs. The increased AF-miRNA expression contributes to maintaining HSCs in a more quiescent state by downregulating fibrosis-associated genes like collagens and other ECM components [9,103]. I further showed that two different PPARG agonists, pioglitazone and PGJ2, can modulate the AF-miRNA network in HSCs. PGJ2 is an endogenous high-affinity PPARG ligand consistently reported to inhibit HSC activation *in vitro* [61,62,187,188,197]. *In vivo*, PGJ2 was able to increase PPARG expression and to attenuate acute liver injury and inflammation in a 24 h mouse model of acute hepatitis [199]. However, studying the efficacy of long-term *in vivo* administration of PGJ2 remains challenging due to its instability [185,203]. This also limits its application as therapeutic drug to treat fibrotic patients. In contrast, pioglitazone is a synthetic small molecule activator of PPARG that belongs to the TZD family [61]. It is frequently reported to attenuate HSC activation, collagen deposition, and other fibrotic and inflammatory parameters in *in vitro* and *in vivo* fibrosis models [64,187,188,204]. Given that pioglitazone is more stable than PGJ2 and is able to reduce fibrosis progression not only in rodents but also in several clinical trials with NASH patients [41,67], it is likely that it also modulates the AF-miRNA network more reliably than PGJ2 in human HSCs.

PPARG agonists have been studied as anti-fibrotic compounds for over a decade [204,205]. The here described AF-miRNA network is one of several signaling networks through which PPARG is known to maintain HSC quiescence [43,103,205]. PPARG is a negative regulator of SMAD-dependent TGF-β-induced fibrotic responses [43], and serves as anti-inflammatory mediator in the communication between metabolic and inflammatory reactions [205]. By demonstrating that PPARG agonists decrease expression of structural ECM components through AF-miRNAs, I expand our molecular understanding of how PPARG agonists exert their anti-fibrotic effects in HSCs.

5.4.4 Limited Success of PPARG-mediated Modulation of the AF-miRNA Network to Target Liver Fibrosis *in vivo* and Recommendations for Alternative *in vivo* Approaches

In **Project C**, I aimed to collectively modulate AF-miRNA expression by activating their transcription factor PPARG to reduce fibrosis progression via the AF-miRNA network identified by us in Winkler *et al.*

(2020) (**Project A**) [103]. However, I could neither show that the PPARG agonist pioglitazone increased AF-miRNA expression in the *in vivo* model of CCl_4-induced murine liver fibrosis nor in the *in vitro* model of culture-activated pHSCs. Nevertheless, I demonstrated *in vitro* in immortalized HSC cell lines, that the PPARG agonists pioglitazone and PGJ2 are both able to enhance AF-miRNA expression directly through PPARG, and that the AF-miRNAs decrease the expression of fibrotic target genes of the AF-miRNA network. This confirms that PPARG-mediated AF-miRNA modulation is a possible approach to reduce the fibrotic activity of HSCs.

There are several possible reasons why AF-miRNA modulation by pioglitazone was effective in cell culture experiments but not in pHSCs. For one, the HSC cell lines were treated with a 4-fold higher pioglitazone concentration than the pHSCs. Furthermore, HSC cell lines were treated for 24 h while pHSCs were treated for seven days to ensure pHSC activation [7,103], so that a potential early short-term peak in AF-miRNA upregulation may have been overlooked in pHSCs. Additionally, the strongest AF-miRNA upregulation was observed in the PPARG-overexpressing GRX-Pparg cell line while culture-activated pHSCs are characterized by a drastic reduction in PPARG gene and protein expression [188,197]. Adjustments of the experimental conditions of pHSC treatment, such as an earlier onset of pioglitazone administration when PPARG levels are still high, testing more timepoints during pHSC activation, or the treatment of pHSCs with either higher pioglitazone concentrations or alternative PPARG agonists such as PGJ2, may nevertheless allow AF-miRNA modulation in pHSCs.

There are also several possible explanations for why AF-miRNA upregulation was not observed upon pioglitazone treatment in the *in vivo* CCl_4 fibrosis model. First, pioglitazone may in general not be able to induce PPARG-mediated AF-miRNA upregulation in HSCs. However, this hypothesis can be excluded because the *in vitro* experiments on immortalized HSC cell lines showed successful AF-miRNA upregulation upon pioglitazone treatment. Second, given that AF-miRNA expression was analyzed in whole liver isolates, HSC-specific AF-miRNA modulation is possibly masked by effects in other cell types, especially hepatocytes as most abundant cell type of the liver [7]. Yet, pioglitazone treatment of Hepa1-6 cells did not modulate AF-miRNA expression *in vitro*, suggesting that such off-target effects do not occur *in vivo.* Third, since orally administered pioglitazone is not targeted to HSCs specifically [61,202], it may largely be sequestered in other parts of the organism without reaching HSCs in sufficient amounts to increase PPARG-mediated AF-miRNA expression. The *in vivo* effect of orally administered pioglitazone on the two cell types can be studied by isolating both hepatocytes and HSCs from perfused livers of fibrosis-induced and pioglitazone-treated animals [191,192]. Such an experiment will allow to determine whether orally administered pioglitazone is successfully delivered to HSCs, whether it exerts HSC-specific AF-miRNA modulation, and whether the AF-miRNAs are, in accordance with Hepa1-6 experiments, indeed not modulated in hepatocytes *in vivo*. In case HSCs are

insufficiently targeted by orally administered pioglitazone, its effect on HSCs may be improved by increasing the pioglitazone dosage beyond the here used 30 mg/kg body weight [206].

There are three alternative approaches besides pioglitazone to potentially reduce fibrosis progression *in vivo* through the AF-miRNA network: i) the use of other, more effective PPARG agonists, ii) the overexpression of ectopic PPARG, and iii) the administration of the AF-miRNAs directly in form of synthetic miRNA mimics. As part of this study and our publication, we demonstrated that all three approaches are feasible *in vitro* [103]. *In vivo*, multiple alternative synthetic PPARG agonists of the TZD family besides pioglitazone (e.g. rosiglitazone), synthetic non-TZD PPARG agonists (e.g. KR62776 or GW570) and also pan-PPAR agonists (e.g. lanifibranor) are extensively studied as anti-fibrotic compounds [188,194,205] and may also mediate their effects through the AF-miRNA network. However, all these synthetic compounds are conventionally administered orally, which does not allow targeted delivery to HSCs [35,61]. Liposome-based parenteral delivery systems are a valuable pharmacological approach for cell-specific targeting, since they promise to protect their cargo from degradation, provide increased drug concentration in the target cell, and reduce putative off-target effects in other cell types [35]. First successes in drug delivery to HSCs have been described using liposomes coated with human serum albumin decorated with mannose-6-phosphate (M6P-HSA). M6P-HSA binds to the M6P/insulin-like growth factor II receptor (M6P/IGFIIR) highly expressed on the cell surface of activated HSCs, and induces liposome fusion with the HSC membrane to release its cargo [35]. Interestingly, rosiglitazone delivered in such M6P-HSA-coated liposomes was shown to reduce CCl_4-mediated fibrosis in rats more successfully than plain rosiglitazone [207], making liposome-based delivery systems a promising approach to increase the therapeutic efficacy of many PPARG agonists. A similar liposome-based approach may also be applied to deliver synthetic PPARG-encoding mRNA or AF-miRNA mimics to HSCs to replenish endogenous PPARG or AF-miRNA levels, respectively [35,208,209].

Overall, I demonstrated here that oral administration of pioglitazone to induce PPARG-mediated AF-miRNA modulation is not a suitable approach to target liver fibrosis *in vivo*. The fact that PPARG is a well-known regulator of diverse anti-fibrotic pathways besides the AF-miRNA network makes it, on the one hand, a promising target for anti-fibrotic interventions but on the other hand, makes it difficult to differentiate AF-miRNA-dependent and AF-miRNA-independent effects of PPARG agonists [43,205]. Therefore, I propose an alternative experimental strategy, where a miRNA mimic cocktail comprised of the 8 AF-miRNAs of the network is packaged into M6P-HSA-coated liposomes to deliver them to HSCs specifically. This way, the specific effects of replenished AF-miRNA levels in controlled concentrations will allow a better understanding of the anti-fibrotic potential of the AF-miRNAs during *in vivo* liver fibrogenesis.

6 Conclusion

This study identifies and characterizes the PPARG-regulated AF-miRNA network, that acts in HSCs as a significant contributor to fibrosis and the fibrotic tumor microenvironment (**Project A**) [103]. Biologically, this study thereby demonstrates how a limited number of functionally connected miRNAs can collectively regulate complex biological processes, in this case fibrosis signaling.

This study further demonstrates that the AF-miRNA network is not only conserved between human and mouse, but also to the rat as additional model organism (**Project B**). By comparing different stages of BDL-mediated, TAA-induced, and CCl_4-induced liver fibrosis in rat and mouse with fibrotic HCC in *SRF-VP16*^{iHep} mice, I showed that the expression patterns of the AF-miRNAs are highly context-specific. AF-miRNA expression varies most strongly between the non-tumorous fibrotic ECM in the fibrosis models on the one hand and the fibrotic tumor microenvironment of HCC on the other hand.

Molecularly, it was shown that the PPARG-regulated AF-miRNA network can be modulated *in vitro* through overexpression or activation of the AF-miRNAs' collective transcription factor PPARG (**Project C**). PPARG agonists are well-studied therapeutic drugs to target liver fibrosis [204]. By demonstrating that the PPARG agonists pioglitazone and PGJ2 decrease expression of fibrotic ECM components through AF-miRNAs, this study expands our molecular understanding of how PPARG agonists exert their anti-fibrotic effects in HSCs. Even though *in vivo*, oral administration of pioglitazone did neither result in upregulation of the AF-miRNAs nor in reduction of fibrogenesis, alternative PPARG agonists or HSC-targeted delivery methods may nevertheless be effective *in vivo*. Another promising approach is the administration of a synthetic AF-miRNA mimic cocktail that allows direct inhibition of the fibrotic target genes of the AF-miRNA network.

With the vastly expanding recognition of miRNA function in disease, their potential as blood serum markers and therapeutic drugs is increasingly shifting into scientific focus [210–212]. The thorough characterization of the AF-miRNAs and their functional network in this study contributes to our molecular understanding of chronic liver disease progression from fibrosis to HCC and may facilitate the identification of potential therapeutic targets or predictors of disease outcome in the future.

7 References

[1] Baglieri, J., Brenner, D. A. & Kisseleva, T. The role of fibrosis and liver-associated fibroblasts in the pathogenesis of hepatocellular carcinoma. *Int. J. Mol. Sci.* **20**, 1723 (2019).

[2] Hernandez-Gea, V., Toffanin, S., Friedman, S. L. & Llovet, J. M. Role of the microenvironment in the pathogenesis and treatment of hepatocellular carcinoma. *Gastroenterology* **144**, 512–527 (2013).

[3] Barry, A. E., Baldeosingh, R., Lamm, R. *et al.* Hepatic Stellate Cells and Hepatocarcinogenesis. *Front. Cell Dev. Biol.* **8**, 709 (2020).

[4] Francque, S., Szabo, G., Abdelmalek, M. F. *et al.* Nonalcoholic steatohepatitis: the role of peroxisome proliferator-activated receptors. *Nat. Rev. Gastroenterol. Hepatol.* **18**, 24–39 (2021).

[5] Llovet, J. M., Kelley, R. K., Villanueva, A. *et al.* Hepatocellular carcinoma. *Nat. Rev. Dis. Prim.* **7**, 6 (2021).

[6] Sung, H., Ferlay, J., Siegel, R. L. *et al.* Global Cancer Statistics 2020: GLOBOCAN Estimates of Incidence and Mortality Worldwide for 36 Cancers in 185 Countries. *CA. Cancer J. Clin.* **71**, 209–249 (2021).

[7] Friedman, S. L. Hepatic Stellate Cells: Protean, Multifunctional, and Enigmatic Cells of the Liver. *Physiol. Rev.* **88**, 125–172 (2008).

[8] Affo, S., Yu, L. X. & Schwabe, R. F. The Role of Cancer-Associated Fibroblasts and Fibrosis in Liver Cancer. *Annu. Rev. Pathol. Mech. Dis.* **12**, 153–186 (2017).

[9] Tsuchida, T. & Friedman, S. L. Mechanisms of hepatic stellate cell activation. *Nat. Rev. Gastroenterol. Hepatol.* **14**, 397–411 (2017).

[10] Pellicoro, A., Ramachandran, P., Iredale, J. P. & Fallowfield, J. A. Liver fibrosis and repair: Immune regulation of wound healing in a solid organ. *Nat. Rev. Immunol.* **14**, 181–194 (2014).

[11] Sepanlou, S. G., Safiri, S., Bisignano, C. *et al.* The global, regional, and national burden of cirrhosis by cause in 195 countries and territories, 1990–2017: a systematic analysis for the Global Burden of Disease Study 2017. *Lancet Gastroenterol. Hepatol.* **5**, 245–266 (2020).

[12] Khan, S. & Saxena, R. Regression of Hepatic Fibrosis and Evolution of Cirrhosis: A Concise Review. *Adv. Anat. Pathol.* **28**, 408–414 (2021).

[13] Weiskirchen, R., Ph, D., Tacke, F. & Ph, D. Liver Fibrosis: Which Mechanisms Matter? *Clin. Liver Dis.* **8**, 94–99 (2016).

[14] El-Serag, H. B. Hepatocellular Carcinoma. *N. Engl. J. Med.* **365**, 1118–1127 (2011).

[15] Forner, A., Reig, M. & Bruix, J. Hepatocellular carcinoma. *Lancet* **391**, 1301–1314 (2018).

[16] Ettrich, T. J., Schwerdel, D., Dolnik, A. *et al.* Genotyping of circulating tumor DNA in cholangiocarcinoma reveals diagnostic and prognostic information. *Sci. Rep.* **9**, 13261 (2019).

[17] Urban, S. K., Mocan, T., Sänger, H., Lukacs-Kornek, V. & Kornek, M. Extracellular Vesicles in Liver Diseases: Diagnostic, Prognostic, and Therapeutic Application. *Semin. Liver Dis.* **39**, 70–77 (2019).

[18] Dizdar, L., Fluegen, G., van Dalum, G. *et al.* Detection of circulating tumor cells in colorectal cancer patients using the GILUPI CellCollector: results from a prospective, single-center study. *Mol. Oncol.* **13**, 1548–1558 (2019).

[19] Llovet, J. M., Brú, C. & Bruix, J. Prognosis of hepatocellular carcinoma: the BCLC staging classification. *Semin. Liver Dis.* **19**, 329–338 (1999).

[20] Pelizzaro, F., Ramadori, G. & Farinati, F. Systemic therapies for hepatocellular carcinoma: an evolving landscape. *Hepatoma Res.* **7**, 36 (2021).

[21] Finn, R. S., Qin, S., Ikeda, M. *et al.* Atezolizumab plus Bevacizumab in Unresectable Hepatocellular Carcinoma. *N. Engl. J. Med.* **382**, 1894–1905 (2020).

[22] Berumen, J., Baglieri, J., Kisseleva, T. & Mekeel, K. Liver fibrosis: Pathophysiology and clinical implications. *WIREs Mech. Dis.* **13**, e1499 (2021).

[23] Ishak, K., Baptista, A., Bianchi, L. *et al.* Histological grading and staging of chronic hepatitis. *J. Hepatol.* **22**, 696–699 (1995).

[24] Kleiner, D. E., Brunt, E. M., Van Natta, M. *et al.* Design and validation of a histological scoring system for nonalcoholic fatty liver disease. *Hepatology* **41**, 1313–1321 (2005).

[25] Goodman, Z. D. Grading and staging systems for inflammation and fibrosis in chronic liver diseases. *J. Hepatol.* **47**, 598–607 (2007).

[26] Patel, K., Bedossa, P. & Castera, L. Diagnosis of liver fibrosis: Present and future. *Semin. Liver Dis.* **35**, 166–183 (2015).

[27] Hernandez-Gea, V. & Friedman, S. L. Pathogenesis of liver fibrosis. *Annu. Rev. Pathol. Mech. Dis.* **6**, 425–456 (2011).

[28] Li, S., Sun, X., Chen, M. *et al.* Liver Fibrosis Conventional and Molecular Imaging Diagnosis Update. *J. Liver* **08**, 236 (2019).

[29] Luedde, T., Kaplowitz, N. & Schwabe, R. F. Cell death and cell death responses in liver disease: mechanisms and clinical relevance. *Gastroenterology* **147**, 765-783.e4 (2014).

[30] Lurie, Y., Webb, M., Cytter-Kuint, R., Shteingart, S. & Lederkremer, G. Z. Non-invasive diagnosis of liver fibrosis and cirrhosis. *World J. Gastroenterol.* **21**, 11567–11583 (2015).

[31] Thapa, B. R. & Walia, A. Liver function tests and their interpretation. *Indian J. Pediatr.* **74**, 663–671 (2007).

[32] Giannini, E. G., Testa, R. & Savarino, V. Liver enzyme alteration: a guide for clinicians. *Can. Med. Assoc. J.* **172**, 367–379 (2005).

[33] Siddiqui, M. S., Yamada, G., Vuppalanchi, R. *et al.* Diagnostic Accuracy of Noninvasive Fibrosis Models to Detect Change in Fibrosis Stage. *Clin. Gastroenterol. Hepatol.* **17**, 1877-1885.e5 (2019).

[34] Peng, Y., Qi, X. & Guo, X. Child-pugh versus MELD score for the assessment of prognosis in liver cirrhosis a systematic review and meta-analysis of observational studies. *Med.* **95**, e2877 (2016).

[35] Bartneck, M., Warzecha, K. T. & Tacke, F. Therapeutic targeting of liver inflammation and fibrosis by nanomedicine. *Hepatobiliary Surg. Nutr.* **3**, 364–376 (2014).

[36] Yang, L. L. Anatomy and Physiology of the Liver. In *Anesthesia for Hepatico-Pancreatic-Biliary Surgery and Transplantation* (eds. Milan, Z. & Goonasekera, C.) 15–40 (Springer, Cham, 2021).

[37] Xu, J., Liu, X., Koyama, Y. *et al.* The types of hepatic myofibroblasts contributing to liver fibrosis of different etiologies. *Front. Pharmacol.* **5**, 167 (2014).

[38] Kisseleva, T. & Brenner, D. Molecular and cellular mechanisms of liver fibrosis and its regression. *Nat. Rev. Gastroenterol. Hepatol.* **18**, 151–166 (2021).

[39] She, H., Xiong, S., Hazra, S. & Tsukamoto, H. Adipogenic Transcriptional Regulation of Hepatic Stellate Cells*. *J. Biol. Chem.* **280**, 4959–4967 (2005).

[40] Hazra, S., Xiong, S., Wang, J. *et al.* Peroxisome Proliferator-activated Receptor γ Induces a Phenotypic Switch from Activated to Quiescent Hepatic Stellate Cells. *J. Biol. Chem.* **279**, 11392–11401 (2004).

[41] Zisser, A., Ipsen, D. H. & Tveden-Nyborg, P. Hepatic stellate cell activation and inactivation in NASH-fibrosis—roles as putative treatment targets? *Biomedicines* **9**, 365 (2021).

[42] Bhattacharyya, S., Wu, M., Fang, F. *et al.* Early growth response transcription factors: key mediators of fibrosis and novel targets for anti-fibrotic therapy. *Matrix Biol.* **30**, 235–242 (2011).

[43] Ghosh, A. K., Quaggin, S. E. & Vaughan, D. E. Molecular basis of organ fibrosis: Potential therapeutic approaches. *Exp. Biol. Med.* **238**, 461–481 (2013).

[44] Lee, Y. A., Wallace, M. C. & Friedman, S. L. Pathobiology of liver fibrosis: a translational success story. *Gut* **64**, 830–841 (2015).

[45] Yanguas, S. C., Cogliati, B., Willebrords, J. *et al.* Experimental models of liver fibrosis. *Arch. Toxicol.* **90**, 1025–1048 (2016).

[46] Llovet, J. M., Villanueva, A., Marrero, J. A. *et al.* Trial Design and Endpoints in Hepatocellular Carcinoma: AASLD Consensus Conference. *Hepatology* **73 Suppl 1**, 158–191 (2021).

[47] Mueller, S. Does pressure cause liver cirrhosis? The sinusoidal pressure hypothesis. *World J. Gastroenterol.* **22**, 10482–10501 (2016).

[48] Kim, M. N., Kim, S. U., Kim, B. K. *et al.* Increased risk of hepatocellular carcinoma in chronic hepatitis B patients with transient elastography-defined subclinical cirrhosis. *Hepatology* **61**, 1851–1859 (2015).

[49] Akima, T., Tamano, M. & Hiraishi, H. Liver stiffness measured by transient elastography is a predictor of hepatocellular carcinoma development in viral hepatitis. *Hepatol. Res.* **41**, 965–970 (2011).

[50] Weiskirchen, R. & Tacke, F. Cellular and molecular functions of hepatic stellate cells in inflammatory responses and liver immunology. *Hepatobiliary Surg. Nutr.* **3**, 344–63 (2014).

[51] Hanahan, D. & Weinberg, R. A. Hallmarks of Cancer: The Next Generation. *Cell* **144**, 646–674 (2011).

[52] Tao, L.-L., Cheng, Y.-Y., Ding, D. *et al.* C/EBP-α ameliorates CCl4-induced liver fibrosis in mice through promoting apoptosis of hepatic stellate cells with little apoptotic effect on hepatocytes in vitro and in vivo. *Apoptosis* **17**, 492–502 (2012).

[53] Oakley, F., Meso, M., Iredale, J. P. *et al.* Inhibition of inhibitor of kappaB kinases stimulates hepatic stellate cell apoptosis and accelerated recovery from rat liver fibrosis. *Gastroenterology* **128**, 108–120 (2005).

[54] Mendizabal, M., Piñero, F., Ridruejo, E. *et al.* Disease Progression in Patients With Hepatitis C Virus Infection Treated With Direct-Acting Antiviral Agents. *Clin. Gastroenterol. Hepatol.* **18**, 2554-2563.e3 (2020).

[55] Bedossa, P. & Paradis, V. Liver extracellular matrix in health and disease. *J. Pathol.* **200**, 504–515 (2003).

[56] Winkler, J., Abisoye-Ogunniyan, A., Metcalf, K. J. & Werb, Z. Concepts of extracellular matrix remodelling in tumour progression and metastasis. *Nat. Commun.* **11**, 5120 (2020).

[57] Barker, H. E., Cox, T. R. & Erler, J. T. The rationale for targeting the LOX family in cancer. *Nat. Rev. Cancer* **12**, 540–552 (2012).

[58] Mann, J. & Mann, D. A. Transcriptional regulation of hepatic stellate cells. *Adv. Drug Deliv. Rev.* **61**, 497–512 (2009).

[59] Odagiri, N., Matsubara, T., Sato-Matsubara, M. *et al.* Anti-fibrotic treatments for chronic liver diseases: The present and the future. *Clin. Mol. Hepatol.* **27**, 413–424 (2021).

[60] Ratziu, V., Sanyal, A., Harrison, S. A. *et al.* Cenicriviroc Treatment for Adults With Nonalcoholic Steatohepatitis and Fibrosis: Final Analysis of the Phase 2b CENTAUR Study. *Hepatology* **72**, 892–905 (2020).

[61] Sauer, S. Ligands for the Nuclear Peroxisome Proliferator-Activated Receptor Gamma. *Trends Pharmacol. Sci.* **36**, 688–704 (2015).

[62] Marra, F., Efsen, E., Romanelli, R. G. *et al.* Ligands of peroxisome proliferator-activated receptor gamma modulate profibrogenic and proinflammatory actions in hepatic stellate cells. *Gastroenterology* **119**, 466–478 (2000).

[63] Li, S., Ghoshal, S., Sojoodi, M. *et al.* Pioglitazone Reduces Hepatocellular Carcinoma Development in Two Rodent Models of Cirrhosis. *J. Gastrointest. Surg.* **23**, 101–111 (2019).

[64] Kon, K., Ikejima, K., Hirose, M. *et al.* Pioglitazone prevents early-phase hepatic fibrogenesis caused by carbon tetrachloride. *Biochem. Biophys. Res. Commun.* **291**, 55–61 (2002).

[65] Ibrahim, S. A., Mohamed, M. Z., El-Tahawy, N. F. & Abdelrahman, A. M. Antifibrotic effects of bezafibrate and pioglitazone against thioacetamide-induced liver fibrosis in albino rats. *Can. J. Physiol. Pharmacol.* **99**, 313–320 (2021).

[66] Yuan, G.-J., Zhang, M.-L. & Gong, Z.-J. Effects of PPARg agonist pioglitazone on rat hepatic fibrosis. *World J. Gastroenterol.* **10**, 1047–1051 (2004).

[67] Musso, G., Cassader, M., Paschetta, E. & Gambino, R. Thiazolidinediones and advanced liver fibrosis in nonalcoholic steatohepatitis: A meta-analysis. *JAMA Intern. Med.* **177**, 633–640 (2017).

[68] Cusi, K., Orsak, B., Bril, F. *et al.* Long-Term Pioglitazone Treatment for Patients With Nonalcoholic Steatohepatitis and Prediabetes or Type 2 Diabetes Mellitus: A Randomized Trial. *Ann. Intern. Med.* **165**, 305–315 (2016).

[69] Sanyal, A. J., Chalasani, N., Kowdley, K. V *et al.* Pioglitazone, vitamin E, or placebo for nonalcoholic steatohepatitis. *N. Engl. J. Med.* **362**, 1675–1685 (2010).

[70] Ratziu, V., Giral, P., Jacqueminet, S. *et al.* Rosiglitazone for nonalcoholic steatohepatitis: one-year results of the randomized placebo-controlled Fatty Liver Improvement with Rosiglitazone Therapy (FLIRT) Trial. *Gastroenterology* **135**, 100–110 (2008).

[71] Fraile, J. M., Palliyil, S., Barelle, C., Porter, A. J. & Kovaleva, M. Non-alcoholic steatohepatitis (NASH) – A review of a crowded clinical landscape, driven by a complex disease. *Drug Des. Devel. Ther.* **15**, 3997–4009 (2021).

[72] Winter, J., Jung, S., Keller, S., Gregory, R. I. & Diederichs, S. Many roads to maturity: microRNA biogenesis pathways and their regulation. *Nat. Cell Biol.* **11**, 228–234 (2009).

[73] Morishita, A., Oura, K., Tadokoro, T. *et al.* MicroRNAs in the Pathogenesis of Hepatocellular Carcinoma: A Review. *Cancers (Basel).* **13**, 514 (2021).

[74] Szabo, G. & Bala, S. MicroRNAs in liver disease. *Nat. Rev. Gastroenterol. Hepatol.* **10**, 542–552 (2013).

[75] Bartel, D. P. MicroRNA Target Recognition and Regulatory Functions. *Cell* **136**, 215–233 (2009).

[76] Pasquinelli, A. E. MicroRNAs and their targets: recognition, regulation and an emerging reciprocal relationship. *Nat. Rev. Genet.* **13**, 271–282 (2012).

[77] O'Brien, J., Hayder, H., Zayed, Y. & Peng, C. Overview of microRNA biogenesis, mechanisms of actions, and circulation. *Front. Endocrinol.* **9**, 402 (2018).

[78] Huntzinger, E. & Izaurralde, E. Gene silencing by microRNAs: contributions of translational repression and mRNA decay. *Nat. Rev. Genet.* **12**, 99–110 (2011).

[79] Lewis, B. P., Shih, I., Jones-Rhoades, M. W., Bartel, D. P. & Burge, C. B. Prediction of Mammalian MicroRNA Targets. *Cell* **115**, 787–798 (2003).

[80] Eulalio, A., Huntzinger, E. & Izaurralde, E. Getting to the Root of miRNA-Mediated Gene Silencing. *Cell* **132**, 9–14 (2008).

[81] Plotnikova, O., Baranova, A. & Skoblov, M. Comprehensive Analysis of Human microRNA–mRNA Interactome. *Front. Genet.* **10**, 933 (2019).

[82] Alles, J., Fehlmann, T., Fischer, U. *et al.* An estimate of the total number of true human miRNAs. *Nucleic Acids Res.* **47**, 3353–3364 (2019).

[83] Ha, M. & Kim, V. N. Regulation of microRNA biogenesis. *Nat. Rev. Mol. Cell Biol.* **15**, (2014).

[84] Hausser, J. & Zavolan, M. Identification and consequences of miRNA-target interactions-beyond repression of gene expression. *Nat. Rev. Genet.* **15**, 599–612 (2014).

[85] Bracken, C. P., Scott, H. S. & Goodall, G. J. A network-biology perspective of microRNA function and dysfunction in cancer. *Nat. Rev. Genet.* **17**, 719–732 (2016).

[86] Bartel, D. P. MicroRNAs: Genomics, Biogenesis, Mechanism, and Function. *Cell* **116**, 281–297 (2004).

[87] Ramalingam, P., Palanichamy, J. K., Singh, A. *et al.* Biogenesis of intronic miRNAs located in clusters by independent transcription and alternative splicing. *RNA* **20**, 76–87 (2014).

[88] Filipowicz, W., Bhattacharyya, S. N. & Sonenberg, N. Mechanisms of post-transcriptional regulation by microRNAs: are the answers in sight? *Nat. Rev. Genet.* **2008**, 102–114 (2008).

[89] Schanen, B. C. & Li, X. Transcriptional regulation of mammalian miRNA genes. *Genomics* **97**, 1–6 (2011).

[90] de Rie, D., Abugessaisa, I., Alam, T. *et al.* An integrated expression atlas of miRNAs and their promoters in human and mouse. *Nat. Biotechnol.* **35**, 872–878 (2017).

[91] Krol, J., Loedige, I. & Filipowicz, W. The widespread regulation of microRNA biogenesis, function and decay. *Nat. Rev. Genet.* **11**, 597–610 (2010).

[92] Treiber, T., Treiber, N. & Meister, G. Regulation of microRNA biogenesis and its crosstalk with other cellular pathways. *Nat. Rev. Mol. Cell Biol.* **20**, 5–20 (2019).

[93] Gebert, L. F. R. & MacRae, I. J. Regulation of microRNA function in animals. *Nat. Rev. Mol. Cell Biol.* **20**, 21–37 (2019).

[94] Rüegger, S. & Großhans, H. MicroRNA turnover: When, how, and why. *Trends Biochem. Sci.* **37**, 436–446 (2012).

[95] O'Reilly, S. MicroRNAs in fibrosis: opportunities and challenges. *Arthritis Res. Ther.* **18**, 11 (2016).

[96] Morishita, A. & Masaki, T. miRNA in hepatocellular carcinoma. *Hepatol. Res.* **45**, 128–141 (2015).

[97] Roy, S., Benz, F., Luedde, T. & Roderburg, C. The role of miRNAs in the regulation of inflammatory processes during hepatofibrogenesis. *Hepatobiliary Surg. Nutr.* **4**, 24–33 (2015).

[98] Marquez, R. T., Bandyopadhyay, S., Wendlandt, E. B. *et al.* Correlation between microRNA expression levels and clinical parameters associated with chronic hepatitis C viral infection in humans. *Lab. Invest.* **90**, 1727–1736 (2010).

[99] Murakami, Y., Toyoda, H., Tanaka, M. *et al.* The Progression of Liver Fibrosis Is Related with Overexpression of the miR-199 and 200 Families. *PLOS ONE* **6**, e16081 (2011).

[100] Kwiecinski, M., Elfimova, N., Noetel, A. *et al.* Expression of platelet-derived growth factor-C and insulin-like growth factor I in hepatic stellate cells is inhibited by miR-29. *Lab. Invest.* **92**, 978–987 (2012).

[101] McDaniel, K., Huang, L., Sato, K. *et al.* The let-7/Lin28 axis regulates activation of hepatic stellate cells in alcoholic liver injury. *J. Biol. Chem.* **292**, 11336–11347 (2017).

[102] Palanichamy, J. K. & Rao, D. S. miRNA dysregulation in cancer: Towards a mechanistic understanding. *Front. Genet.* **5**, 1–10 (2014).

[103] Winkler, I., Bitter, C., Winkler, S. *et al.* Identification of Pparγ-modulated miRNA hubs that target the fibrotic tumor microenvironment. *Proc. Natl. Acad. Sci. U. S. A.* **117**, 454–463 (2020).

[104] Ohrnberger, S., Thavamani, A., Braeuning, A. *et al.* Dysregulated serum response factor triggers formation of hepatocellular carcinoma. *Hepatology* **61**, 979–989 (2015).

[105] Wiebel, F. F., Rennekampff, V., Vintersten, K. & Nordheim, A. Generation of mice carrying conditional knockout alleles for the transcription factor SRF. *Genesis* **32**, 124–126 (2002).

[106] Sandström, J., Heiduschka, P., Beck, S. C. *et al.* Degeneration of the mouse retina upon dysregulated activity of serum response factor. *Mol. Vis.* **17**, 1110–1127 (2011).

[107] Dalton, S. & Treisman, R. Characterization of SAP-1, a protein recruited by serum response factor to the c-fos serum response element. *Cell* **68**, 597–612 (1992).

[108] Hammad, S., Braeuning, A., Meyer, C. *et al.* A frequent misinterpretation in current research on liver fibrosis: the vessel in the center of CCl4-induced pseudolobules is a portal vein. *Arch. Toxicol.* **91**, 3689–3692 (2017).

[109] Ghallab, A., Myllys, M., H. Holland, C. *et al.* Influence of Liver Fibrosis on Lobular Zonation. *Cells* **8**, 1556 (2019).

[110] Tag, C. G., Sauer-Lehnen, S., Weiskirchen, S. *et al.* Bile duct ligation in mice: induction of inflammatory liver injury and fibrosis by obstructive cholestasis. *J. Vis. Exp.* e52438 (2015).

[111] Kountouras, J., Billing, B. H. & Scheuer, P. J. Prolonged bile duct obstruction: a new experimental model for cirrhosis in the rat. *Br. J. Exp. Pathol.* **65**, 305–311 (1984).

[112] Delire, B., Stärkel, P. & Leclercq, I. Animal models for fibrotic liver diseases: What we have, what we need, and what is under development. *J. Clin. Transl. Hepatol.* **3**, 53–66 (2015).

[113] Wallace, M., Hamesch, K., Lunova, M. *et al.* Standard Operating Procedures in Experimental Liver Research: Thioacetamide model in mice and rats. *Lab. Anim.* **49**, 21–29 (2015).

[114] Darlington, G. J., Bernhard, H. P., Miller, R. A. & Ruddle, F. H. Expression of liver phenotypes in cultured mouse hepatoma cells. *J. Natl. Cancer Inst.* **64**, 809–819 (1980).

[115] Meurer, S. K., Alsamman, M., Sahin, H. *et al.* Overexpression of Endoglin Modulates TGF-β1-Signalling Pathways in a Novel Immortalized Mouse Hepatic Stellate Cell Line. *PLOS ONE* **8**, e56116 (2013).

[116] Weiskirchen, S., Tag, C. G., Sauer-Lehnen, S., Tacke, F. & Weiskirchen, R. Isolation and culture of primary murine hepatic stellate cells. *Methods Mol. Biol.* **1627**, 165–191 (2017).

[117] Borojevic, R., Monteiro, A. N. A. A., Vinhas, S. A. *et al.* Establishment of a continuous cell line from fibrotic schistosomal granulomas in mice livers. *Vitr. Cell. Dev. Biol.* **21**, 382–390 (1985).

[118] Tontonoz, P., Hu, E., Graves, R. A., Budavari, A. I. & Spiegelman, B. M. mPPAR gamma 2: tissue-specific regulator of an adipocyte enhancer. *Genes Dev.* **8**, 1224–1234 (1994).

[119] Ergin, B. Functional molecular genetic dissection of the Ets transcription factors Sap-1 and Elk-1 in immediate-early and neuronal gene expression (PhD thesis). (Eberhard-Karls-Universität Tübingen, 2008).

[120] Schindelin, J., Arganda-Carreras, I., Frise, E. *et al.* Fiji: an open-source platform for biological-image analysis. *Nat. Methods* **9**, 676–682 (2012).

[121] Ruijter, J. M., Ramakers, C., Hoogaars, W. M. H. *et al.* Amplification efficiency: Linking baseline and bias in the analysis of quantitative PCR data. *Nucleic Acids Res.* **37**, e45 (2009).

[122] Gu, Z., Gu, L., Eils, R., Schlesner, M. & Brors, B. circlize implements and enhances circular visualization in R. *Bioinformatics* **30**, 2811–2812 (2014).

[123] Love, M. I., Huber, W. & Anders, S. Moderated estimation of fold change and dispersion for RNA-seq data with DESeq2. *Genome Biol.* **15**, 550 (2014).

[124] Whickham, H. *ggplot2: Elegant Graphics for Data Analysis*. (Springer-Verlag New York, 2016).

[125] Kolde, R. pheatmap: Pretty Heatmaps (R package version 1.0.12). (2019).

[126] Neuwirth, E. RColorBrewer: ColorBrewer Palettes (R package version 1.1-2). (2014).

[127] R Core Team. R: A language and environment for statistical computing. R Foundation for Statistical Computing. (2020).

[128] RStudio Team. RStudio: Integrated Development for R. (2016).

[129] Küster, T., Zumkehr, B., Hermann, C. *et al.* Voluntary ingestion of antiparasitic drugs emulsified in honey represents an alternative to gavage in mice. *J. Am. Assoc. Lab. Anim. Sci.* **51**, 219–223 (2012).

[130] Scholten, D., Trebicka, J., Liedtke, C. & Weiskirchen, R. The carbon tetrachloride model in mice. *Lab. Anim.* **49**, 4–11 (2015).

[131] Liang, W., Menke, A. L., Driessen, A. *et al.* Establishment of a General NAFLD Scoring System for Rodent Models and Comparison to Human Liver Pathology. *PLOS ONE* **9**, e115922 (2014).

[132] Fornes, O., Castro-Mondragon, J. A., Khan, A. *et al.* JASPAR 2020: update of the open-access database of transcription factor binding profiles. *Nucleic Acids Res.* **48**, D87–D92 (2019).

[133] Krebs, S., Fischaleck, M. & Blum, H. A simple and loss-free method to remove TRIzol contaminations from minute RNA samples. *Anal. Biochem.* **387**, 136–138 (2009).

[134] Glasel, J. A. Validity of nucleic acid purities monitored by 260nm/280nm absorbance ratios. *Biotechniques* **18**, 62–63 (1995).

[135] Jones, L. J., Yue, S. T., Cheung, C. Y. & Singer, V. L. RNA quantitation by fluorescence-based solution assay: RiboGreen reagent characterization. *Anal. Biochem.* **265**, 368–374 (1998).

[136] Ruijter, J. M., Pfaffl, M. W., Zhao, S. *et al.* Evaluation of qPCR curve analysis methods for reliable biomarker discovery: Bias, resolution, precision, and implications. *Methods* **59**, 32–46 (2013).

[137] Agarwal, V., Bell, G. W., Nam, J.-W. W. & Bartel, D. P. Predicting effective microRNA target sites in mammalian mRNAs. *Elife* **4**, e05005 (2015).

[138] Paraskevopoulou, M. D., Georgakilas, G., Kostoulas, N. *et al.* DIANA-microT web server v5.0: service integration into miRNA functional analysis workflows. *Nucleic Acids Res.* **41**, W169-73 (2013).

[139] Reczko, M., Maragkakis, M., Alexiou, P., Grosse, I. & Hatzigeorgiou, A. G. Functional microRNA targets in protein coding sequences. *Bioinformatics* **28**, 771–776 (2012).

[140] Bitter, C. Regulation of fibrosis by members of the let-7 miRNA family (Master thesis). (Eberhard Karls Universität Tübingen, 2017).

[141] Sengupta, S., den Boon, J. A., Chen, I.-H. *et al.* MicroRNA 29c is down-regulated in nasopharyngeal carcinomas, up-regulating mRNAs encoding extracellular matrix proteins. *Proc. Natl. Acad. Sci.* **105**, 5874–5878 (2008).

[142] Nishikawa, R., Goto, Y., Kojima, S. *et al.* Tumor-suppressive microRNA-29s inhibit cancer cell migration and invasion via targeting LAMC1 in prostate cancer. *Int. J. Oncol.* **45**, 401–410 (2014).

[143] Huang, H., Huang, X., Luo, S. *et al.* The MicroRNA MiR-29c Alleviates Renal Fibrosis via TPM1-Mediated Suppression of the Wnt/β-Catenin Pathway. *Front. Physiol.* **11**, 331 (2020).

[144] Kriegel, A. J., Liu, Y., Fang, Y., Ding, X. & Liang, M. The miR-29 family: genomics, cell biology, and relevance to renal and cardiovascular injury. *Physiol. Genomics* **44**, 237–244 (2012).

[145] Yin, H., Wang, Y., Wu, Y. *et al.* EZH2-mediated Epigenetic Silencing of miR-29/miR-30 targets LOXL4 and contributes to Tumorigenesis, Metastasis, and Immune Microenvironment Remodeling in Breast Cancer. *Theranostics* **10**, 8494–8512 (2020).

[146] Pinzani, M. PDGF and signal transduction in hepatic stellate cells. *Front. Biosci.* **7**, 1720—1726 (2002).

[147] Hayes, A. J., Benjamin, M. & Ralphs, J. R. Role of actin stress fibres in the development of the intervertebral disc: Cytoskeletal control of extracellular matrix assembly. *Dev. Dyn.* **215**, 179–189 (1999).

[148] Bonnans, C., Chou, J. & Werb, Z. Remodelling the extracellular matrix in development and disease. *Nat. Rev. Mol. Cell Biol.* **15**, 786–801 (2014).

[149] Ikenaga, N., Peng, Z.-W., Vaid, K. A. *et al.* Selective targeting of lysyl oxidase-like 2 (LOXL2) suppresses hepatic fibrosis progression and accelerates its reversal. *Gut* **66**, 1697–1708 (2017).

[150] Cox, E. A., Sastry, S. K. & Huttenlocher, A. Integrin-mediated adhesion regulates cell polarity and membrane protrusion through the Rho family of GTPases. *Mol. Biol. Cell* **12**, 265–277 (2001).

[151] Peters, J. M., Shah, Y. M. & Gonzalez, F. J. The role of peroxisome proliferator-activated receptors in carcinogenesis and chemoprevention. *Nat. Rev. Cancer* **12**, 181–195 (2012).

[152] Lakshmi, S. P., Reddy, A. T. & Reddy, R. C. Transforming growth factor β suppresses peroxisome proliferator-activated receptor γ expression via both SMAD binding and novel TGF-β inhibitory elements. *Biochem. J.* **474**, 1531–1546 (2017).

[153] Hickman, D. L., Johnson, J., Vemulapalli, T. H., Crisler, J. R. & Shepherd, R. Commonly Used Animal Models. *Princ. Anim. Res. Grad. Undergrad. Students* 117–175 (2017).

[154] Rich, L. & Whittaker, P. Collagen and picrosirius red staining: a polarized light assessment of fibrillar hue and spatial distribution. *J. Morphol. Sci.* **22**, 97–104 (2005).

[155] Gupta, R. A., Brockman, J. A., Sarraf, P., Willson, T. M. & DuBois, R. N. Target Genes of Peroxisome Proliferator-activated Receptor γ in Colorectal Cancer Cells. *J. Biol. Chem.* **276**, 29681–29687 (2001).

[156] Hodgkinson, C. P. & Ye, S. Microarray analysis of peroxisome proliferator-activated receptor-gamma induced changes in gene expression in macrophages. *Biochem. Biophys. Res. Commun.* **308**, 505–510 (2003).

[157] Spinella, R., Sawhney, R. & Jalan, R. Albumin in chronic liver disease: structure, functions and therapeutic implications. *Hepatol. Int.* **10**, 124–132 (2016).

[158] Winkler, I. Function of miRNAs in murine liver carcinogenesis (PhD thesis). (Eberhard Karls Universität Tübingen, 2019).

[159] Baron, V., Adamson, E. D., Calogero, A., Ragona, G. & Mercola, D. The transcription factor Egr1 is a direct regulator of multiple tumor suppressors including TGFβ1, PTEN, p53, and fibronectin. *Cancer Gene Ther.* **13**, 115–124 (2006).

[160] Friedman, S. L. Mechanisms of Hepatic Fibrogenesis. *Gastroenterology* **134**, 1655–1669 (2008).

[161] Mott, J. L., Kobayashi, S., Bronk, S. F. & Gores, G. J. mir-29 regulates Mcl-1 protein expression and apoptosis. *Oncogene* **26**, 6133–6140 (2007).

[162] Shimizu, S., Takehara, T., Hikita, H. *et al.* The let-7 family of microRNAs inhibits Bcl-xL expression and potentiates sorafenib-induced apoptosis in human hepatocellular carcinoma. *J. Hepatol.* **52**, 698–704 (2010).

[163] Howe, K. L., Achuthan, P., Allen, J. *et al.* Ensembl 2021. *Nucleic Acids Res.* **49**, D884–D891 (2020).

[164] Hamzeiy, H., Allmer, J. & Yousef, M. Computational Methods for MicroRNA Target Prediction. In *miRNomics: MicroRNA Biology and Computational Analysis. Methods in Molecular Biology* (eds. Yousef, M. & Allmer, J.) vol. 1107, 207–221 (Humana Press, 2014).

[165] Riolo, G., Cantara, S., Marzocchi, C. & Ricci, C. miRNA Targets: From Prediction Tools to Experimental Validation. *Methods Protoc.* **4**, 1 (2021).

[166] Sticht, C., De La Torre, C., Parveen, A. & Gretz, N. miRWalk: An online resource for prediction of microRNA binding sites. *PLOS ONE* **13**, 1–6 (2018).

[167] Tarcin, O., Basaranoglu, M., Tahan, V. *et al.* Time course of collagen peak in bile duct-ligated rats. *BMC Gastroenterol.* **11**, 45 (2011).

[168] Salguero Palacios, R., Roderfeld, M., Hemmann, S. *et al.* Activation of hepatic stellate cells is associated with cytokine expression in thioacetamide-induced hepatic fibrosis in mice. *Lab. Investig.* **88**, 1192–1203 (2008).

[169] Liu, F., Chen, L., Rao, H.-Y. *et al.* Automated evaluation of liver fibrosis in thioacetamide, carbon tetrachloride, and bile duct ligation rodent models using second-harmonic generation/two-photon excited fluorescence microscopy. *Lab. Investig.* **97**, 84–92 (2017).

[170] Sigal, M., Siebert, N., Zechner, D. *et al.* Darbepoetin-α inhibits the perpetuation of necro-inflammation and delays the progression of cholestatic fibrosis in mice. *Lab. Investig.* **90**, 1447–1456 (2010).

[171] Georgiev, P., Jochum, W., Heinrich, S. *et al.* Characterization of time-related changes after experimental bile duct ligation. *Br. J. Surg.* **95**, 646–656 (2008).

[172] Zhang, Y., Guo, J., Li, Y., Jiao, K. & Zhang, Y. let-7a suppresses liver fibrosis via TGFβ/SMAD signaling transduction pathway. *Exp. Ther. Med.* **17**, 3935–3942 (2019).

[173] Cai, P., Mu, Y., Olveda, R. M. *et al.* Circulating miRNAs as footprints for liver fibrosis grading in schistosomiasis. *EBioMedicine* **37**, 334–343 (2018).

[174] Hong, J.-S., Lee, D.-H., Yook, Y. W. *et al.* MicroRNA signatures associated with thioacetamide-induced liver fibrosis in mice. *Biosci. Biotechnol. Biochem.* **81**, 1348–1355 (2017).

[175] Zhang, L., Yang, Z., Huang, W. & Wu, J. H19 potentiates let-7 family expression through reducing PTBP1 binding to their precursors in cholestasis. *Cell Death Dis.* **10**, 168 (2019).

[176] Polikepahad, S., Knight, J. M., Naghavi, A. O. *et al.* Proinflammatory Role for let-7 MicroRNAS in Experimental Asthma*. *J. Biol. Chem.* **285**, 30139–30149 (2010).

[177] Kramer, E. L., Mushaben, E. M., Pastura, P. A. *et al.* Early growth response-1 suppresses epidermal growth factor receptor-mediated airway hyperresponsiveness and lung remodeling in mice. *Am. J. Respir. Cell Mol. Biol.* **41**, 415–425 (2009).

[178] Pritchard, M. T. & Nagy, L. E. Hepatic Fibrosis Is Enhanced and Accompanied by Robust Oval Cell Activation after Chronic Carbon Tetrachloride Administration to Egr-1-Deficient Mice. *Am. J. Pathol.* **176**, 2743–2752 (2010).

[179] Chen, S. J., Ning, H., Ishida, W. *et al.* The early-immediate gene EGR-1 is induced by transforming growth factor-β and mediates stimulation of collagen gene expression. *J. Biol. Chem.* **281**, 21183–21197 (2006).

[180] Khimji, A., Shao, R. & Rockey, D. C. Divergent Transforming Growth Factor-β Signaling in Hepatic Stellate Cells after Liver Injury: Functional Effects on ECE-1 Regulation. *Am. J. Pathol.* **173**, 716–727 (2008).

[181] Liu, Q., Zhang, Y., Yang, S. *et al.* PU.1-deficient mice are resistant to thioacetamide-induced hepatic fibrosis: PU.1 finely regulates Sirt1 expression via transcriptional promotion of miR-34a and miR-29c in hepatic stellate cells. *Biosci. Rep.* **37**, BSR20170926 (2017).

[182] Erhard, F., Haas, J., Lieber, D. *et al.* Widespread context dependency of microRNA-mediated regulation. *Genome Res.* **24**, 906–919 (2014).

[183] Fu, M., Zhang, J., Zhu, X. *et al.* Peroxisome Proliferator-activated Receptor γ Inhibits Transforming Growth Factor β-induced Connective Tissue Growth Factor Expression in Human Aortic Smooth Muscle Cells by Interfering with Smad3. *J. Biol. Chem.* **276**, 45888–45894 (2001).

[184] Ghosh, A. K., Bhattacharyya, S., Lakos, G. *et al.* Disruption of transforming growth factor β signaling and profibrotic responses in normal skin fibroblasts by peroxisome proliferator–activated receptor γ. *Arthritis Rheum.* **50**, 1305–1318 (2004).

[185] Li, J., Guo, C. & Wu, J. 15-Deoxy-Δ-12,14-Prostaglandin J2 (15d-PGJ2), an Endogenous Ligand of PPAR- γ: Function and Mechanism. *PPAR Res.* **2019**, 7242030 (2019).

[186] Ahmadian, M., Suh, J. M., Hah, N. *et al.* Pparγ signaling and metabolism: The good, the bad and the future. *Nat. Med.* **19**, 557–566 (2013).

[187] Kawaguchi, K., Sakaida, I., Tsuchiya, M. *et al.* Pioglitazone prevents hepatic steatosis, fibrosis, and enzyme-altered lesions in rat liver cirrhosis induced by a choline-deficient L-amino acid-defined diet. *Biochem. Biophys. Res. Commun.* **315**, 187–195 (2004).

[188] Galli, A., Crabb, D. W., Ceni, E. *et al.* Antidiabetic thiazolidinediones inhibit collagen synthesis and hepatic stellate cell activation in vivo and in vitro. *Gastroenterology* **122**, 1924–1940 (2002).

[189] Leclercq, I. A., Sempoux, C., Stärkel, P. & Horsmans, Y. Limited therapeutic efficacy of pioglitazone on progression of hepatic fibrosis in rats. *Gut* **55**, 1020–1029 (2006).

[190] Morais, A. D. S., Abarca-Quinones, J., Horsmans, Y., Stärkel, P. & Leclercq, I. A. Peroxisome proliferated-activated receptor γ ligand, pioglitazone, does not prevent hepatic fibrosis in mice. *Int. J. Mol. Med.* **19**, 105–112 (2007).

[191] Mederacke, I., Dapito, D. H., Affò, S., Uchinami, H. & Schwabe, R. F. High-yield and high-purity isolation of hepatic stellate cells from normal and fibrotic mouse livers. *Nat. Protoc.* **10**, 305–315 (2015).

[192] Troeger, J. S., Mederacke, I., Gwak, G.-Y. Y. *et al.* Deactivation of hepatic stellate cells during liver fibrosis resolution in mice. *Gastroenterology* **143**, 1073–1083 (2012).

[193] Alatas, F. S., Matsuura, T., Pudjiadi, A. H., Wijaya, S. & Taguchi, T. Peroxisome Proliferator-Activated Receptor Gamma Agonist Attenuates Liver Fibrosis by Several Fibrogenic Pathways in an Animal Model of Cholestatic Fibrosis. *Pediatr. Gastroenterol. Hepatol. Nutr.* **23**, 346–355 (2020).

[194] Wettstein, G., Luccarini, J.-M., Poekes, L. *et al.* The new-generation pan-peroxisome proliferator-activated receptor agonist IVA337 protects the liver from metabolic disorders and fibrosis. *Hepatol. Commun.* **1**, 524–537 (2017).

[195] Lefere, S., Puengel, T., Hundertmark, J. *et al.* Differential effects of selective- and pan-PPAR agonists on experimental steatohepatitis and hepatic macrophages. *J. Hepatol.* **73**, 757–770 (2020).

[196] Boyer-Diaz, Z., Aristu-Zabalza, P., Andrés-Rozas, M. *et al.* Pan-PPAR agonist lanifibranor improves portal hypertension and hepatic fibrosis in experimental advanced chronic liver disease. *J. Hepatol.* **74**, 1188–1199 (2021).

[197] Miyahara, T., Schrum, L., Rippe, R. *et al.* Peroxisome proliferator-activated receptors and hepatic stellate cell activation. *J. Biol. Chem.* **275**, 35715–35722 (2000).

[198] Coutinho, D. S., Anjos-Valotta, E. A., do Nascimento, C. V. M. F. M. F. *et al.* 15-Deoxy-Delta-12,14-Prostaglandin J2 Inhibits Lung Inflammation and Remodeling in Distinct Murine Models of Asthma. *Front. Immunol.* **8**, 740 (2017).

[199] Chen, K., Li, J., Wang, J. *et al.* 15-Deoxy-Δ12,14-prostaglandin J2 Reduces Liver Impairment in a Model of ConA-Induced Acute Hepatic Inflammation by Activation of PPARγ and Reduction in NF-κB Activity. *PPAR Res.* **2014**, 215631 (2014).

[200] Bartel, D. P. & Chen, C.-Z. Micromanagers of gene expression: the potentially widespread influence of metazoan microRNAs. *Nat. Rev. Genet.* **5**, 396–400 (2004).

[201] Shannon, C. E., Daniele, G., Galindo, C. *et al.* Pioglitazone inhibits mitochondrial pyruvate metabolism and glucose production in hepatocytes. *FEBS J.* **284**, 451–465 (2017).

[202] Tomita, K., Azuma, T., Kitamura, N. *et al.* Pioglitazone prevents alcohol-induced fatty liver in rats through up-regulation of c-Met. *Gastroenterology* **126**, 873–885 (2004).

[203] Scher, J. U. & Pillinger, M. H. 15d-PGJ2: The anti-inflammatory prostaglandin? *Clin. Immunol.* **114**, 100–109 (2005).

[204] Gross, B., Pawlak, M., Lefebvre, P. & Staels, B. PPARs in obesity-induced T2DM, dyslipidaemia and NAFLD. *Nat. Rev. Endocrinol.* **13**, 36–49 (2017).

[205] Zhang, F., Kong, D., Lu, Y. & Zheng, S. Peroxisome proliferator-Activated receptor-γ as a therapeutic target for hepatic fibrosis: From bench to bedside. *Cell. Mol. Life Sci.* **70**, 259–276 (2013).

[206] Elshama, S. S., El-Kenawy, A. E. M. & Osman, H. E. H. Toxicological evaluation of subchronic use of pioglitazone in mice. *Iran. J. Basic Med. Sci.* **19**, 712–719 (2016).

[207] Patel, G., Kher, G. & Misra, A. Preparation and evaluation of hepatic stellate cell selective, surface conjugated, peroxisome proliferator-activated receptor-gamma ligand loaded liposomes. *J. Drug Target.* **20**, 155–165 (2012).

[208] Lam, J. K. W., Chow, M. Y. T., Zhang, Y. & Leung, S. W. S. siRNA versus miRNA as therapeutics for gene silencing. *Mol. Ther. - Nucleic Acids* **4**, e252 (2015).

[209] Schlake, T., Thess, A., Fotin-Mleczek, M. & Kallen, K. J. Developing mRNA-vaccine technologies. *RNA Biol.* **9**, 1319–1330 (2012).

[210] Hanna, J., Hossain, G. S. & Kocerha, J. The Potential for microRNA Therapeutics and Clinical Research. *Front. Genet.* **10**, 478 (2019).

[211] Zhang, S., Cheng, Z., Wang, Y. & Han, T. The Risks of miRNA Therapeutics: In a Drug Target Perspective. *Drug Des. Devel. Ther.* **15**, 721–733 (2021).

[212] Yamada, H., Suzuki, K., Ichino, N. *et al.* Associations between circulating microRNAs (miR-21, miR-34a, miR-122 and miR-451) and non-alcoholic fatty liver. *Clin. Chim. Acta.* **424**, 99–103 (2013).

Appendix

A – Abbreviations

%Area	Percent of stained area per total area
3'UTR	3' untranslated region
5'UTR	5' untranslated region
5S	Ribosomal RNA 5S
A	Adenosine
ACTA2	Actin alpha 2, smooth muscle. Protein also known as alpha smooth muscle actin (α-SMA).
Adamts14	ADAM Metallopeptidase with thrombospondin type 1 motif 14
Adamts15	ADAM Metallopeptidase with thrombospondin type 1 motif 15
ADAR	Adenosine deaminases acting on RNA
Adipor1	Adiponectin receptor 1
AF-miRNA network	The anti-fibrotic microRNA network identified by us in Winkler *et al.* (2020)
AF-miRNAs	The anti-fibrotic microRNAs of the AF-miRNA network: let-7a-5p, let-7c-5p, let-7g-5p, miR-29c-3p, miR-30d-5p, miR-30e-5p, miR-335-3p, and miR-338-3p
AGO	Argonaute protein, essential component of RISC
ALD	Alcoholic liver disease
ALT	Alanine aminotransferase
ANOVA	Analysis of variance
AP	Alkaline phosphatase
AST	Aspartate aminotransferase
B2m	Beta-2 microglobulin
BCL2	B cell lymphoma 2
BCLC	Barcelona Clinic Liver Cancer
BCL-xL	BCL2-like 1, BCL2 family member
BDL	Bile duct ligation
CCl_4	Carbon tetrachloride
CCR2	C-C motif chemokine receptor 2
CCR5	C-C motif chemokine receptor 5
cDNA	Complementary DNA
CMC	Carboxymethyl cellulose sodium salt
CMCP	Center for Model System and Comparative Pathology, Institute of Pathology, Heidelberg University Hospital
Col1a1	Collagen type 1 alpha 1
Col1a2	Collagen type 1 alpha 2
Col4a2	Collagen type 4 alpha 2
Col4a5	Collagen type 4 alpha 5
Col5a2	Collagen type 5 alpha 2
CTGF	Connective tissue growth factor
DGCR8	DiGeorge syndrome critical region 8
DMEM	Dulbecco's Modified Eagle Medium
DMN	Dimethylnitrosamine

E. coli	*Escherichia coli*
EDTA	Ethylenediaminetetraacetic acid
EGR1	Early growth response protein 1
ERK	Extracellular signal-recruited kinase
FAS	Fas cell surface death receptor
FCS	Fetal calf serum
FDA	Food and drug administration
Fluc	Firefly (*Photinus pyralis*) luciferase
FXR	Farnesoid X receptor
Gapdh	Glyceraldehyde-3-phosphate dehydrogenase
Gfap	Glial fibrillary acidic protein
GFP	Green fluorescent protein
GGT	Gamma-glutamyltransferase
Gusb	Beta-glucuronidase
HBV	Hepatitis B virus
HCC	Hepatocellular carcinoma
HCV	Hepatitis C virus
HE	Hematoxylin-eosin
HGF	Hepatocyte growth factor
HGFR	HGF receptor, also known as c-Met
hHCC	Human HCC
Hprt	Hypoxanthine phosphoribosyltransferase 1
HSC	Hepatic stellate cell
I	Inosine
i.p.	Intraperitoneal
IfADo	Leibniz Research Centre for Working Environment and Human Factors
IFIZ	Interfaculty Institute for Cell Biology, University Tübingen
IL	Interleukin
KC	Kupffer cell
Lamc1	Laminin gamma 1
LB	Lysogeny broth
LIN28A	Lin-28 homolog A
lncRNA	Long non-coding RNA
Loxl2	Lysyl oxidase-like 2
Loxl4	Lysyl oxidase-like 4
LSEC	Liver sinusoidal endothelial cell
M6P/IGFIIR	Mannose-6-phosphate/insulin-like growth factor II receptor
M6P-HSA	Human serum albumin decorated with mannose-6-phosphate
MAPK	Mitogen-activated protein kinase
MCL1	Myeloid cell leukemia 1, BCL2 family member
MDM2	Mouse double minute 2 homolog, an E3 ubiquitin-protein ligase
mHCC	Murine HCC
miRNA / miR	MicroRNA
MMP	Matrix metalloproteinase
mRNA	Messenger RNA
mTOR	Mechanistic Target of Rapamycin

NaCl	Sodium chloride
NAFLD	Non-alcoholic fatty liver disease
NASH	Non-alcoholic steatohepatitis
ncRNA	Non-coding RNA
NCT	National Center for Tumor Diseases, Heidelberg, Germany
NF-κB	Nuclear factor kappa B
NK cells	Natural killer cells
NTA	Non-template nucleotide addition
PBS	Phosphate buffered saline
PCR	Polymerase chain reaction
PDGF	Platelet-derived growth factor
Pdgfa	Platelet derived growth factor alpha
Pdgfb	Platelet derived growth factor beta
PD-L1	Programmed cell death 1 ligand 1
PGJ2	15-Deoxy-$\Delta^{12,14}$-prostaglandin J2, a PPARG agonist
pHSC	Primary hepatic stellate cell
Pio	Pioglitazone, a PPARG agonist
Plin2	Perilipin-2
PPAR	Peroxisome proliferator-activated receptor
PPARA	Peroxisome proliferator-activated receptor alpha
PPARD	Peroxisome proliferator-activated receptor delta
PPARG	Peroxisome proliferator-activated receptor gamma
PPRE	Peroxisome proliferator response element
pre-miRNA	Precursor miRNA
pri-miRNA	Primary miRNA
PTEN	Phosphatase and tensin homolog
PU.1	PU box binding protein
qPCR	Quantitative PCR
Raf	Raf (rat fibrosarcoma) proto-oncogene serine/threonine-protein kinase
Ras	Ras (rat sarcoma) GTPase family
Rat	*Rattus norvegicus*
Rho	Rho (Ras homolog) GTPase family
RISC	RNA-induced silencing complex
RNA	Ribonucleic acid
RNase	Ribonuclease
RNA-seq	RNA sequencing
Rnu6	U6 small nuclear RNA
RXR	Retinoid X receptor
SEM	Standard error of the mean
SMAD	Mothers against decapentaplegic homolog
Snord33	Small nucleolar RNA, C/D box 33
Snord35a	Small nucleolar RNA, C/D box 35a
SRF	Serum response factor
sRNA-seq	Small RNA sequencing
TAA	Thioacetamide
TACE	Transarterial chemoembolization

Tbp	TATA-box binding protein
TCGA	The cancer genome atlas
Tgfbr1	Transforming growth factor beta receptor 1
TGF-β	Transforming growth factor beta
TIMP	Tissue inhibitors of metalloproteinases
tk120	*Herpes simplex* virus thymidine kinase basal promoter sequence (-120 to +1)
TNFR1	TNF receptor 1
TNF-α	Tumor necrosis factor alpha
Tpm1	Tropomyosin 1
TRAIL	TNF-related apoptosis-inducing ligand
TRBP	TAR RNA-binding protein
Tris	Trizma base
TUT4	Terminal uridyl transferase 4
TUT7	Terminal uridyl transferase 7
TZD	Thiazolidinedione
U87	U87 small nuclear RNA
VEGF	Vascular endothelial growth factor
VitA	Vitamin A
VP16	*Herpes simplex* viral protein 16
W-o-L	Window of linearity
ZEB1	Zinc Finger E-Box Binding Homeobox 1
ZEB2	Zinc Finger E-Box Binding Homeobox 2

B – List of Figures

C – List of Tables

D – Publications

Winkler, I.*, **Bitter, C.***, Winkler, S., Weichenhan, D., Thavamani, A., Hengstler, J. G., Borkham-Kamphorst, E., Kohlbacher, O., Plass, C., Geffers, R., Weiskirchen, R. & Nordheim, A. Identification of Pparγ-modulated miRNA hubs that target the fibrotic tumor microenvironment *Proc. Natl. Acad. Sci. U. S. A.* **117**, 454–463 (2020).

Prabhala, P., Wright, D. B., Robbe, P., **Bitter, C.**, Pera, T., Ten Hacken, N. H. T., van den Berge, M., Timens, W., Meurs, H., Dekkers, B. G. J. Laminin α4 contributes to airway remodeling and inflammation in asthma. *Am. J. Physiol. - Lung Cell. Mol. Physiol.* **317**, L768–L777 (2019).

*equal contribution

E – Supplementary Figures

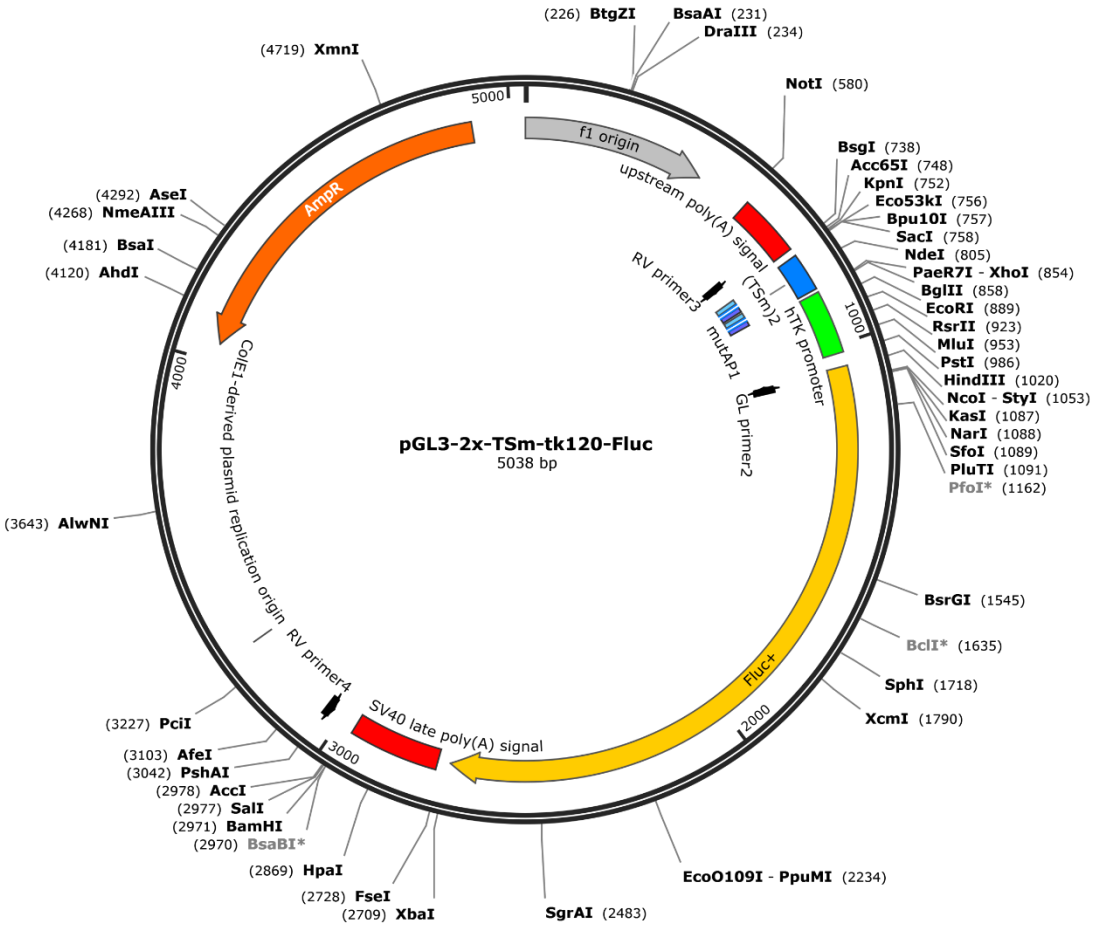

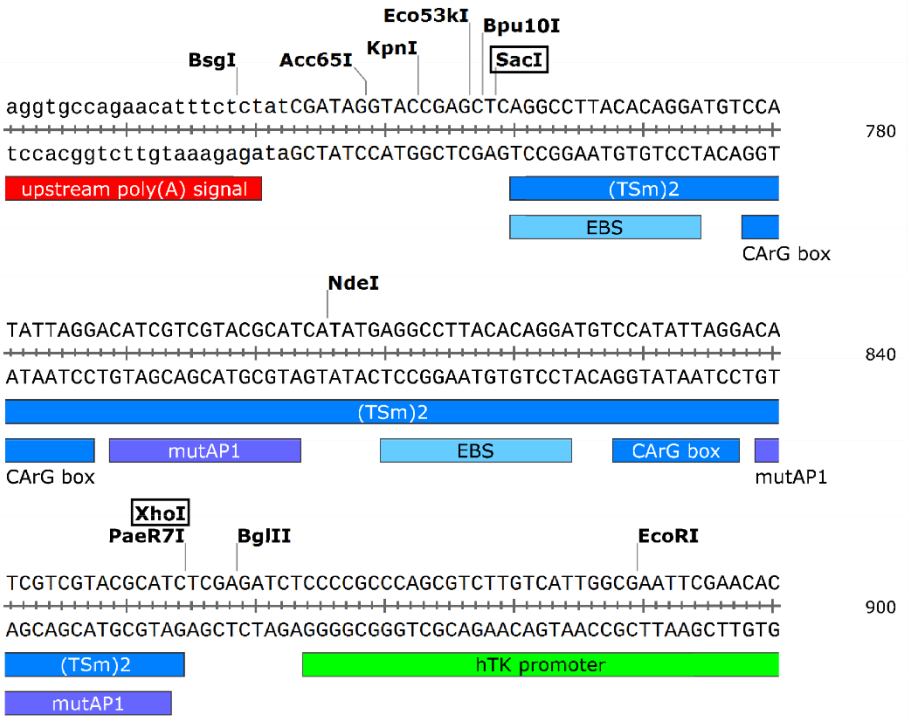

Supplementary Figure 1 | Vectormap and sequence of the transcription factor binding sites of luciferase reporter vector pGL3-2x-TSm-tk120-Fluc. Restriction enzymes SacI and XhoI were used for insert excision. Plasmid was generated by Dr. Bilge Ergin [119].

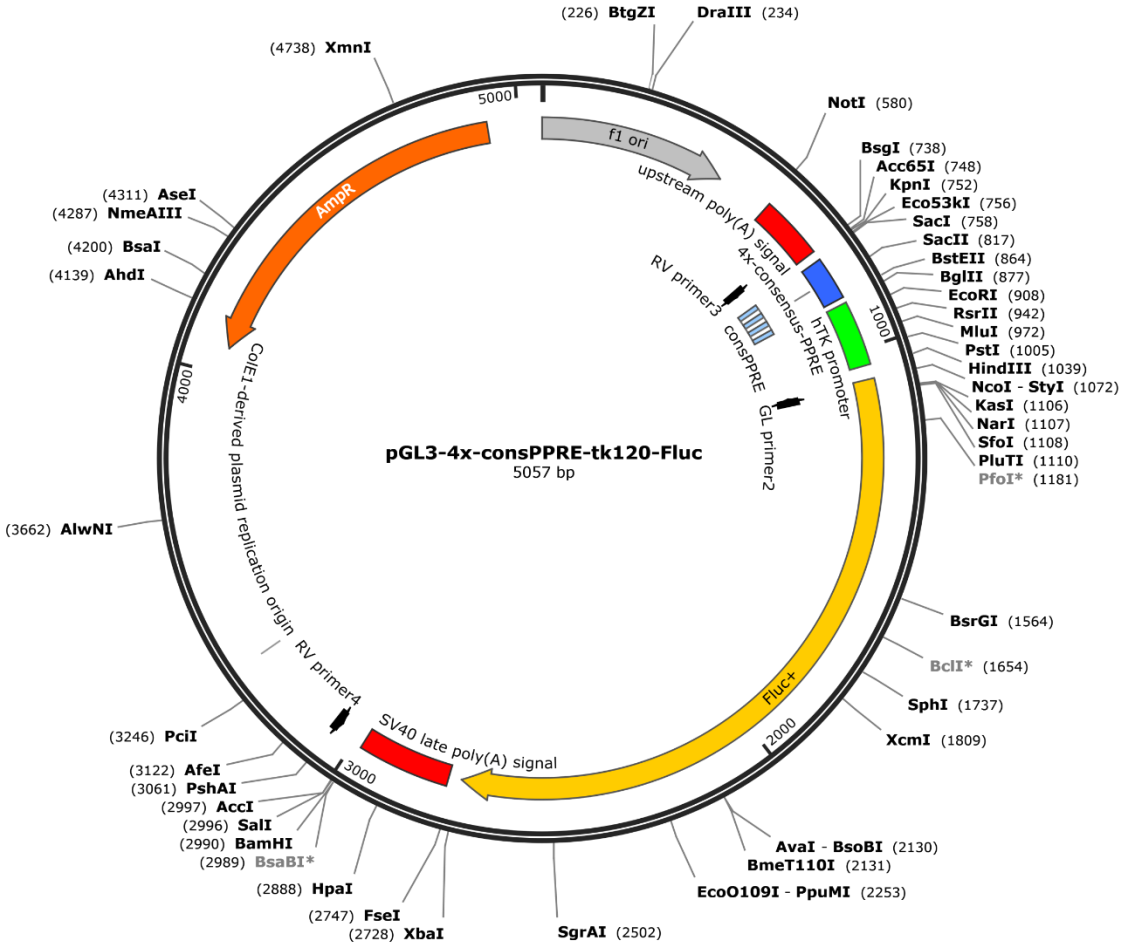

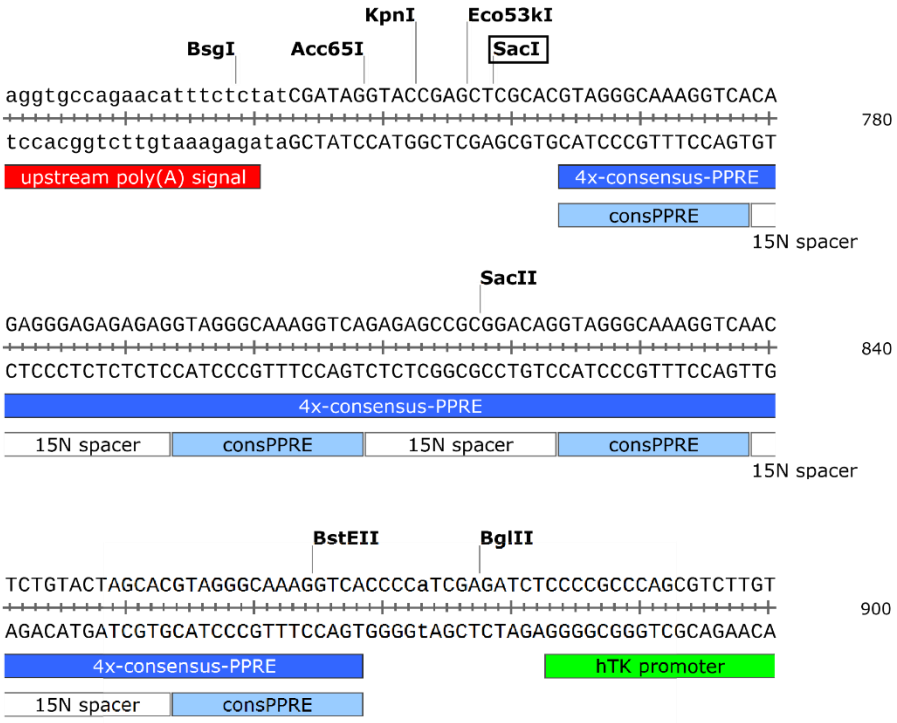

Supplementary Figure 2 | Vectormap and sequence of the inserted PPARG binding sites (4 identical consensus PPREs) of luciferase reporter vector pGL3-consPPRE-tk120-Fluc cloned as part of this study. SacI and XhoI were used for oligonucleotide insertion. Oligonucleotides were designed to lose XhoI site upon correct insertion.

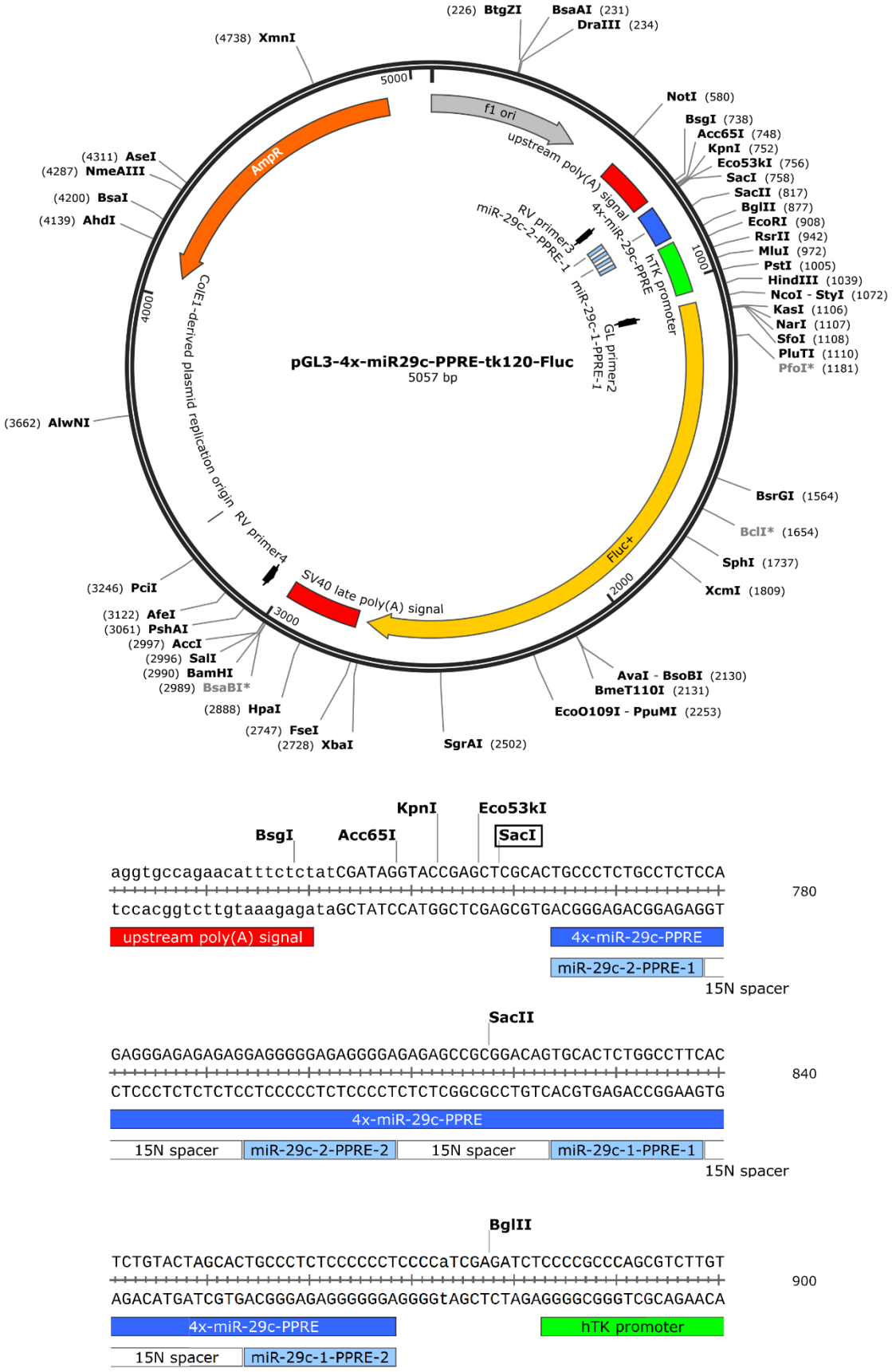

Supplementary Figure 3 | Vectormap and sequence of the inserted PPARG binding sites (4 individual PPREs in the miR-29c promoter region) of luciferase reporter vector pGL3-29cPPRE-tk120-Fluc cloned as part of this study. SacI and XhoI were used for oligonucleotide insertion. Oligonucleotides were designed to lose XhoI site upon correct insertion.

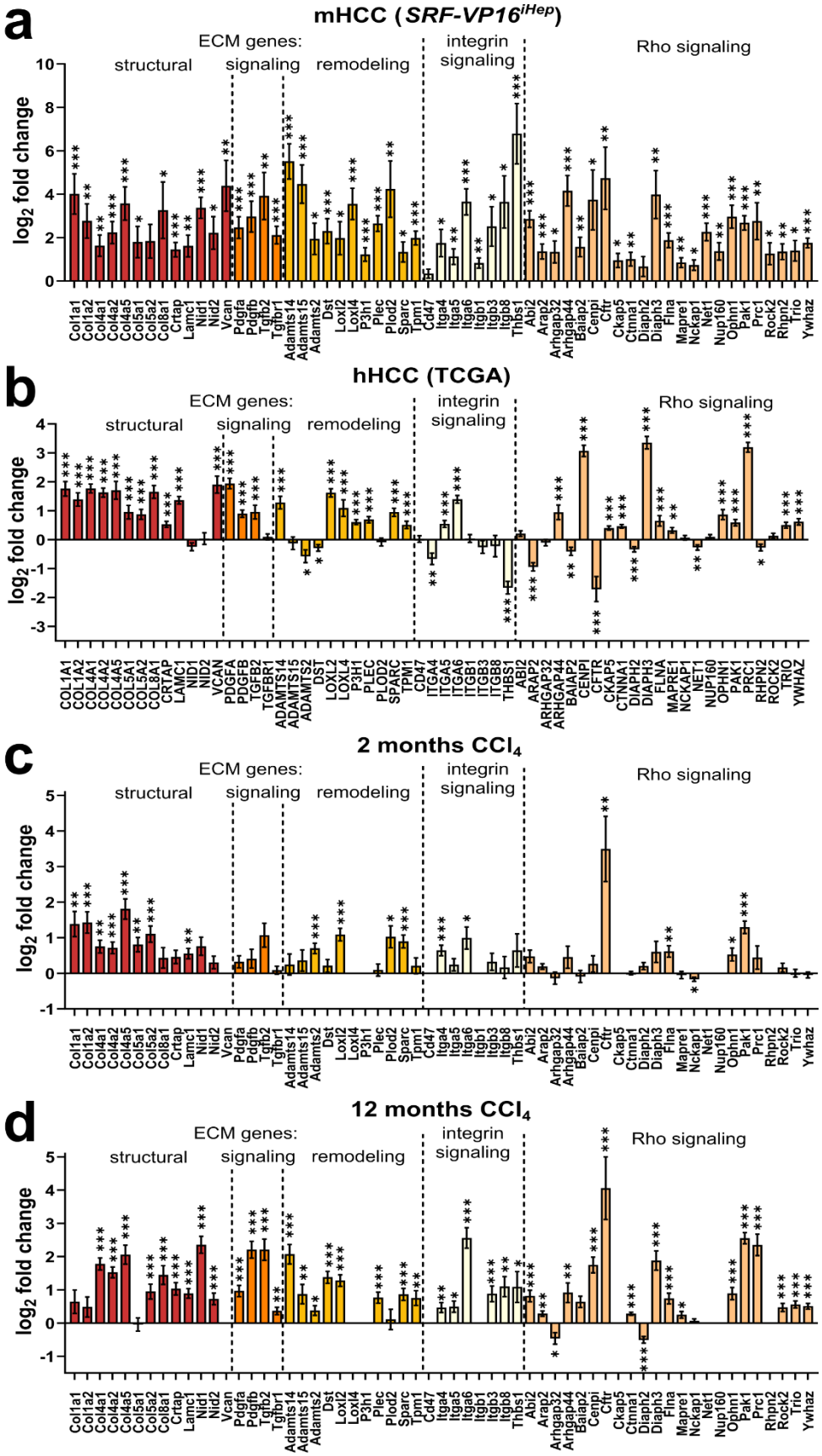

Supplementary Figure 4 | Gene expression of the fibrotic target genes of the AF-miRNA network in (a) murine HCC (*SRF-VP16*^{iHep} tumors), (b) human HCC (TCGA cohort), (c) 2 months and (d) 12 months CCl_4-induced liver fibrosis. Data are shown as mean log_2 fold change in disease (mHCC/hHCC/2 months CCl_4/12 months CCl_4) compared to control (litter mate/healthy liver/2 months oil/12 months oil) in each RNA-seq dataset as analyzed by DESeq2. Data are shown as mean and SEM. *$p_{adj} \leq 0.05$, **$p_{adj} \leq 0.01$, *** $p_{adj} \leq 0.001$.

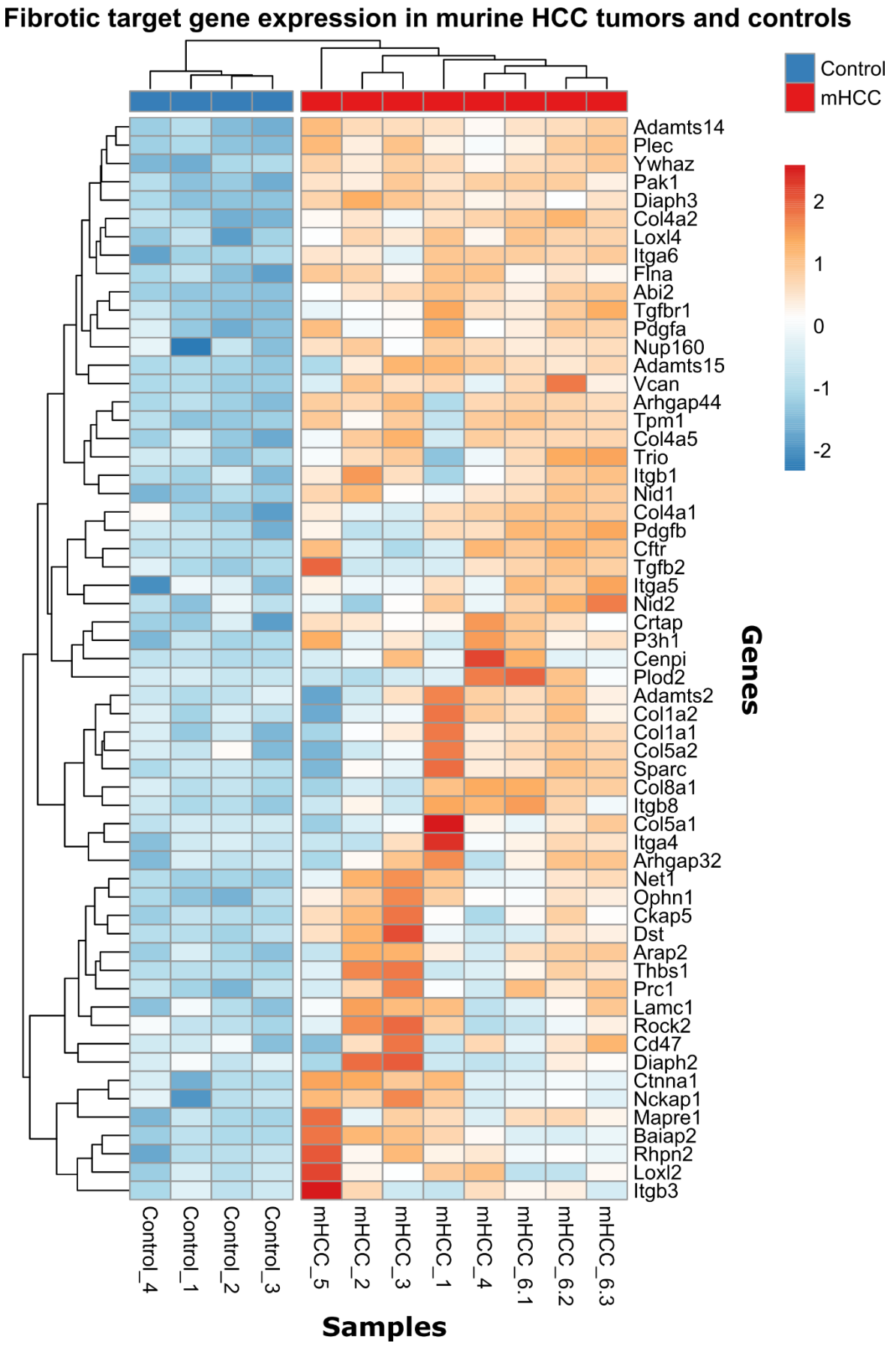

Supplementary Figure 5 | Heatmap of the fibrotic target genes of the AF-miRNA network in murine HCC (*SRF-VP16*^{iHep} tumors) and litter mate controls as determined by RNA-seq. Data are shown as normalized reads (derived from DEseq2 analysis) after z-score transformation.

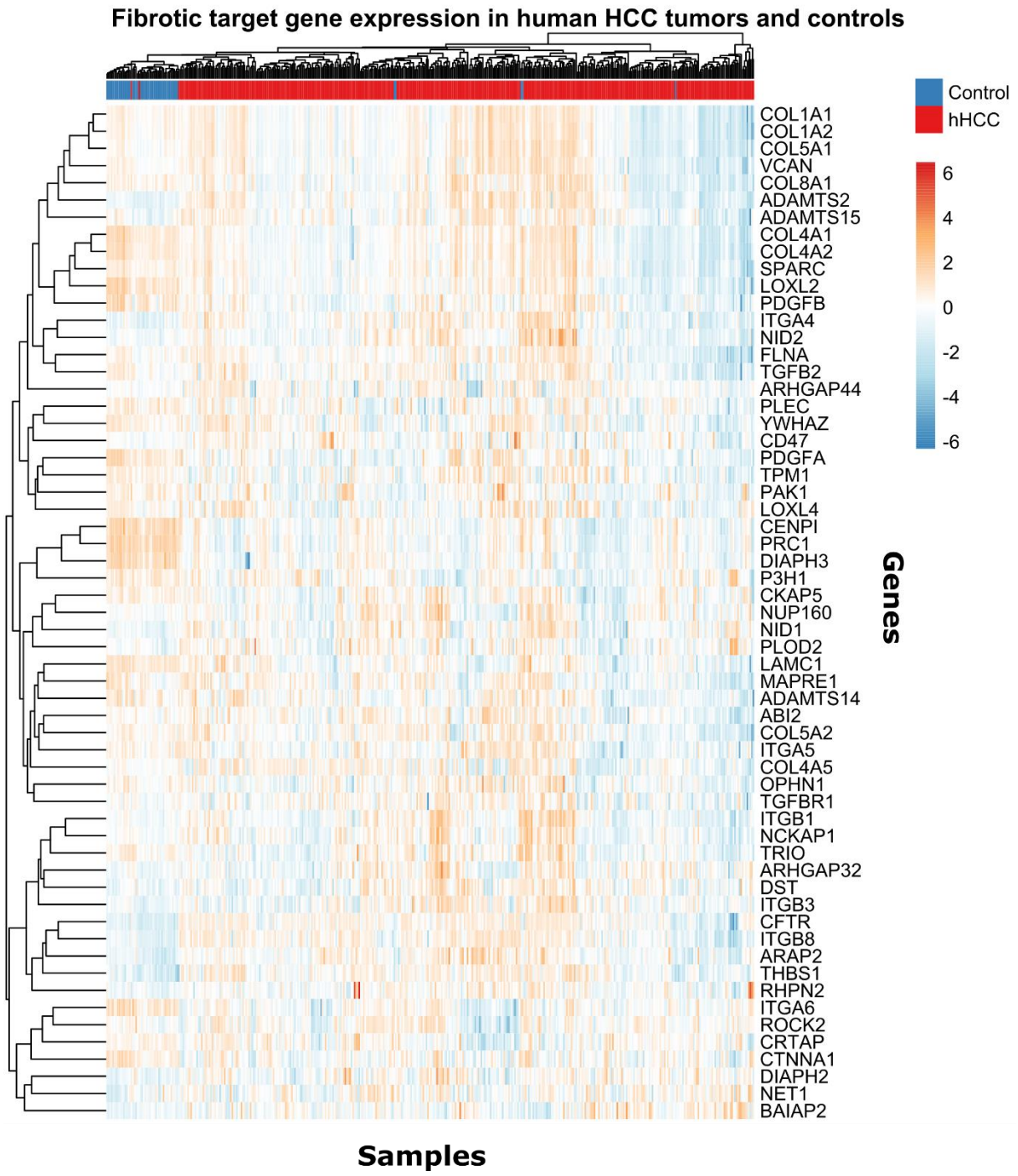

Supplementary Figure 6 | Heatmap of the fibrotic target genes of the AF-miRNA network in human HCC and healthy controls (TCGA cohort) as determined by RNA-seq. Data are shown as normalized reads (derived from DEseq2 analysis) after z-score transformation.

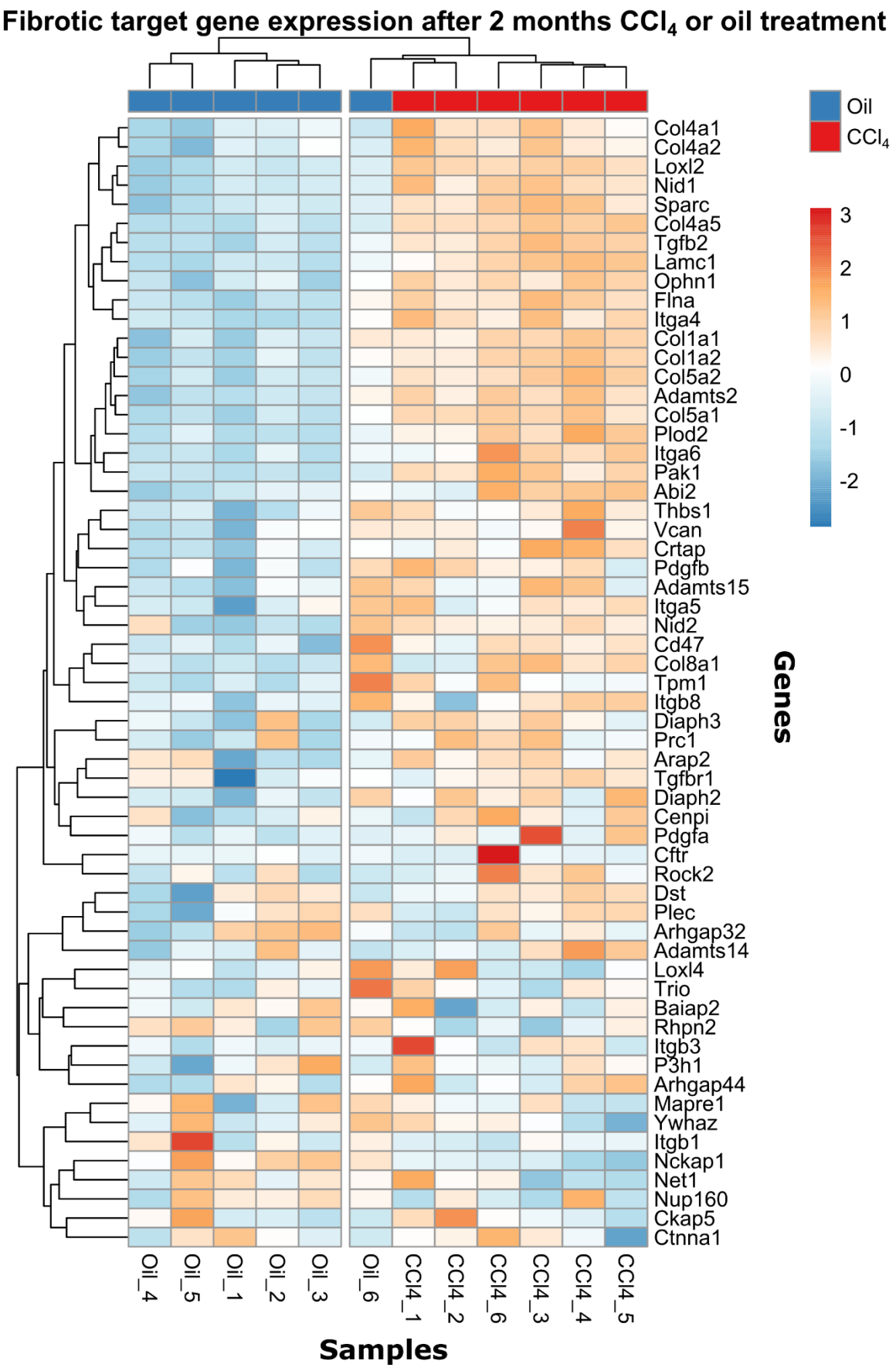

Supplementary Figure 7 | Heatmap of the fibrotic target genes of the AF-miRNA network after 2 months CCl_4 and oil treatment as determined by RNA-seq. Data are shown as normalized reads (derived from DEseq2 analysis) after z-score transformation.

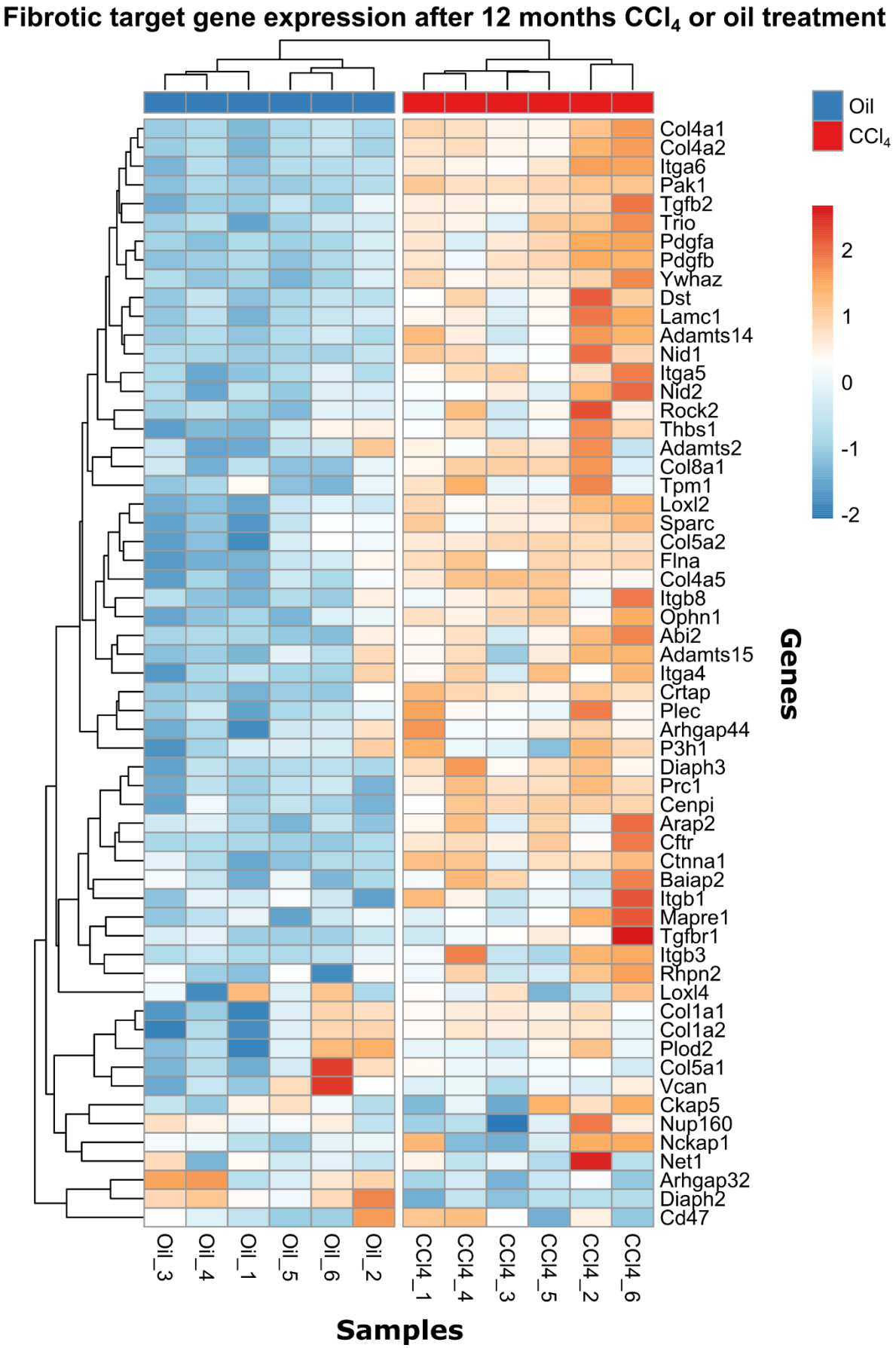

Supplementary Figure 8 | Heatmap of the fibrotic target genes of the AF-miRNA network after 12 months CCl_4 and oil treatment as determined by RNA-seq. Data are shown as normalized reads (derived from DEseq2 analysis) after z-score transformation.

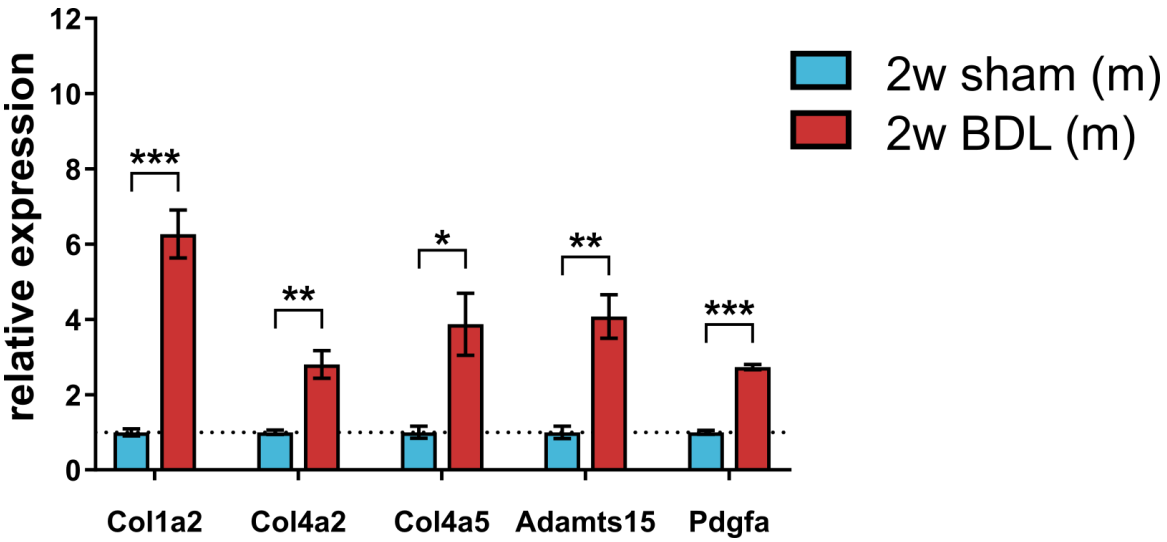

Supplementary Figure 9 | Relative gene expression of further fibrotic target genes of the AF-miRNA network 2 weeks after BDL-mediated liver fibrosis or sham operation in mouse (n=4/group). qPCR data were normalized to *Gapdh* and *Tbp* and then to the mean control group. Statistical comparison by two-sided unpaired t-test. Data are shown as mean and SEM. *p≤0.05, **p≤0.01, *** p≤0.001. BDL – bile duct ligation, w – weeks.

F – Supplementary Data

Supplementary Data 1	ImageJ macro for blinding
Supplementary Data 2	ImageJ macro for %Area quantification
Supplementary Data 3	Code for bioinformatic analysis of RNA-seq data from 2 months and 12 months CCl_4-induced liver fibrosis. Raw reads by Ghallab *et al.* (2019) were analyzed with the R package DESeq2 (v1.22.2).
Supplementary Data 4	List of 40 miRNA:target gene pairs conserved between human, mouse, and rat out of the 8 AF-miRNAs and 14 validated target genes of the network and their miTG scores.

Acknowledgements

I want to express my heartfelt gratitude to everyone who accompanied and supported me during my PhD journey. I only came this far because of all of you.

First and foremost, I especially thank Prof. Dr. Alfred Nordheim for accepting me as his PhD student and for his constant support, guidance, and supervision. I further thank my TAC members Prof. Dr. Ralf-Peter Jansen and Dr. Felicity Jones for their scientific support and valuable advice.

I thank all my collaborators for dedicating their materials, analyses, time, and effort to this study: Prof. Dr. Ralf Weiskirchen, Prof. Dr. Jan G. Hengstler, Dr. Robert Geffers, Dr. Abhishek Thavamani, Sebastian Winkler, Prof Dr. Sebastian Mueller, Teresa Peccerella, Veronika Eckel as well as Dr. med. vet. Tanja Poth and her team at the CMCP.

I am very honored to be supported by the Max Planck's IMPRS Research School "From molecules to Organisms" and the Else Übelmesser foundation, both allowing me to do even better research. A warm thank you to Sarah Danes, Jeanette Müller, and Sibylle Patheiger for their IMPRS workshops and their advice on PhD life inside and outside the lab.

A gigantic thank you goes to all my lovely colleagues from the Nordheim group. Ivana, thank you for all the guidance and patience over the years, for the coffee chats, and all the fun in the lab. Michi, thank you for all your (experi)mental support, from mouse work and study design discussions to an open ear on tough days and a good laugh every day. Thank you also for the Getto Workout sessions and the constant supply of Gehr sweets and home-brewed beer. Siggi, thank you for all the thought and effort you put into my mouse project, and for being such a kind and patient soul. Anke and Heidemi, thank you both so much for all your help in the lab, for the lovely lunch breaks, and for always lending an ear. My thanks and gratitude also to Elena, Stella, Alex, Cansu, Mohan, Pascal, Musti, Nghi, Heide, Sandra, Franziska, Janina, and Munira. You are all incredibly supportive, reliable, and fun to work with!

Finally, I especially thank my friends and my family for always being there, for always encouraging me, and most importantly, for always believing in me: Martin, Lena, Saskia, Jutta, Michael, Lena, Bine, Mathilde, Lena, Tobi, and many more.